Mapping of Urban Tree Canopy Using LiDAR, Oblique Image Viewers and Geographic Object Based Image Analysis (GeOBIA): a Multi-Scale Approach

by

Tyler Wayne Jones

A dissertation submitted to the Graduate Faculty of
Auburn University
in partial fulfillment of the
requirements for the Degree of
Doctorate of Philosophy

Auburn, Alabama
August 4, 2018

Approved by

Art Chappelka, Co-Chair, Professor of Forestry & Wildlife Sciences
Luke Marzen, Co-Chair, Professor of Geosciences
Chandana Mitra, Associate Professor Geosciences
Larry Teeter, Professor of Forestry & Wildlife Sciences

ABSTRACT

The benefits of an urban forest canopy have become more readily understood in recent years. They provide a wealth of environmental, social, and economic benefits such as improved water quality, air temperature regulation, carbon sequestration, air pollution reduction, enhanced human health, better aesthetics, increased property value, and reduction of energy consumption. For this study, a multi-scale analysis is used to determine the efficiency and efficacy of varying remote sensing platforms to capture, model, and measure standard forest metrics. These include industry-standard measurements such as diameter at breast height (DBH) and total stem height. Remotely sensed data platforms such as airborne light detection and ranging (LiDAR), ground-based LiDAR, stereoscopic imaging, and image object construction using object based image analysis have existed for some time, and provide ways to reduce cost and increase efficiency over standard field data collection methods. For this study, data of the same urban forest canopy was examined using data collected from each remote sensing platform and compared directly with data captured using standard in-field forest measurement techniques. The specific objectives being to determine if remote sensing platforms which provide the highest resolutions, specifically spatial resolution, correlate into higher relative accuracy when compared to in-field measurements. These measurements include: 1) at the individual tree scale, DBH, total height, crown width, and total biomass taken for each individual branch along with the bole 2) at the city block scale, these measurments include DBH, total height, species identification, and crown width. 3) at the city scale, these measurments include total height and species identification. The

study areas include: 1) a series of open-grown Nuttall oaks (*Quercus texana*) located approximately 5km northwest of Auburn University, Alabama 2) A single city block located on the campus of Auburn Unversity 3) an urban forested area of the City of Auburn approximately 310 hectares in size. At the local scale each of a series of 7 Nuttall oak trees were scanned using a terrestrial LiDAR scanning system (TLS) from a distance of 5 to 10 meters and from 7 different vantages. Once these data were captured and registered into a comprehensive vector point cloud the trees were destructively sampled in order to aquire accurate linear and volumetric measurements. This information was then compared with those generated from models of the vector point cloud. No significant differences in linear measurements were observed, but a consistent underestimation of overall biomass was observed across all 7 specimen. At the medium scale, a city block of Auburn University's campus had aiborne imagery taken of the entire area from multiple vantage points using oblique oriented passive sensor cameras. These data were used to create a vector point cloud of the study area that were compared to field measurments. No significant differences in linear measurement were observed, minor underestimation of overall biomass was observed compared with estimates based on field measurements. At the city scale, airborne LiDAR (ALS) data were collected and used in conjunction with airborne orthographic imagery to generate a surface model that identifies individual trees. This was accomplished using geographic object based image analysis (GeOBIA) techniques. Once generated the total heights for each individual tree were attributed and compared to a sampling of trees measured in the field. Total heights were found to be underestimated in most observations, but were greater for shorter coniferous trees when

compared to taller deciduous and coniferous trees. In general, this study was useful in comparing the accuracy and relative efficiency of these different remote sensing platforms as they pertain to urban forest measurements. Modern urban forestry relies heavily upon the use of these and other forms of remote sensing to quickly and accurately measure and maintain these vital natural resources.

ACKNOWLEDGEMENTS

The author wishes to thank his major professors, Drs. Art Chappelka and Luke Marzen, for their guidance, input, time, and patience towards his academic career and this dissertation. He would also like to acknowledge the assistance of his committee members, Drs. Chandana Mitra, and Larry Teeter and his outside reader, Dr. Mark Dougherty. He also thanks the Auburn University School of Forestry & Wildlife Scieces and Department of Geosciences for providing funding to make the pursuit of this PhD possible, as well as the U.S. Forest Service-SRS 4952, especially Dudley Hartel for providing funding. He would also like to thank Junshan Liu and Dr. Paul Holley of the Auburn University McWhorter School of Building Science for their technical assistance, and Efrem Robbins for assistance with data collection on long summer days under the oppressive Alabama sun. The author wishes to dedicate this work to his family, his wife Dr. Tiffany Mumford whose love and encouragement made this work possible, and his father and grandfathers: Brad Jones, James Adams, James Gilmore for their examples of using hard work to achieve your goals, and would be proud of his accomplishments.

Table of Contents

List of Tables

List of Figures

Chapter 1. Mapping of Urban Tree Canopy Using LiDAR, Oblique Image Viewers and Geographic Object Based Image Analysis (GeOBIA): An Introduction

The benefits of an urban forest canopy have become more readily understood in recent years. They provide a wealth of environmental, social, and economic benefits such as improved water quality, air temperature regulation, carbon sequestration, air pollution reduction, enhanced human health, better aesthetics, increased property value, and reduction of energy consumption (Nowak et al., 2007; Peper et al., 2007). To maximize urban forests' benefits many cities and municipalities have implemented programs designed to protect and expand forest canopy cover (DCUFA, 2010; Greenworks, 2009; MTNYC, 2007). To make these programs more effective the current extent and distribution of the urban forest canopy must be accurately known (Locke et al., 2010). Presently, the most widely available source of this information is the National Land Cover Dataset (NLCD). Drawbacks to this dataset are its relatively coarse spatial resolution of 30 meters and that the datasets are only periodically updated. These coarse scale datasets are effective for classification at the regional scale, but are ineffective for grouping at the local scale (Homer et al., 2007; Myeol et al., 2001).

In recent years there has been an expansion in the availability of high resolution aerial imagery from both satellite and airborne platforms that have allowed for increases in mapping tree canopy and other landcover types (Rogen and Chen, 2004; Quackenbush et al., 2000). These types of sensors, however, are typically passive, and only collect the electromagnetic radiation reflected off the Earth's surface. This can be problematic because with airborne imagery the data are not collected at the same time, but rather over several days or weeks during different times of the day. This causes variation in the distribution of brightness values from one image to the next,

which causes difficulty during classification as well as varying the degree and direction of shadows cast by tall objects (Rogen and Chen, 2004).

For this study, a multi-scale analysis is used to determine the efficiency and efficacy of varying remote sensing platforms to capture, model, and measure standard forest metrics. These include industry-standard measurements such as diameter at breast height (DBH) and total stem height. These efforts are focused on the health, stand-level stocking, and social contributions that urban forests provide as opposed to commercial level productivity. For this reason, no attempt is made to determine product merchantability, growth & yield, or return on investment (ROI). Several platforms exist for the capture of urban tree metrics, along with long established field measurement methods. Most of these techniques rely upon the inclusion of input parameters such as DBH, total stem height, and crown width to produce accurate estimations of standing biomass, leaf area, carbon sequestration, and more (Avery and Burkhart, 1983).

Remotely sensed data platforms such as airborne light detection and ranging (LiDAR), ground-based LiDAR, stereoscopic imaging, and image object construction using object based image analysis have existed for some time, and provide ways to increase efficiency over standard field data collection methods (Chen et al., 2005; Myeong et al., 2001). Regarding this study, data of the same urban forest canopy will be examined using data captured from each remote sensing platform and compared directly with data captured using standard in-field forest measurement techniques. The hypothesis being that remote sensing platforms, which provide the highest spatial resolution should correlate into higher relative accuracy when compared to in-field measurements. In general, spatial resolution is a function of the distance between the object being observed and the aperture of the device making the observation. For this reason, logic would suggest that airborne LiDAR platforms that measure objects from 1,000 meters or more in

distance while traveling in excess of 250 kilometers per hour would not achieve the same level of spatial resolution as a ground-based LiDAR platform gathering data from the same object less than 15 meters away. However, research has shown that the accuracy of object identification and canopy mapping are not explicitly limited to spatial resolution, but also angle of approach (AOA), laser sensor capture/write limitations, multi-return data layers, and electromagnetic frequency (Huang et al., 2011; Hopkinson et al., 2009; Kato et al., 2004).

Ground-based sensors, while more affordable and portable than airborne units, generally do not possess the same capabilities of their airborne counterparts. This can lead to airborne sensors making up much ground in the terms of data robustness and utility compared to ground-based, however airborne LiDAR does not typically provide the same level of information due to the distance from the target and the number of capture points per unit area compared to ground-based platforms (Gatziolis and Andersen, 2008). Both airborne and ground-based laser scanners utilize active sensors which expel an energy packet, in this case, a beam of light onto an object and measure the reflected energy. Another form of data acquisition involves the use of passive sensors; which capture energy being reflected off an object by some other source. In natural resource applications this source is typically sunlight, but can also include other forms of energy including anthropogenic light sources, geothermal hotspots, and ionizing radiation sources (Scholz and Gruber, 2008).

In this study all three of these platforms are examined using various levels of scale to highlight each one's advantages and limitations. First, a comprehensive literature review (Chapter 2) will highlight the current state of these technologies as well as the relevant history of each type of platform; ground-based LiDAR, airborne LiDAR, and passive camera sensors. Included within this literature review will be ancillary technologies such as geographic object

based image analysis (GeOBIA) which are incorporated into project workflows to increase accuracy and efficiency. Next, in Chapter 3, at the individual tree scale, I will examine a ground-based study of several Nuttall oak (*Quercus texana*) trees that after being heavily scanned using a ground-based system were destructively sampled, measured, and weighed for comparison to digital modeling techniques. Drawbacks and limitations a project at this scale include upper canopy occlusions due to growing-season foliage and economic costs.

Chapter 4 will feature a city block scale project that uses passive sensor camera technology to capture high resolution raster datasets of the study area. The passive sensors in question are oriented in such a manner as to provide a large percentage of image overlap, allowing for the generation of three-dimensional objects via stereoscopic imaging. This is due to the dataset containing a series of five images at each sample coordinate. Four of these are obliques at ninety degree angles relative to the flight path and the fifth is a nadir perspective image giving a "bird's eye view". Overlapping sections of each image allow for viewing of the same object from multiple perspectives. This, in general, permits imaging software to generate vector point clouds from these raster image files. Drawback and limitations of such platforms are seen within the datasets including occlusions to midstory and understory species and brightness value fluctuation from flight line to flight line.

Chapter 5 will assess a city-scale project that uses airborne LiDAR scanning to map, identify, and measure the individual trees of the study area as well as quantify discrepancies with total height measurements. Data, once captured, can be analyzed using many different techniques. Manual interpretation by the end user to aid in digitizing is one of the easiest ways, but this can lead to a bottleneck in terms of project size and scope due to the time required for such manual analysis. Automated mapping procedures exist to bridge this gap, including

geographic object based image analysis (GeOBIA) which allows for automated algorithm construction and execution. This study uses several input datasets captured from varying platforms to map and model overlapping areas of urban forest canopy to achieve image object feature extraction. Drawbacks and limitations include the error prone nature of single point measurement metrics when using relatively low spatial resolution point cloud data. Finally, in chapter 6 I will summarize and discuss the findings and offer possible explanation for shown results as well as offer insight into future research possibilities.

Chapter 2. Literature Review

Several technologies are discussed in the following chapter, each of which bear special significance on understanding the fundamentals of a particular specialty, past research efforts, and current state of the research. Airborne LiDAR scanning systems (ALS) are first discussed along with an introduction into the basics of time-of-flight (TOF) distance measurement and modeling. Terrestrial LiDAR scanning systems (TLS) are then discussed along with much of the recent scientific study into these techniques for natural resource management. Passive camera systems are then described illuminating their fundamental difference when compared to LiDAR scanning systems, and how these technologies allow for dense point cloud construction. Ancillary technologies such as geographic object based image analysis (GeOBIA), polyhedron surface modeling, and scripted algorithm use are also discussed and how they support the primary objectives of the preceding technologies.

2.1 Airborne LiDAR Scanning (ALS)

Airborne LiDAR is used prominently in projects that are at the landscape scale, and in terms of mapping trees, is useful for mapping forest canopy footprints and general heights. In this study it is used in conjunction with high-resolution aerial imagery for performing landscape scale mapping with geographic object based image analysis (GeOBIA). Remote sensing techniques using aerial imagery alone typically have the same problem where variations in light conditions and overarching shadows disrupt traditional pixel-based classifiers. ALS is a technology that can alleviate some of these problems by implementing an active sensor as opposed to the passive sensors used by traditional cameras. An active sensor system relies on two optical beams, the emitted laser beam, and the returned portion of that beam, and is not

vulnerable to shadowing or other variations in natural light (MacFaden et al., 2012; Wehr and Lorh, 1988). The equipment involved in an airborne platform generally include: a laser, a real time kinematic (RTK) corrected global positioning system (GPS) receiver that maintains the aircraft's coordinate position, an inertial measurement unit (IMU) that maintains the aircraft's spatial orientation relative to the ground (equipotential), and an interface between the receivers and data storage devices. To maintain functional RTK correction the receiver must be in range (~40 kilometers) of a base station that is established over a known coordinate and is constantly delivering vector correction data to account for atmospheric aberration. This real time correction is generally used in conjunction with post processing correction (Nilsson, 1996).

While scanning, a laser emits beams of light which encounter an object on the ground. This light is then backscattered and returns to the sensor slightly or significantly weaker than when it was initially emitted, depending on the reflectivity (albedo) of the object encountered (Naesset, 2009). The distance from the source of the light beam and the object that it reflected off of is determined by measuring the amount of time delay between emission and detection. This is possible because the speed at which light travels is fixed, and this type of distance measurement is known as time of flight (TOF) measurement. In general, there are two different types of LiDAR with the former being known as waveform LiDAR which records the backscatter returning to the sensor as a continuous stream of information and the latter being known as discrete-return LiDAR in which the backscatter is quantified into amplitude intervals and recorded at specifically referenced returns (Naesset, 2008). Discrete-return is also known as multi-return LiDAR.

Commercial scanning instruments vary greatly in terms of the number of light beams that can be emitted in a given period of time. In general, the number of beams emitted by a sensor in

one second is known as that sensor's scanning frequency. Depending on the manufacturer and the generation of instrument these can vary from a few thousand beams per second to several hundred thousand beams per second (Gatziolis and Andersen, 2008). This variation in scanning frequency means that higher frequency enabled systems can fly at higher altitudes and at faster speeds while maintaining desired return densities as compared to lower frequency systems. Other system-dependent variables include mirror scanning patterns such as seesaw, parallel, and elliptical as well as beam divergence. This divergence is due to the trajectory of the light beam emitted deviating slightly from the propagation axis to form a cone-like shape as opposed to a true cylinder. Depending on the application, these divergence values typically range from 0.1 to 1.0 milliradian (Baltsavias, 1999). This angular measurement and the operating altitude of the aircraft combine to determine the size of the scanning footprint that the sensor can measure at any given time. This footprint is typically described as the diameter of a beam of light pulses that are intercepted by a plane positioned perpendicularly to the beam axis. Within this footprint the distribution of pulse energy is not uniform, but rather it decreases via two-dimensional Gaussian distribution as it approaches the edge of the footprint's extent (Gatziolis and Andersen, 2008). Another characteristic of the system is the gain factor that is being employed on the backscatter receiving device. This variation in sensitivity is designed to prevent damage to system hardware in the presence of high backscatter energy in the event of highly reflective surfaces.

Other relevant system attributes include the duration of the pulse, the number of returns that can be extracted from a single beam pulse, and the footprint spacing of each scan relative to altitude and velocity (Priestnall, Jaafar and Duncan, 2000). It is from these system attributes that a particular dataset's attributes are determined such as pulse density, return density, return remission, and return number. Pulse density is driven by a system's footprint spacing as

measured over a hypothetical flat plane and is found by dividing one by this squared measurement [1/(footprint spacing^2)]. Return density is the average number of returns per a given unit of area (m^2). This is not to be confused with pulse density due to the prevalence of multi-return systems which in a case of scanning multi-tiered canopy would result in a higher return density than over bare earth, but each of whom would have equal pulse densities. It is because of this location-dependent variation that pulse density, rather than return density, can be used as a standard measurement for LiDAR acquisition (Priestnall, Jaafar and Duncan, 2000).

Return number refers to the rank within the return structure that a particular backscattered beam is observed. For instance, a beam that penetrates highly structured upper canopy before being backscattered by lower canopy would likely register as a second or third return while a beam that penetrated all the way to the ground through the same canopy would register as a last return. Return remission refers to the fraction of beam energy that returns to the sensor as backscatter after encountering an object. This will depend on the reflectivity of the object as well as its range from the sensor and rank within the return structure.

The resulting dataset is generally stored within an interchange format know LAS, short for laser. This file format is the approved file format of the American Society for Photogrammetry and Remote Sensing (ASPRS). This format uses a delimited series of coordinate triplicate along with ancillary data that may be available depending on the system such as return number and remissive value. The data are human readable in that each return is assigned a single line of entry and can be viewed using any text editor assuming sufficient onboard memory to open such large files. File size has been an issue with this technology since the data are inherently large, consisting of perhaps hundreds of millions of returns per file.

Dedicated hard drives with storage in excess of one terabyte are generally employed in an airborne LiDAR project.

The result is a point cloud of XYZ coordinate data that managers and researchers can manipulate to reflect characteristics such as height above ground and texture of various features. This technology has already been utilized in the identification and classification of trees for forest inventory, habitat assessment for wildlife, assessing canopy gaps, and urban feature extraction (Takahashi et al., 2010; Gaulton and Malthus, 2010; Solberg, 2010; Hollaus et al., 2009; Naesset, 2007; Hyde et al., 2006; Bradbury et al., 2005; Rottensteiner, 2003; Priestnall, Jaafar, and Duncan, 2000).

2.2 Terrestrial LiDAR Scanning (TLS) in Urban Canopy Mapping

TLS is typically used in more localized scanning projects intended to cover smaller geographic areas than compared to ALS. In this study a terrestrial scanning system is used to measure seven individual Nuttall oak trees that are later harvested and sampled for linear and volumetric biomass. These results are later compared to those collected using the scanning system. In comparison to the relatively course point clouds generated from airborne LiDAR platforms TLS has become an efficient way of generating an impressively dense point cloud model of a landscape or structure. These systems operate on the same basic principle as ALS by using the consistency of the speed of light where laser pulses are emitted from a known point of origin onto a target and the elapsed time between pulse transmission and reception of the reflected pulse is measured (Bachman, 1979). The distance from the point of origin to the target is half the product of the speed of light and therefore half the total time from pulse transmission to reception. This simple computation means that laser scanners can be manufactured to perform

quickly in the field with some units capable of capturing over 100,000 points per second while still being highly portable.

These dense point cloud methods can be employed to model and accurately measure structured engineering levels of detail in buildings(Wang and Chong, 2015), railway construction (Cowen et al., 2000), power grid layouts (Wang et al., 2009) and other inanimate structures in comparison to the traditionally time consuming field measurements used previously. Initial industrial uses for these LiDAR platforms focused more on man-made structures and landscapes rather than naturally occurring though in recent years this trend has begun to shift toward scanning and modeling of natural resources including forestlands (Watt and Donoghue, 2005).

Urban forests differ greatly in terms of composition and structure when compared to natural forests. Species composition varies greatly and these sites are regularly altered to serve the surrounding community's social goals as well as to reduce risk (Konijnendijk, 2005). Individual trees are more openly grown and exposed to higher quantities of surface water runoff meaning that these specimens exhibit different health, life expectancy, and allometric relationships (Konijnendijk et al, 2005). Modeling these structures was traditionally conducted using either airborne or satellite optical sensors and only more recently with ALS (Shlyakhter et al., 2001; Tan et al., 2007; Teng and Chen, 2009).

These methods have been used for estimating stem-level metrics in forests (MacFarlane et al, 2012; Simonse et al., 2003; Hopkinson et al., 2004), the leaf surface area of individual trees (Hosoi & Omasa, 2006) and to measure directional gap fraction of the foliar canopy (Danson et al., 2007). Efforts have also been made to reconstruct the stem and branch structures from ground scans (Pfeifer et al., 2004; Cheng et al., 2007). Others have developed an approach for producing polygon models of trees reconstructed from ground scans (Xu et al, 2007). These

efforts are nonetheless highly dependent of the type of equipment, distance from target, and other varying factors of the scans. In Hopkinson, a natural stand of Sugar maple (*Acer saccharum*) in southern Ontario were scanned and later sampled. This traditionally pioneer species possess a relatively simple architecture within a natural stand that does not greatly impede the use of scanning systems. However, as a short-lived species that is susceptible to water stress they are not traditionally present in an urban forest landscape (Close, Nguyen, and Kielbaso, 1996). Studies that rely upon the fractal geometry theory of stem and branch architecture are also susceptible to estimation errors from the non-linear structure of both twig and branch (Macfarlane et al., 2012 , Van Noordwijk and Mulia, 2002). This is due to the inherently linear construction of "pipe model" style models (Shinozaki et al., 1964; Makela and Valentine, 2006; Eloy, 2011) which do not only draw their surface models directly from the data points but also estimate areas of zero data points, which has been seen to produce significant error (West et al., 1999; Enquist, 2002; Eloy, 2011). These studies do show, through the use of destructive validation, that existing allometric equation's strong correlation between diameter and biomass can be measured using a ground-based scanning system. This study, instead of relying on such assumptions in branch form, relies instead upon the direct measurement of a relatively dense point cloud with no inference into the inherent structure of branch and stem. To that end, however, estimations of foliar and biomass metrics can become difficult when the scans are of insufficient quality and this constraint has prevented the complete regeneration of a three dimensional tree model that exactly replicates real-world metrics. This has been primarily due to the technical constraints of the scanners and the difficulty of overcoming impeding field conditions that exist during data capture. Scans made in natural forest environments usually require dealing with different levels of obstruction between the various vegetation components

(Hopkinson et al., 2004). In addition, the presence of varying wind conditions will result in a scattering of data points due to the motion of the canopy and foliage. The registration of multiple scans of a given tree acquired from different observation angles will lead to extremely dense point clouds that do not necessarily contribute to any further modeling ability (Huang et al., 2011).

Data processing techniques are required to deal with these and other issues that influence the quality of the end-product such as the presence of structural elements that are finer than the resolving power of the laser scanner (individual needles in a coniferous shoot), the lack of explicit information about leaf or shoot delineation, and the spatial density of the laser beam per unit of volume (Hosoi & Omasa, 2007). It has been observed that ground-based LiDAR can produce point clouds with sufficient density to allow for the extraction of both DBH and tree height. Watt and Donoghue (2005) found that accuracy of these measurements was greatly affected by line of sight and stand density, specifically in dense sitka spruce (*Picea sitchensis*) plantations where scan angle and resolution were driving factors in acquiring enough meaningful information from each stem. Other studies have found both a method for estimating DBH as well as automated stem mapping and tree height determination (Tansey et al., 2009, Lovell et al., 2011, Huang et al., 2011). A recent study using phase-scanning technology in order to measure inventory parameters showed the potential promise of this new technology though the distorting effect that tree leaves exhibit in the point cloud data indicate this area requires further investigation (Yao et al., 2011). Other studies have shown that beyond interpolation of linear metrics these dense point clouds can be used to estimate aboveground biomass, product quality, tree species identification, crown canopy extent and volume (Lin and Herold, 2016; Hackenberg et. al., 2015; Blanchette et. al., 2015; Newnham et. al., 2015; Hopkinson et. al., 2004; Lefsky,

2002). The study by Lin and Herold performs a four part theoretical and field based comparison study involving Boreal forest tree species that achieve up to 90% volumetric accuracy results. These results are based upon field estimates that themselves rely upon the use of a correlation equations, not direct physical measurement of the specimen. Others such as Newnham and Hackenberg evaluate existing allometrics that show a strong predictive ability of terrestrial LiDAR with regard to biomass, but in the cas of Newnham these results are not field validated and though Hackenberg validates with destructive sampling the results are narrowly applied. In general, validation restrictions hamper most studies through either cost and time constraints or the specimen in question being protected or high value in nature. This study uses a routine of data collection, model construction, and field verification that, within its scope, could be applied to all similar oak species using any vendor's scanning/registration products.

Measurements such as diameter at breast height (DBH), tree height, and volume (D^2H) are indispensable information items for management of an urban forest and support future environmental service markets and related green asset accounting protocol recently developed (Pickle, 2014). Given the obvious impracticality of cutting down urban forests to obtain such detailed measurements the next best solution would be to create a method of non-destructive sampling that can capture reliable estimates of these measurements. These standard metrics are long established as effective inputs for determining above ground biomass (Brown, Gillispi, and Lugo, 1989; Schroeder et. al., 1997). The possibility of creating a multi-step algorithm using the techniques described in this study to create a repeatable workflow for generating spatially accurate open-grown Nuttall oak (*Quercus texana*) surface models that can be used for estimating measurements such as volume and leaf area as well as standing biomass is one of the main goals of this study. Nuttall oak was used for this study since it is a commonly grown street

tree in the southern United States (Martin et al. 2011), and our research group has previous experience using this species to predict open-grown crown width equations for urban trees (Martin et al. 2012). As discussed earlier, a TLS scanner functions similarly to ALS platforms by bouncing light off its surroundings creating a series of measurements. This set of measurements known as a point cloud is then stored as a triple series consisting of a vertical angle θ, a horizontal angle ϕ and the distance R between scanner and whatever object is scanned. These coordinate series are then transformed into a Cartesian coordinate system (x, y, z). The coordinate system is generally arbitrary consisting of a point of origin where the scan began. Obviously a major benefit of TLS is the ability to capture data from multiple angles. These multiple datasets must then be combined into a coinciding coordinate system through a process known as registration. Registration methods vary depending on the manufacturer, but for this study the Iterative Closest Point (ICP) algorithm employed by the Leica Geosystems (Norcross, GA) was used. While urban tree canopy mapping procedures have made several advances in accurately predicting both the number of stems and extent of urban forest canopy there still exists an opportunity to enhance these estimates with the incorporation of terrestrial LiDAR (TLS) (Lovell et al., 2011). Inherent deficiencies exist within airborne deployed systems that capture data from several thousand feet away while travelling in excess of 200 kilometers per hour. Lack of sufficiently dense point clouds prevent the majority of tree tops from being actively measured leading to a systemic underestimation of total tree height. With the adoption of ALS urban forestry regimes this underestimation can lead to misrepresentations in overall standing biomass that many urban forest managers and researchers rely upon for quantifying their utility. Given sufficient scanning density parameters and field placement these underestimations of total height are not present with terrestrially deployed systems. With a

relatively sparse number of stems per acre, as are typical of urban forests, these systems can easily capture the true tops of each stem within the same georeferenced coordinate system to which airborne datasets are applied.

Two major platforms of terrestrial LiDAR systems include static tripod mounted systems, and mobile systems. Tripod mounted systems are typically less expensive and do not include onboard RTK corrected GPS receivers. These systems require the unit to be relocated from each scanning position and capture data in a 360° area. The lack of an onboard RTK corrected GPS means that in order to georeference the point cloud data individual benchmarks must be created and tagged with separate, stand-alone RTK units and the associated point cloud data projected manually into the correct coordinate system (Huang et al., 2011). Additionally, without the assistance of positional data these systems have no way of rectifying the point cloud data gathered at each scanstation with subsequent scanstation data. This means positional targets have to be deployed that are visible from each station and can be used as rectification points for the assembly of an overall scanworld. Manually moving these systems and targets require time and significantly limit the range of a single work crew. Mobile systems avoid these types of problems by being mounted on a vehicle chassis capable of constant scanning while in motion. This is possible due to the onboard positional data acquisition that logs each point's coordinate position within a projected coordinate system as opposed to the arbitrarily created coordinate system's used by static systems. However, mobile systems suffer from an obvious drawback given their significantly higher costs compared to the smaller tripod mounted systems.

The resulting point clouds consist of hundreds of millions of spatially disjoined coordinates that have the appearance of meaningful objects to human observers, but no underlying relationship within the database. Creating these links requires establishing spatial

relationships similar to those used with airborne point cloud data in the creation of TIN models. However, the much more robust, and therefore complex, point clouds created from ground-based units continue to prove difficult to accurately model. There are many reasons for this including the tendency for interpolation models to rely upon the z-constant approach where every spatially disjoined point is assumed to occupy a different position along the z plane (Tansey et al., 2009). This problem is overcome with airborne data by applying minute adjustments to each offending point's z-value, but this is not applicable to terrestrial data where the density of the data would lead to an unacceptably large amount of distortion. Instead a series of noise cancelling adjustments must be made along with the inclusion of ground-based data modeling software. For this project a software called 3DReshaper will be used to create three dimensional polyhedron models (TECHNODIGIT; Neyron, France). These are similar to TIN models in that they consist of a non-overlapping series of triangles with varying sizes, however each data point is analyzed individually, regardless of z-value and assigned to a corresponding facet. Using this and several trial-and-error approaches the model can be constructed to closely mimic the appearance of a standing tree and its crown. From this information estimates of volume and surface area can be derived giving forest managers and researchers additional information in quantifying urban forest utility.

2.3 Three Dimensional Image Matching

As discussed earlier, both airborne and terrestrial platforms of active sensor scanning systems have limitations. Particularly hardware limitations such the pulse speed of the scanhead itself or the read/write speed of data storage, but also the size, weight, and widespread availability of such specialized equipment. The second part of this study will focus on the use of

passive sensor technology through widely available digital cameras from less restrictive and expensive platform such as an unmanned aerial vehicle (UAV).

The use of high overlapping imagery for three-dimensional renderings is a well-established photogrammetric procedure (Haala, 2009). Historically this was achieved using pairs of film images taken from slightly differing angles, also called stereoscopic images. Typically, percentage of overlap would range between 40-50% depending on the application. The development of airborne LiDAR scanning techniques proved more economical for surface model generation given the lower requirements for overlap against previous image platforms. These earlier imaging systems required the use of film photography that would typically be scanned into an 8-bit depth digital format with a large percentage of the available 256 brightness values failing to be fully utilized (Perko, 2004). Another disadvantage to these platforms was the "grain noise" that affected the geometric resolution of the imagery. An example would be that with a geometric pixel size of 20 µm with an 8-bit depth per band and 25 cm image width and film image would be represented by 11,500 pixels (Perko, 2004; Perko et al., 2004). A smaller pixel size, 15 µm for instance, would then greatly reduce the radiometric range below 8-bit. In this scenario an image would require a 30 µm pixel to achieve a radiometric range encompassing a full 8-bit (Leberl, 2010; Perko, 2004). These limitations, however, are overcome with the advent of digital imaging systems that routinely capture 13-bit depth imagery with more than 7,000 brightness values per band (Scholz and Gruber, 2008). These systems also provide improved signal-to-noise ratio as well as implement multiple, oblique oriented cameras instead of the traditional single camera thereby greatly reducing the loss of efficiency due to greatly overlapping flight lines. Oblique oriented systems also provide such a considerable excess of

overlapping data that the traditional problem of image occlusions is greatly reduced (Haala, 2009).

The resurgence of three-dimensional imagery from oblique image viewers combined with advances in computer vision have given point clouds derived from such a platform many advantages over active-sensor technology such as: increased planar perspective (Hartley and Zisserman, 2003), photoconsistency across varying datasets (Goesele et al., 2003), three-dimensional model construction in highly variable urban landscapes (Pollefeys et al., 2008), cost effectiveness for at-risk historical site preservation (Snavely et al., 2008), and relative horizontal accuracy at the finer scale (Furukawa et al., 2010). These platforms work on the photogrammetric principles based on the linear condition using both exterior and interior orientation parameters such as principle distance and principle point along with the camera parameters for effective self-calibration (Fraser, 1997). Prior to this, active sensors were the preferred technology for dense 3D recording, replacing passive sensors that had dominated many application areas. Many photogrammetric scientists shifted their research interests to these active scanning practices as a result, slowing advances in automated procedures using photogrammetric technology. Thanks to recent significant improvements in hardware, such as multi-core processing, cluster processing, and algorithms photogrammetry has re-emerged as a competitive technology. Image based surveying and 3D modeling can now deliver results of comparable geometric characteristics to those of active sensor laser scanning for many terrestrial and aerial applications. Though range sensors are more compact than they were some years ago, are still relatively cumbersome and expensive compared to terrestrial digital cameras; their bulkiness can be problematic in some field conditions. The point clouds recorded with range instruments may be geometrically correct at the time of acquisition, but they are not based on redundant

measurements, which can be problematic for projects concerned with absolute accuracy (Fraser, 1997).

Typical photogrammetric quality indicators derived in adjustment procedures are not available for quality evaluation of point clouds produced with range sensors. Moreover, few statistics, which are normally provided by vendors, are provided to describe errors for the entire dataset. Range sensors are normally treated as "black boxes" as they lack well-defined procedures to assess quality on an individual project basis. Though photogrammetric processing can be more labor/processing intensive, can be carried out so that calibration procedures are explicitly stated. This is mainly valid for pure photogrammetric processes, while other calibration tools also fit into the black-box category where mass-point adjustment, divergence, and geometric deformations may be experienced (Remondino et al., 2012). Photogrammetric processing algorithms can suffer problems due to either the initial image quality (atmospheric noise, low radiometric quality, shadows, etc.) or to certain surface materials. This can result in noisy point clouds or difficulties in feature extraction. Furthermore, in order to derive metric 3D results from images, a known distance or ground control points (GCPs) are required in an image based measurement project. In the case of aerial acquisitions, the typical point density of laser scanning datasets is 1 to 25 points/m^2 while an aerial photogrammetric image typically has a ground sampling distance (GSD) of the order of 10 cm, which could theoretically be used to produce a dense point cloud with 100 points/m^2. Several recent publications have compared ranging and imaging techniques based on factors such as accuracy, resolution and dense 3D reconstructions (Kersten and Lindstaedt, 2012; Opitz et al., 2012; Koutsoudis et al., 2014).

Image matching concepts deal with the establishment of correspondences between various image datasets, generally gathered using similar metrics and concerned with the

establishment of correspondences between two or more images (Schenk, 1999). In computer vision, image matching is often called the "stereo correspondences problem" (Szeliski, 2011; Sonka et al., 2014). Image matching requires the establishment of correspondences between primitives extracted from two or more images, along with the determination of the 3D coordinates of matched feature points using projective model. In image space, this process produces a depth map that assigns relative depths to each pixel of an image. The corresponding outcome in object space is the point cloud. Considering an image pair, the disparity is inversely proportional to the camera-to-object distance. Even in situations where the visual understanding and basic geometry relating to the disparity and scene structure are well understood, the automated measurement of such disparities by establishing dense and accurate image correspondences is challenging.

For historical reasons, photogrammetric developments in the field of image matching were mainly related to aerial images and topographic mapping problems. The earliest matching algorithms were developed in the photogrammetry community in the 1950's (Hobrough, 1959; Williams, 1959). In the 1970s, the concepts of epipolar geometry and cross-correlation for image matching were introduced (Helava, 1978). With the advent of digital imaging, research was focused more on automated procedures to both replace manual operator intervention and achieve more powerful matching performance for single points (Forstner, 1982; Ackermann, 1984; Gruen, 1985). In Gruen (1985) and Gruen and Baltsavias (1988), the multi-photo geometrical constraints (MPGC) concept was introduced. Subsequently, the matching procedure was also generalized to object space through the introduction of new techniques and concepts (Wrobel, 1987; Ebner and Heipke, 1988; Helava, 1988). The 1990s was a time of consolidation for image matching and a large number of commercial photogrammetric systems appeared for digital

surface model (DSM) and digital terrain model (DTM) generation from large blocks of near-nadir aerial images. Thus, from sparse (single point) matching, algorithms moved to determination of dense point correspondences. Zhang et al. (1992) presented innovative global matching with probabilistic relaxation, while Maas (1996) introduced a multi-photo, geometrically-constrained (MPGC) approach where features were searched for and matched along epipolar lines. However, in spite of this success, the photogrammetric matching of convergent images in non-traditional reference systems (namely, close-range image blocks) was proving to be problematic and thus new developments in this area were largely confined to the computer vision community where accuracy was not a high priority. Stereo-matching was investigated as early as the mid-1970s (Marr and Poggio, 1976) and developments continued in the 1980s mainly for terrestrial applications (Dhond and Aggarwal, 1989; Ohta and Kanade, 1985; Marr, 1982; Baker and Binford, 1981). Then, in the 1990s, the focus moved to multi-view approaches (Okutomi and Kanade, 1993; Fua and Leclerc, 1995; Narayanan et al., 1998), and then more recently to field programmable gate array (FPGA) and graphics processing unit (GPU) developments in computer architecture (Kalarot et al., 2011), per pixel measurement (Birchfield and Tomasi, 1999), mass energy minimization algorithms (Roy and Cox, 1998; Hirschmuller, 2008) and dynamic programming approaches (Kolmogorov et al., 2006).

To generate the point clouds used for surface model generation intense geoprocessing to determine image orientation must be conducted. In this instance, an imaging model based on the collinearity condition is used for photogrammetric processing. This model uses both exterior and interior orientation parameters such as principle distance and principle point along with the camera parameters for effective self-calibration (Fraser, 1997). The geometric accuracy of these calibration methods have been studied by the German Society of Photogrammetry, Remote

Sensing and Geoinformation (DGPF) and shown to be acceptable with wide ranging applications (Jacobsen et al., 2010).

2.4 Geographic Object Based Image Analysis (GeOBIA)

Within this study, traditionally time-consuming workflows like manual image interpretation and individual object delineation/measurement are assisted with semi-automated computer vision techniques, chief among these are the use of GeOBIA. These considerable advances in image classification and workflow efficiency have garnered widespread appeal and greater use in the last decade (MacFaden, 2012). Traditionally image classification has primarily relied upon the spectral reflectance of individual pixels, which are in turn grouped together where possible. This type of classification works well in relatively homogenous areas, but has considerable difficulty in highly variable urban areas where discreet boundaries between landcover/land are more complex. A solution to these and other problems with pixel based classifiers has come with the development of geographic object based image analysis (GeOBIA). GeOBIA segments, attributes, and classifies image segments based on a variety of characteristics such as spatial extent, shape, texture, and topological characteristics of groups of pixels which better reflects real-world objects and features (Benz et al., 2004). This type of analysis allows for additional spectral attribution as well as giving each image object spatial definition that allows for the creation of neighborhoods and topologies (Blaschke, 2010).

There are various GeOBIA software packages available, but the most widely known and used is Trimble's eCognition (Blaschke, 2010). This package allows for data fusion of both raster and vector datasets, contextual analysis, and hierarchical data structuring. An optional extension to this software called eCognition Server (Trimble Inc. Sunnyvale, CA) enables multi-node batch partitioning and processing that greatly enhances the efficiency of multi-gigabyte

routines. The algorithms used in eCognition have been employed in many mapping studies using various types of raster datasets ranging in spatial, spectral, and radiometric resolution. These include studies to measure landcover mosaics (Syed, Dare, and Jones, 2005) of wetlands, woodlands, grasslands, and mountainous regions (Maier, Tiede, and Dorren, 2008; Pascual et al., 2008;), to measure urban sprawl in both agricultural (Lucas et al. 2007; Suarez et al., 2005)and desert regions (Jacquin, Misakova, and Gay, 2008), derive surface models from input LiDAR datasets (Im, Jensen, and Hodgson, 2008), and addressing workflows for data fusion of raster and vector data structures (Chen, Chiang, and Teo, 2005)

Additional studies have shown that individual stems of both coniferous and deciduous forests can be identified and crown diameters measured using ALS (Popescu Wynne and Nelson, 2003). Further studies have even shown that individual tree metrics such as diameter at breast height (DBH) can be derived from these airborne platforms to within an accuracy of 10% (Popescu, 2007). Disadvantages exist, however, with the optical platforms due to the presence of shadows cast by taller objects as well as the comparatively coarse spatial resolution of the ALS point cloud when compared to the more dense and robust point clouds generated using terrestrial LiDAR scanning (TLS). Attempts at more detailed mapping of stem characteristics such as biomass and carbon sequestration by incorporating ALS into 3D models have produced varying results given that the data are gathered from only nadir perspective providing little peripheral data points (Kato et al., 2009; Kwak et al., 2007; Koch et al., 2006).

The incorporation of high resolution airborne LiDAR into GeOBIA analysis has enabled urban forest canopy mapping in a number of areas and has proven that these data are even more integral to classification than multispectral imagery (MacFaden et al., 2012; O'Neil-Dunne, 2011; O'Neil-Dunne, MacFaden, and Grove, 2010). However, these analyses are still time

consuming and require a great deal of pre-processing when a study area is highly heterogeneous. Pre-processing of LiDAR data tends to vary by the original intended application of the data as well as the vendor that is supplying it. In many cases these data are classified using various third-party software such as QCoherent's LP360 LiDAR processing software either by the vendor that supplied it. Studies have been conducted that demonstrate this software's ability to supply semi-automated ASPRS compliant classification of both forested and non-forested landscapes (Latif, Aman, and Ghazali, 2011; Hippenstiel and Brownson, 2012; Jordan et al., 2012). It appears in some instances (Montealegre et al. 2015; Tinker et al., 2011), however, that the vendor-supplied, post-processing using industry standard software such as LP360 (GeoCue Group Inc. Madison, AL) was not necessary in order to achieve acceptable classification. In those instances, the classifications needed to identify high vegetation and buildings could be gathered with eCognition in a more automated fashion than the only semi-automated workflows of LP360.

Chapter 3. Estimating Urban Tree Canopy Using Terrestrial LiDAR Scanning

3.1 Abstract

Trees grown in an urban environment are typically from a selected list of suitable species due to their appearance as well as suitability for limited water availability and soil compaction factors. A popular oak species in recent decades has been the Nuttall oak (*Quercus texana*). A total of seven Nuttall oaks were scanned using a terrestrial LiDAR scanner and modeled for comparison to manual measurements. These trees were then destructively sampled in place to measure their above-ground biomass. Two approaches were utilized in order to make analysis flexible and provide further insight: a whole-tree approach, and a subsequent branch-by-branch approach. The biomass data were compiled and statistically compared against digital models of each tree that were created from the LiDAR scans. Modeling either each tree as a whole or each branch individually allowed researchers to compare the accuracy of remotely sensed data to those gathered using destructive methods in the field. These resulted in a Pearson coefficient of .977 and linear regression R^2 value of .99 for the LiDAR derived measurements predictive ability in comparison to the manually derived measurements. This indicates an ability of this ground based LiDAR model to predict both the linear dimentions and volumetrics of the standing specimens without the need for such labor intensive and expensive sampling given the sensitivity and value of urban forests.

3.2 Introduction

Terrestrial light distance and ranging (LiDAR) scanning has become an efficient way of generating an impressively dense point cloud model of a landscape or structure. Using the

consistency of the speed of light these sensors emit laser pulses from a known point of origin onto a target and measure the elapsed time between pulse transmission and reception of the reflected pulse (Bachman, 1979). The distance from the point of origin to the target is half the product of the speed of light and therefore half the total time from pulse transmission to reception. This simple computation means that laser scanners can be manufactured to perform quickly in the field with some units capable of capturing over 100,000 points per second.

Urban forests differ greatly in terms of composition and structure when compared to natural forests. Species composition varies greatly and these sites are regularly altered to serve the surrounding community's social goals as well as to reduce risk (Konijnendijk et al., 2005). Individual trees are more openly grown and exposed to higher quantities of surface water runoff meaning that these specimens exhibit different health, life expectancy, and allometric relationships (Konijnendijk et al, 2005). Modeling these structures was traditionally conducted using either airborne or satellite optical sensors and only more recently with ALS (Shlyakhter et al., 2001; Tan et al., 2007; Teng and Chen, 2009).

These methods have been used for estimating stem-level metrics in forests (MacFarlane et al, 2014; Simonse et al., 2003; Hopkinson et al., 2004), the leaf surface area of individual trees (Hosoi and Omasa, 2006) and to measure directional gap fraction of the foliar canopy (Danson et al., 2007). Efforts have also been made to reconstruct the stem and branch structures from ground scans (Pfeifer et al., 2004; Cheng et al., 2007). Others have developed an approach for producing polygon models of trees reconstructed from ground scans (Xu et al, 2007). These efforts are nonetheless highly dependent of the type of equipment, distance from target, and other varying factors of the scans. In Hopkinson, a natural stand of Sugar maple (*Acer saccharum*) in southern Ontario were scanned and later sampled. This traditionally pioneer species possess a

relatively simple architecture within a natural stand that does not greatly impede the use of scanning systems. However, as a short-lived species that is susceptible to water stress they are not traditionally present in an urban forest landscape (Close, Nguyen, and Kielbaso, 1996). Studies that rely upon the fractal geometry theory of stem and branch architecture are also susceptible to estimation errors from the non-linear structure of both twig and branch (Macfarlane et al., 2014; Van Noordwijk and Mulia, 2002). This is due to the inherently linear construction of "pipe model" style models (Eloy, 2011; Makela and Valentine, 2006; Shinozaki et al., 1964) which do not only draw their surface models directly from the data points but also estimate areas of zero data points, which has been seen to produce significant error (Eloy, 2011; Enquist, 2002; West et al., 1999). These studies do show, through the use of destructive validation, that existing allometric equation's strong correlation between diameter and biomass can be measured using a ground-based scanning system. This study, instead of relying on such assumptions in branch form, relies instead upon the direct measurement of a relatively dense point cloud with no inference into the inherent structure of branch and stem. To that end, however, estimations of foliar and biomass metrics can become difficult when the scans are of insufficient quality and this constraint has prevented the complete regeneration of a three dimensional tree model that exactly replicates real-world metrics. This has been primarily due to the technical constraints of the scanners and the difficulty of overcoming impeding field conditions that exist during data capture. Scans made in natural forest environments usually require dealing with different levels of obstruction between the various vegetation components (Hopkinson et al., 2004). In addition, the presence of varying wind conditions will result in a scattering of data points due to the motion of the canopy and foliage. The registration of multiple scans of a given tree acquired from different observation angles will lead to extremely dense

point clouds that do not necessarily contribute to any further modeling ability (Huang et al., 2011).

Data processing techniques are required to deal with these and other issues that influence the quality of the end-product such as the presence of structural elements that are finer than the resolving power of the laser scanner (individual needles in a coniferous shoot), the lack of explicit information about leaf or shoot delineation, and the spatial density of the laser beam per unit of volume (Hosoi & Omasa, 2007). It has been observed that ground-based LiDAR can produce point clouds with sufficient density to allow for the extraction of both DBH and tree height. Watt and Donoghue (2005) found that accuracy of these measurements was greatly affected by line of sight and stand density, specifically in dense Sitka spruce (*Picea sitchensis*) plantations where scan angle and resolution were driving factors in acquiring enough meaningful information from each stem. Other studies have found both a method for estimating DBH as well as automated stem mapping and tree height determination (Tansey et al., 2009, Lovell et al., 2011, Huang et al., 2011). A recent study using phase-scanning technology in order to measure inventory parameters showed the potential promise of this new technology though the distorting effect that tree leaves exhibit in the point cloud data indicate this area requires further investigation (Yao et al., 2011). Other studies have shown that beyond interpolation of linear metrics these dense point clouds can be used to estimate aboveground biomass, product quality, tree species identification, crown canopy extent and volume (Lin and Herold, 2016; Hackenberg et. al., 2015; Blanchette et. al., 2015; Newnham et. al., 2015; Hopkinson et. al., 2004; Lefsky, 2002). In Lin and Herold, a four part theoretical and field based comparison study involving Boreal forest tree species that achieve up to 90% volumetric accuracy results. These results are based upon field estimates that themselves rely upon the use of a correlation equations, not direct

physical measurement of the specimen. Others such as Newnham and Hackenberg evaluate existing allometrics that show a strong predictive ability of terrestrial LiDAR with regard to biomass, but in the case of Newnham these results are not field validated and though Hackenberg validates with destructive sampling the results are narrowly applied (Newnham et al., 2015; Hackenberg et al., 2015).. In general, validation restrictions hamper most studies through either cost and time constraints or the specimen in question being protected or high value in nature. This study uses a routine of data collection, model construction, and field verification that, within its scope, could be applied to all similar oak species using any vendor's scanning/registration products.

Measurements such as diameter at breast height (DBH), tree height, and volume (D^2H) are indispensable information items for management of an urban forest and support future environmental service markets and related green asset accounting protocol recently developed (Pickle, 2014). Given the obvious impracticality of cutting down urban forests to obtain such detailed measurements the next best solution would be to create a method of non-destructive sampling that can capture reliable estimates of these measurements. These standard metrics are long established as effective inputs for determining above ground biomass (Brown, Gillispi, and Lugo, 1989; Schroeder et. al., 1997). The possibility of creating a multi-step algorithm using the techniques described in this study to create a repeatable workflow for generating spatially accurate open-grown Nuttall oak (*Quercus texana*) surface models that can be used for estimating measurements such as volume and leaf area as well as standing biomass is one of the main goals of this study. Nuttall oak was used for this study since it is a commonly grown street tree in the southern United States (Martin et al. 2011), and our research group has previous experience using this species to predict open-grown crown width equations for urban trees

(Martin et al. 2012). While urban tree canopy mapping procedures have made several advances in accurately predicting both the number of stems and extent of urban forest canopy there still exists an opportunity to enhance these estimates with the incorporation of terrestrial LiDAR (TLS) (Lovell et al., 2011). Inherent deficiencies exist within airborne deployed systems that capture data from over a thousand meters away while travelling in excess of 200 kilometers per hour. Lack of sufficiently dense point clouds prevent the majority of tree tops from being actively measured leading to a systemic underestimation of total tree height. With the adoption of ALS urban forestry regimes this underestimation can lead to misrepresentations in overall standing biomass that many urban forest managers and researchers rely upon for quantifying their utility. Given sufficient scanning density parameters and field placement these underestimations of total height are not present with terrestrially deployed systems. With a relatively sparse number of stems per acre, as are typical of urban forests, these systems can easily capture the true tops of each stem within the same georeferenced coordinate system to which airborne datasets are applied.

Using these data one can employ methods to model and accurately measure a tree's physical structure in comparison to traditionally time consuming field measurements in either natural or urban environments. However, urban forests differ greatly in terms of composition and structure when compared to natural forests. Species compositions vary greatly and these sites are regularly altered to serve the surrounding community's social goals as well as to reduce liability (Konijnendijk, 2005). Individual trees are more open-grown and exposed to higher quantities of surface water runoff meaning that these specimens exhibit different health, life expectancy, and allometric relationships. Modeling these structures has traditionally been conducted using either airborne or satellite optical sensors or more recently with ALS (Shlyakhter et al., 2001; Tan et

al., 2007; Teng and Chen, 2009). Studies have shown that individual stems of both coniferous and deciduous forests can be identified and crown diameters measured using ALS (Popescu, Wynne, and Nelson, 2003). Further studies have even show that individual tree metrics such as diameter at breast height (DBH) can be derived from these airborne platforms to within an accuracy of 10% (Popescu, 2007). Disadvantages exist, however, with the optical platforms due to the presence of shadows cast by taller objects as well as the comparatively coarse spatial resolution of the ALS point cloud when compared to TLS. Attempts at more detailed mapping of stem characteristics such as biomass and carbon sequestration by incorporating ALS into 3D models have produced varying results given that the data are gathered from only nadir perspective providing little peripheral data points (Koch et al., 2006; Kato et al., 2009; Kwak et al., 2007).

It has been observed that TLS can produce point clouds with sufficient density to allow for the extraction of both DBH and tree height (Watt and Donoghue, 2005). Watt and Donoghue found that accuracy of these measurements was greatly affected by line of sight and stand density, specifically in dense Sitka Spruce (*Picea sitchensis*) plantations where scan angle and resolution were driving factors in acquiring enough meaningful information from each stem. Other studies have found both a method for estimating DBH as well as automated stem mapping and tree height determination (Tansey et al. 2009, Lovell et al. 2011, Huang et al. 2011). A recent study using phase-scanning technology TLS in order to measure inventory parameters showed the potential promise of this new technology though the distorting effect that tree leaves exhibit in the point cloud data indicate this area requires further investigation (Yao et al. 2011).

TLS is typically used in more localized scanning projects intended to cover a smaller geographic area than compared to ALS. In this study a terrestrial scanning system is used to

measure 7 individual Nuttall oak trees that are later harvested and sampled for linear and volumetric biomass. These results are later compared to those collected using the scanning system. In comparison to the relatively course point clouds generated from airborne LiDAR platforms TLS has become an efficient way of generating an impressively dense point cloud model of a landscape or structure. Using these dense point clouds methods can be employed to model and accurately measure structured engineering levels of detail in buildings (Wang and Chong, 2015), railway construction (Cowen et al., 2000), power grid layouts (Wang et al., 2009) and other inanimate structures in comparison to the traditionally time consuming field measurements of the past. Initial industrial uses for these LiDAR platforms focused more on man-made structures and landscapes rather than naturally occurring though in recent years this trend has begun to shift toward scanning and modeling of natural resources including forestlands (Watt and Donoghue, 2005).

Measurements such as DBH, height, biomass and volume are indispensible information for the management of an urban forest, and to support future environmental service markets and related green asset accounting protocol recently developed (Pickle, 2014). Algorithms for determining urban tree biomass and canopy coverage for southern United States urban trees are just now being developed (Blood et al., 2017; Martin et al. 2012). However, more information is critically needed in this area to ensure the models are accurate and precise.

Given the obvious impracticality of cutting down urban forests to obtain such detailed measurements the next best solution would be to create a method of non-destructive sampling that can reasonably approximate the same data. The possibility of creating a multi-step algorithm using Terrestrial LiDAR to create a repeatable workflow for generating spatially accurate surface models that can be used for estimating measurements such as volume and leaf

area as well as standing biomass is the main goal of this study. Specific objectives include the digital modeling and field measuring of specimens to be compared directly to one another. Open-grown Nuttall oak was used for this study since it is a commonly grown street tree in the southern United States (Martin et al. 2011), and our research group has previous experience using this species to predict open-grown crown width equations for urban trees (Martin et al. 2012, Jones et al. 2016).

3.3 Methods

The methodology for this research focuses on the use of multi-perspective TLS to generate workable surface model structure for calculating foliar and stem metrics. Seven open-grown Nuttall oak trees of approximately 12 years of age and moderate size were selected and scanned using a tripod mounted laser scanner. These particular trees were chosen due to their representation of a typical urban oak tree (species, age, growth spacing) and that they were grown on Auburn University land for research purposes. Two destructive sampling methodologies were applied, the first was to measure each tree's volume as a single whole-stem measurement (Jones et al., 2016). The second, utilized later, was to measure each tree's volume on a branch-by-branch basis, allowing for further analysis of the distribution of volume measurement error, increase the number of observation units, and improve the overall accuracy of the model.

3.3.1 Study Site

The study site is an Auburn University School of Forestry and Wildlife Sciences research station located approximately 5 km from Auburn University in Auburn, Alabama, shown in

Figure 1 below. Data were collected using a Leica ScanStation C-10 (Leica Geosystems, Norcross, GA) from multiple angles from a distance of 8-10 meters.

Figure 3.1 Research site located 5km. from Auburn University, Alabama

3.3.2 Data

This particular sensor uses time of flight (TOF) to sense and record the coordinates of objects encountered by a light pulse. The emitted light pulse has a wavelength of 532 nm giving the sweeping laser scan a green color. This scanner when set to maximum capacity collects data at approximately 50,000 points per second from a maximum distance of 300m depending on the reflectivity (albedo) of the surface being scanned. Onboard there is an integrated 4 megapixel (1920x1920 pixel) camera that captures 3-band (RGB) images. The camera's field of view is 17

degrees, creating a rectified "dome" of 260 images at every ScanStation. Tripod mounted twin targets were set up over established benchmarks and used as common points for registration of each individual scan into a single comprehensive "scanworld".

3.3.3 Terrestrial Laser Scanning

Though multiple registration methods exist, this project focuses on the Iterative Closest Point (ICP) algorithm due to its widespread use and software availability. In its basic form this algorithm consists of six major stages: 1) Selection of a set of points in both a reference and matching point cloud 2) Matching these points to samples 3) Weighting the corresponding pairs 4) Rejecting certain pairs based on looking at each pair individually 5) Assigning an error metric 6) Minimizing that error metric (Rusinkiewicz and Levoy, 2001). These basics steps are altered depending upon the specific software being used which for this project consists of the software manufacturer's proprietary information. These modeled trees would then be analyzed digitally for both linear and volumetric measurements, which would then be correlated against biomass using the US Forest Service's Forest Inventory & Analysis (FIA) allometric tables. Of the seven stems measured, three were analyzed in the first field sampling season using a whole-stem approach whereby the entire stem was aggregated into a single measure of biomass (Jones et al.,2016). This initial methodology proved limiting in several respects, specifically with analysis of statistical distribution of error throughout the canopy and a low number of observation units. As a result, the four remaining trees were analyzed using a branch-by-branch approach whereby in addition to teach the measurements taken using the whole-tree approach each of the tree's branches were also individually identified, weighed, and modeled for biomass. This approach provided additional insight into the overall distribution of modeling error throughout the canopy that a whole-tree approach could not provide.

Point cloud information was collected on two separate occasions, both within the growing season for this particular species. The first was on June 8th, 2013 and the second on September 10, 2015. The first scan encompassed the three trees analyzed using the whole-tree approach with the second scan encompassing the four trees analyzed using the branch-by-branch approach. The methodology was altered from the first experiment to increase the analysis capabilities of the second scan, while also including the measurements from the first. By measuring on a branch-by-branch basis the overall number of data observations are increased and the distribution of the model's error can be more accurately determined. Each of the two methods of field measurements were taken using the same equipment in the same conditions and, other than being measured using single branches, are identical in nature. Immediately after scanning, the trees were physically measured for diameter at breast height (1.37 m above ground-line DBH), total height, crown base height, crown width from north to south, crown width from east to west, percentage of crown missing, crown dieback, and crown light exposure. Total tree and crown-base height were measured using a laser hypsometer (either a MDL LaserAce® hypsometer or a Laser Technology, Inc. TruPulse™ 360B rangefinder). Total tree height was determined by measuring from the ground-line to the top of the tree, and crown base height was recorded as the height to the lowest branch of significance. Crown width was determined by taking two measurements from the crown edges at 90 degree angles and then averaging them. All data were collected using the USDA Forest Service i-Tree Eco tree inventory protocol (Martin et al. 2011, i-Tree 2010). Dieback and percent missing crown were determined for each tree (i-Tree Eco 2010). Branch dieback was estimated by observing the tree from all sides and then calculating percent dieback. Ranges of <1, 1-10, 11-25, 26-50, 51-75, 76-99, and 100% dieback were used to assign tree conditions of excellent, good, fair, poor, critical, dying, and dead,

respectively. Percent missing crown was determined in a similar fashion (i-Tree Eco, 2010). Each tree's metrics were analyzed using the i-Tree Eco individual tree characteristics toolkit for management related biomass figures such as ground area, leaf area, annual carbon storage, and gross carbon storage.

3.3.4 Destructive Sampling

Above-ground biomass was then assessed by manually removing and weighing each tree section. In the initial whole-tree approach leaves for each tree were then weighed using a portable scale to the nearest gram to determine total foliar mass. For the four trees analyzed using the branch-by-branch approach each major branch from the base and moving upward toward the top was harvested, defoliated, and weighed, illustrated in Figures 3.2 and 3.3 below. The central stem was then cut and measured for green weight to the nearest gram, taper, and total length as well as branches these measurements were used in determining each tree's total biomass, shown in Figure 3.4 below. Measurements of mass were then used to compute volume using established green weight per unit volume ratios for Nuttall Oak (Schlaegel and Willson, 1983).

Figure 3.2 Twigs/branches being field measured using scale

Figure 3.3 Nuttall oak being sampled and measured branch-by-branch

Figure 3.4 Nuttall oak bole being felled for measurement

Scan data were registered using an ICP algorithm with the proprietary parameters of the Cyclone software. Fourteen scans from varying angles were combined for an overall 360 degree raw scan containing more than 215 million points. The relevant points from each of the trees were removed, cleaned of obvious noise, and copied into a temporary modelspace using the Cyclone software suite.

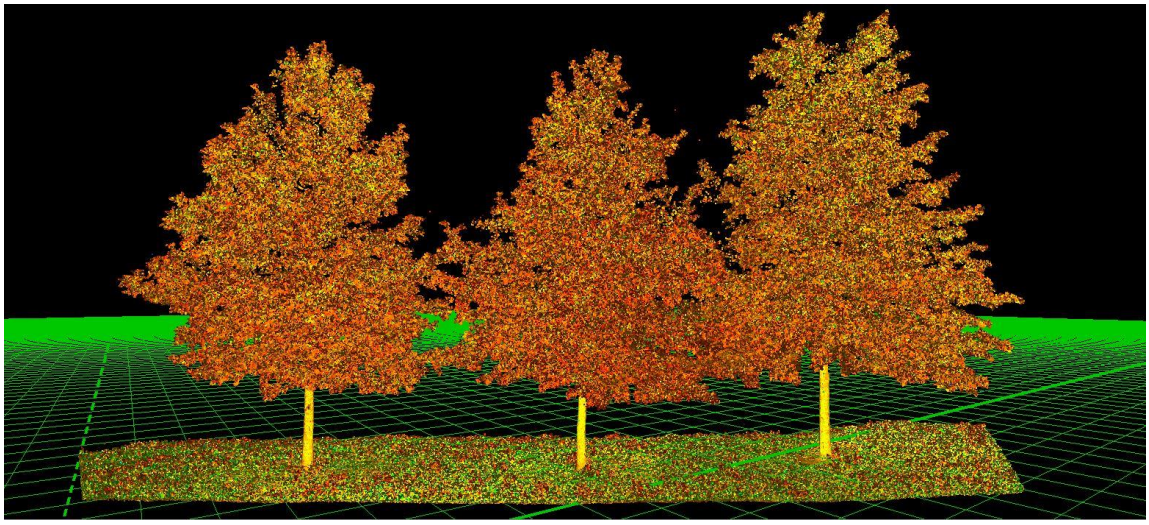

Figure 3.5 Initial LiDAR scan of Nuttall Oaks (taken June 8, 2013)

Detailed meshes of each tree were created using a multi-step algorithm employing point cloud refinement and thinning using 3DReshaper software suite which allows the user to generate surface models with independently defined parameters for density, point deviation, and volumetric thresholds. Using this method linear metrics of each tree, such as height and dbh, were measured within a CAD environment and compared with those taken during destructive sampling. Next, foliar surface area measurements were taken from the generated surface models for each tree's canopy as an estimate of leaf area. These were statistically compared to measurements of surface area taken during destructive sampling. Finally, estimates of volume where generated from the closed polyhedrons representing either the entire stem as a whole or individually identified branches of each tree, as in the case for the branch-by-branch specimens. These volumes where combined with density measurements taken during destructive sampling in order to generate estimates of mass. Biomass of each observation unit within the branch-by-branch approach was measured and modeled further using a variety of methods to enhance its integrity and realistic appearance. These included initial simple mesh creation with sampling

distances of every 0.1 meters. This creates a skeletonized underlying mesh with high accuracy in respect to basic metrics such as height, diameter, and overall crown width. Once this was done a series of refining meshes were then created using more and more of the available points within the cloud at ever decreasing sample sizes. This approach allowed for the consideration and removal of noisy points that fell outside of each mesh's particular standard deviation of points. These parameters were continuously applied until a volume similar to those measured using destructive sampling was reached.

Simple linear regression was employed in order to quantify the differences in measurements within the 129 sample dataset. This particular regression is appropriate because it concerns using input points with one independent variable and one dependent variable to find a linear function that, as accurately as possible, predicts the dependent variable values as a function of the independent variables. Also, a Pearson correlation coefficient was generated for each of the sample datasets in order to measure the linear correlation between the two variables. This widely used coefficient has a value between +1 and −1, where 1 is total positive linear correlation, 0 is no linear correlation, and −1 is total negative linear correlation.

3.4 Results

3.4.1 Linear Measurements

When each tree's linear measurements were taken using point cloud derived surface models the results showed that these digital measurements were less than 1% by distance when compared to those taken in the field. There were two field experiments, one in June 2013 where a whole-tree approach was taken and one in September 2015 where a branch by branch method was employed. In both field sessions the measurement for linear metrics was done using the

same methods. The measurements from experiment 1 can be found in Table 3.1 and experiment 2 found in Table 3.2.

TABLE 3.1

FIELD EXPERIMENT 1, NUTTALL OAK TREES (Auburn, Alabama)

LINEAR MEASUREMENTS (Whole-Tree Approach; June, 2013)

	Field Measurements			Measured From Point Cloud		
Tree ID Number	1	2	3	1	2	3
DBH (cm)	15.49	14.22	17.78	15.5	14.2	17.8
Total Height (m)	8.38	8.41	9.88	8.4	8.4	9.9
Crown-Base Height (m)	1.37	1.49	1.8	1.4	1.5	1.8
Crown-Width N/S (m)	6.25	6.4	7.62	6.2	6.5	7.7
Crown-Width E/W (m)	5.49	6.4	7.01	5.6	6.6	7.1
% Crown Missing*	5	0	0	NA	NA	NA
Crown Dieback*	0	0	0	NA	NA	NA
Crown Light Exposure**	5	4	3	NA	NA	NA
*measured in 5% intervals **scale of 0-5 (5 high, 0 low)						

TABLE 3.2

FIELD EXPERIMENT 2, NUTTALL OAK TREES (Auburn, Alabama)

LINEAR MEASUREMENTS (Branch-by-Branch Approach; July, 2015)

	Field Measurements				Measured From Point Cloud			
Tree ID Number	1	2	3	4	1	2	3	4
DBH (cm)	18.54	17.01	16.76	19.05	18.5	17	16.7	19
Total Height (m)	10.72	10.38	10.50	12.21	10.7	10.3	10.5	12.2
Crown-Base Height (m)	0.85	1.52	1.65	1.18	0.8	1.5	1.6	1.2
Crown-Width N/S (m)	7.89	7.13	7.25	6.92	7.9	7.1	7.2	6.9
Crown-Width E/W (m)	7.95	6.95	6.52	7.32	8.0	7.0	6.5	7.3
% Crown Missing*	0	0	0	0	NA	NA	NA	NA
Crown Dieback*	0	0	0	0	NA	NA	NA	NA
Crown Light Exposure**	5	4	3	5	NA	NA	NA	NA
*measured in 5% intervals **scale of 0-5 (5 high, 0 low)								

These results show an average difference between the measurements to be minimal at less than 1% difference in total height and crown base height. Session 1's whole-tree approach yielded digitally measured total heights of 8.4, 8.4, 9.9 meters compared to field measurements of 8.38, 8.41, 9.88 meters. Each of session 2's branch-by-branch approach specimens had digitally measured total heights of 10.7, 10.3, 10.5, and12.2 meters compared to field measured total heights of 10.72, 10.38, 10.50, and 12.21 meters respectively. Or, simply stated, the results show an average difference between the two measurements to be minimal at less than once percentage of difference with respect to each one's linear metrics.

3.4.2 Volume Measurements

Trees analyzed using the branch-by-branch approach were modeled using the same basic methods as the whole-stem, but with each branch generating its own stand-alone polyhedron (n=129). This required identifying each branch as it moved upward in the canopy within the digital model-space, clipping it into a temporary model-space, and analyzing its volume. For the four trees analyzed in this way that created 129 individual branches, each with their own digitally measured biomass and field measured biomass. These measurements are shown in Table 3.3 below. Volume estimates using the US Forest Service i-Tree Eco analysis model are shown in Table 3.4.

TABLE 3.3
VOLUMETRIC MEASUREMENTS, NUTTALL OAK TREES (Auburn, Alabama)
BRANCH-BY-BRANCH APPROACH (July, 2015)

	Tree #4		
Branch #	Field Mass (kg)	Digital Mass (kg)	Percentage Change
1	50	48.3	0.034
2	4.7	3.3	0.298
3	1.2	0.8	0.333
4	2.7	0.9	0.667
5	2.1	1.7	0.190
6	1.7	0.4	0.765
7	8.1	6.6	0.185
8	7.3	6.2	0.151
9	6.2	5.7	0.081
10	7.9	9.8	-0.241
11	3.3	0.9	0.727
12	3	1.6	0.467
13	5.2	5.5	-0.058
14	6.7	4.7	0.299
15	1.1	0.4	0.636
16	2.7	2	0.259

17	3.5	2.7	0.229
18	2.7	1.9	0.296
19	2.5	2.2	0.120
20	5.5	4.1	0.255
21	2.5	1	0.600
22	3.7	3.9	-0.054
23	18.5	18.1	0.022
24	0.3	0	N/A
25	1	0	N/A
26	3.1	0.8	0.742
27	1.1	0.3	0.727
28	2.2	1.1	0.500
29	0	0	N/A
30	0.3	0	N/A
STEM	111	84	0.243

	Tree #5		
Branch #	Field Mass (kg)	Digital Mass (kg)	
1	1.3	1.1	0.154
2	4	3.6	0.100
3	1.1	0.9	0.182
4	0.4	0.1	0.750
5	1.9	1.4	0.263
6	5.5	5	0.091
7	0.4	0	N/A
8	4.7	3.4	0.277
9	1.3	1	0.231
10	2.8	2.2	0.214
11	0.1	0	N/A
12	4.9	4.1	0.163
13	3.2	2.2	0.313
14	3.7	3.1	0.162
15	1.7	1	0.412
16	1.3	1	0.231
17	2.8	1.6	0.429
18	0.2	0	N/A
19	1	0.7	0.300
20	1.3	1	0.231

21	1.9	1.3	0.316
22	1.4	1	0.286
23	0.8	0.5	0.375
24	2.2	1.8	0.182
25	2.4	1.7	0.292
26	1.5	1.2	0.200
27	2.2	1.9	0.136
28	1.3	0.8	0.385
29	2.5	2	0.200
30	3	2.1	0.300
31	1.8	1.1	0.389
32	0.3	0	N/A
33	1.3	1	0.231
34	2.2	1.8	0.182
35	2.5	1.9	0.240
36	1.4	1.5	-0.071
37	0.3	0	N/A
38	1.8	1.2	0.333
39	1.2	1	0.167
40	0.3	0.2	0.333
41	0.8	0.5	0.375
STEM	120.7	111.6	0.075
	Tree #6		
Branch #	Field Mass (kg)	Digital Mass (kg)	
1	17.2	17.3	-0.006
2	2	1.1	0.450
3	0.7	0.5	0.286
4	1.7	0.9	0.471
5	2	1.3	0.350
6	4.9	4.4	0.102
7	0.7	0.5	0.286
8	2.7	2.4	0.111
9	2.5	1.7	0.320
10	1.9	1.8	0.053
11	1.9	1	0.474
12	1.9	1.2	0.368
13	1.3	1	0.231

14	2.4	2.4	0.000
15	2.1	2	0.048
16	3.2	3.1	0.031
17	1.2	0.8	0.333
18	0.9	0.5	0.444
19	0.3	0.5	-0.667
20	0.8	0.6	0.250
21	1.9	0.9	0.526
22	17	16.1	0.053
23	23.6	21.5	0.089
STEM	131.4	136	-0.035
	Tree #7		
Branch #	Field Mass (kg)	Digital Mass (kg)	
1	6	5.2	0.133
2	4.9	4.4	0.102
3	9.2	9.1	0.011
4	1.5	1.2	0.200
5	3.6	3.3	0.083
6	0.1	0	N/A
7	0.1	0	N/A
8	0.1	0	N/A
9	7.2	6.1	0.153
10	7.2	6.6	0.083
11	0.1	0	N/A
12	9.5	9.3	0.021
13	1.7	1.1	0.353
14	4.8	4.4	0.083
15	1.9	1.6	0.158
16	2	1.3	0.350
17	2.3	2	0.130
18	0.9	0.6	0.333
19	4.7	4	0.149
20	67.4	62.9	0.067
21	0.3	0	N/A
22	0.9	0.4	0.556
23	7.4	6.3	0.149
24	0.4	0.1	0.750

25	0.4	0.2	0.500
26	1.1	1.1	0.000
27	1	0.5	0.500
28	1.2	0.9	0.250
29	2.6	1.8	0.308
30	1.7	1	0.412
31	2.2	1.9	0.136
STEM	154.2	149.6	0.030

TABLE 3.4
BIOMASS ESTIMATES, NUTTALL OAK TREES (Auburn, Alabama)
US FOREST SERVICE i-TREE ECO MODELER (July, 2015; credit Dudlye Hartel)

DBH (cm)	Height (m)	Ground Area (m2)	Leaf Area (m2)	Leaf Biomass (kg)	Leaf Area Index	Carbon Storage (kg)	Gross Carbon Seq (kg/yr)
15.5	8.4	27.20	127.28	12.56	4.68	39.41	5.47
14.2	8.4	32.20	149.85	14.80	4.66	31.99	4.84
17.8	9.9	0.42	158.58	15.66	3.77	56.18	6.75
18.5	10.7	48.87	297.75	29.39	6.08	62.85	7.22
17.0	10.4	38.55	226.68	22.38	5.87	50.80	6.37
16.8	10.5	36.88	153.57	15.16	4.16	49.05	6.24
19.1	12.2	39.58	306.48	30.25	7.74	68.26	7.60

For further comparison the field measurments for the study area were compiled using the US Forest Service i-Tree Eco biomass estimation parameters (i-Tree Eco, 2010). This modeler uses various field gathered measurements as inputs and estimates the gross carbon sequestration of an individual tree per year as well as estimates of standing stem carbon storage in pounds. These results show an average estimated carbon sequestration of the seven specimen trees of 44 kilograms per year with an overall carbon storage of 358 kilograms. These results were provided by Dudley Hartel of the the U.S. Forest Service-SRS 4952.

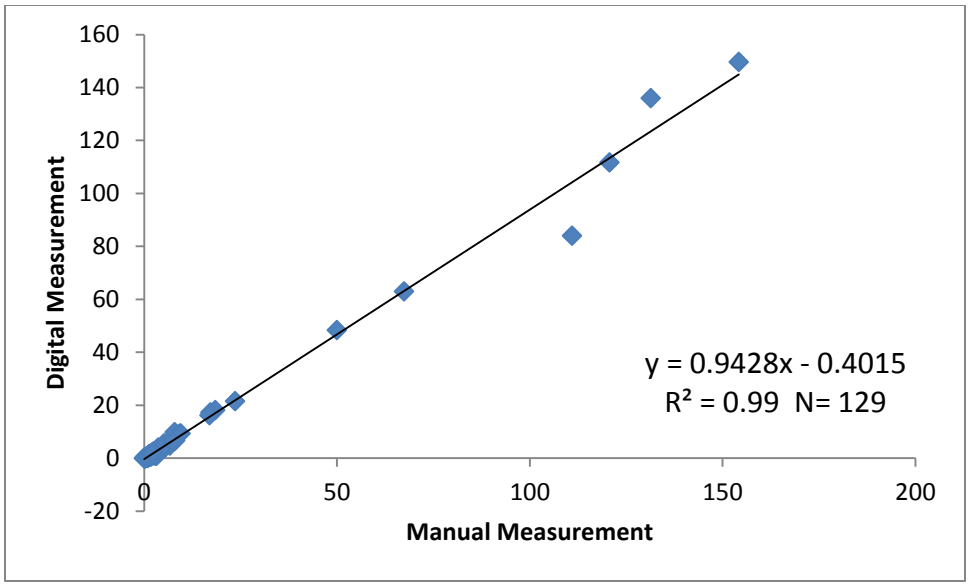

FIGURE 3.6 Linear Regression Analysis for Manual vs. Digital Measurement Nuttall Oak Trees, (Auburn, Alabama; July 2015)

Volumetric measurement results indicate a strong, positive relationship between the manual and digitally acquired measurements. A Pearson correlation coefficient of 0.997 exists between the two with Y(digital) as a predictive measure of X (manual). Also, linear regression analysis shows an R^2 value of 0.99 and is illustrated in Figure 3.6. Totals for all four branch-by-branch approach trees showed the digital measurements underestimated total above-ground biomass by 11% with consistent underestimation for varying size branches. This consistency is perhaps explainable as a function of the scan data not having sufficient coverage of the tops of horizontal branches due to occlusions, a natural limit to ground-based time of flight (TOF) scanning.

3.5 Discussion

Remote sensing technologies provide a means for tree metric quantification by allowing resources to be measured quickly and indirectly when compared to traditional forest inventory methods. Here, a local scale ground-based study of several Nuttall oak trees was performed

which relied upon the use of a terrestrial scanning system. This system was used to construct a relatively dense point cloud of 7 trees, each of which were immediately destructively sampled. This sampling included two field measurement methodologies, whole-tree and branch-by-branch. The modification from experiment 1's whole-tree to experiment 2's branch-by-branch approach were based on initial results and statistical examination. Using a whole tree approach the number of observable units were relatively low and did not provide much analysis beyond comparing linear and volumetric measurements directly. By acquiring the data on a branch-by-branch approach the number of observations can be increased as well as provide information into the distribution of volume throughout the canopy. These results show an average difference between the measurements to be minimal at less than 1% difference in total height and crown base height.

Similar studies have examined the relationship between vector point cloud metrics and above-ground biomass, but have lacked the intensive field sampling results presented here (Macfarlane et al., 2012; Xu et al., 2007; Hopkinson, 2004). Unlike previous studies, the specimens were sampled on an individual branch basis. This provides further context of the distribution of volume throughout the canopy as well as improving statistical analysis by providing additional observations. The combination of appropriate urban tree species selection, destructive sampling, and individual branch analysis make these results unique in the field of terrestrial LiDAR laser scanning for aboveground biomass estimation of urban forests. Generalized information concerning urban tree metrics should be derived from appropriately long lived urban tree species, as opposed to short lived pioneer species or Boreal forest conifers (Hopkinson, 2004).

Linear measurement results indicate that surface models generated using this algorithm mimic within a percentage point DBH, total height, and crown base height which are the typical field measurements of forest inventory (Avery and Burkhart, 1983). Slightly larger differences were apparent in crown width measurements but could be due to the inherent difficulty in capturing highly accurate field measurements such as these with standing timber. It appears likely that the measurements taken from the constructed surface model are more accurate than those taken in the field for this reason. A semi-automated biomass inventory routine on a branch-by-branch basis is a new concept in the field of urban forest inventory, yet these results would indicate it as a possible solution to traditional measurements if tested in further studies.

Visual inspection of the surface models in comparison to photography and high resolution point cloud appear to show bridging of gaps within the canopy that are not actually present. This is possibly due to the complex structural nature of a tree's canopy causing a high number of point returns to fall within two spatially disjoined sections of canopy for which the iterative point refining is unable to correctly classify. However, overestimation across this small sample show relative consistency. This consistency in overestimation could prove useful in developing surface model allometric equation correlations. Larger sample sizes are needed to reliably infer these results, but if such a relationship were to exist a standardized modeling algorithm could be developed that gave acceptable surface area and volumetric results without the need for destructive sampling.

These results have shown that the differences between linear measurements are relatively minor when compared to the field methods, and the volumetric measurements are consistently underestimated due to visual occlusions due to line-of-sight restrictions and tree structure. This underestimation's consistency lends itself to the notion that such missing biomass, while not

statistically insignificant, can be calibrated into a ground-based scanning workflow based on scan point density. Point density is a function of hardware limitations, proximity to the object(s) being scanned, and canopy conditions present at the time. Further research into these functions could isolated and quantify these drivers of underestimation and provide insight into such a calibration. Also, expansion of these methods into varying age and size classes would provide more information into the distribution of underestimation. As these results have shown, overestimation using these methods do not present much challenge due to the polyhedron models being scaled up from smaller, less complex, structures, rather than a parsing down of larger objects as in similar studies (Popescu and Zhao, 2008; Hosoi and Omasa, 2006). Larger sample sizes are needed to draw further conclusions, but these results also indicate an ability for ground-based scanning to mimic industry standard metrics for biomass measurement without the need for destructive sampling of the area in question. As most urban tree inventory projects are within sensitive sites where such methods are unable to be used, this type of workflow would serve as a timely replacement. Overall, these results have shown that a semi-automated branch-by-branch analysis using ground based LiDAR scanning systems offer a viable alternative to traditional measurements. Given advancments in scanning technology, such as mobile LiDAR, these units are becoming lighter, faster, and more deployable than ever before (Zhao et al., 2017). Including these types of remote sensing platforms offer the possibility of urban forest resource managers to monitor and inventory resources at a scale and regularity that are generally less feasible using traditional measurement and inventory methods. Showing that these technologies, among other advancements in the field, to be a useful and timely supplement and possible replacement.

References

Bachman, C. G. (1979). Laser radar systems and techniques. Dedham, Mass., Artech House, Inc., 1979. 203 p.

Blood, A., Starr, G., Escobedo, F. J., Chappelka, A., Wiseman, P. E., Sivakumar, R., & Staudhammer, C. L. (2016). Resolving uncertainties in predictive equations for urban tree crown characteristics of the southeastern United States: Local and general equations for common and widespread species. Urban Forestry & Urban Greening, 20, 282-294.

Brown, Sandra, Andrew JR Gillespie, and Ariel E. Lugo. "Biomass estimation methods for tropical forests with applications to forest inventory data."Forest science 35, no. 4 (1989): 881-902.

Cheng, Z. L., Zhang, X. P., & Chen, B. Q. (2007). Simple reconstruction of tree branches from a single range image. Journal of computer science and technology, 22(6), 846-858.

Close, R. E., Nguyen, P. V., & Kielbaso, J. J. (1996). Urban vs. natural sugar maple growth: I. Stress symptoms and phenology in relation to site characteristics. Journal of Arboriculture, 22, 144-150

Danson, F. M., Hetherington, D., Morsdorf, F., Koetz, B., & Allgower, B. (2007). Forest canopy gap fraction from terrestrial laser scanning. IEEE Geoscience and remote sensing letters, 4(1), 157-160.

Eloy C (2011) Leonardo's rule, self-similarity and wind-induced stresses in trees. Phys Rev Lett 107:1–5. doi: 10.1103/PhysRevLett.107.258101

Enquist B.J. (2002) Universal scaling in tree and vascular plant allometry: toward a general quantitative theory linking plant form and function from cells to ecosystems. Tree Physiol 22:1045–1064

Hackenberg, Jan, Heinrich Spiecker, Kim Calders, Mathias Disney, and Pasi Raumonen. "SimpleTree—An Efficient Open Source Tool to Build Tree Models from TLS Clouds." Forests 6, no. 11 (2015): 4245-4294.

Hopkinson, Chris, Laura Chasmer, Colin Young-Pow, and Paul Treitz. "Assessing forest metrics with a ground-based scanning lidar." Canadian Journal of Forest Research 34, no. 3 (2004): 573-583.

Hosoi, F., & Omasa, K. (2006). Voxel-based 3-D modeling of individual trees for estimating leaf area density using high-resolution portable scanning lidar. IEEE transactions on geoscience and remote sensing, 44(12), 3610-3618.

Huang, H., Z. Li, P. Gong, X. Cheng, N. Clinton, C. Cao, W. Ni, L. Wang, , Automated methods for measuring DBH and tree heights with commercial scanning LiDAR. Photogrammetry Engineering & Remote Sensing. Volume 77 219-227 (2011).

Jones, T., Marzen, L., & Chappelka, A. (2016). Mapping, Modeling, and Estimating Tree Measurements of Urban Tree Canopy Structure Using Terrestrial LiDAR Scanning. Papers in Applied Geography, 2(2), 236-242.

Kato et al., Capturing tree crown formation through implicit surface reconstruction using airborn lidar data. Remote Sensing of Environment, 113(6): 1148-1162 (2009).

Koch, A., U. Heyder and H. Weinacker, , Detection of Individual Tree Crowns in Airborn Lidar Data. Photogrammetric Engineering & Remote Sensing, 72(4): 357-363 (2006).

Konijnendijk, C.C., Nillsson, K., Randrup, T. and Schipperijn, J., , Urban Forests and Trees: A Reference Book (Berlin/Heidelberg: Springer) (2005).

Kwak, D. A., W.K. Lee, J.H. Lee, G. Biging and P. Gong, , Detection of individual trees and estimation of tree height using LiDAR data. Journal of Forest Research, 12(6): 425-434 (2007).

Lefsky, Michael A., Warren B. Cohen, David J. Harding, Geoffrey G. Parker, Steven A. Acker, and S. Thomas Gower. "Lidar remote sensing of above-ground biomass in three biomes." Global ecology and biogeography 11, no. 5 (2002): 393-399.

Lin, Yi, and Martin Herold. "Tree species classification based on explicit tree structure feature parameters derived from static terrestrial laser scanning data." Agricultural and Forest Meteorology 216 (2016): 105-114.

Lovell, J., D. Jupp, G. Newnham, D. Culvenor, 2011, Measuring tree stem diameters using intensity profiles from ground-based scanning LiDAR from a fixed viewpoint. ISPRS Journal of Photogrammetry and Remote Sensing. Volume 77 pp. 219-227

MacFarlane, D.W., Kuyah, S., Mulia, R., Dietz, J., Muthuri, C., and Van Noordwijk, M. 2014. Evaluating a non-destructive method for calibrating tree biomass equations derived from tree branching architecture. Trees: Structure and Function. DOI 10.1007/s00468-014-0993-2

Makela A, Valentine H.T. (2006) Crown ratio influences allometric scaling in trees. Ecology 87(12):2967–2972

Martin, N.A., A.H. Chappelka, G. J. Keever, and E.F. Loewenstein. 2011, A 100% tree inventory using i-Tree Eco protocol: A case study at Auburn University, Alabama. Arbor. & Urban For. 37: 207-212.

Martin, N.A., A.H. Chappelka, E.F. Loewenstein G.J. Keever and G. Somers. 2012, Predictive open-grown crown width equations for three oak species planted in a southern urban locale Arbor.& Urban For. 38: 57-62.

Popescu, S., R. Wynne, R. Nelson, 2003, Measuring Individual Tree Crown Diameter with LiDAR and Assessing its Influence on Estimating Forest Volume and Biomass. Canadian Journal of Remote Sensing, doi: 10.5589/m03-027

Pfeifer, N., Gorte, B., & Winterhalder, D. (2004, July). Automatic reconstruction of single trees from terrestrial laser scanner data. In Proceedings of 20th ISPRS Congress (pp. 114-119). Istanbul: ISPRS.

Schroeder, P., Brown, S., Mo, J., Birdsey, R. and Cieszewski, C., 1997. Biomass estimation for temperate broadleaf forests of the United States using inventory data. Forest Science, 43(3), pp.424-434.

Shinozaki K, Yoda K, Hozumi K, Kira T (1964a) A quantitative analysis of plant form—the pipe model theory I. Basic analysis. Jpn J Ecol 14:97–105

Shlyakhter, I., M. Rozenoer, u. Doresey and S. Teller, 2001, Reconstructing 3D tree models from instrumented photographs. IEEE Computer Graphics and Applications, 21(3): 53-61

Simonse, M., Aschoff, T., Spiecker, H., & Thies, M. (2003). Automatic determination of forest inventory parameters using terrestrial laser scanning. In Proceedings of the scandlaser scientific workshop on airborne laser scanning of forests (Vol. 2003, pp. 252-258).

Tan, P. J., Dowe, D. L., & Dix, T. I. (2007). Building classification models from microarray data with tree-based classification algorithms. In Australasian Joint Conference on Artificial Intelligence (pp. 589-598). Springer, Berlin, Heidelberg.

Tansey, K., N. Selmes, A. Anstee, N. Tate, A. Denniss. 2009, Estimating tree and stand variables in a Corsican pine woodland from terrestrial laser scanner data. International Journal of Remote Sensing. Volume 30 pp. 5195-5209

Teng, C. and Y. Chen, 2009, Image-based tree modeling from a few images with very narrow viewing range. The Visual Computer, 25(4):297-307.

Van Noordwijk M, Mulia R (2002) Functional branch analysis as tool for fractal scaling above- and belowground trees for their additive and non-additive properties. Ecol Model 149:41–51

West GB, Brown JH, Enquist BJ (1999) A general model for the structure and allometry of plant vascular systems. Nature 400:664–667

Yao, T., X. Yang, F. Zhao, Z. Wang, Q. Zhang, D. Jupp, J. Lovell, D. Culvenor, G. Newnham, W. Ni-Meister, 2011, Measuring forest structure and biomass in New England forest stands using echidna ground-based LiDAR. Remote Sensing of Environment, Volume 115 pp. 2965-2974.

Watt, P., D. Donoghue, 2005, Measuring forest structure with terrestrial laser scanning. International Journal of Remote Sensing, 26 pp. 1437-1446

Wang, K., Ming, Z., & Chua, T. S. (2009, July). A syntactic tree matching approach to finding similar questions in community-based qa services. In Proceedings of the 32nd international ACM SIGIR conference on Research and development in information retrieval (pp. 187-194). ACM.

Zhao, G., Lian, M., Li, Y., Duan, Z., Zhu, S., Mei, L., & Svanberg, S. (2017). Mobile lidar system for environmental monitoring. Applied Optics, 56(5), 1506-1516.

Chapter 4. Tree Metric Estimation Using Matching Oblique Stereoscopic Imagery: A Field Study Comparison

4.1 Abstract

Imaging sensors provide a means of mapping and modeling urban landscapes through either active or passive means. Recently, active scanning systems such as light detection and ranging (LiDAR) have been popular due to their discrete data capturing methods and ability to penetrate canopy cover to provide multiple return values for mid-canopy components. However, recent advances in both digital camera size/weight and stereoscopic point cloud generation have seen a shift toward passive sensor technology on unmanned aerial vehicles (UAV). This shift provides an increase in efficiency and repeatability of continuous monitoring projects and it also reduces the upfront costs associated with an active laser scanning project. In this study, an area of urban trees is mapped and modeled using data captured from an oblique stereoscopic image sensor system. Raw image data is mosaicked, geocoded, and analyzed using the Agisoft PhotoScan software suite to generate three-dimensional point clouds. These data are modeled to produce surface models from which above-ground metrics can be derived. This was then compared against field measurements to determine the relative accuracy of the point cloud. Results show a strong correlation (R^2=.994) between measurements taken using field methods and those derived from the generated surface model with an average underestimation of 11.5% across all species. These results indicate an ability to derive satisfactory aboveground urban tree

biomass from relatively simple and accessible remote sensing platforms, a useful step forward in the inventory and management of these valuable natural resources.

4.2 Introduction

Overlapping imagery for three-dimensional viewing is a well-established photogrammetric procedure (Haala, 2009). Historically this was achieved using pairs of film images taken from slightly differing angles, also called stereoscopic images. Typically, percentage of overlap would range between 40-50% depending on the application. The development of airborne light detection and ranging (LiDAR) scanning techniques proved more economical for surface model generation given the lower requirements for overlap against previous image platforms. With advancements in data capture techniques and digital camera miniaturization there has been a shift toward unmanned aerial vehicle (UAV) mounted image capture workflows. One of the most notable advances involved the shift from analog film to digital media. Film traditionally is scanned at a radiometric resolution of 8-bits which rarely yields an entire 256 unique brightness values. By comparison, digital sensors consistently produce 13-bits, or over 7,000 unique brightness values (Leberl et al., 2010; Scholz and Gruber, 2008). Photogrammetric platforms also benefit from a, generally, even distribution of data values across a larger capture area when compared to a laser scanner system. For this reason, large numbers of images from these passive sensor systems can provide enough data points for dense point cloud reconstruction (Rosnell and Honkavaara, 2012).

Due to the non-penetrating nature of a passive sensor system there are areas of occlusion that occur when employing a photogrammetric derived point clouds. In general, cameras are not going to be able to view all areas of the canopy, stem, or nearby ground features that are

occluded by neighboring canopy or building structures. Active laser sensors with discrete scanning systems are able to avoid this issue by relying on a pulsed light packet of higher energy than the reflected atmospheric light of a passive system (Wallace et al., 2016). Rather than have a directly measured coordinate position, relative to a georeferenced aircraft or UAV, point clouds derived from images are created using computer vision techniques such as structure from motion (SfM). SfM employs uses well defined geometrical features that have been viewed from multiple perspectives of differing angular viewpoints to generate a three-dimensional point cloud (Snavely, Seitz, and Szeliski, 2008). This and other computer vision techniques are constructed parallel to advancements in imaging algorithms such as scale invariant feature transform (SIFT), and parallel graphics processing units (GPU). Studies have shown that these data, compared to an airborne laser scanning system, have differences of canopy metrics and delineation of forest components (Lisein, 2013; Dandois and Ellis, 2013). Also, it has been shown that photogrammetric workflows capture additional spectral information and produce higher detail in the upper canopy, denser shading capabilities for computer vision interpretation, higher spectral bandwidth, and other advantages over active-sensor technology (Wallace et al., 2016; Furukawa et al., 2010; Shan et al., 2013; Pollefeys et al., 2008; Snavely et al., 2008; Goesele et al., 2007; Hartley and Zisserman, 2003). The result is data that managers and researchers can analyze to reflect characteristics such as height above ground and texture of various features. This technology has already been utilized in the identification and classification of trees for forest inventory, habitat assessment for wildlife, assessing canopy gaps, and urban feature extraction (Takahashi et al., 2010; Gaulton and Malthus, 2010; Solberg, 2010; Hollaus et al., 2009; Naesset, 2007; Hyde et al., 2006; Bradbury et al., 2005; Rottensteiner, 2003; Priestnall, Jaafar, and Duncan, 2000). Previous studies have focused on stand-level metrics (Solberg, 2010), or have

lacked individual stem validation (Hollaus et al., 2009; Hyde et al., 2006). In this study biomass estimates will be at the individual stem level and validation will be performed on all trees within the study area using standard field measurement techniques (Avery and Burkhart, 1983).

The resurgence of three-dimensional imagery from oblique image viewers combined with advances in computer vision have given point clouds derived from such a platform many advantages over active-sensor technology such as: increased planar perspective (Hartley and Zisserman, 2003), photoconsistency across varying datasets (Goesele et al., 2003), three-dimensional model construction in highly variable urban landscapes (Pollefeys et al., 2008), cost effectiveness for at-risk historical site preservation (Snavely et al., 2008), and relative horizontal accuracy at the finer scale (Furukawa et al., 2010). These platforms work on the photogrammetric principles based on the linear condition using both exterior and interior orientation parameters such as principle distance and principle point along with the camera parameters for effective self-calibration (Fraser, 1997). Prior to this, active sensors were the preferred technology for dense 3D recording, replacing passive sensors that had dominated many application areas. Many photogrammetric scientists shifted their research interests to these active scanning practices as a result, slowing advances in automated procedures using photogrammetric technology. Thanks to recent significant improvements in hardware, such as multi-core processing, cluster processing, and algorithms photogrammetry has re-emerged as a competitive technology. Image based surveying and 3D modeling can now deliver results of comparable geometric characteristics to those of active sensor laser scanning for many terrestrial and aerial applications. Though range sensors are more compact than they were some years ago, are still relatively cumbersome and expensive compared to terrestrial digital cameras; their bulkiness can be problematic in some field conditions. The point clouds recorded with range instruments may

be geometrically correct at the time of acquisition, but they are not based on redundant measurements, which can be problematic for projects concerned with absolute accuracy (Fraser, 1997).

For historical reasons, photogrammetric developments in the field of image matching were mainly related to aerial images and topographic mapping problems. The earliest matching algorithms were developed in the photogrammetry community in the 1950's (Hobrough, 1959; Williams, 1959). In the 1970s, the concepts of epipolar geometry and cross-correlation for image matching were introduced (Helava, 1978). With the advent of digital imaging, research was focused more on automated procedures to both replace manual operator intervention and achieve more powerful matching performance for single points (Forstner, 1982; Ackermann, 1984; Gruen, 1985). In the 1980's the multi-photo geometrical constraints (MPGC) concept was introduced (Gruen and Baltsavias, 1988; Gruen, 1985). Subsequently, the matching procedure was also generalized to object space through the introduction of new techniques and concepts (Wrobel, 1987; Ebner and Heipke, 1988; Helava, 1988). The 1990s was a time of consolidation for image matching and a large number of commercial photogrammetric systems appeared for digital surface model (DSM) and digital terrain model (DTM) generation from large blocks of near-nadir aerial images. Thus, from sparse (single point) matching, algorithms moved to determination of dense point correspondences. Zhang et al. (1992) presented innovative global matching with probabilistic relaxation, while Maas (1996) introduced a multi-photo, geometrically-constrained (MPGC) approach where features were searched for and matched along epipolar lines. However, in spite of this success, the photogrammetric matching of convergent images in non-traditional reference systems (namely, close-range image blocks) was proving to be problematic and thus new developments in this area were largely confined to the

computer vision community where accuracy was not a high priority. In this field, stereo-matching was investigated as early as the 1970's (Marr and Poggio, 1976) and developments continued in the 1980's mainly for terrestrial applications (Baker and Binford, 1981; Marr, 1982; Ohta and Kanade, 1985; Dhond and Aggarwal, 1989). Then, in the 1990's, the focus moved to multi-view approaches (Okutomi and Kanade, 1993; Fua and Leclerc, 1995; Narayanan et al., 1998), and then more recently to field programmable gate array (FPGA) and graphics processing unit (GPU) developments in computer architecture (Kalarot et al., 2011), per-pixel measurement (Birchfield and Tomasi, 1999), global energy minimization algorithms (Roy and Cox, 1998; Hirschmuller, 2008) and dynamic programming approaches (Kolmogorov et al., 2006).

To generate the point clouds used for surface model generation intense geoprocessing to determine image orientation must be conducted. In this instance, an imaging model based on the collinearity condition is used for photogrammetric processing. This model uses both exterior and interior orientation parameters such as principle distance and principle point along with the camera parameters for effective self-calibration (Fraser, 1997). The geometric accuracy of these calibration methods have been studied by the German Society of Photogrammetry, Remote Sensing and Geoinformation (DGPF) and shown to be acceptable with wide ranging applications (Jacobsen et al., 2010).

In this study an urban forested area at a scale encompassing most of a city block (0.86 hectares) in Auburn, Alabama is examined. Specific objectives consist of generating photogrammetricaly derived vector point clouds from a series of overlapping airborne oblique images and using these data to model standing urban forest trees. These surface models would then be used to estimate standing biomass of each individual stem within the study area. These would be compared directly to estimates of standing biomass using standard field data

measurements such as diameter at breast height, total height, crown width, etc. using existing allometric equations.

4.3 Methods

4.3.1 Study Site

For this study a series of overlapping images were taken over the study area in Auburn, Alabama (32.5934° N, 85.4952° W) in September, 2014. The study area consists of the majority of Auburn's Samford Park, a representative urban forested area with many species of both native and non-native trees. The imaging system is a Midas 5 oblique aerial photography system (Track'Air B.V., Kissimmee, Florida) using five cardinally mounted Canon EOS-1Ds Mark III (Canon Inc., Tokyo, Japan) cameras, depicted in Figure 1 below. Four of these are mounted at a 45° angle with a fifth mounted in a flat-plane nadir orientation. Further technical specifications concerning the Midas 5 system are shown in Table 1 below.

4.3.2 MIDAS Camera Assembly

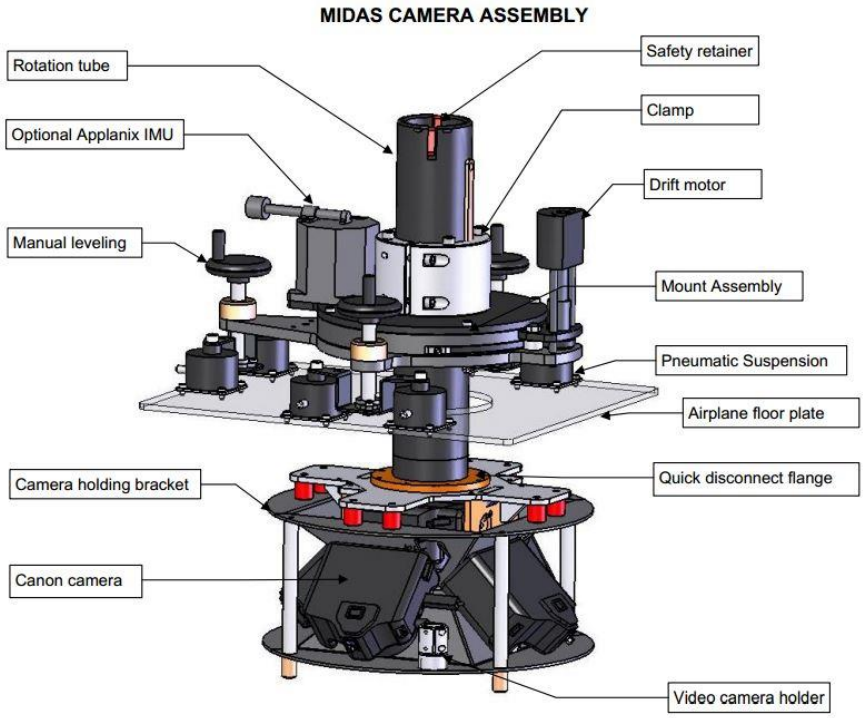

Figure 4.1 MIDAS Camera Assembly (credit: The Sanborn Map Company, Inc.)

Table 4.1 Technical specifications for MIDAS camera assembly

MDC Power requirements	24-28 Volts at 12-13 Amp
Amp Size	19 x 13 x 15 inch (490 x 330 x 390 mm)
Navigation/camera control	Integrated XTRACK flight system
GPS	Integrated Garmin 15
Cameras	Canon EOS 1Ds Mk III
Radiometric Resolution	14-bit
Images	5 x 21 Mega pixels raw images
IMU	Integrated Applanix POSAV 310

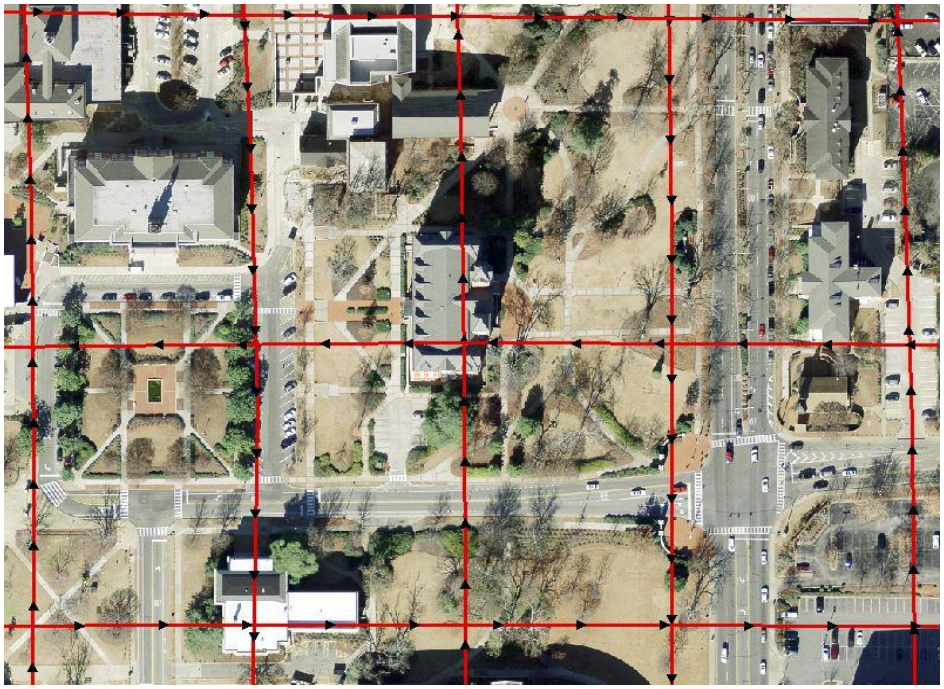

Figure 4.2 Flightlines every 200x400 feet, image captures shown in black (imagery taken 2014)

During flight each camera is triggered to capture an image at the exact same moment. These images contain between 40 to 70% overlap with adjacent images from either parallel or converging flightlines, shown in Figure 4.2 above. These areas of overlap, viewed from two or more angles, provide the passive stereoscopic information that can be utilized for three-dimensional point cloud generation. This occurs after each image is projected back into a single common plane and each pixel is corrected for various optical distortions (Scholz and Gruber, 2008). To rectify the images into a single common plane ground control points had to be gathered. These consisted of immobile objects viewable from a plurality of images and measureable from a ground-based receiver. For these reasons, open area manhole covers were chosen due to their high visibility a common denotation on the ground for each cover's center point being cast into the iron itself. In all 33 of these ground control points were identified and

marked using a real-time kinematics (RTK) corrected Leica-GS14 receiver (Leica Geosystems, Norcross, GA).

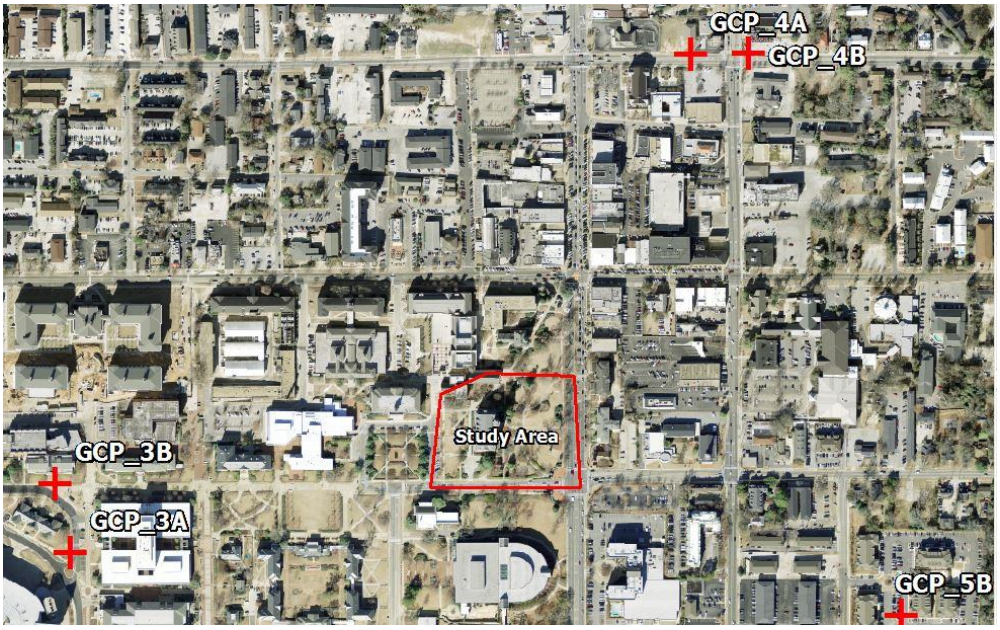

Figure 4.3 Sample of ground control points (GCPs) shown surrounding study area

4.3.3 Assembling Point Clouds

Parsing the accompanying metadata each relevant image was sub-selected within the Agisoft Photoscan Professional software suite, without requiring recopying of the required data that were tens of gigabytes in size. This meant that while the complete analysis of tie-in points would still be required in order to minimize horizontal error, dense point cloud generation would only be necessary for the study area. This workflow was chosen due to the extended nature of pixel-by-pixel analysis that is processor intensive and prone to hardware and software failure before completion, resulting in the loss of the project. Even with these shortcuts the overall processing time for a single 4-core laptop possessing 32-gigabytes of random access memory (RAM) was approximately 100 hours. Upon completion, these data can be exported into

universal point cloud file formats that function within most software packages including ERDAS Imagine (Intergraph Corp., Huntsville, AL), and ESRI's ArcGIS for Desktop.

Within the Agisoft program each of the relevant photographs, 5 from each capture vantage point, were imported and indexed to their corresponding flight line number, capture station number, and cardinal direction. To ensure accuracy and data integrity each indexing file was analyzed using a batch script cursor to prevent accidental duplicates or overwrites prior to initial project assembly after initial efforts showed minor naming errors within the vendor supplied dataset. This is necessary to prevent indexing errors from being misinterpreted later as occlusions within the imagery resulting in unmapped areas. Once imported the overall project file was created and analyzed for "tie-in" points using the Agisoft construction toolbar. These points were used as anchors for the generation of coarse point clouds that represented only a predetermined fraction of the full raster dataset. Using trial and error, these steps were repeated until a coarse point cloud with the lowest achievable horizontal accuracy, less than 1% across the entire study area, was achieved. This "skeleton" dataset was then used to generate a dense point cloud of the study area averaging approximately 3,800 points per square meter of vegetated surface. Once created, these data were exported into an American Standard Code for Information Interchange (ASCII) formatted text file describing each point's coordinate pair (XY), elevation (Z), and color (RGB).

Figure 4.4 Portion of the study area shown using point cloud generated from oblique image viewers.

4.3.4 Interpolation of Surfaces

These data were cleaned for any obvious noise points and subdivided into smaller areas that only encompassed a few trees. From these smaller modelspace projects each individual tree was identified and assigned a temporary modelspace for measurement and imported into the 3DReshaper (Landrivon Technodigit, Neyron, France) software suite for surface modeling. Using the available tools within 3DReshaper each tree surface was modeled using a similar workflow to those discussed in Chapter 3. These models were coarser in nature due to the lower point density of the resulting photogrammetric workflow compared to an active terrestrial LiDAR scanning system. The resulting models were measured for crown width, total height, and diameter at breast height (DBH) with each measurement being entered into a spreadsheet containing that tree's identification number. In total there were 57 trees within the study area,

including many smaller ornamental stems such as Japanese zelcova (serrate) and common crepemyrtle (indica). Due to their small size and overhanging occlusions from larger stems these were not all able to be modeled and were ignored, leaving 41 measured and modeled trees within the study area.

For comparison, the trees were physically measured for diameter at breast height (1.37 m above ground-line DBH), total height, crown base height, crown width from north to south, crown width from east to west, percentage of crown missing, crown dieback, and crown light exposure. Total tree and crown-base height were measured using a laser hypsometer (either a MDL LaserAce® hypsometer or a Laser Technology, Inc. TruPulse™ 360B rangefinder). Total tree height was determined by measuring from the ground-line to the top of the tree, and crown base height was recorded as the height to the lowest branch of significance. Crown width was determined by taking two measurements from the crown edges at 90 degree angles and then averaging them. All data were collected using the USDA Forest Service i-Tree Eco tree inventory protocol (Martin et al. 2011, i-Tree 2010). Dieback and percent missing crown were determined for each tree (i-Tree Eco 2010). Branch dieback was estimated by observing the tree from all sides and then calculating percent dieback. Ranges of <1, 1-10, 11-25, 26-50, 51-75, 76-99, and 100% dieback were used to assign tree conditions of excellent, good, fair, poor, critical, dying, and dead, respectively. Percent missing crown was determined in a similar fashion (i-Tree Eco, 2010). Each tree's metrics were analyzed using the i-Tree Eco individual tree characteristics toolkit for management related biomass figures such as ground area, leaf area, annual carbon storage, and gross carbon storage. Each tree is identified by its tree id value and i-Tree eco species code index. A full species code index can be found in the appendix.

Using the photogrammetric data each overlapping section of imagery was used to generate a three dimensional point cloud. Thus shifting the data structure from a raster model to a vector one, and allowing for the inference of z-values. This resulting dataset therefore contained tabular data for each point denoting a projected horizontal pairing (xy), elevation, and the original RBG brightness values. When a tree is isolated it appears as a single object to a human observer, but each data point is spatially isolated from those surrounding it. To group these isolated points into a single spatial object, one with a height, diameter, and volume, requires the relevant data points to be analyzed and interpolated using various methods. One of the least complex is simple linear interpolation, where an interpolated surface is constructed between each pair of points. Simple interpolation methods such as this are relatively quick to perform, but are incapable of weighting more or less relevant points in order to preserve a logical shape. The results are objects that appear full of empty space or strangely divergent tree branches that fuse and split without reason. In general, a combination of methods must be employed to achieve meaningful results, most of which are not explicitly detailed by software vendors due to their financial investment in such products.

Table 4.2 Field Measurements of all species
Auburn, Alabama (June, 2016)

Tree ID	Species	DBH (cm)	Total Height (m)	Percent Dieback	Crown Radius (m)
4291	QUST	108.97	19.83	25%	12.85
4292	QUPH	28.70	10.34	<1%	3.91
4293	QUPH	36.07	11.17	<1%	4.47
4294	QUPH	29.97	11.17	<1%	3.91
4295	QUPH	29.97	11.73	<1%	3.91
4296	ACSA2	26.67	9.22	<1%	3.91
4297	ULPA	29.72	5.87	<1%	3.63
4298	QUPA	77.47	16.76	<1%	7.82
4301	QUSH	44.20	12.01	<1%	5.87
4302	ULPA	26.67	7.82	<1%	4.47

4303	QUPA	38.10	11.17	<1%	5.31
4304	QUNU	29.21	9.50	<1%	4.47
4307	QUAL	95.50	18.44	25%	7.82
4308	QUPH	29.21	10.06	<1%	3.91
4309	QUPH	36.32	12.29	<1%	3.91
4310	QUPH	29.46	12.01	<1%	4.47
4313	QUSH	25.40	7.54	<1%	3.91
4314	ULPA	33.53	8.66	<1%	5.87
4315	QUNU	22.35	6.98	<1%	3.07
4316	LA6	38.86	8.38	<1%	4.19
4317	LA6	38.35	8.66	<1%	5.03
4318	LA6	46.23	6.98	<1%	4.19
4319	ULAL	75.95	23.74	10%	11.17
4320	COFL	23.11	6.70	<1%	2.79
4321	ILOP	29.21	9.22	<1%	3.91
4322	JUNI	68.07	18.44	25%	7.82
4323	ULAL	68.07	23.74	10%	10.06
4330	ILSP	20.07	8.10	<1%	2.79
4331	QUSH	30.99	9.22	<1%	4.47
4332	ILOP	32.00	8.94	<1%	3.07
4333	MAGR	28.70	8.94	<1%	3.35
4334	QUNU	29.21	8.66	<1%	3.91
4335	ACLE	25.40	7.26	<1%	3.35
4337	LA6	31.24	6.98	<1%	3.07
4339	ACPA	29.46	4.19	<1%	3.63
4360	QUAL	21.84	7.54	<1%	3.35
4364	ILSP	20.83	7.82	<1%	2.79
4366	LA6	27.94	8.66	<1%	3.91
4367	LA6	39.37	7.26	<1%	3.91
4368	LA6	26.92	7.82	<1%	3.91
4369	QUNU	20.57	10.06	<1%	3.07

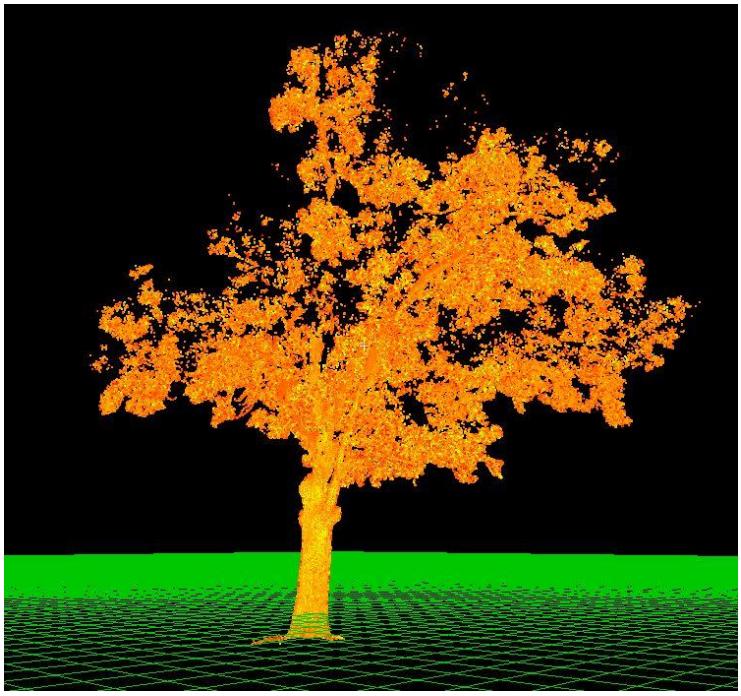

Figure 4.5 Point cloud showing isolated tree within modelspace (Auburn, Alabama; June, 2016)

4.4 Results

4.4.1 Field Measurements

Each tree was identified using the accompanying field measurements and modeled to best convey the structure of the tree. For specimens that were relatively open-grown, meaning few other trees were nearby, a sufficient number of data points existed and modeling yielded fairly complete polyhedrons. Others, however, were within close proximity to neighboring trees or were understory growth and yielded fewer usable data points and sometimes incomplete polyhedrons. This problem highlights the inherent limitations of a passive sensor system that lacks the ability to "see through" moderate canopy structure. In general, there was sufficient point spacing to permit reconstruction and identification of the most important metrics needed for volumetric interpolation, namely total height, canopy width, and DBH. This required

isolating each stem and removing noisy or neighboring points that interfered with a meaningful model.

Each of the trees within the study area were measured using both the previously described field methods and photogrammetricaly derived point clouds. Measurements such as DBH, total height, crown radius, and volume were taken for each specimen within the study area and the results of these are shown in Table 4.3 below.

Table 4.3 Volumes determined using photogrammetricaly derived digital point cloud and field measurements taken in Auburn, Alabama (June, 2016)

Tree ID	Species ID	DBH (cm)	Total Height (m)	Crown Radius (m)	Volume Digital (m^3)	Volume Field (m^3)	Volume Difference (m^3)
4291	QUST	109.0	21.6	14.0	17.23	20.18	-2.95
4292	QUPH	28.7	11.3	4.3	0.49	0.73	-0.24
4293	QUPH	36.1	12.2	4.9	1.31	1.25	0.06
4294	QUPH	30.0	12.2	4.3	0.77	0.86	-0.09
4295	QUPH	30.0	12.8	4.3	0.92	0.9	0.02
4296	ACSA2	26.7	10.1	4.3	0.45	0.56	-0.11
4297	ULPA	29.7	6.4	4.0	0.34	0.44	-0.10
4298	QUPA	77.5	18.3	8.5	8.42	8.62	-0.20
4301	QUSH	44.2	13.1	6.4	1.84	2.01	-0.17
4302	ULPA	26.7	8.5	4.9	0.36	0.48	-0.12
4303	QUPA	38.1	12.2	5.8	1.4	1.39	0.01
4304	QUNU	29.2	10.4	4.9	0.64	0.69	-0.05
4307	QUAL	95.5	20.1	8.5	14.01	14.41	-0.40
4308	QUPH	29.2	11.0	4.3	0.63	0.74	-0.11

4309	QUPH	36.3	13.4	4.3	1.11	1.39	-0.28
4310	QUPH	29.5	13.1	4.9	0.74	0.89	-0.15
4313	QUSH	25.4	8.2	4.3	0.33	0.42	-0.09
4314	ULPA	33.5	9.5	6.4	0.8	0.83	-0.03
4315	QUNU	22.4	7.6	3.4	0.22	0.3	-0.08
4316	LA6	38.9	9.1	4.6	0.71	1.08	-0.37
4317	LA6	38.4	9.5	5.5	0.63	1.09	-0.46
4318	LA6	46.2	7.6	4.6	1.16	1.28	-0.12
4319	ULAL	75.9	25.9	12.2	10.25	11.74	-1.49
4320	COFL	23.1	7.3	3.0	0.22	0.31	-0.09
4321	ILOP	29.2	10.1	4.3	0.44	0.67	-0.23
4322	JUNI	68.1	20.1	8.5	6.41	7.32	-0.91
4323	ULAL	68.1	25.9	11.0	7.59	9.43	-1.84
4330	ILSP	20.1	8.8	3.0	0.19	0.28	-0.09
4331	QUSH	31.0	10.1	4.9	0.88	0.76	0.12
4332	ILOP	32.0	9.8	3.4	0.65	0.78	-0.13
4333	MAGR	28.7	9.8	3.7	0.61	0.63	-0.02
4334	QUNU	29.2	9.5	4.3	0.47	0.63	-0.16
4335	ACLE	25.4	7.9	3.7	0.32	0.4	-0.08
4337	LA6	31.2	7.6	3.4	0.73	0.58	0.15
4339	ACPA	29.5	4.6	4.0	0.26	0.31	-0.05
4360	QUAL	21.8	8.2	3.7	0.27	0.31	-0.04
4364	ILSP	20.8	8.5	3.0	0.19	0.29	-0.10
4366	LA6	27.9	9.5	4.3	0.55	0.58	-0.03

4367	LA6	39.4	7.9	4.3	0.87	0.96	-0.09
4368	LA6	26.9	8.5	4.3	0.45	0.49	-0.04
4369	QUNU	20.6	11.0	3.4	0.31	0.36	-0.05

4.4.1 Point Cloud Measurements

Comparing the two datasets shown in Table 4.3, a trend can be seen between the volumes generated via field measurements and those gathered from the digital point cloud. Compared across all species the point cloud generated volumes were within 11.5% by total volume to volumes generated using field data. This percentage represents an underestimation of volume on average by 0.28 cubic meters. To put this into perspective, one of the smallest trees in the study area, tree number 4360, a white oak (*Quercus alba*) with a DBH of 28.6 centimeters and total height of 8.23 meters has an estimated volume of 0.27 cubic meters. For the oak species (*Quercus*) this underestimation shrinks to 8.5% of total volume compared to non-native ornamentals such as crepe myrtle (*Lagerstroemia indica*) and Chinese elm (*Ulmus parvifolia*) which exhibit a total volume underestimation of 15.7%.

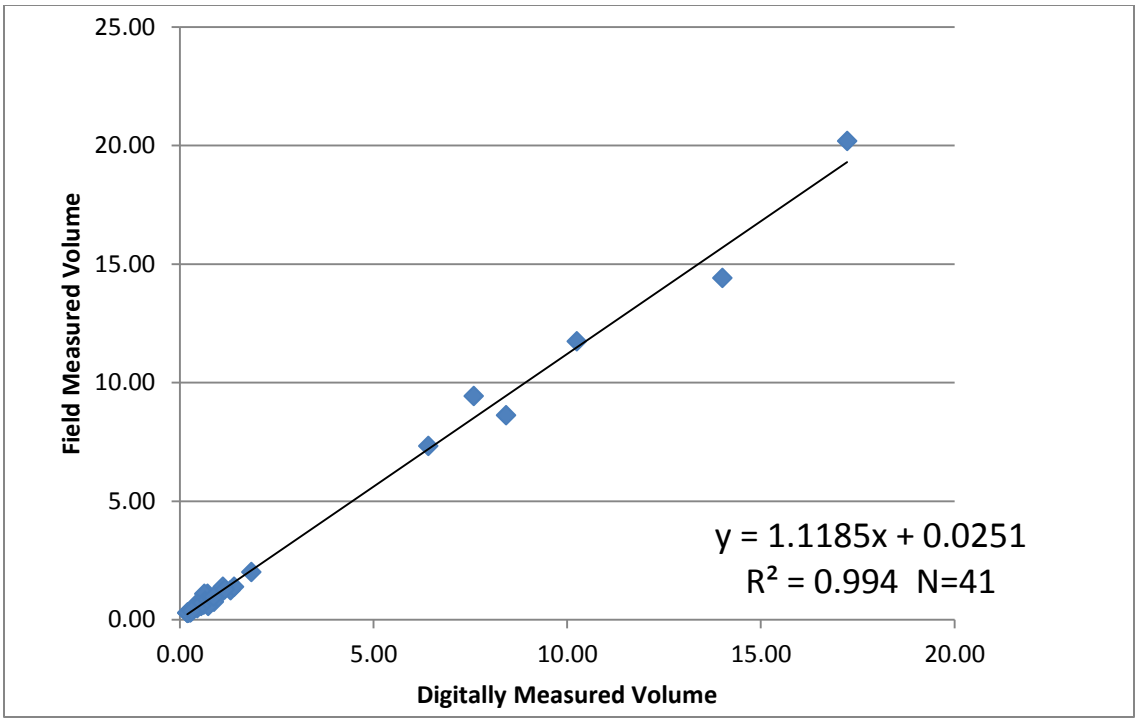

Figure 4.6 Regression Analysis Field Measurement Volumes and Digitally Measured Volumes for all Species in Study Site (Auburn, Alabama; June 2016)

4.4.2 Statistical Analysis

Plotted on a scatter chart (Figure 4.6) the observations show a consistency towards underestimation with the R^2 for the entire dataset at .994. Meaning that the digitally derived measurements yield lower overall volume for the same specimen when compared to the volumes derived from field methods. A trendline showing simple linear regression illustrates the relative position of the observations. Also, a paired t-test was used to examine the two observed values in order to measure the null hypothesis that they are unrelated to one another. This paired t-test distribution showed an observed p-value of 0.004, or that there was very little evidence that the predicted digital volume is not a consistent predictor of field measured volume. This consistency lends itself to the suspicion of occlusions within the point cloud, as a result of line-of-sight obstructions within the imagery, have possibly obscured a portion of each stem.

4.5 Discussion

Here, a medium scale project that uses passive sensor camera technology to capture high resolution raster datasets of a study area encompassing a nearly a city block. The passive sensors in question are oriented in such a manner as to provide a large percentage of image overlap, allowing for the generation of three-dimensional objects via stereoscopic imaging. This is due to the dataset containing a series of five images at each sample coordinate. Four of these are obliques at ninety degree angles relative to the flight path and the fifth is a nadir perspective image giving a "bird's eye view". Overlapping sections of each image allow for viewing of the same object from multiple perspectives. This, in general, permits imaging software to generate vector point clouds from these raster image files. From these point clouds a model reconstruction each tree is generated. Standard metrics such as total height, dbh, and crown width can then be taken and compared to measurements taken using traditional field methods. Measurements from each model allowed for the inference of each tree's volume. This could then be compared to those measurements taken from the ground in order to determine the relative precision of the model. In this study the trees in question were not destructively sampled so there can be no comparison of the model's accuracy. However, most urban tree and canopy measurement schemes use these metrics without destructive sampling due to either economic constraints or the inherent value of the study site (Nowak and Crane, 2000).

Comparing the two datasets, a trend can be seen between the volumes generated via field measurements and those gathered from the digital point cloud. Compared across all species the point cloud generated volumes were within 11.5% by total volume to volumes generated using field data. This percentage represents an underestimation of volume on average by 0.28 cubic meters. To put this into perspective, one of the smallest trees in the study area, tree number 4360,

a white oak (Quercus alba) with a DBH of 21.8 centimeters and total height of 8.3 meters has an estimated volume of 0.27 cubic meters. For the oak species (*Quercus*) this underestimation shrinks to 8.5% of total volume compared to non-native ornamentals such as Crepe Myrtle (*Lagerstroemia indica*) and Chinese Elm (*Ulmus parvifolia*) which exhibit a total volume underestimation of 15.7%. This distribution of error lends itself to the suspicion of occlusions within the point cloud, as a result of line-of-sight obstructions within the imagery, have obscured a portion of each stem, and smaller ornamentals in particular. Differences in total volume signal an underestimation when compared to those seen using traditional field methods. This underestimation is likely due to overhead occlusions that prevent the camera from "seeing" obscured objects such as stem and branch sections. Upon visual inspection, it is noticed that in the more dense portions of the study area several gaps in coordinate data can be observed. These gaps occur in areas where one would expect to find branch continuity, but due to overhead obstruction these branches cannot be observed/measured. Occlusions due to these line-of-sight obstructions can be partially mitigated by decreasing the distance between each flight line. This will decrease the Y-axis view angle of each image and permit a larger percentage of the occluded areas to be imaged by the airborne sensor. Also, increasing the frequency of image capture can reduce the X-axis view angle, further mitigating occlusions, but this solution is subject to hardware limitations such as read/write speed, onboard data storage, and camera shutter speed. As these are rapidly advancing technologies it can be assumed that future studies will be capable of increasing the image capture frequencies presented within this study. Future studies would also likely benefit from increases in spatial, spectral, and radiometric capabilities in passive camera technology, but since these limitations do not appear to be a limiting factor in the study presented here it is difficult to say how far these would go toward increasing the precision of a

similar study. Using airborne imaging sensors to inventory natural resources is not a new idea, but using these data in conjunction with emerging modeling technologies is a rapidly changing scientific pursuit. A multitude of imaging software packages combined with vector point cloud derivation software and polyhedron surface modeling parameters allow users and managers several options for how best to derive accurate metrics. This study is only one combination of the possibilities, specifically, using the MIDAS capture platform with RTK corrected GCPs to generate an urban forest volume inventory across several commonly seen urban species. Overall, these techniques proved useful in the measuring of urban forest canopy using a passive sensor system. These types of systems are likely to see rapid evolution in the near future and provide a meaningful resourse to both managers and researchers.

References

Ackermann, F. (1984). Digital image correlation: performance and potential application in photogrammetry. The Photogrammetric Record, 11(64), 429-439.

Avery, T. and Burkhart, H., (1983), Forest Measurements. McGraw Hill Book Company, New York, New York

Baker, H. H., & Binford, T. O. (1981). An iterative image registration technique with an application to stereo vision. In Proceedings of the International Joint Conference on Artificial Intelligence.

Birchfield, S., & Tomasi, C. (1999). Depth discontinuities by pixel-to-pixel stereo. International Journal of Computer Vision, 35(3), 269-293.

Bradbury et al., "Modeling relationships between birds and vegetation structure using airborne LIDAR data: a review with case studies from agricultural and woodland environments," Ibis 147(3), 443–452 (2005), http://dx.doi.org/10.1111/ibi.2005.147.issue-3.

Dandois, J. P., & Ellis, E. C. (2013). High spatial resolution three-dimensional mapping of vegetation spectral dynamics using computer vision. Remote Sensing of Environment, 136, 259-276.

Dhond, U. R., & Aggarwal, J. K. (1989). Structure from stereo-a review. IEEE transactions on systems, man, and cybernetics, 19(6), 1489-1510.

Ebner, H., & Heipke, C. (1988). Integration of digital image matching and object surface reconstruction. International Archives of Photogrammetry and Remote Sensing, 27(B11), 534-545.

Förstner, W. (1982). On the geometric precision of digital correlation. Int. Arch. Photogrammetry & Remote Sensing, 24(3), 176-189.

Fraser, R. (1997). U.S. Patent No. 5,664,115. Washington, DC: U.S. Patent and Trademark Office.

Fua, P., & Leclerc, Y. G. (1995). Object-centered surface reconstruction: Combining multi-image stereo and shading. International Journal of Computer Vision, 16(1), 35-56.

Furukawa, Y., Curless, B., Seitz, S. M. and Szeliski, R., 2010. Towards internet-scale multi-view stereo. Proceedings of IEEE Conference on Computer Vision and Pattern Recognition, 143: 4–1441

Gaulton R. and T. J. Malthus, "LIDAR mapping of canopy gaps in continuous cover forests: a comparison of canopy height model and point cloud based techniques," Int. J. Rem. Sens. 31(5), 1193–1211 (2010), http://dx.doi.org/10.1080/01431160903380565.

Goesele, M., Snavely, N., Curless, B., Hoppe, H. and Seitz, S. M.,. Multi-view stereo for community photo collections. 11th International Conference on Computer Vision, 2: 265–270. (2007).

Gruen, A. (1985). Adaptive least squares correlation: a powerful image matching technique. South African Journal of Photogrammetry, Remote Sensing and Cartography, 14(3), 175-187.

Gruen, A., & Baltsavias, E. P. (1988). Geometrically constrained multiphoto matching. Photogrammetric engineering and remote sensing, 54(5), 633-641.

Haala, N. (2009, September). Comeback of digital image matching. In Photogrammetric Week (Vol. 9, pp. 289-301). Wichmann Verlag Heidelberg.

Hartley, R. and Zisserman, A.,. Multiple View Geometry in Computer Vision. Second edition. Cambridge University Press, Cambridge, UK. (2003).

Hirschmuller, H. (2008). Stereo processing by semiglobal matching and mutual information. IEEE Transactions on pattern analysis and machine intelligence, 30(2), 328-341.

Hobrough, G. L. (1959). Automatic stereo plotting. Photogrammetric Engineering, 25(5), 763-769.

Hollaus et al., "Growing stock estimation for alpine forests in Austria: a robust LIDAR based approach," Can. J. Forest Res. 39(7), 1387–1400 (2009), http://dx.doi.org/10.1139/X09-042.

Hyde et al., "Mapping forest structure for wildlife habitat analysis using multi-sensor (LIDAR, SAR/InSAR, ETMþ, Quickbird) synergy," Rem. Sens. Environ. 102(1–3), 63–73 (2006), http://dx.doi.org/10.1016/j.rse.2006.01.021.

Kolmogorov, V. (2006). Convergent tree-reweighted message passing for energy minimization. IEEE transactions on pattern analysis and machine intelligence, 28(10), 1568-1583.

Kalarot, R., Morris, J., Berry, D., & Dunning, J. (2011). Analysis of real-time stereo vision algorithms on GPU. In International Conference on Image and Vision Computing New Zealand (IVCNZ).

Kersten, T. P., & Lindstaedt, M. (2012, October). Image-based low-cost systems for automatic 3D recording and modelling of archaeological finds and objects. In Euro-Mediterranean Conference (pp. 1-10). Springer, Berlin, Heidelberg.

Koutsoudis, A., Vidmar, B., Ioannakis, G., Arnaoutoglou, F., Pavlidis, G., & Chamzas, C. (2014). Multi-image 3D reconstruction data evaluation. Journal of Cultural Heritage, 15(1), 73-79.

Leberl, F., Irschara, A., Pock, T., Meixner, P., Gruber, M., Scholz, S., & Wiechert, A. (2010). Point clouds. Photogrammetric Engineering & Remote Sensing, 76(10), 1123-1134.

Lisein, J., Pierrot-Deseilligny, M., Bonnet, S., & Lejeune, P. (2013). A photogrammetric workflow for the creation of a forest canopy height model from small unmanned aerial system imagery. Forests, 4(4), 922-944.

Maas, H. G. (1996). Automatic DEM generation by multi-image feature based matching. International Archives of Photogrammetry and Remote Sensing, 31, 484-489.

Marr, D., & Poggio, T. (1976). Cooperative computation of stereo disparity. Science, 194(4262), 283-287.

Marr, D. (1982). Vision: A Computational Investigation Into. WH Freeman.

Narayanan, P. J., Rander, P. W., & Kanade, T. (1998). Constructing virtual worlds using dense stereo. In Computer Vision, 1998. Sixth International Conference on (pp. 3-10). IEEE.

Naesset E., "Airborne laser scanning as a method in operational forest inventory: status of accuracy assessments accomplished in Scandinavia," Scand. J. Forest Res. 22(5), 433–442 (2007), http://www.tandfonline.com/doi/abs/10.1080/02827580701672147.

Ohta, Y., & Kanade, T. (1985). Stereo by intra-and inter-scanline search using dynamic programming. IEEE Transactions on pattern analysis and machine intelligence, (2), 139-154.

Okutomi, M., & Kanade, T. (1993). A multiple-baseline stereo. IEEE Transactions on pattern analysis and machine intelligence, 15(4), 353-363.

Opitz, S., Wünnemann, B., Aichner, B., Dietze, E., Hartmann, K., Herzschuh, U., ... & Plotzki, A. (2012). Late Glacial and Holocene development of Lake Donggi Cona, north-eastern Tibetan Plateau, inferred from sedimentological analysis. Palaeogeography, Palaeoclimatology, Palaeoecology, 337, 159-176.

Pollefeys, M. et al., Detailed real-time urban 3D reconstruction from video. International Journal of Computer Vision, 78(2–3): 143–167. (2008)

Priestnall G., J. Jaafar, and A. Duncan, "Extracting urban features from LIDAR digital surface models," Comput. Environ. Urban Syst. 24(2), 65–78 (2000), http://dx.doi.org/10.1016/S0198-9715(99)00047-2.

Rosnell, T., & Honkavaara, E. (2012). Point cloud generation from aerial image data acquired by a quadrocopter type micro unmanned aerial vehicle and a digital still camera. Sensors, 12(1), 453-480.

Roy, S., & Cox, I. J. (1998). A maximum-flow formulation of the n-camera stereo correspondence problem. In Computer Vision, 1998. Sixth International Conference on (pp. 492-499). IEEE.

Rottensteiner F., "Automatic generation of high-quality building models from LIDAR data," IEEE Comput. Graph. Applic. 23(6), 42–50 (2003), http://dx.doi.org/10.1109/MCG.2003.1242381.

Remondino, F., Del Pizzo, S., Kersten, T. P., & Troisi, S. (2012, October). Low-cost and open-source solutions for automated image orientation–A critical overview. In Euro-Mediterranean Conference (pp. 40-54). Springer, Berlin, Heidelberg.

Scholz, S., & Gruber, M. (2008). Radiometric Quality of UltraCam Images. In Proceedings of the 21st ISPRS Congress Beijing 2008, International Archives of Photogrammetry, Remote Sensing and Spatial Information Sciences (pp. 1682-1750).

Szeliski, R., Uyttendaele, M., & Steedly, D. (2011). Fast poisson blending using multi-splines. In Computational Photography (ICCP), 2011 IEEE International Conference on (pp. 1-8). IEEE.

Schenk, T. (1999). Digital photogrammetry: Vol. I: Background, fundamentals, automatic orientation produceres. TerraScience.

Sonka, M., Hlavac, V., & Boyle, R. (2014). Image processing, analysis, and machine vision. Cengage Learning.

Solberg S., "Mapping gap fraction, LAI and defoliation using various ALS penetration variables," Int. J. Rem. Sens. 31(5), 1227–1244 (2010), http://dx.doi.org/10.1080/01431160903380672.

Snavely, N., Seitz, S. M. and Szeliski, R.,. Modeling the world from Internet photo collections. International Journal of Computer Vision, 80(2): 189–210 (2008).

Shan, Q., Adams, R., Curless, B., Furukawa, Y. and Sietz, S. M., 2013. The visual Turing test for scene reconstruction. Vision Conference., 3D: 25–32

Snavely, N., Seitz, S. M. and Szeliski, R.,. Modeling the world from Internet photo collections. International Journal of Computer Vision, 80(2): 189–210 (2008).

Takahashi et al., "Stand volume estimation by combining low laser-sampling density LIDAR data with QuickBird panchromatic imagery in closed-canopy Japanese cedar (Cryptomeria japonica) plantations," Int. J. Rem. Sens. 31(5), 1281–1301 (2010), http://dx.doi.org/10.1080/01431160903380623.

Wallace, L., Lucieer, A., Malenovský, Z., Turner, D., & Vopěnka, P. (2016). Assessment of forest structure using two UAV techniques: A comparison of airborne laser scanning and structure from motion (SfM) point clouds. Forests, 7(3), 62.

Wrobel, B. (1987, February). Facets stereo vision (FAST vision)—a new approach to computer stereo vision and to digital photogrammetry. In ISPRS Intercommission Conf. Fast Processing of Photogrammetric Data (pp. 231-258).

Zhang, Y. J. (1996). A survey on evaluation methods for image segmentation. Pattern recognition, 29(8), 1335-1346.

Chapter 5. Measuring Canopy Height Using Airborne LiDAR Scanning: A City-Scale Approach

5.1 Abstract

Airborne LiDAR scanning (ALS) provides a platform to remotely sense large areas of standing timber in a short period of time. Generally, scanning systems are mounted to fixed-wing aircraft with a nadir orientation that permits either single or multi-return data capture. Due to the discrete nature of a vector point cloud, spacing between individual points contain no data and have to either be ignored or interpolated based on the data points surrounding them. This could result in underestimation of total stem height due to the apex of each stem falling within point spaces of zero data. In this study a typical area of urban tree cover in Auburn, Alabama are examined determine if underestimation is present, and to what extent. Data gathered using an airborne LiDAR scanning system is parsed for individual stems using an object-based image analysis routine and total heights are compared to those gathered in the field using traditional measurement techniques. Results showed an average total height underestimation of 6.6% across all size classes with higher rates of underestimation in shorter trees (<12m) compared to the average underestimation of taller trees. Overall, these techniques showed that mapping and measuring of urban forest canopy using a GeOBIA assisted workflow are useful tools for both natural resource managers and researchers.

5.2 Introduction

Urban forests provide a wealth of environmental, social, and economic benefits such as improved water quality, air temperature regulation, carbon sequestration, air pollution reduction, enhanced human health, better aesthetics, increased property value, and reduction of energy

consumption (Nowak et al., 2007; Peper et al., 2007). The canopy's structure in particular can provide insights into functional characteristics and processes of tree growth, and can reveal important information on the forest response to disturbance at the individual tree, stand, community, and ecosystem level (Parker et al. 2004; Rhoads et al. 2004). The structure of a canopy is generally defined using metrics such as canopy closure, defined as the fraction of the sky obscured by foliage within a crown (Lefsky et al. 1999) and often relies on visual canopy assessments (Whitney and Johnson 1984; Seischab et al. 1993). Another is leaf area index (LAI) which generally calls for direct measurement involving destructive sampling of the canopy (Gower and Norman, 1991). Mature coniferous trees, which include all southern pines, generally have a more conical overall shape and smaller horizontal footprint than mature deciduous trees, which include all oaks, ashes, maples, and elms (Reitberger, 2008). This smaller horizontal footprint means any overhead scanning system, such as airborne LiDAR, will have fewer points of measurement from which to determine total stem height.

Airborne LiDAR is used prominently in projects that are at the landscape scale, and in terms of mapping trees, is useful for mapping forest canopy footprints and general heights. In this study it is used in conjunction with high-resolution aerial imagery for performing landscape scale mapping with geographic object based image analysis (GeOBIA). Remote sensing techniques using aerial imagery alone typically have the same problem where variations in light conditions and overarching shadows disrupt traditional pixel-based classifiers. ALS is a technology that can alleviate some of these problems by implementing an active sensor as opposed to the passive sensors used by traditional cameras. An active sensor system relies on two optical beams, the emitted laser beam and the returned portion of that beam, and is not vulnerable to shadowing or other variations in natural light (MacFaden et al., 2014; Wehr and

Lorh, 1988). The equipment involved in an airborne platform generally include: a laser, a real time kinematic (RTK) corrected global positioning system (GPS) receiver that maintains the aircraft's coordinate position, an inertial measurement unit (IMU) that maintains the aircraft's spatial orientation relative to the ground (equipotential), and an interface between the receivers and data storage devices. To maintain functional RTK correction the receiver must be in range (~40 kilometers) of a base station that is established over a known coordinate and is constantly delivering vector correction data to account for atmospheric aberration. This real time correction is generally used in conjunction with post processing correction (Nilsson, 1996).

In this study the focus is on the use of active-sensor airborne LiDAR for the mapping and measuring of urban forest total heights at the city scale. These measurements are a widely utilized input for urban tree allometric equations and their accuracy directly reflected in urban forest biomass estimations. Such airborne platforms provide a way to collect individual stem information on a large area in a relatively short period of time. However, their relatively coarse point density may underestimate crucial metrics for stand-level biomass estimation (Andersen Reutebuch and McGaughey, 2006). Using LiDAR data captured over the city of Auburn, Alabama this study will derive total heights from individual stems in a semi-automated manner and compare those results with total height measurements taken in the field manually. This technology has already been utilized in the identification and classification of trees for forest inventory, habitat assessment for wildlife, assessing canopy gaps, and urban feature extraction (Takahashi et al., 2010; Gaulton and Malthus, 2010; Solberg, 2010; Hollaus et al., 2009; Naesset, 2007; Hyde et al., 2006; Bradbury et al., 2005; Rottensteiner, 2003; Priestnall, Jaafar, and Duncan, 2000). Traditionally these studies have focused on stand-level metrics (Solberg, 2010), lacked individual stem validation (Hollaus et al., 2009; Hyde et al., 2006), or relied upon mostly

manual workflows for feature identification (Holopainen et al., 2013). This study uses a semi-automated process involving GeOBIA for identifying and extracting individual stem metrics and relies upon in-field validation on randomly selected individual trees.

Active remote sensing methods such as airborne LiDAR provide non-destructive methods for directly gathering three dimensional distribution of vegetation canopy components, high resolution topographic elevation, and relatively highly accurate estimates of vegetation height, cover, and other aspects of canopy structure. LiDAR systems can be classified into either discrete return or waveform sampling systems. Waveform LiDAR systems compensate for lower spatial resolution with a finer, and fully digitized, vertical resolution, providing full sub-meter vertical profiles (Coops et al., 2007). By comparison, discrete return LiDAR, with spatial resolution of a meter or less, typically record only one to five returns per laser footprint (Lim et al. 2003; Schenk et al. 2001; Blair et al. 1999). While scanning, a laser emits beams of light which encounter an object on the ground. This light is then backscattered and returns to the sensor slightly or significantly weaker than when it was initially emitted, depending on the reflectivity (albedo) of the object encountered (Naesset, 2009). The distance from the source of the light beam and the object that it reflected off of is determined by measuring the amount of time delay between emission and detection. This is possible because the speed at which light travels is fixed, and this type of distance measurement is known as time of flight (TOF) measurement. Other relevant system attributes include the duration of the pulse, the number of returns that can be extracted from a single beam pulse, and the footprint spacing of each scan relative to altitude and velocity (Priestnall, Jaafar and Duncan, 2000). It is from these system attributes that a particular dataset's attributes are determined such as pulse density, return density, return remission, and return number.

Commercial scanning instruments vary greatly in terms of the number of light beams that can be emitted in a given period of time. In general, the number of beams emitted by a sensor in one second is known as that sensor's scanning frequency. Depending on the manufacturer and the generation of instrument these can vary from a few thousand beams per second to several hundred thousand beams per second (Gatziolis and Andersen, 2008). This variation in scanning frequency means that higher frequency enabled systems can fly at higher altitudes and at faster speeds while maintaining desired return densities as compared to lower frequency systems. Other system-dependent variables include mirror scanning patterns such as seesaw, parallel, and elliptical as well as beam divergence. This divergence is due to the trajectory of the light beam emitted deviating slightly from the propagation axis to form a cone-like shape as opposed to a true cylinder. Depending on the application, these divergence values typically range from 0.1 to 1.0 milliradian (Baltsavias, 1999). This angular measurement and the operating altitude of the aircraft combine to determine the size of the scanning footprint that the sensor can measure at any given time. This footprint is typically described as the diameter of a beam of light pulses that are intercepted by a plane positioned perpendicularly to the beam axis. Within this footprint the distribution of pulse energy is not uniform, but rather it decreases via two-dimensional Gaussian distribution as it approaches the edge of the footprint's extent (Gatziolis and Andersen, 2008). Another characteristic of the system is the gain factor that is being employed on the backscatter receiving device. This variation in sensitivity is designed to prevent damage to system hardware in the presence of high backscatter energy in the event of highly reflective surfaces.

Other relevant system attributes include the duration of the pulse, the number of returns that can be extracted from a single beam pulse, and the footprint spacing of each scan relative to altitude and velocity (Priestnall, Jaafar and Duncan, 2000). It is from these system attributes that a

particular dataset's attributes are determined such as pulse density, return density, return remission, and return number. Pulse density is driven by a system's footprint spacing as measured over a hypothetical flat plane and is found by dividing one by this squared measurement [1/(footprint spacing^2)]. Return density is the average number of returns per a given unit of area (m^2). This is not to be confused with pulse density due to the prevalence of multi-return systems which in a case of scanning multi-tiered canopy would result in a higher return density than over bare earth, but each of whom would have equal pulse densities. It is because of this location-dependent variation that pulse density, rather than return density, can be used as a standard measurement for LiDAR acquisition (Priestnall, Jaafar and Duncan, 2000).

Return number refers to the rank within the return structure that a particular backscattered beam is observed. For instance, a beam that penetrates highly structured upper canopy before being backscattered by lower canopy would likely register as a second or third return while a beam that penetrated all the way to the ground through the same canopy would register as a last return. Return remission refers to the fraction of beam energy that returns to the sensor as backscatter after encountering an object. This will depend on the reflectivity of the object as well as its range from the sensor and rank within the return structure.

The resulting dataset is generally stored within an interchange format know LAS, short for laser. This file format is the approved file format of the American Society for Photogrammetry and Remote Sensing (ASPRS). This format uses a delimited series of coordinate triplicate along with ancillary data that may be available depending on the system such as return number and remissive value. The data are human readable in that each return is assigned a single line of entry and can be viewed using any text editor assuming sufficient onboard memory to open such large files. File size has been an issue with this technology since

the data are inherently large, consisting of perhaps hundreds of millions of returns per file. Dedicated hard drives with storage in excess of one terabyte are generally employed in an airborne LiDAR project.

The result is a point cloud of XYZ coordinate data that managers and researchers can manipulate to reflect characteristics such as height above ground and texture of various features. This technology has already been utilized in the identification and classification of trees for forest inventory, habitat assessment for wildlife, assessing canopy gaps, and urban feature extraction (Takahashi et al., 2010; Gaulton and Malthus, 2010; Solberg, 2010; Hollaus et al., 2009; Naesset, 2007; Hyde et al., 2006; Bradbury et al., 2005; Rottensteiner, 2003; Priestnall, Jaafar, and Duncan, 2000).

This study examines a study area at the city block scale using both orthographic imagery and airborne LiDAR data to identify individual trees using standard LiDAR software in conjunction with geographic object based image analysis (GeOBIA). Once mapped, these trees are attributed with individual total height metrics derived from the airborne LiDAR dataset using GeOBIA. The main objective is to determine if using these data fusion techniques can create an accurate city scale urban forest canopy inventory. To measure accuracy, a subset of randomly selected trees were inspected in the field using traditional methods with results compared to those attributed using the GIS model.

5.3 Methods

5.3.1 Data

Pulse density is driven by a system's footprint spacing as measured over a hypothetical flat plane and is found by dividing one by this squared measurement [1/(footprint spacing2)].

Return density is the average number of returns per a given unit of area (m2). For this study, a sampling of urban trees were scanned using a Leica ALS-50 discrete laser scanner at an altitude of approximately 1,200 meters and speed of 110 knots. Sidelap spacing of 50% and flightline spacing of approximately 300 meters were employed in accordance with widely used industry standards (Popescu, 2012). These data were supplied by the City of Auburn's GIS Department with acquisition parameters set by local municipalities. The data were clipped to encompass only the interior urban forested area of the city while also bounding aircraft flight lines and local roadways. Specifically I-85 to the south and College Street to the west, shown in Figure 1 below. Further details concerning data acquisition parameters can be found in Table 5.1 below.

5.3.2 Study Site

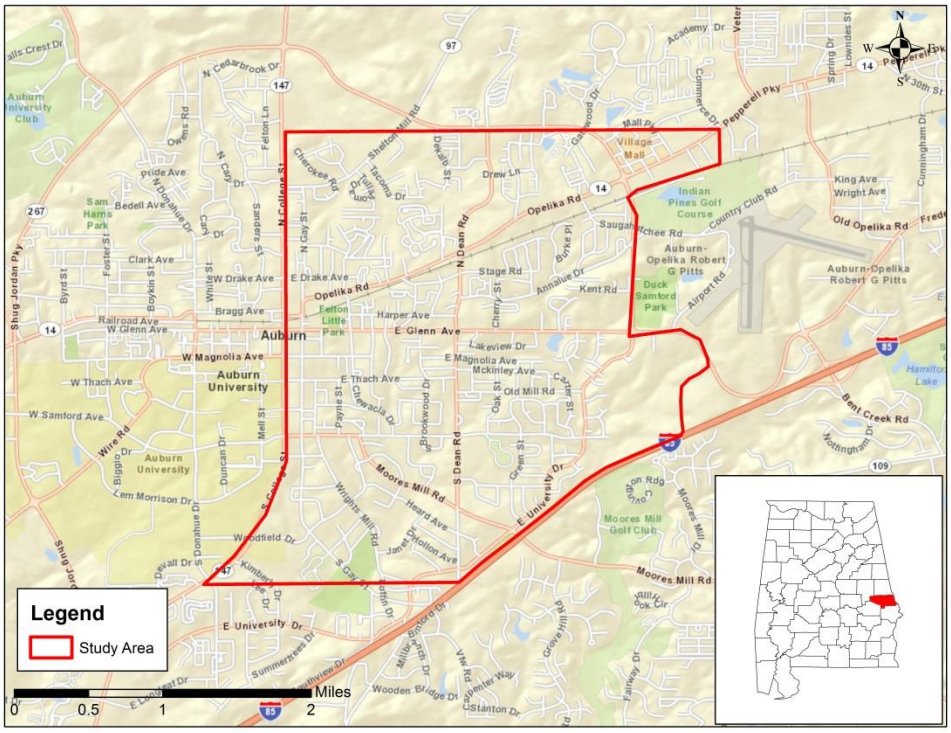

Figure 5.1 Study site in urban forested area within Auburn, Alabama

Table 5.1 LiDAR acquisition specifications, Auburn, Alabama, March 1–April 15, 2014.

Sensor	Leica ALS-50
Flight altitude	4,000 ft (1,219 m)
Repetition rate	93,300 kz
Scan frequency	34 kz
Airspeed	110 knots
Field of View	40 deg
Sidelap	50%
Flight line spacing	1000 ft (305 m)
Average point spacing	2.2 ft
Horizontal accuracy	0.328 ft (0.1 m) RMSE
Vertical accuracy	0.17 ft (0.049 m) @ 95% CI

For stem identification within the GeOBIA modeling workflow 4-band, 6-inch spatial resolution ortho imagery was used. This imagery was captured at the same time as the airborne LiDAR data described above using an accompanying passive sensor system. The data have been georeferenced according to vendor specific parameters including orthorectification using the same visible ground points marked with real time kinematics (RTK) enabled GPS that have been carrier phase corrected to within single centimeter horizontal accuracy. Passive sensor system parameters can be viewed in Table 5.2 below.

Table 5.2 Description of ortho imagery, Auburn, Alabama, March 1–April 15, 2014.

Spectral Resolution	4-Band (RGB,NIR)
Spatial Resolution	6-inch (.15 m)
Radiometric	8-bit (0-255)
Horizontal Deviation	< 6%
Crab	< 5°
Flight altitude	4,000 ft. (1,219 m)

Airspeed	110 knots
Flight line spacing	1000 ft. (305 m)
Endlap	60%
Sidelap	30% (± 5%)
Horizontal accuracy	0.328 ft (0.1 m) RMSE
Vertical accuracy	0.17 ft (0.049 m) @ 95% CI

5.3.3 Classified Point Cloud

Data from multiple flightlines were first mosaicked together, then trimmed to include a study area covering the urban interior of the City of Auburn, Alabama. LiDAR data were additionally QA/QC inspected using GeoCue's LP360 software suite to identify classified above-ground objects. Minor occlusions around roadway and bridge embankments were noticed, but did not impact the quality of the discrete LiDAR data points on the objects of interest (i.e. standing trees) within the study area. The data were then imported into a LAS Dataset where ground features were separated from above-ground features using the vendor supplied classification.

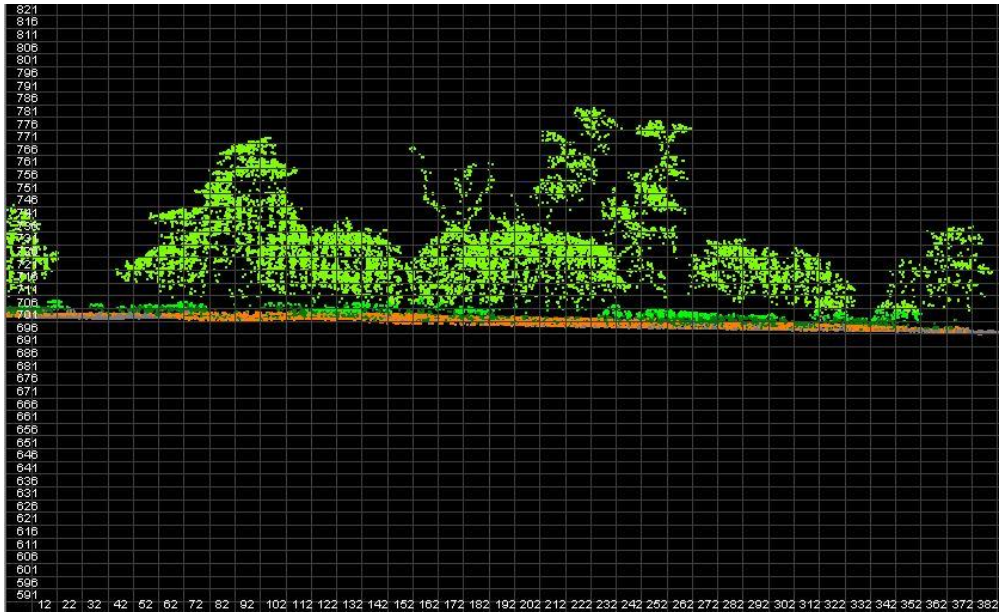

Figure 5.2 Classified point cloud data for urban tree cover showing trees (green) and ground (brown) classifications (Auburn, Alabama; March, 2014)

5.3.4 GeOBIA Classification

After this, each were rasterized using natural neighbor interpolation with zero point thinning and sampling sizes equal to the dataset's point spacing. Using these newly created digital surface and digital elevation models map algebra was employed to create a single normalized digital surface model (nDSM) raster output. Ortho images were mosaicked using ERDAS Imagine's MosaicPro software suite. Each image was color corrected using an illumination equalization histogram matching scheme where seamlines for each ortho image were feathered to a distance of 50 meters. This created a single image output with matching histogram values and a seamless appearance. The resulting data were imported into the eCognition Developer 8.0 software suite (Trimble Inc. Sunnyvale, California) a widely utilized object-based analysis software, to be analyzed for individual stem identification. Various weighted values were assigned to each of the layers in an iterative segmentation scheme that was

used to produce multiple levels of image object primitives. Using trial-and-error, these primitives were re-segmented and merged to create accurate single-stem image objects shown in Figure 5.5 below.

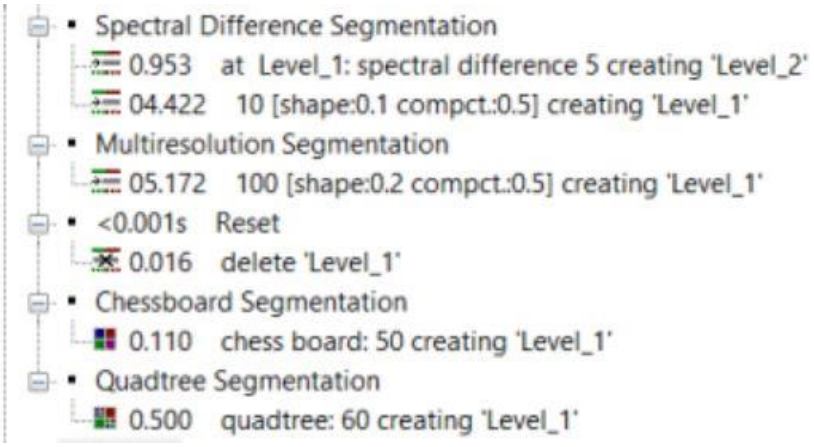

Figure 5.3 Sample of segmentation ruleset used to create image objects in eCognition

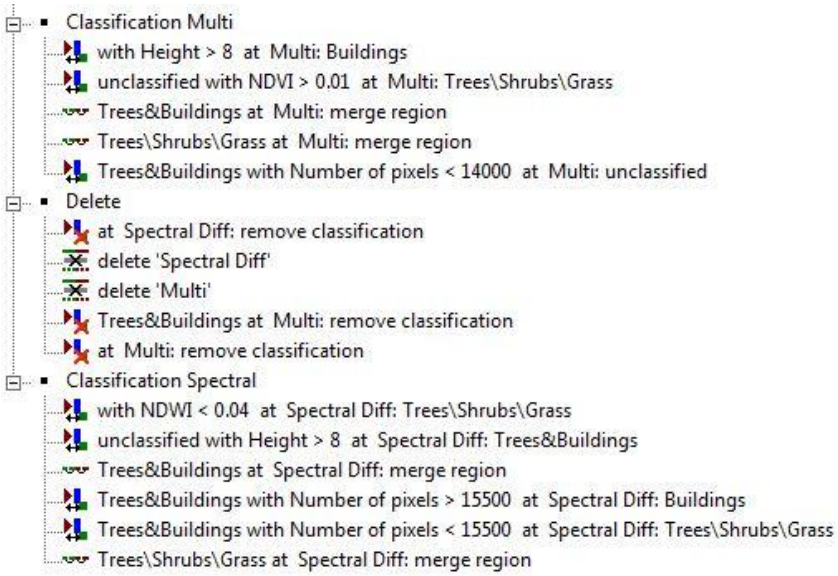

Figure 5.4 Sample of classification ruleset used to classify image objects into candidate classes in eCognition

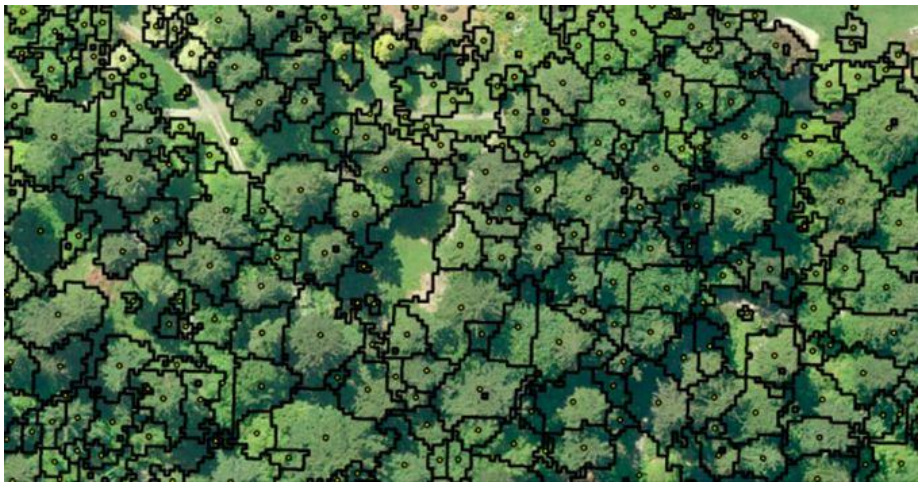

Figure 5.5 eCognition ruleset and tree identification after GeOBIA segmentation (Auburn, Alabama; March, 2014)

Each image object is attributed with the tabular data of all input layers as well as every successive segmentation layer, meaning no data are lost from the workflow. Using the nDSM layer for height relative to the ground each image object (i.e. tree) has an associated maximum height value. Using the ArcGIS random number function, a random series of 30 trees were exported into an inspection output table showing, among other attributes, their locations and their maximum height values. Using these data each stem was visited in the field and measured for total height using a laser rangefinder/hypsometer. Varying distances to each tree were necessary to obtain a clear view of their tops, but distances never exceeded 30 meters horizontally. These field obtained values were then compared with those obtained from the GeOBIA model. Total heights from the LiDAR derived dataset were differenced from those gathered in field in order to determine the percentage of difference. Each total height was then plotted using simple linear regression which uses input points with one independent variable and one dependent variable to find a linear function that, as accurately as possible, predicts the dependent variable values as a function of the independent variables.

5.4 Results

5.4.1 GeOBIA Urban Canopy

Each tree ID number coincides with its position within the random selection routing, with 1 being the first tree assigned and 30 being the last. Significant digits as shown are commiserate with the scale accuracy of both the LiDAR system as well as the digital hypsometer used in the field.

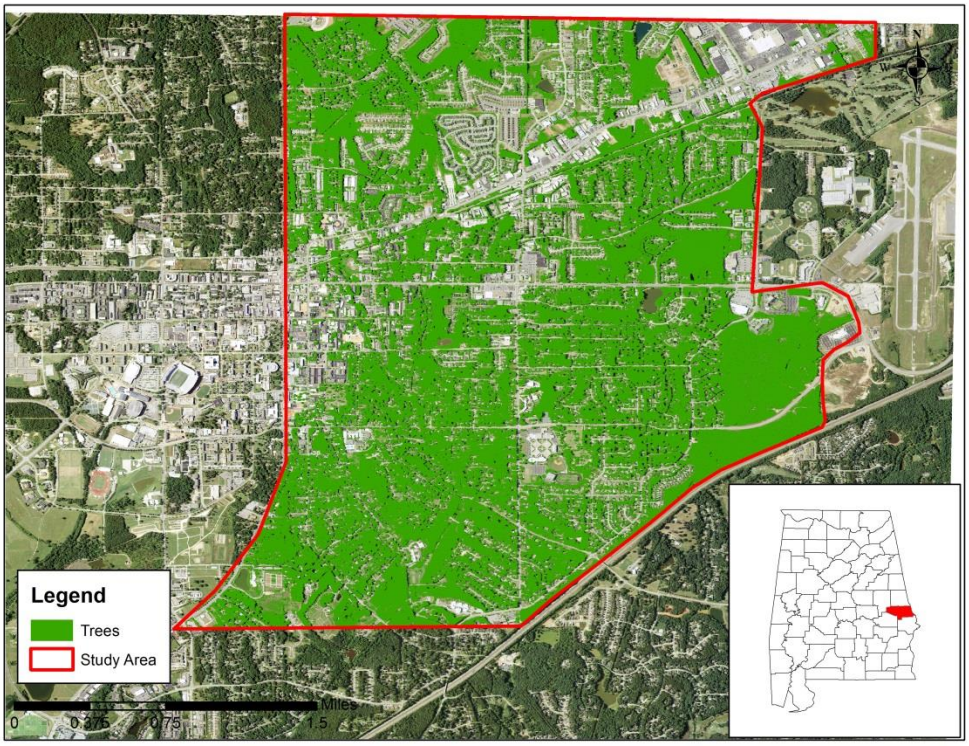

Figure 5.6 GeOBIA classified trees (green) within the study area (Auburn, Alabama)

5.4.2 Airborne Laser Scanning Total Heights

Table 5.3 Field measured total heights and LiDAR generated total heights of randomly selected field inspected trees (Auburn, Alabama)

Tree ID#	LiDAR Total Height (m)	Field Total Height (m)	Different % LiDAR/Field
1	8.445122	9.207317	-0.09
2	12.56098	13.47561	-0.07
3	8.902439	9.939024	-0.12
4	10.97561	11.12805	-0.01
5	9.603659	10.30488	-0.07
6	13.38415	14.26829	-0.07
7	16.89024	17.86585	-0.06
8	6.432927	7.560976	-0.18
9	13.59756	14.5122	-0.07
10	15.7622	17.04268	-0.08
11	8.780488	9.481707	-0.08
12	11.7378	13.07927	-0.11
13	14.5122	15.73171	-0.08
14	18.84146	18.90244	0.00
15	15.88415	17.16463	-0.08
16	12.56098	14.11585	-0.12
17	14.11585	15.03049	-0.06
18	10.03049	10.39634	-0.04
19	16.40244	17.5	-0.07
20	8.323171	9.512195	-0.14

21	13.53659	14.32927	-0.06
22	12.89634	14.69512	-0.14
23	16.43293	16.92073	-0.03
24	14.20732	16.21951	-0.14
25	18.96341	19.20732	-0.01
26	17.28659	17.37805	-0.01
27	15.09146	15.60976	-0.03
28	12.53049	13.65854	-0.09
29	10.42683	10.70122	-0.03
30	8.810976	9.72561	-0.10
Avg.	12.92988	13.82317	-0.08

The extent of the GeOBIA classification scheme is shown in Figure 5.6 above. These data reflect the urban tree canopy extent for the study area. Based on these results the urban canopy extent is 1,558,077 m^2 (155.8 hectares) of the study area's 3,131,542 m^2 (313.1 hectares) or 49.75% of the entire area. This percentage of canopy cover is above the US Forest Service's recommendation for urban canopy extent of 40% (Nowak et al., 2010). In an attempt to assess the accuracy of the GeOBIA generated urban canopy layer the entire data layer was overlaid with a series of 30 randomly generated location points. Each of these 30 locations were inspected for accuracy by visual comparison to the airborne imagery with an accurate position being one that is forested and an inaccurate position being one that is unforested. This visual validation found 28 of the 30 inspection sites were correctly classified as forested areas with 2 locations that were incorrectly classified as forested areas. In one case the misclassification came from a

residential home with elevated patio that contain what appear to be planted vegetation. The elevation above the surrounding area combined with the spectral signature of the green vegetation indicate that the errors were of commission on the part of the classification algorithm. Future study should investigate ways of exempting these types of logic tree errors as the algorithm's robustness are one of it's core strengths. The more thought and logic put into how the machine is segmenting, attributing, and classifying the objects the more accurate and usefufthe resulting product will be for end users and resource managers.

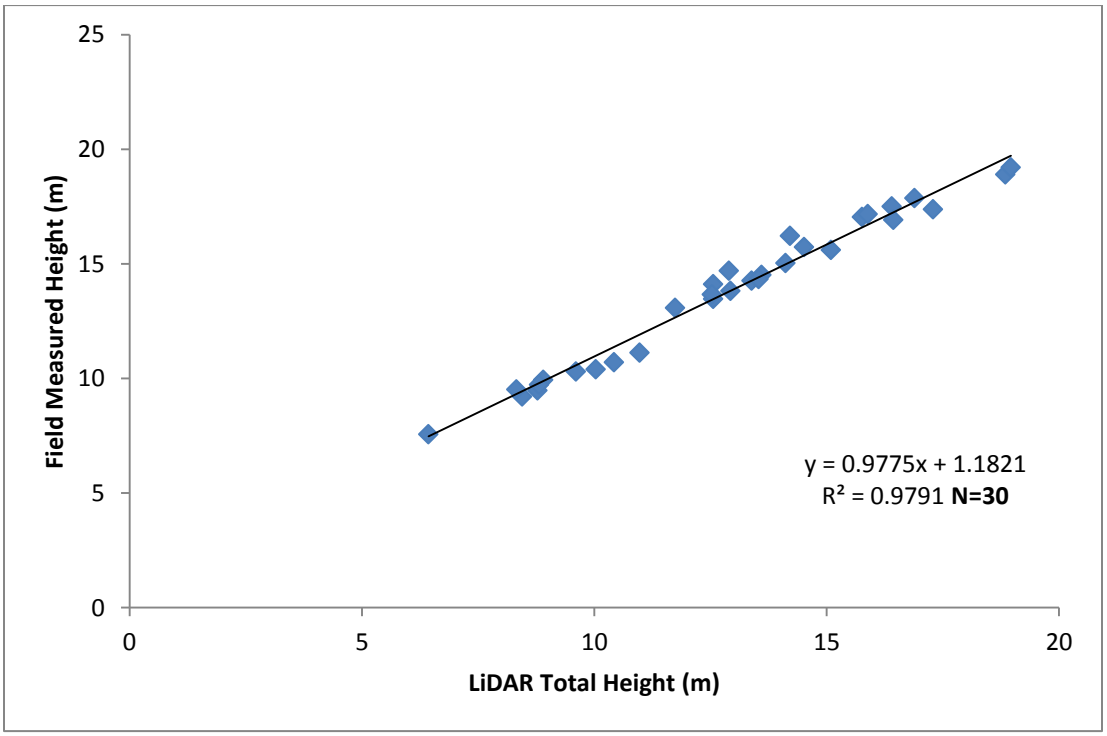

Figure 5.7 Linear regression plot for field measured height and LiDAR generated height measurements, each observation shown as a blue dot (Auburn, Alabama)

5.4.3 Regression Analysis

The data from both the LiDAR model and field measurements are plotted in Figure 5.7 above using a simple linear regression. This shows that the data coincide with an R^2 of .97 with an average underestimation of 6.6%. That is, the underestimation of the airborne LiDAR derived total heights when compared to total heights derived using field measurements. This underestimation was not consistently applied throughout the entire data range, however. Further inspection of the data shows trees with lower total heights, < 12 meters, showed an average underestimation of 8.3% compared to trees over 12 meters with an average underestimation of 5.9%. Examining this further, by comparing softwood species to hardwood species showed that at approximately 12 meters in total height the average underestimation of the two became more similar than for stems at less than 12 meters. Specifically, underestimation of hardwoods and softwoods at less than 12 meters showed an underestimation of 7.6 and 8.7% respectively. For hardwoods and softwoods over 12 meters this shrinks to 5.5 and 6.1% respectively. This appears likely due to the tendency of mature pine canopies to "flatten" into a larger average horizontal area compared to non-mature pines (Avery and Burkhart, 1983). This larger average horizontal area at maximum total height would increase the likelihood of a discrete LiDAR pulse return being correctly captured. Smaller trees with more conical overall shapes would not possess these features and point spacing of the laser scanning system would serve as a direct driver of individual stem height accuracy. This would mean as the average horizontal point spacing of a scanning system decreased the likelihood of a correctly measured discrete LiDAR point would increase. Each scanning project, based on their overall goal, should be oriented so as to minimize this underestimation. Considerations on scanning system style, such as discrete or waveform, as well as airspeed, altitude, and pulse speed should be taken into account and weighed for their

cost/benefit as most scanning projects likely are compromises between a host of end-users from various disciplines or municipal departments. In general, a reduction in the airspeed and/or flight altitude will result in an inversely proportional increase in the average horizontal point spacing of any particular scanning system. These assumptions are, of course, predicated on the safe operational parameters of the aircraft as well as federal, state, and local regulations regarding operating altitude over populated areas.

5.5 Discussion

The combination of passive camera imaging with active sensor airborne LiDAR provides a wealth of information that can be used for urban tree canopy mapping. Multiple workflows and software suites have been created for analyzing these data, but most are specialized in nature and only provide solutions to a small subset of a general GIS workflow. The incorporation of GeOBIA into these analyses offers the ability for data fusion techniques that no other individual software can provide. In this instance, using eCognition's object oriented segmentation, attribution, and classification workflows allow the user to incorporate both raster and vector datasets, each of varying resolutions and spatial extents, into a single routine for generating urban forest extent. This could offer researchers and managers a more affordable option for analysis given the cost of many software suites and the time required to gain sufficient experience using them. However, eCognition's user interface is not especially intuitive or easy to use for the beginner. It's mixture of graphical user interface (GUI) and command line scripting require either prior experience or detailed examples, which is not currently offered.

Airborne LiDAR systems provide a remote sensing platform that can cover large areas in a relatively short period of time. Data can be collected over an area of hundreds of square miles

in a matter of days, compared to ground measurement methods which require large crews of workers and cover only a fraction of the same area. These data are not without their limitations, however, since only minimal inference concerning merchantability of the interior bole can be established when gathered for coniferous stands or during leaf-on conditions. This presents a challenge to commercial producers given that merchantability is seen as a necessary metric regarding value, as opposed to municipal managers who are primarily concerned with aboveground biomass, canopy closure, carbon sequestration, etc. For these managers there can be a wealth of information derived from an airborne platform at a relatively low cost when compared to ground measurements. Other possibilities for future investigation include the fusion of active sensor scanning data with passive sensor data from varying angular perspectives, permitting photogrammetric point cloud derivation for additional component identification and measurement. As this is an ever expanding field of study there will certainly be plenty of changes to come. In general, remotes sensing technologies combined with GIS workflows provide a relatively small number of individuals the ability to map, measure, inventory, and analyze more data covering larger areas than are possible using only traditional field methods. In this study a city scale project covering hundreds of acres and thousands of trees were mapped and analyzed to a reasonable degree of accuracy and required only an active processing time of ten to twelve hours. This does not include planning and pre-processing, of course, but these workflows could be expanded to include adjacent cities or rural areas not included in this particular study without much additional processing time required. It is in that expandibility that the usefulness of these remote sensing platforms and GeOBIA become apparent.

References

Andersen, H. E., Reutebuch, S. E., & McGaughey, R. J. (2006). A rigorous assessment of tree height measurements obtained using airborne lidar and conventional field methods. Canadian Journal of Remote Sensing, 32(5), 355-366.

Baltsavias, E. P. (1999). Airborne laser scanning: existing systems and firms and other resources. ISPRS Journal of Photogrammetry and Remote sensing, 54(2-3), 164-198.

Blair, J. B., Rabine, D. L., & Hofton, M. A. (1999). The Laser Vegetation Imaging Sensor: a medium-altitude, digitisation-only, airborne laser altimeter for mapping vegetation and topography. ISPRS Journal of Photogrammetry and Remote Sensing, 54(2-3), 115-122.

Bradbury et al., "Modelling relationships between birds and vegetation structure using airborne LIDAR data: a review with case studies from agricultural and woodland environments," Ibis 147(3), 443–452 (2005), http://dx.doi.org/10.1111/ibi.2005.147.issue-3.

Coops, N. C., Hilker, T., Wulder, M. A., St-Onge, B., Newnham, G., Siggins, A., & Trofymow, J. T. (2007). Estimating canopy structure of Douglas-fir forest stands from discrete-return LiDAR. Trees, 21(3), 295.

Gaulton R. and T. J. Malthus, "LIDAR mapping of canopy gaps in continuous cover forests: a comparison of canopy height model and point cloud based techniques," Int. J. Rem. Sens. 31(5), 1193–1211 (2010), http://dx.doi.org/10.1080/01431160903380565.

Gatziolis, D., & Andersen, H. E. (2008). A guide to LIDAR data acquisition and processing for the forests of the Pacific Northwest. Gen. Tech. Rep. PNW-GTR-768. Portland, OR: US Department of Agriculture, Forest Service, Pacific Northwest Research Station. 32 p, 768.

Gower, S. T., & Norman, J. M. (1991). Rapid estimation of leaf area index in conifer and broad-leaf plantations. Ecology, 72(5), 1896-1900.

Hollaus et al., “Growing stock estimation for alpine forests in Austria: a robust LIDAR based approach,” Can. J. Forest Res. 39(7), 1387–1400 (2009), http://dx.doi.org/10.1139/X09-042.

Holopainen, M., Kankare, V., Vastaranta, M., Liang, X., Lin, Y., Vaaja, M., ... & Kukko, A. (2013). Tree mapping using airborne, terrestrial and mobile laser scanning–A case study in a heterogeneous urban forest. Urban forestry & urban greening, 12(4), 546-553.

Hyde et al., “Mapping forest structure for wildlife habitat analysis using multi-sensor (LIDAR, SAR/InSAR, ETMþ, Quickbird) synergy,” Rem. Sens. Environ. 102(1–3), 63–73 (2006), http://dx.doi.org/10.1016/j.rse.2006.01.021.

Lim, K., Treitz, P., Wulder, M., St-Onge, B., & Flood, M. (2003). LiDAR remote sensing of forest structure. Progress in physical geography, 27(1), 88-106.

Lefsky, Michael A., Warren B. Cohen, David J. Harding, Geoffrey G. Parker, Steven A. Acker, and S. Thomas Gower. "Lidar remote sensing of above-ground biomass in three biomes." *Global ecology and biogeography* 11, no. 5 (2002): 393-399.

MacFaden, S. W., O'Neil-Dunne, J. P., Royar, A. R., Lu, J. W., & Rundle, A. G. (2012). High-resolution tree canopy mapping for New York City using LIDAR and object-based image analysis. Journal of Applied Remote Sensing, 6(1), 063567.

Naesset E., “Airborne laser scanning as a method in operational forest inventory: status of accuracy assessments accomplished in Scandinavia,” Scand. J. Forest Res. 22(5), 433–442 (2007), http://www.tandfonline.com/doi/abs/10.1080/02827580701672147.

Naesset E., “Effects of different sensors, flying altitudes, and pulse repetition frequencies on forest canopy metrics and biophysical stand properties derived from small-footprint airborne laser data” Remote Sensing of Environment. Vol 113. Iss. 1. pgs 148-159. https://doi.org/10.1016/j.rse.2008.09.001

Nilsson, M. (1996). Estimation of tree heights and stand volume using an airborne lidar system. Remote sensing of environment, 56(1), 1-7.

Nowak D. J. and D. E. Crane, "Carbon storage and sequestration by urban trees in the USA," Environ. Pollut. 116(3), 381–389 (2002), http://dx.doi.org/10.1016/S0269-7491 (01)00214-7.

Parker, G. G., Harding, D. J., & Berger, M. L. (2004). A portable LIDAR system for rapid determination of forest canopy structure. Journal of Applied Ecology, 41(4), 755-767.

Peper, P. J., McPherson, E. G., Simpson, J. R., Gardner, S. L., Vargas, K. E., Xiao, Q., & WATT, F. (2007). New York City, New York municipal forest resource analysis. Washington, District of Columbia: Center for Urban Forest Research, United States Department of Agriculture, Forest Service, Pacific Southwest Research Station.

Priestnall G., J. Jaafar, and A. Duncan, "Extracting urban features from LIDAR digital surface models," Comput. Environ. Urban Syst. 24(2), 65–78 (2000), http://dx.doi.org/10 .1016/S0198-9715(99)00047-2.

Reitberger, J., Krzystek, P., & Stilla, U. (2008). Analysis of full waveform LIDAR data for the classification of deciduous and coniferous trees. International journal of remote sensing, 29(5), 1407-1431.

Rottensteiner F., "Automatic generation of high-quality building models from LIDAR data," IEEE Comput. Graph. Applic. 23(6), 42–50 (2003), http://dx.doi.org/10.1109/MCG.2003 .1242381.

Solberg S., "Mapping gap fraction, LAI and defoliation using various ALS penetration variables," Int. J. Rem. Sens. 31(5), 1227–1244 (2010), http://dx.doi.org/10.1080/ 01431160903380672.

Schenk, T. (1999). Digital photogrammetry: Vol. I: Background, fundamentals, automatic orientation produceres. TerraScience.

Takahashi et al., "Stand volume estimation by combining low laser-sampling density LIDAR data with QuickBird panchromatic imagery in closed-canopy Japanese cedar (Cryptomeria japonica) plantations," Int. J. Rem. Sens. 31(5), 1281–1301 (2010), http:// dx.doi.org/10.1080/01431160903380623.

Seischab, F. K., Bernard, J. M., & Eberle, M. D. (1993). Glaze storm damage to western New York forest communities. Bulletin of the Torrey Botanical Club, 64-72.

Wehr A.and U. Lohr, "Airborne laser scanning—an introduction and overview," ISPRS J. Photogramm. Rem. Sens. 54(2–3), 68–82 (1988), http://dx.doi.org/10.1016/S0924-2716 (99)00011-8.

Whitney, H. E., & Johnson, W. C. (1984). Ice storms and forest succession in southwestern Virginia. Bulletin of the Torrey Botanical Club, 429-437.

Chapter 6. Conclusions and Discussion

The utility provided by urban forests in modern cityscapes are well documented and widely accepted. Urban forests provide a wealth of environmental, social, and economic benefits such as improved water quality, air temperature regulation, carbon sequestration, air pollution reduction, enhanced human health, better aesthetics, increased property value, and reduction of energy consumption (Nowak et al., 2007; Peper et al., 2007). To maximize urban forests' benefits many cities and municipalities have implemented programs designed to protect and expand forest canopy cover (DCUFA, 2010; Greenworks, 2009; MTNYC, 2007). To make these programs more effective the current extent and distribution of the urban forest canopy must be accurately known (Locke et al., 2010). Meaning that beyond simply acknowledging the existence of such resources managers and municipalities seek to quantify them in such a manner as they can be more effectively distributed among their users.

6.1 Estimating Urban Tree Canopy Using Terrestrial Laser Scanning

Remote sensing technologies provide the means for such quantification by allowing resources to be measured quickly and indirectly when compared to traditional forest inventory methods. In chapter 3 a local scale ground-based study of several Nuttall oak (*Quercus texana*) trees was performed which relied upon the use of a terrestrial scanning system. This system was used to construct a relatively dense point cloud of 7 trees, each of which were immediately destructively sampled. This sampling included two field measurement methodologies, whole-tree and branch-by-branch. The modification from experiment 1's whole-tree to experiment 2's branch-by-branch approach were based on initial results and statistical examination. Using a whole tree approach the number of observable units were relatively low and did not provide

much analysis beyond comparing linear and volumetric measurements directly. By acquiring the data on a branch-by-branch approach the number of observations can be increased as well as provide information into the distribution of volume throughout the canopy. These results show an average difference between the measurements to be minimal at less than 1% difference in total height and crown base height. Session 1's whole-tree approach yielded digitally measured total heights of 8.4, 8.4, 9.9 meters compared to field measurements of 8.38, 8.41, 9.88 meters. Each of session 2's branch-by-branch approach specimens had digitally measured total heights of 10.7, 10.3, 10.5, and12.2 meters compared to field measured total heights of 10.72, 10.38, 10.50, and 12.21 meters respectively. Or, simply stated, the results show an average difference between the two measurements to be minimal at less than once percentage of difference with respect to each one's linear metrics.

Volumetric measurement results indicate a strong, positive relationship between the manual and digitally acquired measurements. A Pearson correlation coefficient of 0.997 exists between the two with Y(digital) as a predictive measure of X (manual). Also, linear regression analysis shows an R^2 value of 0.99 and is illustrated in Figure 3.1. Totals for all four branch-by-branch approach trees showed the digital measurements underestimated total above-ground biomass by 11% with consistent underestimation for varying size branches. This consistency is perhaps explainable as a function of the scan data not having sufficient coverage of the tops of horizontal branches due to occlusions, a natural limit to ground-based time of flight (TOF) scanning.

Linear measurement results indicate that surface models generated using this algorithm mimic within a percentage point DBH, total height, and crown base height which are the typical field measurements of forest inventory (Avery and Burkhart, 1983). Slightly larger differences

were apparent in crown width measurements but could be due to the inherent difficulty in capturing highly accurate field measurements such as these with standing timber. It appears likely that the measurements taken from the constructed surface model are more accurate than those taken in the field for this reason.

Visual inspection of the surface models in comparison to photography and high resolution point cloud appear to show bridging of gaps within the canopy that are not actually present. This is possibly due to the complex structural nature of a tree's canopy causing a high number of point returns to fall within two spatially disjoined sections of canopy for which the iterative point refining is unable to correctly classify. However, overestimation across this small sample show relative consistency. This consistency in overestimation could prove useful in developing surface model allometric equation correlations. Larger sample sizes are needed to reliably infer these results, but if such a relationship were to exist a standardized modeling algorithm could be developed that gave acceptable surface area and volumetric results without the need for destructive sampling.

These results have shown that the differences between linear measurements are relatively minor when compared to the field methods, and the volumetric measurements are consistently underestimated due to visual occlusions due to line-of-sight restrictions and tree structure. This underestimation's consistency lends itself to the notion that such missing biomass, while not statistically insignificant, can be calibrated into a ground-based scanning workflow based on scan point density. Point density is a function of hardware limitations, proximity to the object(s) being scanned, and canopy conditions present at the time. Further research into these functions could isolated and quantify these drivers of underestimation and provide insight into such a calibration. Also, expansion of these methods into varying age and size classes would provide

more information into the distribution of underestimation. As these results have shown, overestimation using these methods do not present much challenge due to the polyhedron models being scaled up from smaller, less complex, structures, rather than a parsing down of larger objects as in similar studies (Popescu and Zhao, 2008; Hosoi and Omasa, 2006). The major drawback of this kind of dense point cloud model generation is the economic costs associated with gathering such dense point clouds using a stationary scanning system such as the one used in this study. In order gather the required data a field scanning session lasting over 6 hours was needed. At the city scale this would not be desirable due to the large investment in labor, but recent advances in scanning systems would largely mitigate these issues. Mobile terrestrial scanning systems already exist that permit the moving capture of data points in much less time than shown within this study (Herrero-Huerta, Lindenbergh, and Rodríguez-Gonzálvez, 2018). Larger sample sizes are needed to draw further conclusions, but these results also indicate an ability for ground-based scanning to mimic industry standard metrics for biomass measurement without the need for destructive sampling of the area in question. As most urban tree inventory projects are within sensitive sites where such methods are unable to be used, this type of workflow would serve as a timely replacement.

6.2 Tree Estimation Using Matching Oblique Stereoscopic Imagery: A Field Study Approach

In chapter 4 a medium scale project that uses passive sensor camera technology to capture high resolution raster datasets study area encompassing a nearly a city block. The passive sensors in question are oriented in such a manner as to provide a large percentage of image overlap, allowing for the generation of three-dimensional objects via stereoscopic imaging. This is due to the dataset containing a series of five images at each sample coordinate. Four of these

are obliques at ninety degree angles relative to the flight path and the fifth is a nadir perspective image giving a "bird's eye view". Overlapping sections of each image allow for viewing of the same object from multiple perspectives. This, in general, permits imaging software to generate vector point clouds from these raster image files. From these point clouds a model reconstruction each tree is generated. Standard metrics such as total height, dbh, and crown width can then be taken and compared to measurements taken using traditional field methods. Comparing the two datasets, a trend can be seen between the volumes generated via field measurements and those gathered from the digital point cloud. Compared across all species the point cloud generated volumes were within 11.5% by total volume to volumes generated using field data. This percentage represents an underestimation of volume on average by 0.28 cubic meters. To put this into perspective, one of the smallest trees in the study area, tree number 4360, a white oak (Quercus alba) with a DBH of 8.6 inches and total height of 27 feet has an estimated volume of 0.27 cubic meters. For the oak species (*Quercus*) this underestimation shrinks to 8.5% of total volume compared to non-native ornamentals such as Crepe Myrtle (*Lagerstroemia indica*) and Chinese Elm (*Ulmus parvifolia*) which exhibit a total volume underestimation of 15.7%. This distribution of error lends itself to the suspicion of occlusions within the point cloud, as a result of line-of-sight obstructions within the imagery, have obscured a portion of each stem, and smaller ornamentals in particular. Occlusions due to line-of-sight obstructions can be partially mitigated by decreasing the distance between each flight line. This will decrease the Y-axis view angle of each image and permit a larger percentage of the occluded areas to be imaged by the airborne sensor. Also, increasing the frequency of image capture can reduce the X-axis view angle, further mitigating occlusions, but this solution is subject to hardware limitations such as read/write speed, onboard data storage, and camera shutter speed. As these are rapidly advancing

technologies it can be assumed that future studies will be capable of increasing the image capture frequencies presented within this study. Future studies would also likely benefit from increases in spatial, spectral, and radiometric capabilities in passive camera technology, but since these limitations do not appear to be a limiting factor in the study presented here it is difficult to say how far these would go toward increasing the precision of a similar study.

6.3 Measuring Canopy Height Using Airborne LiDAR Scanning: a city-scale approach

Chapter 5 examines a city-scale project that uses airborne LiDAR scanning to map, identify, and measure the individual trees of the study area as well as quantify discrepancies with total height measurements. Data, once captured, can be analyzed using many different techniques. Manual interpretation by the end user to aid in digitizing is one of the easiest ways, but this can lead to a bottleneck in terms of project size and scope due to the time required for such manual analysis. Automated mapping procedures exist to bridge this gap, including geographic object based image analysis (GeOBIA) which allows for automated algorithm construction and execution. This study uses several input datasets captured from varying platforms to map and model overlapping areas of urban forest canopy to achieve image object feature extraction. Specifically, extracting individual trees from the study area in order to assign individual total heights. These height values were taken from the corresponding airborne LiDAR dataset which encompasses the entire study area. Once identified and assigned a total height value a random selection of trees were measured manually using traditional field methods. Results show that the data coincide with an R^2 of 0.97 with an average underestimation of 6.6%. That is, the underestimation of the airborne LiDAR derived total heights when compared to total heights derived using field measurements. This underestimation was not consistently applied throughout the entire data range, however. Further inspection of the data shows trees with lower

total heights, < 12 meters, showed an average underestimation of 8.3% compared to trees over 12 meters with an average underestimation of 5.9%. Examining this further, by comparing softwood species to hardwood species showed that at approximately 12 meters in total height the average underestimation of the two became more similar than for stems at less than 12 meters. Specifically, underestimation of hardwoods and softwoods at less than 12 meters showed an underestimation of 7.6 and 8.7% respectively. For hardwoods and softwoods over 12 meters this shrinks to 5.5 and 6.1% respectively. This appears likely due to the tendency of mature pine canopies to "flatten" into a larger average horizontal area compared to non-mature pines (Avery and Burkhart, 1983). This larger average horizontal area at maximum total height would increase the likelihood of a discrete LiDAR pulse return being correctly captured. Smaller trees with more conical overall shapes would not possess these features and point spacing of the laser scanning system would serve as a direct driver of individual stem height accuracy. This would mean as the average horizontal point spacing of a scanning system decreased the likelihood of a correctly measured discrete LiDAR point would increase. Each scanning project, based on their overall goal, should be oriented so as to minimize this underestimation. Considerations on scanning system style, such as discrete or waveform, as well as airspeed, altitude, and pulse speed should be taken into account and weighed for their cost/benefit as most scanning projects likely are compromises between a host of end-users from various disciplines or municipal departments. In general, a reduction in the airspeed and/or flight altitude will result in an inversely proportional increase in the average horizontal point spacing of any particular scanning system. These assumptions are, of course, predicated on the safe operational parameters of the aircraft as well as federal, state, and local regulations regarding operating altitude over populated areas.

6.4 Sythesis and Future Directions

Airborne LiDAR systems provide a remote sensing platform that can cover large areas in a relatively short period of time. Data can be collected over an area of hundreds of square miles in a matter of days, compared to ground measurement methods which require large crews of workers and cover only a fraction of the same area. These data are not without their limitations, however, since only minimal inference concerning merchantability of the interior bole can be established. This presents a challenge to commercial producers given that merchantability is seen as a necessary metric regarding value, as opposed to municipal managers who are primarily concerned with aboveground biomass, canopy closure, carbon sequestration, etc. For these managers there can be a wealth of information derived from an airborne platform at a relatively low cost when compared to ground measurements. In general, natural resource managers have access to publicly available datasets that include the type of data described here. Many either do not know the urban tree metrics that can be derived from this data or lack the technical skills to implement such a GIS workflow. Using these methods relatively acceptable results can be derived which include stand-level and individual stem level metrics. Future investigations should focus on the generation of automated workflows that require only input datasets without unique customization requirements, such as those shown here. Other possibilities for future investigation include the fusion of active sensor scanning data with passive sensor data from varying angular perspectives, permitting photogrammetric point cloud derivation for additional component identification and measurement.

References

Ackermann, F. (1984). Digital image correlation: performance and potential application in photogrammetry. The Photogrammetric Record, 11(64), 429-439.

Avery, T. and Burkhart, H., (1983), Forest Measurements. McGraw Hill Book Company, New York, New York

Andersen, H. E., Reutebuch, S. E., & McGaughey, R. J. (2006). A rigorous assessment of tree height measurements obtained using airborne lidar and conventional field methods. Canadian Journal of Remote Sensing, 32(5), 355-366.

Baltsavias, E. P. (1999). Airborne laser scanning: existing systems and firms and other resources. ISPRS Journal of Photogrammetry and Remote sensing, 54(2-3), 164-198.

Baker, H. H., & Binford, T. O. (1981). An iterative image registration technique with an application to stereo vision. In Proceedings of the International Joint Conference on Artificial Intelligence.

Benz et al., (2004). "Multi-resolution, object-oriented fuzzy analysis of remote sensing data for GIS-ready information," ISPRS J. Photogramm. Rem. Sens. 58(3–4), 239–258 (2004), http://dx.doi.org/10.1016/j.isprsjprs.2003.10.002.

Birchfield, S., & Tomasi, C. (1999). Depth discontinuities by pixel-to-pixel stereo. International Journal of Computer Vision, 35(3), 269-293.

Blaschke T., (2010) "Object based image analysis for remote sensing," ISPRS J. Photogramm. Rem. Sens. 65(1), 2–16, http://dx.doi.org/10.1016/j.isprsjprs.2009.06.004.

Blood, A., Starr, G., Escobedo, F. J., Chappelka, A., Wiseman, P. E., Sivakumar, R., & Staudhammer, C. L. (2016). Resolving uncertainties in predictive equations for urban tree crown characteristics of the southeastern United States: Local and general equations for common and widespread species. Urban Forestry & Urban Greening, 20, 282-294.

Bradbury et al., (2005) "Modelling relationships between birds and vegetation structure using airborne LIDAR data: a review with case studies from agricultural and woodland environments," Ibis 147(3), 443–452, http://dx.doi.org/10.1111/ibi.2005.147.issue-3.

Brown, Sandra, Andrew JR Gillespie, and Ariel E. Lugo. (1989) "Biomass estimation methods for tropical forests with applications to forest inventory data."*Forest science* 35, no. 4: 881-902.

Bucksch, A. and Lindenbergh, R., , Campino (2008) "a skeletonization method for point cloud processing." ISPRS Journal of Photogrammetry and Remote Sensing, 63, pp. 115–127.

Bucksch, A., Lindenbergh, R. and Meneti, M., (2009). Applications for point cloud skeletonizationin forestry and agriculture. Reports of Geodesy, Special Issue of the IX Konferencji naukowo-technicznej "Aktualne Problemy w Geodezji Inzynieryjne", 87, p. 11

Bucksch, A., Lindenbergh, R. and Meneti, M., , (2010). SkelTre – robust skeleton extractionfrom imperfect point clouds. "Special issue on 3D object retrieval 2009". The Visual Computer, 26, pp. 1283–1300

Bunting P. J. and R. M. Lucas, (2006). "The delineation of tree crowns in Australian mixed species forests using hyperspectral Compact Airborne Spectrographic Imager (CASI) data," Rem.Sens. Environ. 101(2), 230–248, http://dx.doi.org/10.1016/j.rse.2005.12.015.

Chen L., T. Chiang, and T. Teo, (2005). "Fusion of LIDAR and high resolution images for forest canopy modeling," in Proc. 26th Asian Conf. Remote Sensing 2005 Annual Conference, Hanoi, Vietnam

Cheng, Z. L., Zhang, X. P., & Chen, B. Q. (2007). Simple reconstruction of tree branches from a single range image. Journal of computer science and technology, 22(6), 846-858.

City of New York, (2010). "Street tree planting requirements for new buildings," Department of Parks & Recreation, http://www.nycgovparks.org/services/forestry/street-tree-planting-requirements-for-new-buildings (accessed 11/17/16).

Close, R. E., Nguyen, P. V., & Kielbaso, J. J. (1996). Urban vs. natural sugar maple growth: I. Stress symptoms and phenology in relation to site characteristics. *Journal of Arboriculture*, *22*, 144-150.

Coops, N. C., Hilker, T., Wulder, M. A., St-Onge, B., Newnham, G., Siggins, A., & Trofymow, J. T. (2007). Estimating canopy structure of Douglas-fir forest stands from discrete-return LiDAR. Trees, 21(3), 295.

Cote, J.-F., Widlowski, J.-L., Fournier, R.A. and Verstraete, M.M., (2009). The structural and radiative consistency of three-dimensional tree reconstructions from terrestrial LiDAR. Remote Sensing of Environment, 113, pp. 1067–1081

Cowen, D. J., Jensen, J. R., Hendrix, C., Hodgson, M., Schill, S. R., & Macchiaverna, F. (2000). A GIS-assisted rail construction econometric model that incorporates LIDAR data. Photogrammetric Engineering and Remote Sensing, 66(11), 1323-1328.

Dandois, J. P., & Ellis, E. C. (2013). High spatial resolution three-dimensional mapping of vegetation spectral dynamics using computer vision. Remote Sensing of Environment, 136, 259-276.

Danson, F. M., Hetherington, D., Morsdorf, F., Koetz, B., & Allgower, B. (2007). Forest canopy gap fraction from terrestrial laser scanning. IEEE Geoscience and remote sensing letters, 4(1), 157-160.

DC Urban Forestry Administration. (2010). "District of Columbia assessment of urban forest resources and strategy," Urban Forestry Administration, District Department of Transportation, Government of the District of Columbia, http://dc.gov/DC/DDOT/On+Your+Street/Urban+Forestry/DC+Assessment+of+Urban+Forest+Resources+and+Strategy+-+June+2010 (accessed 11/19/17).

Dhond, U. R., & Aggarwal, J. K. (1989). Structure from stereo-a review. IEEE transactions on systems, man, and cybernetics, 19(6), 1489-1510.

Dorren L. K., B. Maier, and A. C. Seijmonsbergen, "Improved Landsat-based forest mapping in steep mountainous terrain using object-based classification," For. Ecol. Manage. 183(1–3), 31–46 (2003), http://dx.doi.org/10.1016/S0378-1127(03)00113-0.

Ebner, H., & Heipke, C. (1988). Integration of digital image matching and object surface reconstruction. International Archives of Photogrammetry and Remote Sensing, 27(B11), 534-545.

Eloy C (2011) Leonardo's rule, self-similarity and wind-induced stresses in trees. Phys Rev Lett 107:1–5. doi: 10.1103/PhysRevLett.107.258101

Enquist B.J. (2002) Universal scaling in tree and vascular plant allometry: toward a general quantitative theory linking plant form and function from cells to ecosystems. Tree Physiol 22:1045–1064

Forstner, W. (1982). On the geometric precision of digital correlation. Int. Arch. Photogrammetry & Remote Sensing, 24(3), 176-189.

Fraser, R. (1997). U.S. Patent No. 5,664,115. Washington, DC: U.S. Patent and Trademark Office.

Fua, P., & Leclerc, Y. G. (1995). Object-centered surface reconstruction: Combining multi-image stereo and shading. International Journal of Computer Vision, 16(1), 35-56.

Furukawa, Y., Curless, B., Seitz, S. M. and Szeliski, R., (2010). Towards internet-scale multi-view stereo. Proceedings of IEEE Conference on Computer Vision and Pattern Recognition, 143: 4–1441.

Gatziolis, D., & Andersen, H. E. (2008). A guide to LIDAR data acquisition and processing for the forests of the Pacific Northwest. Gen. Tech. Rep. PNW-GTR-768. Portland, OR: US Department of Agriculture, Forest Service, Pacific Northwest Research Station. 32 p, 768.

Gaulton R. and T. J. Malthus, (2010) "LIDAR mapping of canopy gaps in continuous cover forests: a comparison of canopy height model and point cloud based techniques," Int. J. Rem. Sens. 31(5), 1193–1211, http://dx.doi.org/10.1080/01431160903380565.

Goesele, M., Snavely, N., Curless, B., Hoppe, H. and Seitz, S. M., (2007). Multi-view stereo for community photo collections. 11th International Conference on Computer Vision, 2: 265–270.

Gower, S. T., & Norman, J. M. (1991). Rapid estimation of leaf area index in conifer and broad-leaf plantations. Ecology, 72(5), 1896-1900.

Gruen, A. (1985). Adaptive least squares correlation: a powerful image matching technique. South African Journal of Photogrammetry, Remote Sensing and Cartography, 14(3), 175-187.

Gruen, A., & Baltsavias, E. P. (1988). Geometrically constrained multiphoto matching. Photogrammetric engineering and remote sensing, 54(5), 633-641.

Hackenberg, Jan, Heinrich Spiecker, Kim Calders, Mathias Disney, and Pasi Raumonen. (2015). "SimpleTree—An Efficient Open Source Tool to Build Tree Models from TLS Clouds." *Forests* 6, no. 11: 4245-4294.

Hartley, R. and Zisserman, A., (2003). Multiple View Geometry in Computer Vision. Second edition. Cambridge University Press, Cambridge, UK.

Herrero-Huerta, M., Lindenbergh, R., & Rodríguez-Gonzálvez, P. (2018). Automatic tree parameter extraction by a Mobile LiDAR System in an urban context. PloS one, 13(4), e0196004.

Hirschmuller, H. (2008). Stereo processing by semiglobal matching and mutual information. IEEE Transactions on pattern analysis and machine intelligence, 30(2), 328-341.

Homer et al., "Completion of the 2001 national land cover database for the conterminous United States," Photogramm. Eng. Rem. Sens. 73(4), 337–341 (2007), http://www.epa.gov/mrlc/pdf/april-07-highlight.pdf.

Haala, N. (2009, September). Comeback of digital image matching. In Photogrammetric Week (Vol. 9, pp. 289-301). Wichmann Verlag Heidelberg.

Hobrough, G. L. (1959). Automatic stereo plotting. Photogrammetric Engineering, 25(5), 763-769.

Hollaus et al., "Growing stock estimation for alpine forests in Austria: a robust LIDAR based approach," Can. J. Forest Res. 39(7), 1387–1400 (2009), http://dx.doi.org/10.1139/X09-042.

Holopainen, M., Kankare, V., Vastaranta, M., Liang, X., Lin, Y., Vaaja, M., ... & Kukko, A. (2013). Tree mapping using airborne, terrestrial and mobile laser scanning–A case study in a heterogeneous urban forest. Urban forestry & urban greening, 12(4), 546-553.

Hopkinson, Chris, Laura Chasmer, Colin Young-Pow, and Paul Treitz. "Assessing forest metrics with a ground-based scanning lidar." *Canadian Journal of Forest Research* 34, no. 3 (2004): 573-583.

Hosoi, F., & Omasa, K. (2006). Voxel-based 3-D modeling of individual trees for estimating leaf area density using high-resolution portable scanning lidar. IEEE transactions on geoscience and remote sensing, 44(12), 3610-3618.

Huang, H., Z. Li, P. Gong, X. Cheng, N. Clinton, C. Cao, W. Ni, L. Wang,. (2011). Automated methods for measuring DBH and tree heights with commercial scanning LiDAR. Photogrammetry Engineering & Remote Sensing. Volume 77 219-227

Hyde et al., (2006) "Mapping forest structure for wildlife habitat analysis using multi-sensor (LIDAR, SAR/InSAR, ETMþ, Quickbird) synergy," Rem. Sens. Environ. 102(1–3), 63–73, http://dx.doi.org/10.1016/j.rse.2006.01.021.

i-Tree., (2010). i-Tree Software Suite v3.1 User's Manual. http://www.itreetools.org/resources/manuals/iTree%20Eco%20Users%20Manual.pdf

Im J., J. R. Jensen, and M. E. Hodgson, (2008). "Object-based land cover classification using highposting-density LIDAR data," GISci. Rem. Sens. 45(2), 209–228, http://dx.doi.org/ 10.2747/1548-1603.45.2.209.

Jacquin A., L. Misakova, and M. Gay, (2008) "A hybrid object-based classification approach for mapping urban sprawl in periurban environment," Landsc. Urban Plan. 84(2), 152–165 , http://dx.doi.org/10.1016/j.landurbplan.2007.07.006.

Jones, T., Marzen, L., & Chappelka, A. (2016). Mapping, Modeling, and Estimating Tree Measurements of Urban Tree Canopy Structure Using Terrestrial LiDAR Scanning. Papers in Applied Geography, 2(2), 236-242.

Kalarot, R., Morris, J., Berry, D., & Dunning, J. (2011). Analysis of real-time stereo vision algorithms on GPU. In International Conference on Image and Vision Computing New Zealand (IVCNZ).

Kato et al., (2009).Capturing tree crown formation through implicit surface reconstruction using airborn lidar data. Remote Sensing of Environment, 113(6): 1148-1162

Kersten, T. P., & Lindstaedt, M. (2012, October). Image-based low-cost systems for automatic 3D recording and modelling of archaeological finds and objects. In Euro-Mediterranean Conference (pp. 1-10). Springer, Berlin, Heidelberg.

Koch, A., U. Heyder and H. Weinacker, (2006). Detection of Individual Tree Crowns in Airborn Lidar Data. Photogrammetric Engineering & Remote Sensing, 72(4): 357-363

Kolmogorov, V. (2006). Convergent tree-reweighted message passing for energy minimization. IEEE transactions on pattern analysis and machine intelligence, 28(10), 1568-1583.

Konijnendijk, C.C., Nillsson, K., Randrup, T. and Schipperijn, J., (2005). Urban Forests and Trees: A Reference Book (Berlin/Heidelberg: Springer)

Koutsoudis, A., Vidmar, B., Ioannakis, G., Arnaoutoglou, F., Pavlidis, G., & Chamzas, C. (2014). Multi-image 3D reconstruction data evaluation. Journal of Cultural Heritage, 15(1), 73-79.

Kwak, D. A., W.K. Lee, J.H. Lee, G. Biging and P. Gong, , Detection of individual trees and estimation of tree height using LiDAR data. Journal of Forest Research, 12(6): 425-434 (2007).

Laliberte et al., (2004) "Object-oriented image analysis for mapping shrub encroachment from 1937 to 2003 in southern New Mexico," Rem. Sens. Environ. 93(1–2), 198–210 , http://dx.doi.org/10.1016/j.rse.2004.07.011.

Leberl, F., Irschara, A., Pock, T., Meixner, P., Gruber, M., Scholz, S., & Wiechert, A. (2010). Point clouds. Photogrammetric Engineering & Remote Sensing, 76(10), 1123-1134.

Lefsky, Michael A., Warren B. Cohen, David J. Harding, Geoffrey G. Parker, Steven A. Acker, and S. Thomas Gower. "Lidar remote sensing of above-ground biomass in three biomes." *Global ecology and biogeography* 11, no. 5 (2002): 393-399.

Lim, K., Treitz, P., Wulder, M., St-Onge, B., & Flood, M. (2003). LiDAR remote sensing of forest structure. Progress in physical geography, 27(1), 88-106.

Lin, Yi, and Martin Herold. "Tree species classification based on explicit tree structure feature parameters derived from static terrestrial laser scanning data." *Agricultural and Forest Meteorology* 216 (2016): 105-114.

Lisein, J., Pierrot-Deseilligny, M., Bonnet, S., & Lejeune, P. (2013). A photogrammetric workflow for the creation of a forest canopy height model from small unmanned aerial system imagery. Forests, 4(4), 922-944.

Locke et al., "Prioritizing preferable locations for increasing urban tree canopy in New York City," Cities. Environ. 3(1), 1–18 (2010), http://escholarship.bc.edu/cate/vol3/iss1/4.

Lovell, J., D. Jupp, G. Newnham, D. Culvenor, 2011, Measuring tree stem diameters using intensity profiles from ground-based scanning LiDAR from a fixed viewpoint. ISPRS Journal of Photogrammetry and Remote Sensing. Volume 77 pp. 219-227

Lucas et al., "Rule-based classification of multi-temporal satellite imagery for habitat and agricultural land cover mapping," ISPRS J. Photogramm. Rem. Sens. 62(3), 165–185 (2007), http://dx.doi.org/10.1016/j.isprsjprs.2007.03.003.

Maas, H. G. (1996). Automatic DEM generation by multi-image feature based matching. International Archives of Photogrammetry and Remote Sensing, 31, 484-489.

MacFaden, S. W., O'Neil-Dunne, J. P., Royar, A. R., Lu, J. W., & Rundle, A. G. (2012). High-resolution tree canopy mapping for New York City using LIDAR and object-based image analysis. Journal of Applied Remote Sensing, 6(1), 063567.

Maier B., D. Tiede, and L. Dorren, "Characterizing mountain forest structure using landscape metrics on LIDAR-based canopy surface models," Chapter 7.2 in Object Based Image Analysis, T.Blaschke, S. Lang, and G. J. Hay, Eds., pp. 625–644, Springer-Verlag, Berlin (2008).

Makela A, Valentine H.T. (2006) Crown ratio influences allometric scaling in trees. Ecology 87(12):2967–2972

Marr, D. (1982). Vision: A Computational Investigation Into. WH Freeman.

Marr, D., & Poggio, T. (1976). Cooperative computation of stereo disparity. Science, 194(4262), 283-287.

Martin, N.A., A.H. Chappelka, G. J. Keever, and E.F. Loewenstein. 2011, A 100% tree inventory using i-Tree Eco protocol: A case study at Auburn University, Alabama. Arbor. & Urban For. 37: 207-212.

Martin, N.A., A.H. Chappelka, E.F. Loewenstein G.J. Keever and G. Somers. 2012, Predictive open-grown crown width equations for three oak species planted in a southern urban locale Arbor.& Urban For. 38: 57-62.

MacFarlane, D.W., Kuyah, S., Mulia, R., Dietz, J., Muthuri, C., and Van Noordwijk, M. 2014. Evaluating a non-destructive method for calibrating tree biomass equations derived from tree branching architecture. Trees: Structure and Function. DOI 10.1007/s00468-014-0993-2

Moeller M. S. and T. Blaschke, "Monitoring LULC dynamics in the urban-rural fringe," in Anais XII Simposio Brasileiro de Sensoriamento Remoto, April 16–21, 2005, pp. 3821–3828, Instituto Nacional de Pesquisas Espaciais (INPE), Goiania, Brazil (2005).

Moeller M. S. and T. Blaschke, "A new index for the differentiation of vegetation fractions in urban neighborhoods based on satellite imagery," in Am. Soc. Photogramm. Remote Sensing 2006 Annual Conference, Reno, Nevada, May 1–5, 2006, 7 p (2006).

Montealegre, A. L., Lamelas, M. T., & de la Riva, J. (2015). A comparison of open-source LiDAR filtering algorithms in a mediterranean forest environment. IEEE Journal of Selected Topics in Applied Earth Observations and Remote Sensing, 8(8), 4072-4085.

Myeong et al., "Urban cover mapping using digital, high-spatial resolution aerial imagery," Urban Ecosyst. 5(4), 243–256 (2001), http://dx.doi.org/10.1023/A:1025687711588.

Narayanan, P. J., Rander, P. W., & Kanade, T. (1998, January). Constructing virtual worlds using dense stereo. In Computer Vision, 1998. Sixth International Conference on (pp. 3-10). IEEE.

Naesset E., "Airborne laser scanning as a method in operational forest inventory: status of accuracy assessments accomplished in Scandinavia," Scand. J. Forest Res. 22(5), 433–442 (2007), http://www.tandfonline.com/doi/abs/10.1080/02827580701672147.

Naesset E., "Effects of different sensors, flying altitudes, and pulse repetition frequencies on forest canopy metrics and biophysical stand properties derived from small-footprint airborne laser data" Remote Sensing of Environment. Vol 113. Iss. 1. pgs 148-159. https://doi.org/10.1016/j.rse.2008.09.001

Nilsson, M. (1996). Estimation of tree heights and stand volume using an airborne lidar system. Remote sensing of environment, 56(1), 1-7.

Nowak D. J. and D. E. Crane, "Carbon storage and sequestration by urban trees in the USA," Environ. Pollut. 116(3), 381–389 (2002), http://dx.doi.org/10.1016/S0269-7491 (01)00214-7.

Ohta, Y., & Kanade, T. (1985). Stereo by intra-and inter-scanline search using dynamic programming. IEEE Transactions on pattern analysis and machine intelligence, (2), 139-154.

Okutomi, M., & Kanade, T. (1993). A multiple-baseline stereo. IEEE Transactions on pattern analysis and machine intelligence, 15(4), 353-363.

Opitz, S., Wünnemann, B., Aichner, B., Dietze, E., Hartmann, K., Herzschuh, U., ... & Plotzki, A. (2012). Late Glacial and Holocene development of Lake Donggi Cona, north-eastern Tibetan Plateau, inferred from sedimentological analysis. Palaeogeography, Palaeoclimatology, Palaeoecology, 337, 159-176.

Parker, G. G., Harding, D. J., & Berger, M. L. (2004). A portable LIDAR system for rapid determination of forest canopy structure. Journal of Applied Ecology, 41(4), 755-767.

Pascual et al., "Object-based semi-automatic approach for forest structure characterization using LIDAR data in heterogeneous Pinus sylvestris stands," For. Ecol. Manage. 255(11), 3677–3685 (2008), http://dx.doi.org/10.1016/j.foreco.2008.02.055.

Peper, P. J., McPherson, E. G., Simpson, J. R., Gardner, S. L., Vargas, K. E., Xiao, Q., & WATT, F. (2007). New York City, New York municipal forest resource analysis. Washington, District of Columbia: Center for Urban Forest Research, United States Department of Agriculture, Forest Service, Pacific Southwest Research Station.

Pickle, A, 21st Century Water Asset Accounting: Case Studies Report. Nicholas Institute for Environmental Policy Solutions. ISBN: 9781780405124

Pfeifer, N., Gorte, B., & Winterhalder, D. (2004, July). Automatic reconstruction of single trees from terrestrial laser scanner data. In Proceedings of 20th ISPRS Congress (pp. 114-119). Istanbul: ISPRS.

Pollefeys, M. et al., Detailed real-time urban 3D reconstruction from video. International Journal of Computer Vision, 78(2–3): 143–167. (2008)

Popescu, S., R. Wynne, R. Nelson, 2003, Measuring Individual Tree Crown Diameter with LiDAR and Assessing its Influence on Estimating Forest Volume and Biomass. Canadian Journal of Remote Sensing, doi: 10.5589/m03-027

Popescu, S., 2007, Estimating biomass of individual trees using airborne LiDAR. Biomass and Bioenergy, Vol. 31 Issue 9 pp. 646-655

Priestnall G., J. Jaafar, and A. Duncan, "Extracting urban features from LIDAR digital surface models," Comput. Environ. Urban Syst. 24(2), 65–78 (2000), http://dx.doi.org/10 .1016/S0198-9715(99)00047-2.

Quackenbush L. J., P. F. Hopkins, and G. J. Kinn, "Developing forestry products from high resolution digital aerial imagery," Photogramm. Eng. Rem. Sens. 66(11), 1337–1346 (2000), http://asprs.org/a/publications/pers/2000journal/November/2000_nov_1337-1346 .pdf.

Reitberger, J., Krzystek, P., & Stilla, U. (2008). Analysis of full waveform LIDAR data for the classification of deciduous and coniferous trees. International journal of remote sensing, 29(5), 1407-1431.
Remondino, F., Del Pizzo, S., Kersten, T. P., & Troisi, S. (2012). Low-cost and open-source solutions for automated image orientation–A critical overview. In Euro-Mediterranean Conference (pp. 40-54). Springer, Berlin, Heidelberg.

Rogan J. and D. M. Chen, "Remote sensing technology for mapping and monitoring landcover and land-use change," Progr. Plan. 61(4), 301–325 (2004), http://www.clarku.edu/ departments/geography/pdfs/Rogan %26 Chen 2004.pdf Chen 2004.pdf.

Rosnell, T., & Honkavaara, E. (2012). Point cloud generation from aerial image data acquired by a quadrocopter type micro unmanned aerial vehicle and a digital still camera. Sensors, 12(1), 453-480.

Rottensteiner F., "Automatic generation of high-quality building models from LIDAR data," IEEE Comput. Graph. Applic. 23(6), 42–50 (2003), http://dx.doi.org/10.1109/MCG.2003 .1242381.

Roy, S., & Cox, I. J. (1998). A maximum-flow formulation of the n-camera stereo correspondence problem. In Computer Vision, 1998. Sixth International Conference on (pp. 492-499). IEEE.

Schenk, T. (1999). Digital photogrammetry: Vol. I: Background, fundamentals, automatic orientation produceres. TerraScience.

Scholz, S., & Gruber, M. (2008). Radiometric Quality of UltraCam Images. In Proceedings of the 21st ISPRS Congress Beijing 2008, International Archives of Photogrammetry, Remote Sensing and Spatial Information Sciences (pp. 1682-1750).

Schroeder, P., Brown, S., Mo, J., Birdsey, R. and Cieszewski, C., 1997. Biomass estimation for temperate broadleaf forests of the United States using inventory data. *Forest Science*, *43*(3), pp.424-434.

Seischab, F. K., Bernard, J. M., & Eberle, M. D. (1993). Glaze storm damage to western New York forest communities. Bulletin of the Torrey Botanical Club, 64-72.

Shan, Q., Adams, R., Curless, B., Furukawa, Y. and Sietz, S. M., 2013. The visual Turing test for scene reconstruction. Vision Conference., 3D: 25–32

Shinozaki K, Yoda K, Hozumi K, Kira T (1964a) A quantitative analysis of plant form—the pipe model theory I. Basic analysis. Jpn J Ecol 14:97–105

Shlyakhter, I., M. Rozenoer, u. Doresey and S. Teller, 2001, Reconstructing 3D tree models from instrumented photographs. IEEE Computer Graphics and Applications, 21(3): 53-61

Simonse, M., Aschoff, T., Spiecker, H., & Thies, M. (2003, September). Automatic determination of forest inventory parameters using terrestrial laser scanning. In Proceedings of the scandlaser scientific workshop on airborne laser scanning of forests (Vol. 2003, pp. 252-258).

Snavely, N., Seitz, S. M. and Szeliski, R.,. Modeling the world from Internet photo collections. International Journal of Computer Vision, 80(2): 189–210 (2008).

Solberg S., "Mapping gap fraction, LAI and defoliation using various ALS penetration variables," Int. J. Rem. Sens. 31(5), 1227–1244 (2010), http://dx.doi.org/10.1080/01431160903380672.

Sonka, M., Hlavac, V., & Boyle, R. (2014). Image processing, analysis, and machine vision. Cengage Learning.

Suarez et al., "Use of airborne LIDAR and aerial photography in the estimation of individual tree heights in forestry," Comput. Geosci. 31(2), 253–262 (2005), http://dx.doi.org/10.1016/j.cageo.2004.09.015.

Syed S., P. Dare, and S. Jones, "Automatic classification of land cover features with high resolution imagery and LIDAR data: an object-oriented approach," in Proc. SSC2005 Spatial Intelligence, Innovation and Praxis: The National Biennial Conference of the Spatial Sciences Institute, September 2005, Melbourne, Australia, pp. 512–522

(2005).

Szeliski, R., Uyttendaele, M., & Steedly, D. (2011, April). Fast poisson blending using multi-splines. In Computational Photography (ICCP), 2011 IEEE International Conference on (pp. 1-8). IEEE.

Takahashi et al., "Stand volume estimation by combining low laser-sampling density LIDAR data with QuickBird panchromatic imagery in closed-canopy Japanese cedar (Cryptomeria japonica) plantations," Int. J. Rem. Sens. 31(5), 1281–1301 (2010), http://dx.doi.org/10.1080/01431160903380623.

Tan, P. J., Dowe, D. L., & Dix, T. I. (2007, December). Building classification models from microarray data with tree-based classification algorithms. In Australasian Joint Conference on Artificial Intelligence (pp. 589-598). Springer, Berlin, Heidelberg.

Tansey, K., N. Selmes, A. Anstee, N. Tate, A. Denniss. 2009, Estimating tree and stand variables in a Corsican pine woodland from terrestrial laser scanner data. International Journal of Remote Sensing. Volume 30 pp. 5195-5209

Tao, G. and Y Yasuoka, 2002, Combining high resolution satellite imagery and airborne laser scanning dat for generating bareland DEM in urban areas. International Archives of the Photogrammetry, Remote Sensing and Spatial Information Sciences, 30.

Teng, C. and Y. Chen, 2009, Image-based tree modeling from a few images with very narrow viewing range. The Visual Computer, 25(4):297-307.

Tinkham, W. T., Huang, H., Smith, A., Shrestha, R., Falkowski, M. J., Hudak, A. T., ... & Marks, D. G. (2011). A comparison of two open source LiDAR surface classification algorithms. Remote Sensing, 3(3), 638-649.

Van Noordwijk M, Mulia R (2002) Functional branch analysis as tool for fractal scaling above- and belowground trees for their additive and non-additive properties. Ecol Model 149:41–51

Wallace, L., Lucieer, A., Malenovský, Z., Turner, D., & Vopěnka, P. (2016). Assessment of forest structure using two UAV techniques: A comparison of airborne laser scanning and structure from motion (SfM) point clouds. Forests, 7(3), 62.

Wang, K., Ming, Z., & Chua, T. S. (2009). A syntactic tree matching approach to finding similar questions in community-based qa services. In Proceedings of the 32nd international ACM SIGIR conference on Research and development in information retrieval (pp. 187-194). ACM.

Watt, P., D. Donoghue, 2005, Measuring forest structure with terrestrial laser scanning. International Journal of Remote Sensing, 26 pp. 1437-1446

Wehr A.and U. Lohr, “Airborne laser scanning—an introduction and overview,” ISPRS J. Photogramm. Rem. Sens. 54(2–3), 68–82 (1988), http://dx.doi.org/10.1016/S0924-2716 (99)00011-8.

West GB, Brown JH, Enquist BJ (1999) A general model for the structure and allometry of plant vascular systems. Nature 400:664–667

Whitney, H. E., & Johnson, W. C. (1984). Ice storms and forest succession in southwestern Virginia. Bulletin of the Torrey Botanical Club, 429-437.

Wrobel, B. (1987). Facets stereo vision (FAST vision)—a new approach to computer stereo vision and to digital photogrammetry. In ISPRS Intercommission Conf. Fast Processing of Photogrammetric Data (pp. 231-258).

Xiangyu Wang, Heap-Yih Chong, 2015 "Setting new trends of integrated Building Information Modelling (BIM) for construction industry", Construction Innovation, Vol. 15 Issue: 1, pp.2-6, https://doi.org/10.1108/CI-10-2014-0049

Yao, T., X. Yang, F. Zhao, Z. Wang, Q. Zhang, D. Jupp, J. Lovell, D. Culvenor, G. Newnham, W. Ni-Meister, 2011, Measuring forest structure and biomass in New England forest stands using echidna ground-based LiDAR. Remote Sensing of Environment, Volume 115 pp. 2965-2974.

Zhang, Y. J. (1996). A survey on evaluation methods for image segmentation. Pattern recognition, 29(8), 1335-1346.

Appendix

i-Tree Eco (UFORE) Species Code List

SppCode	Genus	Species Name	Common Name
AB	Abies		fir spp
AB1	Abelia		abelia spp
AB3	Abutilon		Indian mallow spp
ABAL	Adonidia	alba	Silver fir
ABAL3	Abies	alba	European silver fir
ABAM	Abies	amabilis	Pacific silver fir
ABBA	Abies	balsamea	Balsam fir
ABBE	Abutilon	berlandieri	Berlandier indian mallow
ABBO	Abies	borisii-regis	Bulgarian fir
ABBR	Abies	bracteata	Bristlecone fir
ABCH	Abelia	chinensis	Abelia
ABCO	Abies	concolor	White fir
ABER	Abutilon	eremitopetalum	Hiddenpetal indian mallow
ABFR	Abies	fraseri	Fraser fir
ABGR	Abies	grandis	Grand fir
ABGR3	Abutilon	grandifolium	Hairy indian mallow
ABGR4	Abelia	x grandiflora	Glossy abelia
ABHO	Abies	holophylla	Manchurian fir
ABHO2	Abies	homolepis	Japanese fir
ABLA	Abies	lasiocarpa	Subalpine fir
ABLO	Abies	concolor v lowiana	Sierra white fir
ABMA	Abies	magnifica	California red fir
ABME2	Abutilon	menziesii	Ko'oloa 'ula
ABNO	Abies	nordmanniana	Nordman fir
ABPA	Abutilon	palmeri	Palmer's indian mallow
ABPH	Abies	x phanerolepis	Bracted balsam fir
ABPI	Abies	pinsapo	Abeto de espaÑa
ABPR	Abies	procera	Noble fir
ABSA2	Abutilon	sandwicense	Greenflower indian mallow
ABSH	Abies	x shastensis	Shasta red fir
ABVI2	Abutilon	virginianum	Van dyke's indian mallow
AC	Acer		maple spp
AC1	Acokanthera		acokanthera spp
AC10	Acrocomia		acrocomia spp
AC2	Acalypha		copperleaf spp

AC3	Acca		acca spp
AC5	Achyranthes		chaff flower spp
AC7	Acnistus		acnistus spp
AC8	Acoelorrhaphe		Paurotis palm spp
ACAM2	Acalypha	amentacea	Match me if you can
ACAN	Acacia	aneura	Mulga
ACAN4	Acacia	anegadensis	Blackbrush wattle
ACAR	Acnistus	arborescens	Hollowheart
ACAT	Achyranthes	atollensis	Hawai'i chaff flower
ACAU	Acacia	auriculaeformis	Earleaf acacia
ACBA	Acer	barbatum	Florida maple

ACBA2	Acacia	baileyana	Bailey acacia
ACBE	Acacia	berlandieri	Guajillo
ACBE2	Acalypha	berteriana	Berteron acalypha
ACBI	Acacia	binervia	Coast Mayll
ACBI3	Acalypha	bisetosa	Streambank copperleaf
ACBU	Acer	buergerianum	Trident maple
ACCA	Acer	campestre	Hedge maple
ACCA1	Acacia	cardiophylla	Wyalong wattle
ACCA2	Acacia	caven	Roman cassie
ACCAQU	Acer	campestre 'Queen Elizabeth'	Queen eliz hedge maple
ACCH	Acacia	choriophylla	Cinnecord
ACCI	Acer	circinatum	Vine maple
ACCO	Acacia	confusa	Small philippine acacia
ACCO2	Acacia	constricta	Whitethorn acacia
ACCO5	Acacia	cornigera	Bullhorn wattle
ACCY2	Acacia	cyclops	Cyclops acacia
ACDE	Acacia	decurrens	Green acacia
ACDE3	Acacia	dealbata	Silver wattle
ACEL	Acacia	elata	Cedar wattle
ACFA	Acacia	farnesiana	Sweet acacia
ACFI	Acacia	fimbriata	Fringed Wattle
ACFL	Acacia	floribunda	Gossamer wattle
ACFR	Acer	x freemanii	Freeman maple
ACFRJE	Acer	x freemanii jeffersred	Autumn blaze
ACGI	Acer	ginnala	Amur maple
ACGL	Acer	glabrum	Rocky mountain maple
ACGR	Acer	griseum	Paperbark maple
ACGR2	Acacia	greggii	Catclaw acacia
ACGR3	Acer	grandidentatum	Bigtooth maple
ACHI2	Acalypha	hispida	Bristly copperleaf
ACHO	Acacia	howittii	Sticky Wattle
ACIM	Acacia	implexa	Lightwood
ACIR	Acacia	irrorata	Green Wattle
ACIT	Acacia	iteaphylla	Flinders range wattle
ACJA2	Acer	japonicum	Fullmoon maple
ACKO	Acacia	koa	Koa
ACKO2	Acacia	koaia	Koaoha
ACLE	Acer	leucoderme	Chalk maple
ACLE1	Acacia	leucoclada	Northern Silver Wattle
ACLI	Acacia	linifolia	Flax-leaved Wattle
ACLO	Acacia	longifolia	Sydney golden wattle
ACLOLO	Acacia	longifolia longifolia	Sallow wattle
ACLOSO	Acacia	longifolia sophorae	Coastal wattle
ACMA	Acer	macrophyllum	Bigleaf maple
ACMA1	Acacia	maidenii	Maiden's Wattle

ACMA2	Acacia	macracantha	Porknut
ACME	Acacia	melanoxylon	Blackwood
ACME2	Acacia	mellifera	Black thorn acacia
ACME3	Acrocomia	media	Corozo
ACME80	Acacia	mearnsii	Black wattle
ACMI	Acacia	millefolia	Milfoil wattle
ACMO	Acer	mono	Painted maple
ACMO1	Acer	monspessulanum	Montpelier Maple
ACMU	Acacia	muricata	Spineless wattle
ACMU2	Achyranthes	mutica	Blunt chaff flower
ACNE	Acer	negundo	Boxelder
ACNE4	Acacia	neovernicosa	Viscid acacia
ACNI	Acer	nigrum	Black maple
ACNI2	Acacia	nilotica	Gum arabic tree
ACNI3	Acacia	nigrescens	Knob thorn
ACOB	Acer	oblongum	Evergreen maple
ACOB1	Acokanthera	oblongifolia	Dune poison bush
ACPA	Acer	palmatum	Japanese maple
ACPA1	Acacia	parvipinnula	Silver Stemmed Wattle
ACPA8	Acacia	paradoxa	Paradox acacia
ACPA81	Acacia	parramattensis	South wales wattle
ACPADI	Acer	palmatum 'Dissectum'	Lace-leaf maple
ACPE	Acer	pensylvanicum	Striped maple
ACPE1	Acacia	pendula	Weeping myall
ACPI	Acacia	pinetorum	Pineland wattle
ACPL	Acer	platanoides	Norway maple
ACPLCK	Acer	platanoides 'Crimson King'	Crimson king norway maple
ACPLCO	Acer	platanoides 'Columnare'	Columnar maple
ACPLFA	Acer	platanoides 'Fairview'	Fairview norway maple
ACPLQE	Acer	platanoides 'Queen Eliz'	Queen eliz norway maple
ACPLSC	Acer	platanoides 'Schwedleri'	Schwedleri norway maple
ACPO2	Acacia	podalyriifolia	Pearl wattle
ACPO3	Acacia	polyacantha	Catechu tree
ACPO4	Acalypha	portoricensis	Puerto rico copperleaf
ACPR	Acacia	pravissima	Ovens wattle
ACPR1	Acacia	prominens	Golden Rain Wattle
ACPS	Acer	pseudoplatanus	Sycamore maple
ACPS1	Acer	pseudosieboldianum	Korean maple
ACPSSP	Acer	pseudoplatanus 'Spaethii'	Spaethii sycamore maple
ACPY3	Acacia	pycnantha	Golden wattle
ACRE	Acacia	recifiens	Acacia recifiens

ACRE2	Acacia	retinodes	Water wattle
ACRE4	Acacia	retusa	Catch and keep
ACRE9	Acacia	redolens	Bank catclaw
ACRI	Acacia	rigidula	Blackbrush acacia
ACRO	Acacia	roemeriana	Roundflower catclaw
ACRU	Acer	rubrum	Red maple
ACRU1	Acacia	rubida	Red-stem Wattle
ACRUAR	Acer	rubrum 'Armstrong'	Scarlet maple
ACRUGR	Acer	rubrum 'Gerling'	Gerling red maple
ACRUMO	Acer	rubrum 'Morgan'	Morgan red maple
ACRUOC	Acer	rubrum 'October glory'	October glory red maple
ACRURS	Acer	rubrum 'Red Sunset'	Red sunset red maple
ACSA	Acacia	saligna	Orange wattle
ACSA1	Acer	saccharinum	Silver maple
ACSA2	Acer	saccharum	Sugar maple
ACSA2GR	Acer	saccharum 'Green Mountain'	Green mtn sugar maple
ACSA3	Acacia	salicina	Willow acacia
ACSC	Acacia	schottii	Schott's wattle
ACSC2	Acacia	schaffneri	Schaffner's wattle
ACSE	Acacia	semperflorens	Aromo en flor
ACSE2	Acca	sellowiana	Feijoa
ACSP	Acer	spicatum	Mountain maple
ACSP1	Acacia	spectabilis	Mudgee Wattle
ACSP2	Acacia		acacia spp
ACSP3	Achyranthes	splendens	Maui chaff flower
ACSP4	Acacia	sphaerocephala	Bee wattle
ACST	Acacia	stenophylla	Shoestring acacia
ACSU	Acacia	suaveolens	Sweet Wattle
ACTA	Acer	tataricum	Tatar maple
ACTE	Acacia	terminalis	Sunshine Wattle
ACTO	Acacia	tortuosa	Twisted acacia
ACTO2	Acacia	tortilis	Umbrella thorn
ACTO5	Acrocomia	totai	Grugru palm
ACTR	Acer	truncatum	Purple blow maple
ACTR1	Acer	triflorum	Three-flower maple
ACVE	Acacia	verniciflua	Varnish wattle
ACVE2	Acacia	verticillata	Prickly moses
ACVI	Acacia	visco	Acacia visco
ACVI2	Acrocomia	vinifera	Coyol palm
ACVO	Acacia	vogeliana	Macata bourse bastard
ACWI	Acalypha	wilkesiana	Copperleaf
ACWR	Acoelorraphe	wrightii	Paurotis palm
ACWR2	Acacia	greggii v wrightii	Wright acacia
AD1	Adansonia		adansonia spp

AD2	Adelia		wild lime spp
AD3	Adenanthera		beadtree spp
AD5	Adenostoma		chamise spp
AD6	Adolphia		prickbush spp
AD7	Adonidia		Adonidia spp
ADCA2	Adolphia	californica	California prickbush
ADDI3	Adansonia	digitata	Baobab
ADFA	Adenostoma	fasciculatum	Chamise
ADIN	Adolphia	infesta	Junco
ADME	Adonidia	merrilli	Manilla palm
ADPA	Adenanthera	pavonina	Red beadtree
ADRI	Adelia	ricinella	Wild lime
ADSP	Adenostoma	sparsifolium	Redshank
ADVA	Adelia	vaseyi	Vasey's wild lime
AE	Aesculus		buckeye spp
AE1	Aegiphila		spiritweed spp
AE2	Aeonium		aeonium spp
AEBU	Aesculus	x bushii	Bush's chesnut
AECA	Aesculus	x carnea	Red horsechestnut
AECA2	Aesculus	californica	California buckeye
AECABR	Aesculus	x carnea 'Briottii'	Briottii horsechestnut
AECAST	Aesculus	x carnea 'Stafford'	Stafford red hrsechestnut
AECH	Aesculus	chinensis	Aesculus chinensis
AEEL	Aegiphila	elata	Tall spiritweed
AEFL	Aesculus	flava	Yellow buckeye
AEGL	Aesculus	glabra	Ohio buckeye
AEHA2	Aeonium	haworthii	Haworth's aeonium
AEHI	Aesculus	hippocastanum	Horsechestnut
AEHY	Aesculus	x hybrida	Hybrid chesnut
AEIN5	Aegiphila	integrifolia	Entireleaf spiritweed
AEMA	Aegiphila	martinicensis	Caribbean spiritweed
AEMA2	Aesculus	x marylandica	Maryland chesnut
AEMU	Aesculus	x mutabilis	Chesnut
AENE	Aesculus	x neglecta	Dwarf buckeye
AEPA	Aesculus	pavia	Red buckeye
AEPA2	Aesculus	parviflora	Bottlebrush buckeye
AESY	Aesculus	sylvatica	Painted buckeye
AEWO	Aesculus	x worlitzensis	Aesculus x worlitzensis
AF	Afrormosia		afromosia spp
AF1	Afrocarpus		afrocarpus spp
AFFA	Afrocarpus	falcatus	Outeniqua yellowwood
AFLA	Afrormosia	laxiflora	Afrormosia laxiflora
AG	Agathis		agathis spp
AG1	Agarista		Florida hobblebush spp
AG2	Agrostis		bentgrass spp
AG3	Agonis		agonis spp
AG4	Ageratina		snakeroot spp

AGAU	Agathis	australis	Kauri
AGCU	Agrostis	curtisii	Bristle bent
AGFL	Agonis	flexuosa	Peppermint tree
AGHA4	Ageratina	havanensis	Havana snakeroot
AGLA	Agathis	lanceolata	Koghis kauri
AGMA	Agathis	macrophylla	Pacific kauri
AGPO2	Agarista	populifolia	Florida hobblebush
AGRE3	Ageratina	resiniflua	Resinous snakeroot
AGRO	Agathis	robusta	Queensland kauri
AI1	Ailanthus		ailanthus spp
AI2	Aiphanes		aiphanes spp
AIAL	Ailanthus	altissima	Tree of heaven
AIMI	Aiphanes	minima	Guinea bactris
AL	Alnus		alder spp
AL1	Albizia		albizia spp
AL10	Alloxylon		alloxylon spp
AL11	Alchornea		alchornea spp
AL12	Aloysia		beebrush spp
AL13	Alphitonia		alphitonia spp
AL15	Alsophila		alsophila spp
AL16	Alstonia		alstonia spp
AL18	Alvaradoa		alvaradoa spp
AL2	Alchorneopsis		alchorneopsis spp
AL3	Alectryon		alectryon spp
AL4	Allocasuarina		allocasuarina spp
AL5	Aleurites		aleurites spp
AL6	Alhagi		alhagi spp
AL7	Allamanda		allamanda spp
AL8	Aloe		aloe spp
AL9	Allophylus		allophylus spp
ALAC	Alnus	acuminata	Mexican Alder
ALAD	Albizia	adinocephala	Cream albizia
ALAM	Alvaradoa	amorphoides	Mexican alvaradoa
ALAM5	Alsophila	amintae	Forest alsophila
ALAR	Aloe	arborescens	Tree aloe
ALBL	Allamanda	blanchetii	Purple allamanda
ALBR4	Alsophila	bryophila	Helecho gigante de sierra
ALCA8	Albizia	carbonaria	Naked albizia
ALCH2	Albizia	chinensis	Chinese albizia
ALCO	Alchornea	cordifolia	Iporuru
ALCO2	Alnus	cordata	Italian alder
ALCR9	Allophylus	crassinervis	Palo blanco
ALDI	Allocasuarina	distyla	Shrubby She-oak
ALED	Allophylus	edulis	Chal-chal
ALEX	Alectryon	excelsus	Titoki
ALEX1	Alphitonia	excelsa	Red Ash
ALFA	Albizia	moluccana	Moluca albizia

ALFA4	Alnus	x fallacina	Alder
ALFE	Albizia	ferruginea	Albizia
ALFL	Alloxylon	flammeum	Red Silky Oak
ALFL3	Alchorneopsis	floribunda	Palo de gallina
ALFO	Aleurites	fordi	Tung oil tree
ALGL	Alnus	glutinosa	European alder
ALGR2	Aloysia	gratissima	Whitebrush
ALIN	Alnus	incana	Grey alder
ALIO	Alnus	jorullensis	Evergreen alder
ALJU	Albizia	julibrissin	Mimosa
ALLA	Alchornea	latifolia	Achiotillo
ALLE	Albizia	lebbeck	Acacia amarilla
ALLE2	Albizia	lebbekoides	Indian albizia
ALLI	Allocasuarina	littoralis	Black she-oak
ALLO	Albizia	lophantha	Cape Wattle
ALMA	Alnus	maritima	Seaside alder
ALMA12	Alhagi	maurorum	Camelthorn
ALMA16	Alstonia	macrophylla	Deviltree
ALMA2	Alectryon	macrococcus	Hawai'i alectryon
ALMA9	Aloysia	macrostachya	Rio grande beebrush
ALMO	Aleurites	moluccana	Indian walnut
ALMO11	Aleurites	montana	Mu oil tree
ALNE2	Alnus	nepalensis	Nepal alder
ALOB	Alnus	oblongifolia	Arizona alder
ALPO3	Alphitonia	ponderosa	Hawai'i kauilatree
ALPO7	Alsophila	portoricensis	Puerto rico alsophila
ALPR	Albizia	procera	Tall Albizia
ALRA	Allophylus	racemosus	Palo de caja
ALRH	Alnus	rhombifolia	White alder
ALRU	Alnus	incana ssp. rugosa	Speckled alder
ALRU2	Alnus	rubra	Red alder
ALSA10	Albizia	saponaria	Whiteflower albizia
ALSE	Alnus	serrulata	Hazel alder
ALSI	Alnus	viridis ssp. sinuata	Sitka alder
ALSU	Alectryon	subcinereus	Bird's Eye
ALTE	Alnus	tenuifolla	Mountain alder
ALTO	Allocasuarina	torulosa	Rose she-oak
ALTO1	Alectryon	tomentosus	Hairy Bird's Eye
ALTR6	Aloysia	triphylla	Lemon beebrush
ALVE	Allocasuarina	verticillata	Drooping she-oak
ALVI5	Alnus	viridis	Green alder
ALWR	Aloysia	wrightii	Wright's beebrush
AM	Amelanchier		serviceberry spp
AM1	Amherstia		amherstia spp
AM3	Amelasorbus		amelasorbus spp
AM5	Amorpha		false indigo spp

AM6	Ampelopsis		peppervine spp
AM7	Amphipappus		chaffbush spp
AM8	Amphitecna		amphitecna spp
AM9	Amyris		torchwood spp
AMAR	Amelanchier	arborea	Downy serviceberry
AMAR5	Ampelopsis	arborea	Peppervine
AMBA	Amelanchier	bartramiana	Oblongfruit serviceberry
AMBA2	Amyris	balsamifera	Balsam torchwood
AMCA	Amelanchier	canadensis	Eastern service berry
AMCA5	Amorpha	californica	California false indigo
AMDI4	Amyris	diatrypa	Hairy torchwood
AMEL	Amyris	elemifera	Torchwood
AMFL	Amelanchier	alnifolia	Western serviceberry
AMFR	Amorpha	fruticosa	Desert false indigo
AMFR2	Amphipappus	fremontii	Fremont's chaffbush
AMGE	Amorpha	georgiana	Georgia false indigo
AMGL2	Amorpha	glabra	Mountain false indigo
AMGR	Amelanchier	x grandiflora 'Autumn'	Apple serviceberry
AMHE	Amorpha	herbacea	Clusterspike false indigo
AMHU2	Amelanchier	humilis	Low serviceberry
AMIN2	Amelanchier	interior	Pacific serviceberry
AMIN4	Amelanchier	x intermedia	Intermediate serviceberry
AMJA	Amelasorbus	jackii	Jack's amelasorbus
AMLA	Amelanchier	laevis	Smooth service berry
AMLA2	Amphitecna	latifolia	Black calabash
AMLA3	Amorpha	laevigata	Smooth false indigo
AMMA3	Amyris	madrensis	Mountain torchwood
AMNA2	Amelanchier	nantucketensis	Nantucket serviceberry
AMNE	Amelanchier	x neglecta	Neglected serviceberry
AMNI	Amorpha	nitens	Shining false indigo
AMNO	Amorpha	x notha	Notha indigobush
AMNO4	Amherstia	nobilis	Pride of burma
AMOB2	Amelanchier	obovalis	Coastal serviceberry
AMOU	Amorpha	ouachitensis	Ouachita false indigo
AMPA	Amelanchier	pallida	Pale serviceberry
AMPA4	Amorpha	paniculata	Panicled false indigo
AMPU5	Amelanchier	pumila	Dwarf serviceberry
AMQU	Amelanchier	x quinti-martii	Guint mart's serviceberry
AMRO2	Amorpha	roemeriana	Roemer's false indigo
AMSA	Amelanchier	sanguinea	Roundleaf serviceberry
AMSC2	Amorpha	schwerinii	Schwerin's false indigo
AMTE4	Amyris	texana	Texas torchwood
AMUT	Amelanchier	utahensis	Utah serviceberry
AN	Angophora		angophora spp
AN1	Anacardium		anacardium spp
AN11	Anthocephalus		anthocephalus spp

AN12	Antidaphne		antidaphne spp
AN13	Antidesma		chinalaurel spp
AN14	Antiphytum		saucerflower spp
AN15	Antirhea		quina spp
AN2	Anadenanthera		anadenanthera spp
AN3	Andira		andira spp
AN6	Aniba		aniba spp
AN7	Anisacanthus		desert honeysuckle spp
AN8	Annona		annona spp
ANAC4	Antirhea	acutata	Placa chiquitu
ANBA	Angophora	bakeri	Narrow-leaved apple
ANBR7	Aniba	bracteata	Canelillo
ANCH3	Anthocephalus	chinensis	Anthocephalus Kadam
ANCH4	Annona	cheirimola	Cherimoya
ANCO	Angophora	costata	Smooth-bark angophora
ANCO3	Antirhea	coriacea	Pegwood
ANFL	Angophora	floribunda	Rough-bark angophora
ANGL	Annona	glabra	Pond apple
ANHE4	Antiphytum	heliotropioides	Mexican saucerflower
ANHI	Angophora	hispida	Dwarf Apple
ANIM	Andira	inermis	Cabbagebark tree
ANKA	Antidesma	x kapuae	Kapua chinalaurel
ANLI3	Anisacanthus	linearis	Narrowleaf honeysuckle
ANLU3	Antirhea	lucida	Palo iloron
ANMO	Annona	montana	Mountain soursop
ANMU	Annona	muricata	Soursop
ANOB2	Antirhea	obtusifolia	Quina roja
ANOC	Anacardium	occidentale	Cashew
ANPE13	Anadenanthera	peregrina	Cohoba tree
ANPL2	Antidesma	platyphyllum	Ha'a
ANPO3	Antirhea	portoricensis	Puerto rico quina
ANPU2	Antidesma	pulvinatum	Hame
ANPU6	Anisacanthus	puberulus	Dwarf desert honeysuckle
ANQU2	Anisacanthus	quadrifidus	Wright desert honeysuckle
ANRE	Annona	reticulata	Custard apple
ANSI	Antirhea	sintenisii	Sintenis' quina
ANSQ	Annona	squamosa	Sugar apple
ANTH2	Anisacanthus	thurberi	Thurber's honeysuckle
ANWR6	Antidaphne	wrightii	Wright's catkin mistletoe
AR	Argyrodendron		argyrodendron spp
AR10	Arecastrum		arecastrum palm spp
AR12	Argusia		sea rosemary spp
AR14	Argyrautia		arhyrautia spp
AR15	Argyroxiphium		silversword spp
AR18	Aristotelia		Aristotelia spp
AR2	Aralia		spikenard spp
AR20	Artemisia		sagebrush spp

AR22	Artocarpus		breadfruit spp
AR3	Araucaria		araucaria spp
AR4	Arbutus		madrone spp
AR6	Archontophoenix		archontophoenix spp
AR7	Arctostaphylos		manzanita spp
AR9	Ardisia		marlberry spp
ARAC	Argyrodendron	actinophyllum	Black booyong
ARAL	Archontophoenix	alexandrae	Alexandra palm
ARAL2	Artocarpus	altilis	Breadfruit
ARAL3	Arctostaphylos	alpina	Alpine bearberry
ARAN	Arbutus	andrachne	Cyprus strawberry tree
ARAN2	Arctostaphylos	andersonii	Santa cruz manzanita
ARAR	Araucaria	araucana	Monkeypuzzle tree
ARAR2	Arbutus	arizonica	Arizona madrone
ARAU	Arctostaphylos	auriculata	Mount diablo manzanita
ARBA4	Arctostaphylos	bakeri	Baker's manzanita
ARBE3	Arctostaphylos	x benitoensis	Benito's mazanita
ARBI	Araucaria	bidwillii	Bunya bunya
ARBR	Araucaria	brasiliensis	Araucaria brasileÑa
ARCA11	Artemisia	californica	Coastal sagebrush
ARCA21	Arctostaphylos	catalinae	Santa catalina manzanita
ARCA22	Argyroxiphium	caliginis	Eke silversword
ARCA33	Arctostaphylos	x campbelliae	Campbell manzanita
ARCA5	Arctostaphylos	canescens	Hoary manzanita
ARCH	Aristotelia	chilensis	Maqui
ARCH12	Aralia	chinensis	Chinese angelica tree
ARCI	Arctostaphylos	x cinerea	Waldo manzanita
ARCO	Araucaria	columnaris	Coral reef araucaria
ARCO13	Arctostaphylos	confertiflora	Santa rosa manzanita
ARCO23	Arctostaphylos	x coloradensis	Colorado manzanita
ARCO3	Arctostaphylos	columbiana	Hairy manzanita
ARCR6	Arctostaphylos	cruzensis	La cruz manzanita
ARCR80	Ardisia	crenata	Hen's eyes
ARCU	Archontophoenix	cunninghamiana	King palm
ARCU1	Araucaria	cunninghamii	Hoop pine
ARDE4	Argyrautia	degeneri	Degener's argyrautia
ARED	Arctostaphylos	edmundsii	Little sur manzanita
AREL4	Ardisia	elliptica	Shoebutton
AREL8	Aralia	elata	Japanese angelica tree
ARES	Ardisia	escallonoides	Marlberry
ARGA4	Arctostaphylos	gabrielensis	San gabriel manzanita
ARGL11	Ardisia	glauciflora	Ausubon
ARGL3	Arctostaphylos	glandulosa	Eastwood's manzanita
ARGL4	Arctostaphylos	glauca	Bigberry manzanita
ARGL5	Arctostaphylos	glutinosa	Schreiber's manzanita
ARGN2	Argusia	gnaphalodes	Sea rosemary
ARGR5	Argyroxiphium	grayanum	Hana forest silversword

ARHE	Araucaria	heterophylla	Norfolk island pine
ARHE2	Artocarpus	heterophyllus	Jackfruit
ARHE4	Arctostaphylos	x helleri	Heller's manzanita
ARHI5	Arctostaphylos	hispidula	Gasquet manzanita
ARHO7	Arctostaphylos	hooveri	Hoover's manzanita
ARHU	Aralia	humilis	Arizona spikenard
ARHU1	Araucaria	hunsteinii	Klinki pine
ARIM	Arctostaphylos	imbricata	San bruno manzanita
ARIN2	Arctostaphylos	insularis	Island manzanita
ARJA	Ardisia	japonica	Japanese ardisia
ARJE	Arctostaphylos	x jepsonii	Jepson's manzanita
ARKA	Argyroxiphium	x kai	Argyroxiphium x kai
ARKA2	Argyroxiphium	kauense	Kau silversword
ARLA21	Arctostaphylos	x laxiflora	Lazyflower manzanita
ARLU3	Ardisia	luquillensis	Mountain marlberry
ARLU4	Arctostaphylos	luciana	Santa lucia manzanita
ARMA	Arctostaphylos	manzanita	Whiteleaf manzanita
ARMA2	Arbutus	var. marina	Marina arbutus
ARMA31	Arctostaphylos	malloryi	Mallory's manzanita
ARME	Arbutus	menziesii	Pacific madrone
ARME3	Arctostaphylos	mewukka	Indian manzanita
ARME7	Arctostaphylos	x media	Intermediate manzanita
ARME8	Arctostaphylos	mendocinoensis	Pygmy manzanita
ARMO12	Arctostaphylos	moranii	Moran's manzanita
ARMO2	Arctostaphylos	morroensis	Morro manzanita
ARMO5	Arctostaphylos	montaraensis	Montara manzanita
ARMO6	Arctostaphylos	montereyensis	Monterey manzanita
ARMY	Arctostaphylos	myrtifolia	Ione manzanita
ARNI	Arctostaphylos	nisseniana	Nissenan manzanita
ARNO6	Arctostaphylos	nortensis	Del norte manzanita
AROB	Arctostaphylos	obispoensis	Serpentine manzanita
AROB2	Ardisia	obovata	Guadeloupe marlberry
AROS	Arctostaphylos	osoensis	Oso manzanita
AROT	Arctostaphylos	otayensis	Otay manzanita
ARPA19	Arctostaphylos	pacifica	Pacific manzanita
ARPA21	Arctostaphylos	pallida	Alameda manzanita
ARPA3	Arctostaphylos	pajaroensis	Pajaro manzanita
ARPA4	Arctostaphylos	parryana	Parry manzanita
ARPA6	Arctostaphylos	patula	Greenleaf manzanita
ARPE5	Arctostaphylos	pechoensis	Pecho manzanita
ARPE9	Arctostaphylos	peninsularis	Peninsular manzanita
ARPI	Arctostaphylos	pilosula	La panza manzanita
ARPR	Arctostaphylos	pringlei	Pringle manzanita
ARPU10	Arctostaphylos	purissima	La purissima manzanita
ARRA7	Arctostaphylos	rainbowensis	Rainbow manzanita
ARRE5	Arctostaphylos	refugioensis	Refugio manzanita
ARRE7	Arctostaphylos	regismontana	Kings mountain manzanita

ARRE8	Arctostaphylos	x repens	Pmc manzanita
ARRO	Arecastrum	romanzoffianum	Queen palm
ARRU	Arctostaphylos	rubra	Red fruit bearberry
ARRU2	Arctostaphylos	rudis	Shagbark manzanita
ARSA5	Argyroxiphium	sandwicense	Hawai'i silversword
ARSI	Arctostaphylos	silvicola	Bonny doon manzanita
ARSO	Ardisia	solanacea	China shrub
ARSP	Aralia	spinosa	Devils walking stick
ARST	Arctostaphylos	stanfordiana	Stanford's manzanita
ARTE	Arbutus	xalapensis	Texas madrone
ARTO2	Arctostaphylos	tomentosa	Woollyleaf manzanita
ARTR	Artemisia	tridentata	Big sagebrush
ARTR4	Artemisia	tripartita	Threetip sagebrush
ARUN	Arbutus	unedo	Strawberry tree
ARUV	Arctostaphylos	uva-ursi	Kinnikinnick
ARVI3	Arctostaphylos	virgata	Bolinas manzanita
ARVI4	Arctostaphylos	viscida	Sticky white manzanita
ARVI7	Arctostaphylos	viridissima	Whitehair manzanita
ARVI8	Argyroxiphium	virescens	Greensword
ARWE	Arctostaphylos	wellsii	Wells' manzanita
ARX	Arbutus	x andrachnoides	Hybrid Strawberry tree
AS3	Asimina		pawpaw spp
ASAN6	Asimina	angustifolia	Slimleaf pawpaw
ASIN12	Asimina	incana	Woolly pawpaw
ASNA3	Asimina	x nashii	Nash's pawpaw
ASOB6	Asimina	obovata	Bigflower pawpaw
ASPA18	Asimina	parviflora	Smallflower pawpaw
ASRE7	Asimina	reticulata	Netted pawpaw
ASTE11	Asimina	tetramera	Fourpetal pawpaw
ASTR	Asimina	triloba	Pawpaw
AT1	Atamisquea		atamisquea spp
AT2	Atriplex		saltbush spp
ATCA	Atriplex	canescens	Four winged saltbrush
ATEM	Atamisquea	emarginata	Vomitbush
ATGR2	Atriplex	griffithsii	Griffiths' saltbush
ATHY	Atriplex	hymenelytra	Desertholly
ATJO	Atriplex	johnstonii	Johnson's saltbush
ATLA2	Atriplex	lampa	South american saltbush
ATNA	Atriplex	navajoensis	Navajo saltbush
ATNU	Atriplex	nummularia	Bluegreen saltbush
ATPO	Atriplex	polycarpa	Allscale
ATSP	Atriplex	spinifera	Spinescale saltbush
ATTO	Atriplex	torreyi	Torrey's saltbush
ATVE	Atriplex	vesicaria	Aboriginal saltbush
AU1	Aucuba		acuba spp
AU2	Auerodendron		auerodendron spp
AUJA	Aucuba	japonica	Japanese aucuba

AUPA2	Auerodendron	pauciflorum	Turtlefat
AV	Averrhoa		averrhoa spp
AV1	Avicennia		mangrove spp
AVBI	Averrhoa	bilimbi	Bilimbi
AVCA	Averrhoa	carambola	Star fruit
AVGE	Avicennia	germinans	Black mangrove
AVMA3	Avicennia	marina	Gray mangrove
AY1	Ayenia		ayenia spp
AYAR	Ayenia	ardua	Wingstem ayenia
AYCO	Ayenia	compacta	California ayenia
AYGL	Ayenia	glabra	Smooth ayenia
AZ	Azolla		mosquitofern spp
AZ2	Azara		azara spp
AZCA	Azolla	caroliniana	Carolina mosquitofern
AZFI	Azolla	filiculoides	Pacific mosquitofern
AZME	Azolla	mexicana	Mexican mosquitofern
AZMI	Azolla	microphylla	Azolla microphylla
AZMI2	Azara	microphylla	Boxleaf azara
AZPI	Azolla	pinnata	Feathered mosquitofern
BA	Banksia		banksia spp
BA1	Baccharis		baccharis spp
BA11	Batesimalva		gaymallow spp
BA13	Bauhinia		bauhinia spp
BA2	Bambusa		bamboo spp
BA3	Banara		palo de ramon spp
BA4	Banisteriopsis		banisteriopsis spp
BA5	Backhousia		backhousia spp
BA7	Barleria		Philippine violet spp
BA8	Barleriola		barleriola spp
BA9	Barringtonia		barringtonia spp
BAAE	Banksia	aemula	Wallum Banksia
BAAN	Baccharis	angustifolia	Saltwater false willow
BAAR8	Bambusa	arundinacea	Thorny bamboo
BAAS	Barringtonia	asiatica	Sea putat
BABE2	Bambusa	beecheyana	Beechey's bamboo
BABL	Bauhinia	x blakeana	Blake's bauhinia
BACA	Bauhinia	candicans	Pata de vaca
BACI	Backhousia	citriodora	Lemon-scented Myrtle
BADI3	Baccharis	dioica	Broombush false willow
BAEM	Baccharis	emoryi	Emory's baccharis
BAER	Banksia	ericifolia	Heath-leaved Banksia
BAFO	Bauhinia	forficata	Bauhinia
BAGA	Bauhinia	galpinii	Pride of de kaap
BAGL	Baccharis	glomeruliflora	Silverling
BAHA	Baccharis	halimifolia	Eastern baccharis
BAHO3	Bauhinia	hookeri	Queensland ebony
BAIN	Banksia	integrifolia	Coast banksia

BALO3	Bambusa	longifolia	Longflower bamboo
BALO4	Bambusa	longispiculata	Mahal bamboo
BALU	Bauhinia	lunarioides	Texasplume
BALU2	Barleria	lupulina	Hophead philippine violet
BALU3	Banisteriopsis	lucida	Paralejo de monte
BAMA	Banksia	marginata	Silver banksia
BAMO	Bauhinia	monandra	Mariposa
BAMU3	Bauhinia	multinervia	Petit flamboyant bauhinia
BAMY	Backhousia	myrtifolia	Grey Myrtle
BANE2	Baccharis	neglecta	Rooseveltweed
BAPA3	Bauhinia	pauletia	Railroadfence
BAPI	Baccharis	pilularis	Dwarf chaparral broom
BAPO	Banara	portoricensis	Puerto rico palo de ramon
BAPO6	Bambusa	polymorpha	Polymorph bamboo
BAPR	Barleria	prionitis	Porcupine flower
BAPT	Baccharis	pteronioides	Yerba de pasmo
BAPU	Bauhinia	purpurea	Orchid tree
BARO	Banksia	robur	Swamp Banksia
BASA	Baccharis	salicina	Great plains false willow
BASA2	Baccharis	sarothroides	Desertbroom
BASA4	Baccharis	salicifolia	Mule's fat
BASE	Baccharis	sergiloides	Squaw waterweed baccharis
BASE1	Banksia	serrata	Saw Banksia
BASO	Barleriola	solanifolia	False philippine violet
BATE6	Bambusa	textilis	Textile bamboo
BATO	Bauhinia	tomentosa	St. thomas tree
BATU	Bambusa	tulda	Bamboo
BATU2	Bambusa	tuldoides	Puntingpole bamboo
BAVA	Bauhinia	variegata	Mountain ebony
BAVA2	Banara	vanderbiltii	Vanderbilt palo de ramon
BAVA3	Baccharis	vanessae	Encinitis false willow
BAVI5	Batesimalva	violacea	Purple gaymallow
BAVU2	Bambusa	vulgaris	Common bamboo
BAYU	Bauhinia	yunnanensis	Yunnan bauhinia
BE	Betula		birch spp
BE1	Beaucarnea		beaucarnea spp
BE2	Befaria		befaria spp
BE4	Beilschmiedia		beilschmiedia spp
BE7	Bernardia		myrtlecroton spp
BEAL	Betula	alleghaniensis	Yellow birch
BEAL1	Betula	pubescens	Cut leaved birch
BEAL2	Betula	albo-sinensis	Chinese birch
BEBO	Betula	borealis	Northern birch
BECA2	Berberis	canadensis	American barberry
BECA4	Betula	x caerulea	Blue birch
BEDA	Berberis	darwinii	Darwin's berberis

BEDI2	Bernardia	dichotoma	Caribbean myrtlecroton
BEDU	Betula	x dugleana	Dugle's birch
BEEA	Betula	x eastwoodiae	Eastwood's birch
BEFE	Berberis	fendleri	Colorado barberry
BEHA2	Berberis	harrisoniana	Harrison's barberry
BEHO	Betula	x hornei	Horne's birch
BEIN	Bernardia	incana	Hoary myrtlecroton
BEJA	Betula	x jackii	Jack's birch
BEJU3	Berberis	julianiae	Julian's berberis
BELE	Betula	lenta	Black birch
BEMI	Beilschmiedia	miersii	Belloto del norte
BEMU2	Betula	murrayana	Murray's birch
BEMY	Bernardia	myricifolia	Mouse's eye
BENE4	Betula	neoalaskana	Resin birch
BENI	Betula	nigra	River birch
BEOB	Bernardia	obovata	Desert myrtlecroton
BEOC	Betula	occidentalis	Water birch
BEOT	Berberis	x ottawensis	Ottawa barberry
BEPA	Betula	papyrifera	Paper birch
BEPE	Betula	pendula	European white birch
BEPE2	Beilschmiedia	pendula	Guajon
BEPEGR	Betula	pendula gracilis	Weeping birch
BEPL2	Betula	platyphylla	Asian white birch
BEPO	Betula	populifolia	Gray birch
BEPU	Betula	pumila	Bog birch
BEPU3	Betula	x purpusii	Purpus's birch
BERA2	Befaria	racemosa	Tarflower
BERE	Beaucarnea	recurvata	Ponytail palm
BESA	Betula	x sandbergii	Sandberg's birch
BESP	Berberis		barberry spp
BETH	Berberis	thunbergii	Japanese barberry
BEUB	Betula	uber	Virginia roundleaf birch
BEUT	Betula	x utahensis	Northwestern paper birch
BEUT2	Betula	utilis	Indian paper birch
BEVU	Berberis	vulgaris	Common barberry
BEWI	Berberis	wilcoxii	Wilcox's barberry
BEWI2	Betula	x winteri	Winter's birch
BI	Bismarckia		bismarckia spp
BI1	Bidens		beggarticks spp
BI4	Bischofia		bishopwood spp
BI5	Bixa		bixa spp
BIJA	Bischofia	javanica	Toog
BIME	Bidens	menziesii	Mauna loa beggarticks
BINO	Bismarckia	nobilis	Bismarckia palm
BIOR	Bixa	orellana	Lipsticktree
BIPO	Bischofia	polycarpa	Bischofia polycarpa
BL1	Blighia		blighia spp

BLSA2	Blighia	sapida	Akee
BO	Bolusanthus		bolusanthus spp
BO1	Bobea		'ahakea spp
BO10	Bourreria		strongbark spp
BO11	Bouvardia		bouvardia spp
BO2	Bocconia		bocconia spp
BO6	Bontia		bontia spp
BO7	Borrichia		seaside tansy spp
BO8	Bouchea		bouchea spp
BO9	Bougainvillea		bougainvillea spp
BOAR2	Borrichia	arborescens	Tree seaside tansy
BOBR3	Bobea	brevipes	'akupa
BOCA4	Bourreria	cassinifolia	Smooth strongbark
BODA	Bontia	daphnoides	White alling
BOEL3	Bobea	elatior	'ahakea lau nui
BOFR2	Bocconia	frutescens	Parrotweed
BOGL4	Bougainvillea	glabra	Paperflower
BOOV	Bourreria	succulenta	Bahama strongback
BORA2	Bourreria	radula	Rough strongbark
BOSA2	Bobea	sandwicensis	Hawai'i dogweed
BOSP	Bougainvillea	spectabilis	Great bougainvillea
BOSP2	Bouchea	spathulata	Spoonleaf
BOSP8	Bolusanthus	speciosus	Tree wisteria
BOTE2	Bouvardia	ternifolia	Firecrackerbush
BOTI	Bobea	timonioides	'ahakea
BOVI2	Bourreria	virgata	Roble de guayo
BR	Brahea		palm(brahea) spp
BR1	Brachychiton		brachychiton spp
BR10	Brugmansia		brugmansia spp
BR11	Bruguiera		bruguiera spp
BR12	Brunellia		brunellia spp
BR13	Brunfelsia		Brunfelsia spp
BR14	Brya		coccuswood spp
BR15	Brassaia		brassaia spp
BR3	Breynia		breynia spp
BR5	Brighamia		brighamia spp
BR6	Brongniartia		greentwig spp
BR7	Brosimum		brosimum spp
BR8	Broussaisia		broussaisia spp
BR9	Broussonetia		broussonetia spp
BRAC	Schefflera	actinophylla	Schefflera
BRAC2	Brachychiton	acerifolius	Illwarra Flame Tree
BRAL3	Brosimum	alicastrum	Breadnut
BRAM4	Brunfelsia	americana	American brunfelsia
BRAR	Brahea	armata	Mexican blue palm
BRAR6	Broussaisia	arguta	Kanawao
BRBI	Brachychiton	bidwillii	Little Kurrajong

BRBR	Brahea	brandegeei	San jose hesper palm
BRCA12	Brugmansia	candida	Angel's-trumpet
BRCO6	Brunellia	comocladiifolia	West indian sumac
BRDE4	Brunfelsia	densifolia	Serpentine hill raintree
BRDI	Brachychiton	discolor	Lacebark
BRDI8	Breynia	disticha	Snowbush
BREB	Brya	ebenus	Ebony coccuswood
BRED	Brahea	edulis	Guadalupe palm
BRGY	Bruguiera	gymnorrhiza	Oriental mangrove
BRIN4	Brighamia	insignis	Cabbage on a stick
BRLA5	Brunfelsia	lactea	Vega blanca
BRMI4	Brongniartia	minutifolia	Littleleaf greentwig
BRNI6	Brunfelsia	nitida	Cuban raintree
BROC	Brachychiton	occulneuem	Bottle tree
BRPA	Broussonetia	papyrifera	Paper mulberry
BRPA15	Bruguiera	parviflora	Smallflower bruguiera
BRPO	Brachychiton	populneum	Kurrajong
BRPO3	Brunfelsia	portoricensis	Puerto rico raintree
BRRO	Brighamia	rockii	Molokai ohaha
BRRU	Brachychiton	rupestris	Brachichiton rupestris
BRSU3	Brugmansia	suaveolens	Angel's-tears
BRUN	Brunfelsia	uniflora	Yesterday-today-tomorrow
BU	Bursaria		bursaria spp
BU1	Buchenavia		buchenavia spp
BU2	Bucida		bucida spp
BU3	Buckleya		buckleya spp
BU4	Buddleja		butterflybush spp
BU5	Bunchosia		woodland coffee spp
BU6	Bursera		bursera spp
BU7	Butia		feather palm spp
BU8	Bumelia		bumelia spp
BU9	Buckinghamia		buckinghamia spp
BUAL	Buddleja	alternifolia	Fountain butterflybush
BUAS	Buddleja	asiatica	Dogtail
BUBU	Bucida	buceras	Black olive
BUCA	Butia	capitata	Jelly palm
BUCE	Buckinghamia	celsissima	Ivory Curl Flower
BUDA2	Buddleja	davidii	Orange eye butterflybush
BUDI	Buckleya	distichophylla	Piratebush
BUFA	Bursera	fagaroides	Fragrant bursera
BUGL	Bunchosia	glandulosa	Cafe forastero
BUGL2	Bunchosia	glandulifera	Cafe falso
BULA	Bumelia	lanuginosum	Chittamwood
BULI	Buddleja	lindleyana	Lindley's butterflybush
BUMA	Buddleja	marrubiifolia	Woolly butterflybush
BUMA80	Buddleja	madagascariensis	Smokebush
BUMI	Bursera	microphylla	Elephant tree

BUMI1	Buxus	microphylla	Littleleaf box
BUMO	Bucida	molinetii	Spiny bucida
BUOF	Buddleja	officinalis	Pole butterflybush
BUPO	Buxus	portoricensis	Puerto rico box
BUPO5	Bunchosia	polystachia	Woodland coffee
BURA	Buddleja	racemosa	Wand butterflybush
BUSA	Buddleja	saligna	Squarestem butterflybush
BUSC	Buddleja	scordioides	Escobilla butterflybush
BUSE	Buddleja	sessiliflora	Rio grande butterflybush
BUSE2	Buxus	sempervirens	Common box
BUSI	Bursera	simaruba	Gumbo limbo
BUSP	Buxus		boxwood spp
BUSP1	Bursaria	spinosa	Sweet bursaria
BUTE4	Buchenavia	tetraphylla	Fourleaf buchenavia
BUVA	Buxus	vahlii	Vahl's box
BY1	Byrsonima		byrsonima spp
BYCR	Byrsonima	crassifolia	Maricao cimun
BYLU	Byrsonima	lucida	Long key locustberry
BYSP	Byrsonima	spicata	Doncella
BYWA	Byrsonima	wadsworthii	Almendrillo
CA	Campomanesia		camponmanesia spp
CA1	Carya		hickory spp
CA10	Callicarpa		beautyberry spp
CA11	Callistemon		bottlebrush spp
CA12	Callitris		cypress-pine spp
CA13	Calluna		heather spp
CA14	Calocedrus		incense cedar spp
CA15	Calophyllum		calophyllum spp
CA16	Calotropis		calotropis spp
CA17	Calycanthus		sweetshrub spp
CA18	Calycophyllum		calycophyllum spp
CA19	Castanospermum		castanospermum spp
CA2	Caragana		peashrub spp
CA20	Calyptranthes		mountainbay spp
CA21	Calyptronoma		manac spp
CA22	Camellia		camellia spp
CA24	Camptotheca		camptotheca spp
CA25	Cananga		ilang-ilang spp
CA26	Canella		wild cinnamon spp
CA28	Canotia		canotia spp
CA29	Canthium		canthium spp
CA3	Catalpa		catalpa spp
CA30	Capparis		caper spp
CA33	Carica		papaya spp
CA34	Carissa		carissa spp
CA36	Carmona		scorpionbush spp
CA37	Carnegia		saguaro spp

CA38	Carpenteria		tree anemone spp
CA4	Castanea		chestnut spp
CA40	Carpinus		hornbeam spp
CA41	Carpobrotus		carpobrotus spp
CA42	Caryopteris		caryopteris spp
CA43	Caryota		fishtail palm spp
CA44	Casasia		casasia spp
CA45	Casearia		casearia spp
CA46	Cassine		cassine spp
CA48	Cassipourea		cassipourea spp
CA49	Castela		castela spp
CA5	Caesalpinia		nicker spp
CA50	Castilla		castilla spp
CA52	Casuarina		sheoak spp
CA53	Catesbaea		lilythorn spp
CA54	Casimiroa		casimiroa spp
CA56	Castanopsis		castanopsis spp
CA57	Calodendrum		calodendrum spp
CA6	Cajanus		cajanus spp
CA7	Callicoma		callicoma spp
CA8	Callaeum		callaeum spp
CA9	Calliandra		stickpea spp
CAAC	Camptotheca	acuminata	Happy tree
CAAC3	Casearia	aculeata	Rabo de ranton
CAAC4	Calyptranthes	acevedoi	Puerto rico mountainbay
CAAF2	Cassia	afrofistula	Kenyan shower
CAAM13	Capparis	amplissima	Burro blanco
CAAM14	Callicarpa	ampla	Caparosa
CAAM2	Callicarpa	americana	American beautyberry
CAAQ	Carya	aquatica	Water hickory
CAAR	Caragana	arborescens	Siberian pea tree
CAAR2	Senna	artemisioides	Wormwood senna
CAAR8	Casearia	arborea	Gia verde
CAAU	Castanospermum	australe	Black Bean
CAAU10	Caragana	aurantiaca	Dwarf peashrub
CABA2	Capparis	baducca	Caper
CABE	Carpinus	betulus	European hornbeam
CABEFA	Carpinus	betulus 'Fastigiata'	Fastigate hornbeam
CABI	Catalpa	bignonioides	Southern catalpa
CABR16	Carya	x brownii	Brown's hickory
CABR32	Calycanthus	brockiana	Georgia sweetshrub
CACA	Carpinus	caroliniana	American hornbeam
CACA17	Carpenteria	californica	Tree anemone
CACA2	Calophyllum	antillanum	Maria
CACA26	Caesalpinia	caudata	Tailed nicker
CACA3	Calodendrum	capense	Cape chesnut
CACA38	Carya	carolinae	Southern shagbark hickory

CACA73	Calycophyllum	candidissimum	Degame
CACH	Chrysolepis	chrysophylla	Giant chinkapin
CACI	Callistemon	citrinus	Crimson bottlebrush
CACI19	Caesalpinia	ciliata	Mato
CACL3	Casasia	clusiifolia	Sevenyear apple
CACL7	Caryopteris	x clandonensis	Caryopteris
CACO	Carya	cordiformis	Bitternut hickory
CACO1	Callitris	columellaris	White cypress-pine
CACO24	Carya	x collina	Collin hickory
CACO28	Caesalpinia	coriaria	Divi divi
CACR27	Castanea	crenata	Japanese chestnut
CACU	Casuarina	cunninghamiana	River she-oak
CACY	Capparis	cynophallophora	Jamacia caper
CADE	Castanea	dentata	American chestnut
CADE10	Carya	x demareei	Demaree hickory
CADE11	Casearia	decandra	Wild honeytree
CADE15	Caesalpinia	decapetala	Shoofly
CADE2	Calocedrus	decurrens	Incense cedar
CADI	Callicarpa	dichotoma	Purple beautyberry
CADI12	Caesalpinia	divergens	Small yellow nicker
CADU3	Carya	x dunbarii	Dunbar's hickory
CAED	Casimiroa	edulis	White sapote
CAED3	Carpobrotus	edulis	Hottentot fig
CAEL5	Castilla	elastica	Panama rubbertree
CAEM4	Castela	emoryi	Crucifixion thorn
CAEN	Callitris	endlicheri	Black Cypress Pine
CAEQ	Casuarina	equisetifolia	Australian pine
CAER	Catalpa	erubescens	Purple toned catalpa
CAER3	Castela	erecta	Goatbush
CAES	Calyptranthes	estremenae	Las cuevas mountainbay
CAEX	Cassia	excelsa	Crown of gold tree
CAFE	Caesalpinia	ferrea	Leopard tree(pau-ferro)
CAFI	Cassia	fistula	Canafistula
CAFL	Carya	floridana	Scrub hickory
CAFL2	Calycanthus	floridus	Carolina allspice
CAFL3	Capparis	flexuosa	Falseteeth
CAFR80	Caragana	frutex	Russian peashrub
CAGI	Caesalpinia	gilliesii	Bird or paradise bush
CAGI11	Calotropis	gigantea	Giant milkweed
CAGL	Carya	glabra	Pignut hickory
CAGL11	Casuarina	glauca	Gray sheoak
CAGL2	Callitris	glaucophylla	White cyprus pine
CAGR11	Cassia	grandis	Pink shower
CAGU2	Casearia	guianensis	Guyanese wild coffee
CAGU3	Cassipourea	guianensis	Goatwood
CAHA	Callistemon	x harkness	Gawler hybrid
CAHA10	Calliandra	haematomma	Red powderpuff

CAHA9	Capparis	hastata	Broadleaf caper
CAHO	Canotia	holacantha	Canotia
CAIL	Carya	illinoinensis	Pecan
CAIN21	Capparis	incana	Hoary caper
CAIN4	Calophyllum	inophyllum	Alexandrian laurel
CAIN5	Capparis	indica	Linguam
CAJA	Carpinus	japonica	Japanese hornbeam
CAJA11	Callicarpa	japonica	Japanese callicarpa
CAJA9	Camellia	japonica	Camellia
CAKA5	Caesalpinia	kavaiensis	Uhiuhi
CAKI	Calyptranthes	kiaerskovii	Kiaerskov's lidflower
CAKI1	Callistemon	x kings park spec.	Kings park bottlebrush
CAKR	Calyptranthes	krugii	Limoncillo
CALA	Carya	laciniosa	Shellbark hickory
CALA34	Carya	x laneyi	Laney's hickory
CALE	Cassia	leptophylla	Gold medallion tree
CALE13	Carya	x lecontei	Leconte's hickory
CALE28	Casuarina	lepidophloia	Belah
CALI	Callistemon	linearifolius	Netted Bottle Brush
CALI1	Callistemon	linearis	Narrow-leaved Bottlebrush
CALO	Catalpa	longissima	Haitian catalpa
CALO15	Calliandra	locoensis	Rio Loc stickpea
CALO2	Calophyllum	longifolium	Maria; santa maria
CALU12	Calyptranthes	luquillensis	Luquillo forest lidflower
CALU8	Carya	x ludoviciana	Hickory
CAMA	Callistemon	macropunctatus	Scarlet Bottlebrush
CAMA25	Calyptranthes	martorellii	Martorell's lidflower
CAMA37	Carissa	macrocarpa	Amatungulu
CAMA45	Callaeum	macropterum	Hillyhock
CAME	Caesalpinia	mexicana	Mexican holdback
CAME19	Catesbaea	melanocarpa	Tropical lilythorn
CAMI36	Caryota	mitis	Burmese fishtail palm
CAMO	Castanea	mollissima	Chinese chestnut
CAMO14	Caesalpinia	monensis	Black nicker
CAMY	Carya	myristicformis	Nutmeg hickory
CANE	Cassia	nemophila	Australian senna
CANE33	Cassia	x nealiae	Rainbow shower tree
CANE7	Castanea	x neglecta	Neglected chesnut
CANI17	Casearia	nitida	Smooth honeytree
CANU8	Carya	x nussbaumeri	Nussbaumer's hickory
CAOB	Casuarina	obesa	Swamp Sheoak
CAOC5	Calycanthus	occidentalis	Western sweetshrub
CAOD	Cananga	odorata	Ilan-ilan
CAOD2	Canthium	odoratum	Alahe'e
CAOV	Carya	ovata	Shagbark hickory
CAOV2	Carya	ovalis	Red hickory
CAOV3	Catalpa	ovata	Chinese catalpa

CAPA	Carya	pallida	Sand hickory
CAPA1	Callistemon	pallidus	Lemon bottlebrush
CAPA2	Calyptranthes	pallens	Pale lidflower
CAPA3	Carica	papaya	Papaya
CAPA33	Caesalpinia	parryi	Parry's holdback
CAPA34	Caesalpinia	pauciflora	Fewflower holdback
CAPA43	Catesbaea	parviflora	Smallflower lilythorn
CAPE	Callistemon	pendula	Bottlebrush
CAPE17	Calyptranthes	peduncularis	Maricao lidflower
CAPE2	Caesalpinia	peltophoroides	Sibipiruna
CAPH	Caesalpinia	phyllanthoides	Wait-a-bit vine
CAPO6	Caesalpinia	portoricensis	Brown nicker
CAPO9	Calyptranthes	portoricensis	Puerto rico lidflower
CAPR	Calotropis	procera	Rooster tree
CAPU	Castanea	pumila	Alleghany chinkapin
CAPU13	Caesalpinia	pulcherrima	Pride-of-barbados
CAPU2	Carya	pumilia	Carya
CAPU33	Calliandra	purpurea	Purple stickpea
CAPY	Caragana	pygmaea	Dwarf pea tree
CARE22	Carmona	retusa	Scorpionbush
CARH	Campomanesia	rhombea	Goabiroba miuda
CARH1	Callitris	rhomboidea	Oyster Bay Pine
CARI3	Calyptronoma	rivalis	Puerto rico manac
CARO	Cassia	javanica	Apple blossom
CASA	Camellia	sasanqua	Sasanqua camellia
CASA2	Castanea	sativa	CastaÑo comÚn
CASA4	Capparis	sandwichiana	Native caper
CASA5	Callistemon	salignus	White bottlebrush
CASC16	Carya	x schneckii	Schneck's hickory
CASC33	Cajanus	scarabaeoides	Cajanus
CASE	Callicoma	serratifolia	Callicoma
CASI	Senna	siamea	Siamese cassia
CASI16	Camellia	sinensis	Tea
CASI8	Calyptranthes	sintenisii	Limoncillo de monte
CASP	Catalpa	speciosa	Northern catalpa
CASP11	Caesalpinia	spinosa	Spiny holdback
CASP2	Senna	spectabilis	Casia amarilla
CASSI	Cassia		cassia spp
CAST	Casuarina	stricta	Coast beefwood
CASU33	Calliandra	surinamensis	Surinamese stickpea
CASU34	Calliandra	schultzii	Pink powder puff tree
CASY2	Casearia	sylvestris	Crackopen
CATE	Carya	texana	Black hickory
CATH3	Calyptranthes	thomasiana	Thomas' lidflower
CATO	Carya	alba	Mockernut hickory
CATR12	Calyptranthes	triflora	Threeblossom lidflower
CATW	Calliandra	tweedii	Trinidad flame bush

CAUR	Caryota	urens	Wine palm
CAVI	Callistemon	viminalis	Weeping bottlebrush
CAVI8	Caesalpinia	virgata	Wand holdback
CAVU	Calluna	vulgaris	Heather
CAWI	Canella	winterana	Cinnamon bark
CAWO5	Calyptranthes	woodburyi	Woodbury's lidflower
CAXY	Cassine	xylocarpa	Marbletree
CAZU	Calyptranthes	zuzygium	Myrtle of the river
CE	Ceratopetalum		ceratopetalum
CE1	Ceanothus		ceanothus spp
CE10	Celosia		cock's comb spp
CE13	Cephalanthus		buttonbush spp
CE15	Ceratonia		ceratonia spp
CE17	Cercidiphyllum		katsura tree spp
CE18	Cercis		redbud spp
CE19	Cereus		sweetpotato cactus spp
CE2	Celtis		hackberry spp
CE20	Cestrum		jessamine spp
CE22	Cercidium		cercidium spp
CE3	Cercocarpus		mountain mahogany spp
CE4	Cecropia		pumpwood spp
CE5	Cedrela		cedrela spp
CE6	Cercidium		cercidium spp
CE7	Cedrus		cedar spp
CE8	Ceiba		ceiba spp
CE9	Celastrus		bittersweet spp
CEAD2	Cecropia	adenopus	Ambay pumpwood
CEAL3	Cestrum	alternifolium	Alternateleaf jessamine
CEAP	Ceratopetalum	apetalum	Coachwood
CEAR	Ceanothus	arboreus	Feltleaf ceanthous
CEAR2	Ceanothus	x arcuatus	Arching ceanothus
CEAT	Cedrus	atlantica	Atlas cedar
CEATGL	Cedrus	atlantica glauca	Blue atlas cedar
CEAU	Celtis	australis	European hackberry
CEAU2	Cestrum	aurantiacum	Orange jessamine
CEBA	Ceanothus	x bakeri	Baker's ceanothus
CEBE	Cercocarpus	montanus v glaber	Birchleaf mtn mahogany
CECA	Cercis	canadensis	Eastern redbud
CECO	Ceanothus	cordulatus	Whitethorn ceanothus
CECO2	Ceanothus	connivens	Trailing buckbrush
CECR	Ceanothus	crassifolia	Ceanothus crassifolia
CECU	Ceanothus	cuneatus	Buckbrush
CECY	Ceanothus	cyaneus	San diego buckbrush
CEDE	Cedrus	deodara	Deodar cedar
CEDE2	Ceanothus	dentatus	Sandscrub ceanothus
CEDI	Ceanothus	divergens	Calistoga ceanothus
CEDI6	Cestrum	diurnum	Day jessamine

CEFA3	Cestrum	fasciculatum	Early jessamine
CEFE	Ceanothus	fendleri	Fendler's ceanothus
CEFE2	Ceanothus	ferrisiae	Coyote ceanothus
CEFI2	Cedrela	fissilis	Brazilian cedarwood
CEFL	Parkinsonia	florida	Blue paloverde
CEFL4	Ceanothus	x flexilis	Flexible ceanothus
CEGI	Carnegia	gigantea	Saguaro
CEGR	Ceanothus	greggii	Desert ceanothus
CEGR2	Ceanothus	griseus	Carmel ceanothus
CEGU	Ceratopetalum	gummiferum	NS Wales Christmas Bush
CEHE	Ceanothus	herbaceus	Jersey tea
CEHE3	Cereus	hexagonus	Lady of the night cactus
CEHI3	Cereus	hildmannianus	Hedge cactus
CEIG	Celtis	iguanaea	Iguana hackberry
CEIM	Ceanothus	impressus	Santa barbara ceanothus
CEIN	Ceanothus	integerrimus	Deer brush
CEIN2	Cercocarpus	intricatus	Littleleaf mahogany
CEIN3	Ceanothus	incanus	Coast whitethorn
CEJA	Cercidiphyllum	japonicum	Katsura tree
CEJE	Ceanothus	jepsonii	Jepson ceanothus
CELA	Celtis	laevigata	Sugarberry
CELA2	Cestrum	laurifolium	Galen del monte
CELE	Cercocarpus	ledifolius	Curlleaf mahogany
CELE2	Ceanothus	leucodermis	Chaparral whitethorn
CELE3	Ceanothus	lemmonii	Lemmon's ceanothus
CELI	Cedrus	libani	Cedar of lebanon
CELI2	Celtis	lindheimeri	Lindheimer's hackberry
CELO	Ceanothus	x lobbianus	Lobbian ceanothus
CELO2	Ceanothus	x lorenzenii	Lorenzen's ceanothus
CEMA	Ceanothus	maritimus	Maritime ceanothus
CEMA2	Ceanothus	martinii	Martin's ceanothus
CEME	Ceanothus	megacarpus	Bigpod ceanothus
CEME3	Ceanothus	x mendocinensis	Mendocino ceanothus
CEMI	Parkinsonia	microphylla	Yellow paloverde
CEMI4	Ceanothus	microphyllus	Littleleaf buckbrush
CEMO	Cercocarpus	montanus	Alderleaf mahogany
CENO	Cestrum	nocturnum	Night jessamine
CEOB	Cecropia	obtusifolia	Trumpet tree
CEOC	Celtis	occidentalis	Northern hackberry
CEOC2	Cephalanthus	occidentalis	Button bush
CEOC3	Cercis	canadensis v texensis	Western redbud
CEOD	Cedrela	odorata	Spanish cedar
CEOL	Ceanothus	oliganthus	Hairy ceanothus
CEOP	Ceanothus	ophiochilus	Vail lake ceanothus
CEOR9	Cercis	orbiculata	California redbud
CEOT	Ceanothus	x otayensis	Otay ceanothus

CEPA	Cecropia	palmata	Cecropia
CEPA1	Celtis	paniculata	Native Hackberry
CEPA2	Ceanothus	papillosus	Wartleaf ceanothus
CEPA3	Ceanothus	parryi	Parry ceanothus
CEPA4	Ceanothus	parvifolius	Littleleaf ceanothus
CEPA5	Celosia	palmeri	Palmer's cock's comb
CEPA6	Ceanothus	palmeri	Palmer ceanothus
CEPA8	Celtis	pallida	Spiny hackberry
CEPE	Ceiba	pentandra	Ceiba
CEPE2	Cecropia	schreberiana	Pumpwood
CEPU2	Ceanothus	purpureus	Hollyleaf ceanothus
CERE	Celtis	reticulata	Western hackberry
CERE2	Cercis	reniformis	Southwestern redbud
CERO4	Ceanothus	roderickii	Pine hill buckbrush
CERU	Ceanothus	x rugosus	Rugose ceanothus
CESA	Ceanothus	sanguineus	Redstem ceanothus
CESA3	Cephalanthus	salicifolius	Mexican buttonbush
CESA4	Cestrum	salicifolium	Pussywillow jessamine
CESC	Celastrus	scandens	American bittersweet
CESE5	Ceanothus	serpyllifolius	Coastal plain buckbrush
CESI	Cedrela	sinensis	Chinese toon
CESI2	Cercis	siliquastrum	Arbol de judea
CESI3	Ceratonia	siliqua	Algarrobo europeo
CESI4	Celtis	sinensis	Chinese hackberry
CESO	Ceanothus	sonomensis	Sonoma ceanothus
CESO2	Ceanothus	sorediatus	Jimbrush
CESP	Ceanothus	spinosus	Green bark ceanothus
CETE	Celtis	tenuifolia	Dwarf hackberry
CETE2	Celtis	tetrandra	Eastern nettle tree
CETH	Ceanothus	thyrsiflorus	Blue blossom
CETO	Ceanothus	tomentosus	Woolyleaf ceanothus
CETO1	Celtis	tournefortii	Oriental hackberry
CETR3	Celtis	trinervia	Almex
CETR4	Cercocarpus	traskiae	Catalina island mahogany
CEVA	Ceanothus	x vanrensselaeri	Vanrensselaer ceanothus
CEVE	Ceanothus	velutinus	Snowbrush ceanothus
CEVE2	Ceanothus	verrucosus	Barranca brush
CEVE4	Ceanothus	x veitchianus	Veitch ceanothus
CH	Chamaecyparis		false cypress spp
CH10	Chrysanthemum		daisy spp
CH11	Chamaesyce		sandmat spp
CH13	Charpentiera		papala spp
CH14	Cheirodendron		cheirodendron spp
CH15	Chenopodium		goosefoot spp
CH16	Chilopsis		desert willow spp
CH18	Chiococca		milkberry spp
CH19	Chionanthus		fringetree spp

CH2	Chaenomeles		flowering quince spp
CH20	Chione		chione spp
CH22	Choisya		Mexican orange spp
CH23	Chorisia		Chorisia spp
CH24	Chromolaena		thoroughwort spp
CH26	Chrysobalanus		chrysobalanus spp
CH27	Chrysolepis		chinquapin spp
CH29	Chrysophyllum		chrysophyllum spp
CH3	Chamaerops		fan palm spp
CH30	Chrysothamnus		rabbitbrush spp
CH31	Chitalpa		chitalpa spp
CH32	Chrysalidocarps		butterfly palm spp
CH4	Chamaebatia		mountain misery spp
CH5	Chamaebatiaria		fernbush spp
CH6	Chamaecrista		sensitive pea spp
CH7	Chamaecystis		chamaecystis spp
CH8	Chamaedaphne		leatherleaf spp
CH9	Chamaedorea		chamaedorea spp
CHAL8	Chiococca	alba	West indian milkberry
CHAL9	Chrysothamnus	albidus	Whiteflower rabbitbrush
CHAR17	Chamaesyce	arnottiana	'akoko
CHAR6	Chrysophyllum	argenteum	Bastard redwood
CHAR8	Chamaesyce	articulata	Jointed sandmat
CHAT2	Chamaesyce	atrococca	Koko
CHAU2	Chamaebatia	australis	Southern mountain misery
CHAX2	Chionanthus	axilliflorus	Hueso
CHBI5	Chrysophyllum	bicolor	Chrysophyllum bicolor
CHCA	Chamaedaphne	calyculata	Bog heather
CHCA10	Chrysophyllum	cainito	Star apple
CHCE	Chamaesyce	celastroides	'ekoko
CHCL3	Chamaesyce	clusiifolia	Forest sandmat
CHCO12	Chionanthus	compactus	Bridgotree
CHDE3	Charpentiera	densiflora	Napali coast papala
CHDO3	Cheirodendron	dominii	Domin's club
CHDO4	Chionanthus	domingensis	White rosewood
CHDU	Choisya	dumosa	Mexican orange
CHEL	Charpentiera	elliptica	Ellipticleaf papala
CHFA	Cheirodendron	fauriei	Faurie's club
CHFO4	Cheirodendron	forbesii	Olapa
CHFU	Chamaecyparis	funebris	Mourning cypress
CHGR18	Chamaecrista	greggii	Gregg's sensitive pea
CHGR6	Chrysothamnus	greenei	Greene's rabbitbrush
CHHA2	Chamaesyce	halemanui	Kauai sandmat
CHHE3	Chamaesyce	herbstii	Herbst's sandmat
CHHO4	Chionanthus	holdridgei	Hueso prieto
CHHU	Chamaerops	humilis	Mediterranean fan palm
CHHU2	Chrysothamnus	humilis	Truckee rabbitbrush

CHIC	Chrysobalanus	icaco	Coco plum
CHJA2	Chaenomeles	japonica	Maule's quince
CHKU	Chamaesyce	kuwaleana	Kokomalei
CHLA1	Chaenomeles	speciosa	Japonese quince
CHLA2	Chamaecyparis	lawsoniana	Port orford cedar
CHLI	Chilopsis	linearis	Desertwillow
CHLI3	Chrysothamnus	linifolius	Spearleaf rabbitbrush
CHLI6	Chionanthus	ligustrinus	Cabra blanca
CHLU	Dypsis	lutescens	Areca palm
CHMI2	Chamaebatiaria	millefolium	Fernbush
CHMO2	Chrysothamnus	molestus	Arizona rabbitbrush
CHMU3	Chamaesyce	multiformis	Variable sandmat
CHNA	Ericameria	nauseosa	Rabbitbrush
CHNO	Chamaecyparis	nootkatensis	Alsaka cedar
CHOA	Chenopodium	oahuense	Alaweo
CHOB	Chamaecyparis	obtusa	Hinoki cypress
CHOB2	Charpentiera	obovata	Broadleaf papala
CHOL	Chrysophyllum	oliviforme	Satinleaf
CHOL3	Chamaesyce	olowaluana	Alpine sandmat
CHOV2	Charpentiera	ovata	Koolau range papala
CHPA17	Chiococca	parvifolia	Pineland milkberry
CHPA29	Chamaecystis	palmensis	Tagasaste
CHPA31	Chrysophyllum	pauciflorum	Camito de perro
CHPI	Chamaecyparis	pisifera	Sawara false cypress
CHPL	Cheirodendron	platyphyllum	Lapalapa
CHPO8	Chamaecrista	portoricensis	Puerto rico sensitive pea
CHPR	Chrysanthemum	praecox	Early daisy
CHPR7	Chamaecystis	prolifera	Escabon
CHRE	Chionanthus	retusus	Chinese fringe tree
CHRE3	Chamaesyce	remyi	Remy's sandmat
CHRO2	Chamaesyce	rockii	Koolau range sandmat
CHSE11	Chrysolepis	sempervirens	Bush chinquapin
CHSE17	Chamaedorea	seifrizii	Seifriz's chamaedorea
CHSE5	Chione	seminervis	Puntaj jayuya
CHSI	Chromolaena	sinuata	Wavyleaf thoroughwort
CHSP	Chorisia	speciosa	Palo borracho
CHSP3	Chrysothamnus	spathulatus	Guadalupe rabbitbrush
CHTA	Chitalpa	tashkentensis	Chitalpa
CHTH	Chamaecyparis	thyoides	Atlantic white cedar
CHTO3	Charpentiera	tomentosa	Waianae range papala
CHTR2	Cheirodendron	trigynum	Olapalapa
CHVE4	Chione	venosa	Fatpork
CHVI	Chionanthus	virginicus	Fringe tree
CHVI8	Chrysothamnus	viscidiflorus	Yellow rabbitbrush
CI1	Cibotium		manfern spp
CI3	Cinchona		cinchona spp
CI4	Cinnamomum		cinnamon spp

CI8	Citharexylum		fiddlewood spp
CI9	Citrullus		watermelon spp
CIAU	Citrus	aurantifolia	Lime
CIAU2	Citrus	aurantium	Sour orange
CIBE	Citharexylum	berlandieri	Berlandier's fiddlewood
CIBR3	Citharexylum	brachyanthum	Boxthorn fiddlewood
CIBU2	Cinnamomum	burmannii	Padang cassia
CICA	Cinnamomum	camphora	Camphor tree
CICA8	Citharexylum	caudatum	Juniper berry
CICH	Cibotium	chamissoi	Chamisso's manfern
CIEL2	Cinnamomum	elongatum	Laurel avispillo
CIFR	Citharexylum	fruticosum	Florida fuddlewood
CIGL	Cibotium	glaucum	Hapu'u
CIGR	Citrus	maxima	Shaddock
CILA	Citrullus	lanatus	Water melon
CILI	Citrus	limon	Lemon
CILI2	Citrus	limetta	Bitter orange
CILI3	Citrus	x limonia	Mandarin lime
CIME3	Citrus	medica	Citron
CIME8	Cibotium	menziesii	Hapu'u li
CIMO	Citharexylum	montevidense	Taruma de espinho
CIMO3	Cinnamomum	montanum	Avispillo
CIPA	Citrus	x paradisi	Grapefruit
CIPE3	Citharexylum	x perkinsii	Perkins' fiddlewood
CIPU	Cinchona	pubescens	Quinine
CIRE3	Citrus	reticulata	Tangerine
CISI	Citrus	sinensis	Orange
CISP	Citrus		citrus spp
CISP2	Citharexylum	spinosum	Fiddlewood
CITR7	Citharexylum	tristachyum	Threespike fiddlewood
CIVE2	Cinnamomum	verum	Cinnamon
CL1	Cladrastis		cladrastis spp
CL10	Cliftonia		cliftonia spp
CL11	Clinopodium		clinopodium spp
CL13	Clusia		attorney spp
CL2	Claoxylon		claoxylon spp
CL5	Clermontia		clermontia spp
CL6	Clerodendrum		glorybower spp
CL7	Cleyera		cleyera spp
CL8	Clibadium		clibadium spp
CL9	Clidemia		clidemia spp
CLAC2	Clerodendrum	aculeatum	Haggarbush
CLAC3	Clethra	acuminata	Mountain sweetpepperbush
CLAL	Clethra	alnifolia	Sweet pepperbush
CLAL4	Cleyera	albopunctata	Teta prieta
CLAN7	Clidemia	angustilamia	Narrowleaf terciopelo
CLAR4	Clermontia	arborescens	'oha wai nui

CLAS2	Clinopodium	ashei	Ashe's calamint
CLBU	Clerodendrum	bungei	Rose glorybower
CLCA5	Clermontia	calophylla	Lava clermontia
CLCA6	Clermontia	carinifera	Koloa clermontia
CLCH4	Clerodendrum	chinense	Stickbush
CLCL	Clermontia	clermontioides	Kauai clermontia
CLCL2	Clusia	clusioides	Cupeillo
CLCO10	Clinopodium	coccineum	Scarlet calamint
CLCY5	Clidemia	cymosa	Camasey colorado
CLDE4	Clinopodium	dentatum	Florida calamint
CLDR2	Clermontia	drepanomorpha	Kohala mtn clermontia
CLER	Clibadium	erosum	Carruzo
CLFA	Clermontia	fauriei	Haha'aiakamanu
CLFU	Clermontia	fulva	Yellowflower clermontia
CLGE	Clinopodium	georgianum	Georgia calamint
CLGL2	Clerodendrum	glabrum	Natal glorybower
CLGR3	Clermontia	grandiflora	Bog clermontia
CLGU	Clusia	gundlachii	Grundlach's attorney
CLHA4	Clermontia	hawaiiensis	'oha kepau
CLHI3	Clidemia	hirta	Soapbush
CLIN2	Clerodendrum	inerme	Embrert
CLJA3	Clerodendrum	japonicum	Japanese glorybower
CLJA6	Cleyera	japonica	Sakaki
CLKA	Clermontia	kakeana	Forest clermontia
CLKA2	Clerodendrum	kaempferi	Kaempfer's glorybower
CLKO	Clermontia	kohalae	Waipio valley clermontia
CLLE3	Clermontia	x leptoclada	Clermontia
CLLI3	Clermontia	lindseyana	Hillside clermontia
CLLU	Cladrastis	kentukea	Yellowwood
CLMA24	Clerodendrum	macrostegium	Velvetleaf glorybower
CLMI2	Clusia	minor	Cupey de monte
CLMI3	Clermontia	micrantha	Maui clermontia
CLMO	Cliftonia	monophylla	Buckwheat tree
CLMO5	Clermontia	montis-loa	Mauna loa clermontia
CLMU2	Clermontia	multiflora	Waihee clermontia
CLOB2	Clermontia	oblongifolia	Oahu clermontia
CLPA6	Clermontia	pallida	Wailai pali clermontia
CLPA8	Clermontia	parviflora	Smallflower clermontia
CLPE2	Clermontia	peleana	Pele clermontia
CLPE3	Clermontia	persicifolia	Waioiani clermontia
CLPY2	Clermontia	pyrularia	Hamakua clermontia
CLQU	Clerodendrum	quadriloculare	Shooting star
CLRO	Clusia	rosea	Autograph tree
CLSA	Claoxylon	sandwicense	Po'ola
CLSA5	Clermontia	samuelii	Hana clermontia
CLSP13	Clerodendrum	x speciosum	Java glory bean
CLSP2	Clethra		sweetpepperbush spp

CLSP7	Clerodendrum	speciosissimum	Javanese glorybower
CLST2	Clidemia	strigillosa	Thicket hogwood
CLTH	Clerodendrum	thompsoniae	Bagflower
CLTR	Clerodendrum	trichotomum	Harlequin glorybower
CLTU2	Clermontia	tuberculata	Haleakala clermontia
CLUM5	Clerodendrum	umbellatum	Umbel clerodendrum
CLWA2	Clermontia	waimeae	Swampforest clermontia
CLWA3	Clerodendrum	wallichii	Wallich's glorybower
CN1	Cnemidaria		cnemidaria spp
CN2	Cneoridium		cneoridium spp
CN3	Cnidoscolus		cnidoscolus spp
CNAC	Cnidoscolus	aconitifolius	Treadsoftly
CNDU	Cneoridium	dumosum	Bush rue
CNHO	Cnemidaria	horrida	Deepwoods fern
CO	Corymbia		corymbia spp
CO1	Cornus		dogwood spp
CO10	Coffea		coffee spp
CO11	Cojoba		cojoba spp
CO12	Coleogyne		coleogyne spp
CO13	Colubrina		nakedwood spp
CO14	Colvillea		colvillea spp
CO15	Copernicia		copernicia spp
CO16	Colutea		colutea spp
CO17	Corypha		corypha spp
CO18	Comarostaphylis		summer holly spp
CO19	Comocladia		maidenplum spp
CO2	Corylus		hazelnut spp
CO21	Condalia		snakewood spp
CO23	Conocarpus		button tree spp
CO24	Conostegia		snailwood spp
CO25	Conradina		false rosemary spp
CO26	Copaifera		copaifera spp
CO27	Coprosma		mirrorplant spp
CO28	Corchorus		corchorus spp
CO29	Cordia		cordia spp
CO3	Cotoneaster		cotoneaster spp
CO30	Cordyline		cordyline spp
CO34	Cornutia		cornutia spp
CO35	Coronilla		crownvetch spp
CO36	Corynocarpus		corynocarpus spp
CO39	Cotinus		smoketree spp
CO4	Coccoloba		coccoloba spp
CO40	Cocculus		cocculus spp
CO41	Couroupita		cannonball tree spp
CO42	Coursetia		babybonnets spp
CO43	Cowania		bitterbrush spp
CO5	Coccothrinax		silver palm spp

CO6	Cochlospermum		cochlospermum spp
CO7	Cocos		coconut palm spp
CO8	Codariocalyx		tick trefoil spp
CO9	Codiaeum		codiaeum spp
COAC2	Cotoneaster	acutifolius	Peking cotoneaster
COAD	Cotoneaster	adpressus	Creeping cotoneaster
COAL	Cornus	alternifolia	Alternateleaf dogwood
COAL2	Cordia	alliodora	Capa prieto
COAL3	Coccothrinax	barbadensis	Puerto rican thatch palm
COAL4	Trema	micranthum	Rainforest laurel
COAM	Corylus	americana	American hazlenut
COAM2	Cornus	amomum	Knob-styled dogwood
COAN11	Cordia	angustifolia	Basora
COAR	Coccothrinax	argentata	Florida silverpalm
COAR2	Coffea	arabica	Arabian coffee
COAR3	Colubrina	arborescens	Greenheart
COAR6	Colutea	arborescens	Bladder senna
COAR7	Cornus	x arnoldiana	Arnold dogwood
COAS2	Cornus	asperifolia	Toughleaf dogwood
COAS3	Colubrina	asiatica	Asian nakedwood
COAU	Cordyline	australis	Giant dracaena
COAV	Corylus	avellana	European filbert
COAX	Coursetia	axillaris	Texas babybonnets
COBA4	Cordia	bahamensis	Bahama manjack
COBE3	Cordia	bellonis	Serpentine manjack
COBO2	Cordia	boissieri	Anacahuita
COBO3	Cordia	borinquensis	Muneco
COBU	Cotoneaster	buxifolius	Cotoneaster
COCA	Cornus	capitata	Himalayan Strawberry Tree
COCA1	Corymbia	calophylla	Marri
COCA18	Colubrina	californica	Las animas nakedwood
COCA19	Conradina	canescens	False rosemary
COCI	Corymbia	citriodora	Lemonscented gum
COCO1	Cotinus	coggygria	Smoke tree
COCO11	Condalia	correllii	Correll's snakewood
COCO2	Corylus	colurna	Turkish hazelnut
COCO3	Corylus	cornuta	Beaked hazlenut
COCO5	Cordia	collococca	Red manjack
COCO8	Coccoloba	costata	Uvilla
COCU	Colubrina	cubensis	Cuban nakedwood
COCY3	Coprosma	cymosa	Hawai'i mirrorplant
CODI	Coccoloba	diversifolia	Doveplum
CODI18	Cordia	dichotoma	Fragrant manjack
CODI19	Cotoneaster	divaricatus	Spreading cotoneaster
CODI3	Comarostaphylis	diversifolia	Summer holly
CODO	Comocladia	dodonaea	Poison ash
CODR	Cornus	drummondii	Roughleaf dogwood

COEL	Colubrina	elliptica	Soldierwood
COEL3	Coprosma	elliptica	Bog mirrorplant
COER	Conocarpus	erectus	Button mangrove
COER3	Coprosma	ernodeoides	'aiakanene
COER5	Condalia	ericoides	Javelin bush
COET	Conradina	etonia	Eton rosemary
COEX	Corymbia	eximia	Yellow bloodwood
COFL	Cornus	florida	Flowering dogwood
COFO	Cornus	foemina	Stiff dogwood
COFO2	Coprosma	foliosa	Forest mirrorplant
COFR11	Cotoneaster	frigidus	Tree cotoneaster
COFR2	Cordyline	fruticosa	Tiplant
COFR3	Cotoneaster	franchetii	Orange cotoneaster
COFR9	Cornus	x friedlanderi	Friedlander's dogwood
COGE	Cordia	gerascanthus	Yauco
COGL	Condalia	globosa	Bitter snakewood
COGL17	Coronilla	globosa	White crownvetch
COGL3	Cornus	glabrata	Brown dogwood
COGL4	Comocladia	glabra	Carrasco
COGL5	Colubrina	glandulosa	Glandular nakedwood
COGL6	Cordia	globosa	Curaciao bush
COGL8	Coursetia	glandulosa	Rosary babybonnets
COGL9	Conradina	glabra	Apalachicola rosemary
COGR7	Colubrina	greggii	Sierra nakedwood
COGR8	Conradina	grandiflora	Largeflower rosemary
COGU3	Couroupita	guianensis	Cannonball tree
COGY	Codariocalyx	gyroides	False tick trefoil
COHE12	Corylus	heterophylla	Siberian hazelnut
COHI3	Corchorus	hirsutus	Jackswitch
COHO	Condalia	hookeri	Brazilian bluewood
COHO80	Cotoneaster	horizontalis	Rockspray cotoneaster
COHU80	Cotoneaster	hupehensis	Hupeh cotoneaster
COKA	Coprosma	kauensis	Koi
COKO	Cornus	kousa	Kousa dogwood
COKR	Coccoloba	krugii	Whitewood
COLA	Cocculus	laurifolius	Laurel-leafed snailseed
COLA12	Cordia	laevigata	Smooth manjack
COLA18	Cotoneaster	lacteus	Milkflower cotoneaster
COLA6	Corynocarpus	laevigatus	Karaka nut
COLI7	Cordia	lima	Lija
COLI8	Coffea	liberica	Liberian coffee
COLO4	Coprosma	longifolia	Oahu mirrorplant
COLU5	Cotoneaster	lucidus	Shiny cotoneaster
COMA	Cornus	mas	Cornelian cherry
COMA1	Corymbia	maculata	Spotted gum
COMA2	Corylus	maxima var. purpurea	Purpule giant filbert

COME	Purshia	mexicana	Cliffrose
COME6	Coprosma	menziesii	Hupilo
COMI	Coccoloba	microstachya	Puckhout
COMO2	Coprosma	x molokaiensis	Chelsea's mirrorplant
COMO3	Coprosma	montana	Alpine mirrorplant
COMY	Cordia	myxa	Assyrian plum
CONU	Cocos	nucifera	Coconut palm
CONU2	Cornus	nuttallii	Pacific dogwood
COOB	Cotinus	obovatus	American smoketree
COOB3	Cordia	obliqua	Clammy cherry
COOB4	Cornutia	obovata	Nigua
COOB9	Cornus	obliqua	Silky dogwood
COOC3	Coprosma	ochracea	Maui mirrorplant
COOF2	Copaifera	officinalis	Copaiba
COOP	Colubrina	oppositifolia	Kauila
COPA	Cotoneaster	pannosus	Silverleaf cotoneaster
COPA16	Cordia	parvifolia	Small-leaf geigertree
COPA24	Coccoloba	pallida	Pale seagrape
COPR	Copernicia	prunifera	Carnuaba wax palm
COPU	Coccoloba	pubescens	Moralon
COPU8	Coprosma	pubens	Pubescent mirrorplant
COPY	Coccoloba	pyrifolia	Uvera
COPY2	Cornutia	pyramidata	Azulejo
CORA	Cornus	racemosa	Gray dogwood
CORA13	Colvillea	racemosa	Colville's glory
CORA2	Coleogyne	ramosissima	Blackbrush
CORE4	Coprosma	repens	Creeping mirrorplant
CORH	Coprosma	rhynchocarpa	Woodland mirrorplant
CORI	Cordia	rickseckeri	San bartolome
CORU	Cornus	rugosa	Roundleaf dogwood
CORU17	Conostegia	rufescens	Luquillo mtn snailwood
CORU4	Coccoloba	rugosa	Ortegon
CORU5	Cordia	rupicola	Puerto rico manjack
COSA81	Cornus	sanguinea	Bloodtwig dogwood
COSE2	Cordia	sebestena	Geiger tree
COSE3	Cornus	sessilis	Blackfruit dogwood
COSI	Cordia	sinensis	Cordia sinensis
COSI2	Coccoloba	sintenisii	Uvero de monte
COSI82	Cotoneaster	simonsii	Simons' cotoneaster
COSL	Cornus	x slavinii	Slavin's dogwood
COSP3	Condalia	spathulata	Squawbush
COST	Cornus	sericea	Red osier dogwood
COST6	Colubrina	stricta	Comal nakedwood
COSU	Cordia	sulcata	Moral
COSU2	Cordia	subcordata	Kou
COSW	Coccoloba	swartzii	Swartz's pigeonplum
COTE6	Colubrina	texensis	Texan hogplum

COTE8	Coprosma	ternata	Molokai mirrorplant
COTE9	Coccoloba	tenuifolia	Bahama pigeonplum
COTO	Corymbia	torelliana	Cadaghi
COUT	Corypha	utan	Buri palm
COUV	Coccoloba	uvifera	Sea grape
COVA3	Codiaeum	variegatum	Garden croton
COVA4	Coronilla	valentina	Mediterranean crownvetch
COVE	Coccoloba	venosa	False chiggergrape
COVE4	Conradina	verticillata	Cumberland false rosemary
COVE6	Colubrina	verrucosa	Urban's nakedwood
COVI	Cochlospermum	vitifolium	Silk cottontree
COVI8	Condalia	viridis	Green snakewood
COWA	Condalia	warnockii	Warnock's snakewood
COWA3	Cordia	wagneriorum	Luquillo mountain manjack
COWA4	Coprosma	waimeae	'olena
CR	Crataegus		hawthorn spp
CR11	Cryptocarya		cryptocarya spp
CR12	Cryptomeria		Japanese cedar spp
CR2	Crescentia		crescentia spp
CR4	Crinodendron		Crinodendron spp
CR5	Critonia		Critonia spp
CR6	Crossopetalum		crossopetalum spp
CR7	Crossosoma		rockflower spp
CR8	Crotalaria		rattlebox spp
CR9	Croton		croton spp
CRAE	Crataegus	aestivalis	May hawthorn
CRAE2	Crataegus	aemula	Rome hawthorn
CRAL	Crescentia	alata	Morrito
CRAL14	Crataegus	alma	Bountiful hawthorn
CRAL2	Cryptocarya	alba	Peumo
CRAM4	Crataegus	ambitiosa	Grand rapids hawthorn
CRAN	Crataegus	annosa	Phoenix city hawthorn
CRAN10	Crataegus	anamesa	Fort bend hawthorn
CRAN6	Crataegus	x anomala	Anomalous hawthorn
CRAN9	Crataegus	ancisa	Mississippi hawthorn
CRAP4	Crataegus	apiomorpha	Fort sheridan hawthorn
CRAR6	Crataegus	arborea	Montgomery hawthorn
CRAR7	Crataegus	arcana	Carolina hawthorn
CRAR8	Crataegus	arrogans	Dixie hawthorn
CRAS3	Croton	astroites	Wild marrow
CRAT3	Crataegus	ater	Nashville hawthorn
CRAU2	Crataegus	austromontana	Valley head hawthorn
CRBE	Crataegus	berberifolia	Barbary hawthorn
CRBE4	Croton	betulinus	Beechleaf croton
CRBE5	Crataegus	beadlei	Beadle's hawthorn
CRBE6	Crataegus	beata	Dunbar's hawthorn
CRBI2	Crossosoma	bigelovii	Ragged rockflower

CRBO3	Crataegus	bona	Berks county hawthorn
CRBR	Crataegus	brachyacantha	Blueberry hawthorn
CRBR13	Crataegus	x brevipes	Crataegus x brevipes
CRBR3	Crataegus	brainerdii	Brainerd's hawthorn
CRBR4	Crataegus	brazoria	Brazos hawthorn
CRCA	Crataegus	calpodendron	Pear hawthorn
CRCA22	Crataegus	carrollensis	Eureka springs hawthorn
CRCA4	Crossosoma	californicum	California rockflower
CRCH	Crataegus	chrysocarpa	Fireberry hawthorn
CRCI	Croton	ciliatoglandulifer	Mexican croton
CRCO	Crataegus	pedicellata	Scarlet hawthorn
CRCO13	Crataegus	contrita	Southern hawthorn
CRCO2	Crataegus	coccinioides	Kansas hawthorn
CRCO26	Crataegus	compacta	Clustered hawthorn
CRCO27	Crataegus	corusca	Shiningbranch hawthorn
CRCO32	Crataegus	condigna	River junction hawthorn
CRCO4	Crataegus	coleae	Cole's hawthorn
CRCO7	Crataegus	compta	Adorned hawthorn
CRCO8	Crataegus	consanguinea	Tallahassee hawthorn
CRCO9	Croton	cortesianus	Cortez's croton
CRCR	Crataegus	crus-galli	Cockspur hawthorn
CRCRIN	Crataegus	crus-galli 'Inermis'	Inermis cockspur hawthorn
CRCU	Crescentia	cujete	Calabash tree
CRDA3	Crataegus	dallasiana	Dallas hawthorn
CRDE3	Crataegus	desueta	New york hawthorn
CRDI	Crataegus	dilatata	Broadleaf hawthorn
CRDI10	Crataegus	dissona	Northern hawthorn
CRDI11	Crataegus	distincta	Distinct hawthorn
CRDI3	Crataegus	dispar	Aiken hawthorn
CRDI4	Crataegus	disperma	Spreading hawthorn
CRDI8	Croton	discolor	Lechecillo
CRDI9	Crataegus	dispessa	Mink hawthorn
CRDO	Crataegus	douglasii	Black hawthorn
CRDO3	Crataegus	dodgei	Dodge's hawthorn
CREN	Crataegus	engelmannii	Engelmann's hawthorn
CRER	Crataegus	erythropoda	Cerro hawthorn
CRER3	Crataegus	erythrocarpa	Red hawthorn
CREX2	Crataegus	exilis	Slender hawthorn
CREX3	Crataegus	extraria	Marietta hawthorn
CRFL	Crataegus	flabellata	Fanleaf hawthorn
CRFL2	Crataegus	flava	Yellowleaf hawthorn
CRFR	Croton	fruticulosus	Bush croton
CRFR3	Crataegus	fragilis	Fragile hawthorn
CRFU2	Crataegus	fulleriana	Fuller's hawthorn
CRFU3	Crataegus	furtiva	Albany hawthorn
CRGL	Cryptocarya	glaucescens	Jackwood
CRGL4	Crataegus	glareosa	Port huron hawthorn

CRGR13	Crataegus	grandis	Grand hawthorn
CRGR2	Crataegus	greggiana	Gregg's hawthorn
CRHA2	Crataegus	harbisonii	Harbison's hawthorn
CRHA3	Crataegus	x haemacarpa	Crataegus x haemacarpa
CRHA4	Crataegus	harveyana	Harvey's hawthorn
CRHE3	Crataegus	helvina	Clarkton hawthorn
CRHO5	Crataegus	holmesiana	Holmes' hawthorn
CRHU	Croton	humilis	Pepperbush
CRHU3	Crataegus	x hudsonica	Hudson hawthorn
CRID	Crataegus	ideae	Concord hawthorn
CRIG2	Crataegus	ignave	Bedford springs hawthorn
CRIL2	Crossopetalum	ilicifolium	Christmasberry
CRIM	Crataegus	x immanis	Crataegus x immanis
CRIM3	Croton	impressus	Puerto rico croton
CRIM6	Crataegus	impar	Redclay hawthorn
CRIN	Crataegus	intricata	Biltmore hawthorn
CRIN10	Crataegus	x incaedua	Crataegus x incaedua
CRIN13	Croton	incanus	Torrey's croton
CRIN16	Crataegus	indicens	Mansfield hawthorn
CRIN17	Crataegus	insidiosa	Ozark hawthorn
CRIN18	Crataegus	integra	Lake ella hawthorn
CRIN19	Crataegus	invicta	Fulton hawthorn
CRIN26	Crataegus	inanis	Oldmaid hawthorn
CRIR	Crataegus	iracunda	Stolonbearing hawthorn
CRIR2	Crataegus	irrasa	Blanchard's hawthorn
CRJA	Cryptomeria	japonica	Japanese red cedar
CRJE	Crataegus	jesupii	Jesup's hawthorn
CRJO3	Crataegus	jonesiae	Miss jones' hawthorn
CRKE2	Crataegus	kelloggii	Kellogg's hawthorn
CRKE3	Crataegus	x kennedyi	Kennedy's hawthorn
CRKN	Crataegus	knieskerniana	Knieskern's hawthorn
CRLA	Crataegus	x lavallei	Carriere hawthorn
CRLA11	Crataegus	latebrosa	Densewoods hawthorn
CRLA2	Crataegus	lacrimata	Pensacola hawthorn
CRLA3	Crataegus	lanuginosa	Woolly hawthorn
CRLA4	Crataegus	x laneyi	Laney's hawthorn
CRLA80	Crataegus	laevigata	Smooth hawthorn
CRLA9	Crataegus	lanata	Hoary hawthorn
CRLE5	Crataegus	x lettermanii	Letterman's hawthorn
CRLE8	Crataegus	lemingtonensis	Lemington hawthorn
CRLI12	Crataegus	limnophila	Waterloving hawthorn
CRLI4	Croton	linearis	Grannybush
CRLI5	Crescentia	linearifolia	Higuerito
CRLI6	Crataegus	limata	Warm springs hawthorn
CRLO3	Crotalaria	longirostrata	Longbeak rattlebox
CRLU	Crataegus	lucorum	Grove hawthorn
CRLU2	Croton	lucidus	Firebush

CRLU3	Crataegus	lumaria	Roundleaf hawthorn
CRMA	Crataegus	marshallii	Parsley hawthorn
CRMA11	Crataegus	x maligna	Crataegus x maligna
CRMA3	Crataegus	macrosperma	Bigfruit hawthorn
CRMA4	Crataegus	margarettiae	Margarett's hawthorn
CRMA8	Cryptocarya	mannii	Holio
CRME	Crataegus	mendosa	Albertville hawthorn
CRME1	Crataegus	mexicana	Mexican hawthorn
CRME11	Crataegus	membranacea	Tissueleaf hawthorn
CRME3	Crataegus	meridionalis	Gallion hawthorn
CRME6	Crataegus	menandiana	Menand's hawthorn
CRMI10	Crataegus	mira	Confederate hawthorn
CRMO	Crataegus	x mordenensis	Morden hawthorn
CRMO1	Crataegus	mollis	Downy hawthorn
CRMU11	Crataegus	multiflora	Inkberry hawthorn
CRMU4	Crataegus	munda	Batesburg hawthorn
CRNA4	Crataegus	nananixonii	Nixon's hawthorn
CRNI	Crataegus	nitida	Glossy hawthorn
CRNI4	Crataegus	nitidula	Ontario hawthorn
CRNO2	Crataegus	x notha	Crataegus x notha
CRNU4	Crataegus	nuda	Nude hawthorn
CROP	Crataegus	opaca	Riverflat hawthorn
CROP3	Crataegus	opulens	Rochester hawthorn
CROV2	Crataegus	ovata	Ovateleaf hawthorn
CROX	Crataegus	monogyna	Oneseed hawthorn
CRPA	Crinodendron	patagua	Patagua
CRPA3	Crataegus	panda	Florida hawthorn
CRPE13	Crataegus	pearsonii	Pearson's hawthorn
CRPE14	Crataegus	x peckietta	Peck's hawthorn
CRPE17	Crataegus	pequotorum	Connecticut hawthorn
CRPE2	Crataegus	penita	Great smoky mtn hawthorn
CRPE3	Crataegus	pennsylvanica	Pennsylvania hawthorn
CRPE6	Crataegus	persimilis	Plumleaf hawthorn
CRPE7	Crataegus	perjucunda	Pearthorn
CRPH	Crataegus	phaenopyrum	Washington hawthorn
CRPI	Crataegus	x pilosa	Pilose hawthorn
CRPI3	Crataegus	pinetorum	Pineland hawthorn
CRPI4	Crataegus	piperi	Piper's hawthorn
CRPO	Crataegus	poliophylla	Elegant hawthorn
CRPO11	Crataegus	porrecta	Pittsburgh hawthorn
CRPO4	Croton	poecilanthus	Sabinon
CRPO6	Crescentia	portoricensis	Higuero de sierra
CRPO7	Critonia	portoricensis	Puerto rico thoroughwort
CRPR	Crataegus	pruinosa	Frosted hawthorne
CRPR2	Crataegus	pringlei	Pringle's hawthorn
CRPR4	Crataegus	pratensis	Prairie hawthorn
CRPR5	Crataegus	prona	Illinois hawthorn

CRPU	Crataegus	punctata	Dotted hawthorn
CRPU14	Crataegus	putata	Scranton hawthorn
CRPU8	Crataegus	x puberis	Crataegus x puberis
CRPU9	Crataegus	pulcherrima	Beautiful hawthorn
CRRA6	Crataegus	ravida	Jeweled hawthorn
CRRE11	Crataegus	resima	Gulf hawthorn
CRRE3	Crataegus	reverchonii	Reverchon's hawthorn
CRRH	Crossopetalum	rhacoma	Maidenberry
CRRH2	Crataegus	rhodella	Franklin's hawthorn
CRRI	Crataegus	rivularis	River hawthorn
CRRI2	Croton	rigidus	Yellow balsam
CRRI5	Crataegus	rigens	Gadsden hawthorn
CRRU	Cryptocarya	rubra	Cryptocarya
CRRU10	Crataegus	x rubrocarnea	Crataegus x rubrocarnea
CRRU5	Crataegus	rufula	Rusty hawthorn
CRSA	Crataegus	saligna	Willow hawthorn
CRSA3	Crataegus	sargentii	Sargent's hawthorn
CRSA8	Crotalaria	saltiana	African rattlebox
CRSC4	Crataegus	schuettei	Schuette's hawthorn
CRSC80	Crataegus	scabrida	Rough hawthorn
CRSH3	Crataegus	shaferi	Shafer's hawthorn
CRSI3	Crataegus	x simulata	Crataegus x simulata
CRSO	Croton	sonorae	Sonoran croton
CRSO2	Croton	soliman	Soliman's croton
CRSP	Crataegus	spathulata	Littlehip hawthorn
CRSP5	Crataegus	spatiosa	New london hawthorn
CRSP6	Crataegus	spissa	Essex hawthorn
CRST	Crataegus	stenosepala	Duke hawthorn
CRST6	Croton	stenophyllus	West indian croton
CRSU	Crataegus	succulenta	Fleshy hawthorn
CRSU16	Crataegus	suksdorfii	Suksdorf's hawthorn
CRSU2	Crataegus	submollis	Quebec hawthorn
CRSU3	Crataegus	suborbiculata	Caughuawaga hawthorn
CRSU6	Crataegus	sutherlandensis	Sutherland hawthorn
CRTA2	Crataegus	tanuphylla	Keystone hawthorn
CRTE2	Crataegus	texana	Texas hawthorn
CRTH4	Crataegus	thermopegaea	Graceful hawthorn
CRTI2	Crataegus	tinctoria	Dyed hawthorn
CRTR	Crataegus	tracyi	Tracy's hawthorn
CRTR2	Crataegus	triflora	Threeflower hawthorn
CRTR4	Crataegus	tristis	Minute hawthorn
CRTU2	Crataegus	turnerorum	Turner's hawthorn
CRUN	Crataegus	uniflora	Dwarf hawthorn
CRUV	Crataegus	uvaldensis	Lonestar hawthorn
CRVA	Crataegus	vailiae	Miss vail's hawthorn
CRVA3	Crataegus	valida	Rockmart hawthorn
CRVE11	Crataegus	versuta	Johnny reb hawthorn

CRVI	Crataegus	viridis	Green hawthorn
CRVI3	Crataegus	viburnifolia	Sawtooth hawthorn
CRVU	Crataegus	vulsa	Alabama hawthorn
CRWA	Crataegus	warneri	Warner's hawthorn
CRWE	Crataegus	x websteri	Webster's hawthorn
CRWH	Crataegus	x whittakeri	Whittaker's hawthorn
CRWI2	Croton	wigginsii	Wiggins' croton
CRWO	Crataegus	wootoniana	Wooton's hawthorn
CRX	Crataegus	x smithiana	Red Mexican Hawthorn
CRXA	Crataegus	xanthophylla	Buffalo hawthorn
CU	Cupressus		cypress spp
CU1	Cudrania		cudrania spp
CU4	Cunninghamia		cunninghamia spp
CU5	Cupania		cupania spp
CU6	Cupaniopsis		carrotwood spp
CU8	Cupressocyparis		cupressocyparis spp
CUAB	Cupressus	abramsiana	Santa cruz island cypress
CUAM	Cupania	americana	Guara
CUAN	Cupaniopsis	anacardioides	Carrotwood
CUAR	Cupressus	arizonica	Arizona cypress
CUBA	Cupressus	bakeri	Baker cypress
CUFO2	Cupressus	forbesii	Tecate cypress
CUFU	Cupressus	funebris	Chinese weeping cypress
CUGL	Cupania	glabra	Florida toadwood
CUGO	Cupressus	goveniana	Gowen cypress
CUGU	Cupressus	guadalupensis	Guadaluoe cypress
CULA	Cunninghamia	lanceolata	Blue chinese fir
CULE	Cupressocyparis	leylandii	Leyland cypress
CULU	Cupressus	lusitanica	Cedar-of-Goa
CUMA	Cupressus	macrocarpa	Monterey cypress
CUMA2	Cupressus	macnabiana	Macnab cypress
CUMAAU	Cupressus	macrocarpa aurea	Golden montery cypress
CUSA	Cupressus	sargentii	Sargent cypress
CUSE	Cupressus	sempervirens	Italian cypress
CUTO	Cupressus	torulosa	Bhutan cypress
CUTR	Cupania	triquetra	Guara blanca
CUTR2	Cudrania	tricuspidata	Storehousebush
CUVE	Cupania	vernalis	Camboata vermelho
CY	Cyphomandra		cyphomandra spp
CY1	Cyanea		cyanea spp
CY10	Cyrilla		titi spp
CY11	Cyrtandra		cyrtandra spp
CY12	Cytisus		broom spp
CY2	Cyathea		treefern spp
CY3	Cybianthus		cybianthus spp
CY4	Cycas		cycad spp
CY5	Cyclobalanopsis		Evergreen oak spp

CY6	Cydonia		cydonia spp
CY7	Cynometra		cynometra spp
CY8	Cypholophus		lopleaf spp
CYAC4	Cyanea	aculeatiflora	Haleakala cyanea
CYAL3	Cyrtandra	x alata	Cyrtandra x alata
CYAL4	Cyrtandra	x alnea	Cyrtandra x alnea
CYAM4	Cyrtandra	x ambigua	Ambiguous cyrtandra
CYAN	Cyathea	andina	Parrotfeather treefern
CYAN6	Cyanea	angustifolia	'aku
CYAR	Cyathea	arborea	Tree-fern
CYAR10	Cyanea	arborea	Palmtree cyanea
CYAR13	Cyathea	armata	Creeping treefern
CYAS	Cyanea	asarifolia	Gingerleaf cyanea
CYAS2	Cyanea	aspleniifolia	Spleenwort cyanea
CYAT2	Cyrtandra	x atomigyna	Cyrtandra x atomigyna
CYAX	Cyrtandra	x axilliflora	Axilflower
CYBA5	Cyrtandra	x basipartita	Cyrtandra x basipartita
CYBE	Cyphomandra	betacea	Tamarillo
CYBI3	Cyrtandra	biserrata	Molokai cyrtandra
CYBO3	Cyathea	borinquena	Birdwing treefern
CYCA11	Cyrtandra	x carinata	Cyrtandra x carinata
CYCA12	Cyrtandra	x caudatisepala	Cyrtandra x caudatisepala
CYCA13	Cyrtandra	x caulescens	Cyrtandra x caulescens
CYCA23	Cyanea	calycina	Waianae range rollandia
CYCA8	Cyrtandra	calpidicarpa	Valley cyrtandra
CYCH4	Cyrtandra	x christophersenii	Christoperson's cyrtandra
CYCI	Cycas	circinalis	Queen sago
CYCL	Cyrtandra	x cladantha	Cyrtandra x cladantha
CYCO11	Cyanea	comata	Maui cyanea
CYCO12	Cyanea	copelandii	Treetrunk cyanea
CYCO13	Cyanea	coriacea	Leatherleaf cyanea
CYCO18	Cyathea	cooperi	Cooper's cyathea
CYCO7	Cyrtandra	confertiflora	Lava cyrtandra
CYCO8	Cyrtandra	x conradtii	Conradt's cyrtandra
CYCO9	Cyrtandra	cordifolia	Heartleaf cyrtandra
CYCR3	Cyrtandra	x crassior	Cyrtandra x crassior
CYCR4	Cyrtandra	crenata	Kahana valley cyrtandra
CYCR7	Cyrtandra	x crassifolia	Cyrtandra x crassifolia
CYCU2	Cyrtandra	x cupuliformis	Cyrtandra x cupuliformis
CYCY3	Cyrtandra	cyaneoides	Mapele
CYCY7	Cyanea	cylindrocalyx	Cyanea cylindrocalyx
CYDA2	Cytisus	x dallimorei	Dallimore's spanishbroom
CYDE4	Cyrtandra	dentata	Mountain cyrtandra
CYDE5	Cyanea	degeneriana	Degener's cyanea
CYDU2	Cyanea	dunbarii	Ravine cyanea
CYEL5	Cyanea	elliptica	Ellipticleaf cyanea
CYEL8	Cyanea	eleeleensis	Eleele cyanea

CYFA5	Cyanea	fauriei	Faurie's cyanea
CYFE5	Cyrtandra	x ferrocolorata	Cyrtandra x ferrocolorata
CYFE6	Cyrtandra	x ferruginosa	Cyrtandra x ferruginosa
CYFI5	Cyrtandra	filipes	Gulch cyrtandra
CYFI6	Cyanea	fissa	Kauai cyanea
CYFO2	Cyrtandra	x forbesii	Forbes's cyrtandra
CYFU	Cyathea	furfuracea	Jamaican treefern
CYGA2	Cyrtandra	garnotiana	Hahala
CYGE	Cyrtandra	x georgiana	Georgia cyrtandra
CYGI3	Cyrtandra	giffardii	Forest cyrtandra
CYGI5	Cyanea	giffardii	Kilauea mauna cyanea
CYGL	Cyclobalanopsis	glauca	Cyclobalanopsis glauca
CYGL5	Cyanea	glabra	Smooth cyanea
CYGR12	Cyrtandra	grayi	Gray's cyrtandra
CYGR4	Cyrtandra	gracilis	Palolo valley cyrtandra
CYGR5	Cyrtandra	grandiflora	Largeflower cyrtandra
CYGR6	Cyrtandra	grayana	Pacific cyrtandra
CYGR8	Cyanea	grimesiana	Splitleaf cyanea
CYHA13	Cyanea	habenata	Stream-bed cyanea
CYHA2	Cyrtandra	halawensis	Toothleaf cyrtandra
CYHA3	Cyrtandra	hashimotoi	Maui cyrtandra
CYHA4	Cyrtandra	hawaiensis	Hawai'i cyrtandra
CYHA6	Cyanea	hamatiflora	Wetforest cyanea
CYHA7	Cyanea	hardyi	Oahu cyanea
CYHE4	Cyrtandra	hematos	Singleflower cyrtandra
CYHI5	Cyanea	hirtella	Rustyleaf cyanea
CYHI6	Cyrtandra	x hillebrandii	Hillebrand's cyrtandra
CYHO3	Cyrtandra	x honolulensis	Honolulu cyrtandra
CYHO4	Cyrtandra	x hosakae	Hosaka's cyrtandra
CYHO6	Cyanea	horrida	Prickly cyanea
CYHU2	Cyanea	humboldtiana	Oahu rollandia
CYKA	Cyrtandra	x kaalae	Kaala cyrtandra
CYKA11	Cyanea	kahiliensis	Cyanea kahiliensis
CYKA12	Cyrtandra	kamooloaensis	Kamo'oloa cyrtandra
CYKA2	Cyrtandra	x kahanaensis	Kahanae cyrtandra
CYKA5	Cyrtandra	kalihii	Koolau range cyrtandra
CYKA8	Cyrtandra	kauaiensis	Ulunahele
CYKA9	Cyrtandra	kaulantha	Waikane valley cyrtandra
CYKE	Cyrtandra	kealiae	Wahiawa mtn cyrtandra
CYKI	Cyrtandra	x kipahuluensis	Kipahulu cyrtandra
CYKI2	Cyrtandra	x kipapaensis	Kipapa cyrtandra
CYKO	Cyrtandra	kohalae	Kohala mountain cyrtandra
CYKO3	Cyanea	kolekoleensis	Kolekole cyanea
CYKO4	Cyanea	koolauensis	Palolo valley rollandia
CYKU	Cyanea	kunthiana	Kunth's cyanea
CYKU3	Cyanea	kuhihewa	Limahuli valley cyanea
CYLA12	Cyanea	lanceolata	Lanceleaf cyanea

CYLA6	Cyrtandra	x laevis	Cyrtandra x laevis
CYLA8	Cyrtandra	laxiflora	Oahu cyrtandra
CYLE3	Cyrtandra	lessoniana	Lesson's cyrtandra
CYLE5	Cyanea	leptostegia	Giant kokee cyanea
CYLI6	Cyanea	lindseyana	Lindsey's cyanea
CYLI7	Cyanea	linearifolia	Linearleaf cyanea
CYLI9	Cyrtandra	limahuliensis	Limahuli cyrtandra
CYLO12	Cyanea	longiflora	Ridge rollandia
CYLO3	Cyrtandra	longifolia	Longleaf cyrtandra
CYLO5	Cyanea	lobata	Waihee valley cyanea
CYLO7	Cyanea	longissima	Streambank cyanea
CYLY	Cyrtandra	lydgatei	Lydgate's cyrtandra
CYLY2	Cyrtandra	lysiosepala	Oppositeleaf cyrtandra
CYMA10	Cyanea	macrostegia	Purple cyanea
CYMA12	Cyanea	mannii	Mann's cyanea
CYMA14	Cyanea	marksii	Marks' cyanea
CYMA22	Cyrtandra	macraei	Upland cyrtandra
CYMA24	Cyanea	mauiensis	Cyanea mauiensis
CYMA6	Cyrtandra	macrocalyx	Largecalyx cyrtandra
CYMA7	Cyrtandra	x malacophylla	Cyrtandra x malacophylla
CYMA8	Cyrtandra	x mannii	Mann's cyrtandra
CYMC	Cyanea	mceldowneyi	Mceldowney's cyanea
CYME7	Cyrtandra	menziesii	Ha'i wale
CYME9	Cyanea	membranacea	Papery cyanea
CYMO12	Cypholophus	moluccanus	Hawai'i lopleaf
CYMU10	Cyanea	munroi	Munro's cyanea
CYMU3	Cytisus	multiflorus	White spanishbroom
CYMU5	Cyrtandra	munroi	Lanaihale cyrtandra
CYNU2	Cyrtandra	x nutans	Cyrtandra x nutans
CYOB	Cydonia	oblonga	Quince
CYOB4	Cyanea	obtusa	Bluntlobe cyanea
CYOL3	Cyrtandra	olona	Kauai cyrtandra
CYOP	Cyrtandra	x opaeulae	Opaeula cyrtandra
CYOX2	Cyrtandra	oxybapha	Pohakea gulch cyrtandra
CYPA12	Cyrtandra	paludosa	Kanawao ke'oke'o
CYPA23	Cyanea	parvifolia	Waioli valley rollandia
CYPA6	Cyrilla	parvifolia	Littleleaf titi
CYPA7	Cyathea	parvula	Small treefern
CYPI2	Cyrtandra	pickeringii	Pickering's cyrtandra
CYPI4	Cyanea	pilosa	Hairy cyanea
CYPI5	Cyanea	pinnatifida	Sharktail cyanea
CYPL5	Cyrtandra	platyphylla	'ilihia
CYPL7	Cyanea	platyphylla	Puna cyanea
CYPO2	Cynometra	portoricensis	Oreganillo falso
CYPO4	Cyrtandra	polyantha	Niu valley cyrtandra
CYPO5	Cyanea	pohaku	Pohaku cyanea
CYPR5	Cyrtandra	procera	Bog cyrtandra

CYPR6	Cyrtandra	propinqua	Arrowleaf cyrtandra
CYPR7	Cyrtandra	pruinosa	Frosted cyrtandra
CYPR8	Cyanea	procera	Molokai cyanea
CYPR9	Cyanea	profuga	Mapulehu valley cyanea
CYPU5	Cyrtandra	x pubens	Cyrtandra x pubens
CYPU8	Cyathea	pungens	Spiny treefern
CYPY	Cyanea	pycnocarpa	Manyfruit cyanea
CYQU	Cyanea	quercifolia	Oakleaf cyanea
CYRA	Cyrilla	racemiflora	Swamp cypress
CYRA3	Cyrtandra	x ramosissima	Cyrtandra x ramosissima
CYRE10	Cyanea	remyi	Remy's cyanea
CYRE11	Cycas	revoluta	Sago palm
CYRE8	Cyanea	recta	Kealia cyanea
CYRI3	Cyrtandra	rivularis	River cyrtandra
CYRO4	Cyrtandra	x rockii	Rock's cyrtandra
CYSA2	Cyrtandra	sandwicensis	Hairy cyrtandra
CYSC4	Cytisus	scoparius	Scotchbroom
CYSC6	Cyrtandra	x scabrella	Cyrtandra x scabrella
CYSC7	Cyanea	scabra	Harsh cyanea
CYSE12	Cyanea	sessilifolia	Sessileleaf cyanea
CYSE7	Cyrtandra	sessilis	Windyridge cyrtandra
CYSH	Cyanea	shipmanii	Shipman's cyanea
CYSI	Cybianthus	sintenisii	Puerto rico ridgerunner
CYSO	Cyanea	solanacea	Popolo
CYSO2	Cyanea	solenocalyx	Pua kala
CYSP4	Cyrtandra	spathulata	Spoonleaf cyrtandra
CYSP5	Cyanea	spathulata	Spoonleaf cyanea
CYST5	Cyanea	stictophylla	Kaiholena cyanea
CYST7	Cytisus	striatus	Striated broom
CYST8	Cyanea	st.-johnii	St. john's rollandia
CYSU4	Cyrtandra	x subintegra	Cyrtandra x subintegra
CYSU6	Cyrtandra	subumbellata	Parasol cyrtandra
CYSU8	Cyanea	superba	Mt. kaala cyanea
CYSY	Cyanea	sylvestris	Wahiawa cyanea
CYTE10	Cyathea	tenera	Helecho gigante
CYTI	Cyrtandra	tintinnabula	Laupahoehoe cyrtandra
CYTR6	Cyanea	tritomantha	'aku 'aku
CYTR7	Cyanea	truncata	Punaluu cyanea
CYTU	Cyrtandra	x turbiniformis	Cyrtandra x turbiniformis
CYUM2	Cyrtandra	x umbraculiflora	Cyrtandra umbraculiflora
CYUN5	Cyanea	undulata	Leechleaf cyanea
CYVI4	Cyrtandra	x villicalyx	Cyrtandra x villicalyx
CYVI7	Cyrtandra	viridiflora	Greenleaf cyrtandra
CYVI8	Cytisus	villosus	Hairybroom
CYWA	Cyrtandra	waianaeensis	Waianaeuka cyrtandra
CYWA10	Cyrtandra	x waihoiensis	Sharp-tooth cyrtandra
CYWA4	Cyrtandra	waiolani	Fuzzyflower cyrtandra

CYWA6	Cyrtandra	wawrae	Rockface cyrtandra
DA	Dahlia		dahlia spp
DA1	Dacryodes		dacryodes spp
DA2	Dalbergia		Indian rosewood spp
DA3	Dalea		prairie clover spp
DA4	Daphne		daphne spp
DA5	Daphnopsis		daphnopsis spp
DA6	Dasiphora		shrubby cinquefoil spp
DA7	Davidia		davidia spp
DAAM2	Daphnopsis	americana	Burn nose
DABR2	Dalbergia	brownei	Brown's indian rosewood
DACA9	Dalea	carthagenensis	Cartagena prairie clover
DAEC	Dalbergia	ecastaphyllum	Coinvine
DAEX	Dacryodes	excelsa	Candletree
DAHE2	Daphnopsis	helleriana	Heller's cieneguillo
DAIM	Dahlia	imperialis	Tree dahlia
DAIN	Davidia	involucrata	Dove Tree
DALA11	Daphne	laureola	Spurgelaurel
DAMO3	Dalbergia	monetaria	Moneybush
DAPH	Daphnopsis	philippiana	Emajagua de sierra
DASI	Dalbergia	sissoo	India rosewood
DASP	Psorothamnus	spinosus	Smokethorn
DE10	Dendropemon		leechbush spp
DE11	Dendrophthora		tree destroyer spp
DE12	Derris		derris spp
DE15	Deutzia		pride-of-Rochester spp
DE2	Dedeckera		July gold spp
DE3	Deeringothamnus		false pawpaw spp
DE4	Delissea		delissea spp
DE5	Delonix		delonix spp
DE8	Dendromecon		tree poppy spp
DE9	Dendropanax		dendropanax spp
DEAR	Dendropanax	arboreus	Angelica tree
DEBI4	Dendropemon	bicolor	Puerto rico leechbush
DECA9	Dendropemon	caribaeus	Four-angle leechbush
DECR	Deutzia	crenata	Crenate pride-rochester
DEDO	Dendrophthora	domingensis	Cuban tree destroyer
DEEU	Dedeckera	eurekensis	July gold
DEFA	Delissea	fallax	Hawai'i delissea
DEFL2	Dendrophthora	flagelliformis	Caribbean tree destroyer
DEGR3	Deutzia	gracilis	Slender pride rochester
DEHA3	Dendromecon	harfordii	Harford's tree poppy
DELA3	Dendropanax	laurifolius	Palo de vaca
DELA4	Delissea	laciniata	Cutleaf delissea
DELA6	Delissea	lauliiana	Small-leaf delissea
DEPA10	Deutzia	parviflora	Mongolian pride-rochester
DEPA9	Delissea	parviflora	Smallflower delissea

DEPU5	Dendropemon	purpureus	Smooth leechbush
DEPU6	Deeringothamnus	pulchellus	Royal false pawpaw
DERE	Delonix	regia	Royal poinciana
DERH2	Delissea	rhytidosperma	Kauai delissea
DERI	Dendromecon	rigida	Tree poppy
DERI4	Delissea	rivularis	Plateau delissea
DERU	Deeringothamnus	rugelii	Rugel's false pawpaw
DESC4	Deutzia	scabra	Fuzzy pride-of-rochester
DESI2	Dendropemon	sintenisii	Hicaquillo
DESU	Delissea	subcordata	Koolau range delissea
DEUN2	Delissea	undulata	Leechleaf delissea
DI10	Dirca		leatherwood spp
DI11	Ditta		ditta spp
DI12	Dipholis		willow bustic spp
DI2	Dichrostachys		dichrostachys spp
DI3	Diervilla		bush honeysuckle spp
DI4	Dillenia		dillenia spp
DI6	Diospyros		diospyros spp
DI7	Diphysa		diphysa spp
DI8	Diplacus		bush monkeyflower spp
DIBL3	Diospyros	blancoi	Mabolo
DICA12	Diplacus	calycinus	Kaweah river monkeyflower
DICI2	Dichrostachys	cinerea	Aroma
DIEB2	Diospyros	ebenum	Ebony
DIFA3	Diplacus	fasciculatus	Santa lucia monkeyflower
DIGR5	Diplacus	grandiflorus	Largeflower monkeyflower
DIHI4	Diospyros	hillebrandii	Elama
DIIN6	Dillenia	indica	Chulta
DIKA	Diospyros	kaki	Japanese persimmon
DILI4	Diplacus	linearis	Chaparral monkeyflower
DILO	Diervilla	lonicera	Northern bush honeysuckle
DILO5	Diplacus	lompocensis	Lompoc mesa monkeyflower
DILO6	Diplacus	longiflorus	Southern monkeyflower
DIMA24	Diospyros	maritima	Malaysian persimmon
DIMY	Ditta	myricoides	Jaboncillo
DIOC3	Dirca	occidentalis	Western leatherwood
DIPA9	Dirca	palustris	Eastern leatherwood
DIPU4	Diplacus	puniceus	Red bush monkeyflower
DIRE6	Diospyros	revoluta	Black apple
DIRI	Diervilla	rivularis	Mountain bush honeysuckle
DIRU3	Diplacus	rutilus	Santa susana monkeyflower
DISA	Sideroxylon	salicifolium	Willow bustic
DISA10	Diospyros	sandwicensis	Lama
DISE	Diervilla	sessilifolia	Southern bush honeysuckle

DISI3	Diospyros	sintenisii	Chinese persimmon
DISU11	Dillenia	suffruticosa	Shrubby dillenia
DITE	Diospyros	texana	Texas persimmon
DITH	Diphysa	thurberi	Thurber's diphysa
DIVI	Diospyros	virginiana	Common persimmon
DO	Dombeya		dombeya spp
DO1	Dodonaea		dodonaea spp
DO2	Doryphora		doryphora spp
DO3	Dovyalis		Ceylon gooseberry spp
DOHE2	Dovyalis	hebecarpa	Ceylon gooseberry
DOSA	Doryphora	sassafras	New South Wales Sassafras
DOVI	Dodonaea	viscosa	Florida hopbush
DOWA	Dombeya	wallichii	Dombeya
DR	Dracaena		dracaena spp
DR3	Drimys		winter's bark spp
DR6	Drypetes		drypetes spp
DRAL5	Drypetes	alba	Cafeillo
DRDI	Drypetes	diversifolia	Milkbark
DRDR	Dracaena	draco	Dragon tree
DRFR2	Dracaena	fragrans	Fragrant dracaena
DRGL2	Drypetes	glauca	Varital
DRIL	Drypetes	ilicifolia	Rosewood
DRLA	Drypetes	lateriflora	Guiana palm
DRWI	Drimys	winteri	Canelo
DU1	Dubautia		dubautia spp
DU2	Duranta		duranta spp
DUAR	Dubautia	arborea	Mauna kea dubautia
DUCI	Dubautia	ciliolata	Lava dubautia
DUDE	Dubautia	x demissifolia	Dubautia x demissifolia
DUDO	Dubautia	dolosa	Maui dubautia
DUER	Duranta	erecta	Golden dewdrops
DUFA2	Dubautia	x fallax	Dubautia x fallax
DUIM	Dubautia	imbricata	Bog dubautia
DUKN	Dubautia	knudsenii	Forest dubautia
DULA2	Dubautia	laevigata	Smooth dubautia
DULA4	Dubautia	laxa	Na'ena'e pua melemele
DULI	Dubautia	linearis	Shrubland dubautia
DUME	Dubautia	x media	Dubautia x media
DUME4	Dubautia	menziesii	Mountain dubautia
DUMI	Dubautia	microcephala	Kauai dubautia
DUMO	Dubautia	x molokaiensis	Molokai dubautia
DUMO2	Dubautia	x montana	Dubautia x montana
DUPA3	Dubautia	paleata	Na'ena'e pua kea
DUPA5	Dubautia	pauciflorula	Wahiawa bog dubautia
DUPL	Dubautia	plantaginea	Plantainleaf dubautia
DUPL2	Dubautia	platyphylla	Cinderslope dubautia

DURA	Dubautia	raillardioides	Na'ena'e 'ula
DURE2	Dubautia	reticulata	Netvein dubautia
DUSH	Dubautia	sherffiana	Waianae range dubautia
DUSY	Dubautia	syndetica	Wahiawa dubautia
DY1	Dypsis		dypsis spp
DYDE2	Dypsis	decaryi	Triangle palm
EB1	Ebenopsis		Texas ebony spp
EBEB	Ebenopsis	ebano	Texas ebony
EC3	Echium		vipersbugloss spp
ECCA5	Echium	candicans	Pride of madeira
ED1	Edgeworthia		paperbush spp
EDPA	Edgeworthia	papyrifera	Oriental paperbush
EH1	Ehretia		ehretia spp
EHAC	Ehretia	acuminata	Koda Tree
EHAN	Ehretia	anacua	Knockaway
EHTH	Ehretia	thyrsiflora	Ehretia thyrsiflora
EL	Elaeodendron		elaeodendron spp
EL1	Elaeagnus		elaeagnus spp
EL2	Elaeis		oil palm spp
EL3	Elaeocarpus		elaeocarpus spp
EL4	Eleutherococcus		ginseng spp
EL5	Elliottia		elliottia spp
ELAN	Elaeagnus	angustifolia	Russian olive
ELAU	Elaeodendron	australe	Red Olive Plum
ELBI	Elaeocarpus	bifidus	Kalia
ELCO	Elaeagnus	commutata	Silverberry
ELDE	Elaeocarpus	decipiens	Japanese blueberry tree
ELEU	Elaeocarpus	eumundi	Smooth-leaved Quandong
ELGL	Elaeocarpus	glabripetalus	Elaeocarpus glabripetalus
ELGU	Elaeis	guineensis	African oil palm
ELMU	Elaeagnus	multiflora	Cherry silverberry
ELOB	Elaeocarpus	obovatus	Hard Quandong
ELOR2	Elaeodendron	orientale	False olive
ELPE6	Eleutherococcus	pentaphyllus	Ginseng
ELPU	Elaeagnus	pungens	Thorny elaeagnus
ELPY	Elliottia	pyroliflorus	Copperbush
ELRA	Elliottia	racemosa	Georgia plume
ELRE	Elaeocarpus	reticulatus	Blueberry ash
ELUM	Elaeagnus	umbellata	Autumn olive
EM1	Embelia		embelia spp
EM2	Embothrium		embothrium spp
EM3	Emorya		emorya spp
EMCO	Embothrium	coccineum	Notro
EMPA	Embelia	pacifica	Kilioe
EMSU	Emorya	suaveolens	Emorybush
EN	Endiandra		endiandra spp
EN1	Encelia		brittlebush spp

EN3	Entada		callingcard vine spp
EN4	Enterolobium		enterolobium spp
ENCO2	Enterolobium	contortisiliquum	Pacara earpod tree
ENCY	Enterolobium	cyclocarpum	Ear tree
ENFR	Encelia	frutescens	Button brittlebush
ENPO4	Entada	polystachya	Callingcard vine
ENSI	Endiandra	sieberi	Hard Corkwood
ENVI	Encelia	virginensis	Virgin river brittlebush
EP3	Epilobium		willowherb spp
EPSE3	Epilobium	septentrionale	Northern willowherb
ER1	Eranthemum		eranthemum spp
ER11	Erithalis		blacktorch spp
ER12	Ernodea		ernodea spp
ER15	Erythrina		erythrina spp
ER16	Erythroxylum		coca spp
ER5	Ericameria		ericameria spp
ER7	Eriobotrya		loquat spp
ER8	Eriodictyon		yerba santa spp
ERAL12	Eriodictyon	altissimum	Indian knob mountainbalm
ERAN2	Eriodictyon	angustifolium	Narrowleaf yerba santa
ERAR	Erythroxylum	argentinum	Erythroxylum argentinum
ERAR17	Erythroxylum	areolatum	Swamp-redwood
ERAR27	Ericameria	arborescens	Goldenfleece
ERBE3	Erythrina	berteriana	Machete
ERBI	Erythrina	bidwillii	Bidwill's coral tree
ERBL2	Ericameria	bloomeri	Rabbitbush
ERBR11	Erythroxylum	brevipes	Brisselet
ERBR13	Ericameria	brachylepis	Chaparral goldenbush
ERCA	Erythrina	caffra	Kaffirboom coral tree
ERCA6	Eriodictyon	californicum	California yerba santa
ERCO	Erythrina	coralloides	Naked coral tree
ERCO22	Erythrina	corallodendron	Coral erythrina
ERCR	Erythrina	crista-galli	Cockspur coral tree
ERCR2	Eriodictyon	crassifolium	Thickleaf yerba santa
ERCR7	Ericameria	crispa	Crisped goldenbush
ERDE	Eriobotrya	deflexa	Bronze loquat
EREG	Erythrina	eggersii	Cock's spur
ERER11	Ericameria	ericoides	California goldenbush
ERFA	Erythrina	falcata	Corticeira-da-serra
ERFL7	Erythrina	flabelliformis	Coralbean
ERFR4	Erithalis	fruticosa	Blacktorch
ERFU2	Erythrina	fusca	Bucayo
ERGI5	Ericameria	gilmanii	Whiteflower goldenbush
ERHE	Erythrina	herbacea	Eastern coralbean
ERHU4	Erythrina	humeana	Natal coral tree
ERJA	Eriobotrya	japonica	Loquat tree
ERLI5	Ernodea	littoralis	Coughbush

ERLI6	Ericameria	linearifolia	Narrowleaf goldenbush
ERLY	Erythrina	lysistemon	Lysistemon coral tree
EROD	Erithalis	odorifer	Scented blacktorch
EROP2	Ericameria	ophitidis	Serpentine goldenbush
ERPA15	Ericameria	palmeri	Palmer's goldenbush
ERPA24	Ericameria	parishii	Parish's rabbitbrush
ERPA29	Ericameria	paniculata	Mojave rabbitbrush
ERPA30	Ericameria	parryi	Parry's rabbitbrush
ERPI7	Ericameria	pinifolia	Pinebush
ERPO	Erythrina	poeppigiana	Mountain immortelle
ERPU18	Eranthemum	pulchellum	Blue-sage
ERRE8	Ericameria	resinosa	Columbian goldenbush
ERRO3	Erythroxylum	rotundifolium	Ratwood
ERRU4	Erythroxylum	rufum	Rufous false cocaine
ERSA11	Erythrina	sandwicensis	Wili wili
ERSP	Erythrina	speciosa	Coral tree
ERTE18	Ericameria	teretifolia	Green rabbitbrush
ERTO	Eriodictyon	tomentosum	Woolly yerba santa
ERTR6	Eriodictyon	traskiae	Pacific yerba santa
ERTR7	Eriodictyon	trichocalyx	Hairy yerba santa
ERUI2	Ericameria	x uintahensis	Uinta rubber rabbitbrush
ERUM	Erythrina	umbrosa	Ceibo
ERUR4	Erythroxylum	urbanii	Urban's false cocaine
ERVA7	Erythrina	variegata	Tiger's claw
ERVAOR	Erythrina	variegata v orientalis	Indian coral tree
ERVE	Erythrina	vespertilio	Bat Wing Coral Tree
ERX	Erythrina	x sykesii	Thorny Coral Tree
ES1	Escallonia		redclaws spp
ES3	Esenbeckia		jopoy spp
ESBE	Esenbeckia	berlandieri	Berlandier's jopoy
ESRU4	Escallonia	rubra	Redclaws
EU	Euroschinus		euroschinus spp
EU1	Eucalyptus		gum spp
EU11	Euryops		euryops spp
EU2	Eubrachion		tapeworm-plant spp
EU5	Eucommia		eucommia spp
EU6	Eugenia		stopper spp
EU8	Euphorbia		spurge spp
EU9	Eurya		eurya spp
EU99	Eucryphia		eucryphia spp
EUAC	Eucalyptus	acaciformis	Wattle-leaved peppermint
EUAC1	Eucalyptus	acmenoides	White mahogany
EUAG	Eucalyptus	agglomerata	Blue-leaved stringybark
EUAG1	Eucalyptus	aggregata	Black gum
EUAL	Euonymus	alatus	Winged burningbush
EUAL8	Euonymus	alata	Winged burning bush

EUAL80	Eucalyptus	albens	Whitebox
EUAM	Eucalyptus	amplifolia	Cabbage gum
EUAM3	Eubrachion	ambiguum	Tapeworm-plant
EUAM7	Euonymus	americana	Strawberry bush
EUAM81	Eucalyptus	amygdalina	Blackpeppermint
EUAN	Eucalyptus	andrewsii	New england blackbutt
EUAN1	Eucalyptus	angophoroides	Apple-topped box
EUAO	Eucalyptus	aromaphloia	Scent bark
EUAP	Eucalyptus	apiculata	Narrow-leaved malle ash
EUAP5	Euonymus	aptera	Corky spindletree
EUAS	Eucalyptus	astringens	Brown mallet
EUAT	Euonymus	atropurpurea	Eastern wahoo
EUAX	Eugenia	axillaris	White stopper
EUBA1	Eucalyptus	badjensis	Big Badja gum
EUBA2	Eucalyptus	baeuerlenii	Baeuerlen's gum
EUBA3	Eucalyptus	bakeri	Baker's mallee
EUBA4	Eucalyptus	bancroftii	Bancroft's redgum
EUBA5	Eucalyptus	baueriana	Blue box
EUBA6	Eucalyptus	baxteri	Brown stringy bark
EUBE	Eucalyptus	benthamii	Camden white gum
EUBE1	Eucalyptus	beyeri	Beyer's ironbark
EUBE4	Eugenia	bellonis	Puerto rico stopper
EUBI	Eugenia	biflora	Blackrodwood
EUBL	Eucalyptus	blakelyi	Blakely's redgum
EUBL1	Eucalyptus	blaxlandii	Blaxland's strigybark
EUBO	Eucalyptus	botryoides	Southern mahogany
EUBO1	Eucalyptus	bosistoana	Coast grey box
EUBO3	Eugenia	boqueronensis	Sierra de cayey stopper
EUBO4	Eugenia	borinquensis	Guayabota de sierra
EUBR	Euphorbia	brasiliensis	Euphorbia brasiliensis
EUBR1	Eucalyptus	brookeriana	Brooker's gum
EUBR2	Eucalyptus	bridgesiana	Applebox
EUBU	Eucalyptus	burgessiana	Faulconbridge malle ash
EUBU6	Euonymus	bungeanum	Winterberry
EUCA	Eucalyptus	calophylla	Redgum
EUCA1	Eucalyptus	camaldulensis	Red gum eucalyptus
EUCA10	Eugenia	cacuminis	Cerro torrecilla stopper
EUCA1OV	Eucalyptus	camaldulensis ovata	River red gum
EUCA2	Eucalyptus	camphora	Swamp gum eucalyptus
EUCA3	Eucalyptus	caesia	Gungurru
EUCA4	Eucalyptus	caliginosa	Broad-leaved stringybark
EUCA5	Eucalyptus	cameronii	Diehard stringybark
EUCA6	Eucalyptus	canaliculata	Large-fruit grey gum
EUCA7	Eucalyptus	capitellata	Brown stringybark
EUCAOV	Eucalyptus	camaldulensis x ovata	Eucalyptus camaldulensis

EUCE	Eucalyptus	cephalocarpa	Silver stringybark
EUCH	Eucalyptus	chapmaniana	Bogong gum
EUCH4	Euryops	chrysanthemoides	Bull's eye
EUCI	Eucalyptus	cinerea	Silver dollar eucalyptus
EUCL	Eucalyptus	cladocalyx	Sugargum
EUCLNA	Eucalyptus	cladocalyx nana	Dwarf Sugar gum
EUCO	Eucalyptus	conferruminata	Bald island marlock
EUCO1	Eucalyptus	coccifera	Tasmanian snow gum
EUCO13	Eugenia	corozalensis	Sperry guava
EUCO2	Eucalyptus	conica	Fuzzy box
EUCO24	Euphorbia	cotinifolia	Mexican shrubby spurge
EUCO3	Eucalyptus	cornuta	Yate
EUCO4	Eugenia	confusa	Redberry stopper
EUCO5	Eugenia	cordata	Lathberry
EUCO6	Eucalyptus	consideniana	Yertchuk
EUCO7	Eucalyptus	cordata	Herat-leaved silver gum
EUCR	Eucalyptus	crebra	Narrowleaf red ironbark
EUCR1	Eucalyptus	crenulata	Buxton gum
EUCU	Eucalyptus	cunninghamii	Cliff mallee ash
EUCU1	Eucalyptus	curtisii	Plunkett mallee
EUCU3	Euphorbia	curtisii	Curtis' spurge
EUD4	Eucalyptus	delegatensis	Alpine ash
EUD5	Eucalyptus	dendromorpha	Budawang Ash
EUD6	Eucalyptus	denticulata	Shining gum
EUD8	Eucalyptus	deuaensis	Mongamulla mallee
EUDA	Eucalyptus	dalrympleana	Mountain white gum
EUDA1	Eucalyptus	dawsonii	Slaty box
EUDE	Eucalyptus	deglupta	Mindanao gum
EUDE1	Eucalyptus	dealbata	Tumble-down red gum
EUDE10	Euphorbia	dendroides	Tree spurge
EUDE2	Eucalyptus	deanei	Roundleaf gum
EUDE3	Eucalyptus	decorticans	Gum-topped ironbark
EUDE7	Eucalyptus	desmondensis	Desmond mallee
EUDI	Eucalyptus	diversicolor	Karri eucalyptus
EUDI1	Eucalyptus	dives	Broad-leaved peppermint
EUDO	Eugenia	domingensis	Serrette guave
EUDO2	Eucalyptus	dorrigoensis	Dorrigo white gum
EUDU	Eucalyptus	dumosa	White mallee
EUDU1	Eucalyptus	dunnii	Dunn's white gum
EUDW	Eucalyptus	dwyeri	Dwyer's red gum
EUEA	Eugenia	earhartii	Earhart's stopper
EUEG	Eugenia	eggersii	Guasabara
EUEL	Eucalyptus	elata	River peppermint
EUEL1	Eucalyptus	elliptica	Bendemeer white gum
EUER	Eucalyptus	erythrocorys	Red-cap gum
EUEU	Euonymus	europaea	European spindle tree
EUEU1	Eucalyptus	eugenioides	Thin-leaved stringybark

EUFA	Eucalyptus	fasciculosa	Pink gum
EUFA1	Eucalyptus	fastigata	Brown barrel
EUFA2	Euroschinus	falcata	Ribbonwood
EUFI	Eucalyptus	fibrosa	Broad-leaved red ironbark
EUFI81	Corymbia	ficifolia	Redflower gum
EUFO	Euonymus	fortunei	Winter creeper
EUFO1	Eucalyptus	forrestiana	Fuchsia gum
EUFO3	Eugenia	foetida	Boxleaf stopper
EUFR	Eucalyptus	fraxinoides	White mountain ash
EUGL	Eucalyptus	globulus	Blue gum eucalyptus
EUGL1	Eucalyptus	glaucina	Slaty red gum
EUGL2	Eucalyptus	globoidea	White stringybark
EUGL6	Eugenia	glabrata	Smooth rodwood
EUGLCO	Eucalyptus	globulus v compacta	Dwarf blue gum
EUGO	Eucalyptus	gomphocephala	Tuart
EUGO2	Eucalyptus	goniocalyx	Mountain graygum
EUGOBI	Eucalyptus	globulus bicostata	Southern blue gum
EUGOMA	Eucalyptus	globulus maidenii	Maiden's gum
EUGR	Eucalyptus	grandis	Flooded gum eucalyptus
EUGR1	Eucalyptus	gregsoniana	Wolgan snow gum
EUGU	Eucalyptus	gunnii	Cicer gum eucalyptus
EUGU2	Eucalyptus	gummifera	Red bloodwood
EUHA	Eucalyptus	haemastoma	Scribbly gum
EUHA1	Eucalyptus	hallii	Goodwood gum
EUHA2	Euphorbia	haeleeleana	Kauai spurge
EUHA4	Eugenia	haematocarpa	Luquillo mountain stopper
EUHA9	Euonymus	hamiltoniana	Hamilton's spindletree
EUIN	Eugenia	involucrata	Cerejeira-do-rio-grande
EUJA	Euonymus	japonica	Evergreen euonymus
EUKI	Eucalyptus	kitsoniana	Gippsland mallee
EUKI4	Euonymus	kiautschovica	Creeping strawberry bush
EUKO	Eugenia	koolauensis	Nioi
EULA	Eucalyptus	lacrimans	Weeping snowgum
EULA1	Eucalyptus	lansdowneana	Red-flowered mallee box
EULA2	Eucalyptus	largiflorens	Black box
EULA8	Euphorbia	lactea	Mottled spurge
EULA9	Eugenia	laevis	Bayamon stopper
EULE	Eucalyptus	leucoxylon	White ironbark
EULE2	Eucalyptus	lehmannii	Bushy yate
EULE6	Euphorbia	leucocephala	Pascuita
EULELE	Eucalyptus	leucoxylon leuc.	Yellow gum
EULEME	Eucalyptus	leucoxylon mglocrpa	Large fruit yellow gum
EULI	Eugenia	ligustrina	Privet stopper
EULI1	Eucalyptus	ligustrina	Privet-leaved stringybark
EULO	Eucalyptus	longifolia	Woollybutt

EULU	Eucalyptus	luehmanniana	Yellow-top mallee ash
EUMA	Eucalyptus	macrocarpa	Bluebush
EUMA1	Eucalyptus	macrandra	River yate
EUMA1MA	Eucalyptus	mannifera mannifera	Brittle gum
EUMA2	Eucalyptus	macarthurii	Camden woollybutt
EUMA3	Eucalyptus	macrorhyncha	Red stringybark
EUMA4	Eucalyptus	marginata	Jarrah
EUMA6	Eucalyptus	major	Queensland grey gum
EUMA7	Eucalyptus	mannifera	Red spotted gum
EUME	Eucalyptus	melliodora	Yellow box
EUMI	Eucalyptus	microcorys	Australian tallowwood
EUMI2	Eucalyptus	microtheca	Coolibah tree
EUMI3	Eucalyptus	microcarpa	Narrow-leaved box
EUMI4	Euphorbia	misera	Cliff spurge
EUMI5	Eucalyptus	mitchelliana	Mount Buffalo gum
EUMI6	Eucalyptus	michaeliana	Hillgrove gum
EUMI9	Euphorbia	milii	Christplant
EUMO	Eugenia	monticola	Birdcherry
EUMO1	Eucalyptus	moluccana	Gum-topped box
EUMO2	Eucalyptus	moorei	Narrow-leaved sally
EUMO3	Eucalyptus	morrisbyi	Morrisby's gum
EUMO5	Eucalyptus	x mortoniana	Morton eucalyptus
EUMU	Euryops	multifidus	Hawk's eye
EUMU1	Eucalyptus	multicaulis	Whipstick mallee ash
EUNE	Eucalyptus	neglecta	Omeo gum
EUNE4	Euphorbia	neriifolia	Indian spurgetree
EUNI	Eucalyptus	nicholii	Willow-leaved gimlet
EUNI1	Eucalyptus	nitens	Silvertop
EUNO	Eucalyptus	nortonii	Long-leaved box
EUNO1	Eucalyptus	notabilis	Blue Mountains mahogany
EUNU	Eucalyptus	nutans	Red-flowered moort
EUNY	Eucryphia	x nymansensis	'Namansay' eucryphia
EUOB	Eucalyptus	obliqua	Messmate stringybark
EUOB1	Eucalyptus	obtusiflora	Dongarra mallee
EUOC	Euonymus	occidentalis	Western wahoo
EUOC9	Eucalyptus	occidentalis	Flat-top yate
EUOD	Eucalyptus	odorata	Peppermint box
EUOL	Eucalyptus	olsenii	Woila gum
EUOVOV	Eucalyptus	ovata ovata	Swamp gum
EUPA	Eucalyptus	paniculata	Gray ironbark
EUPA1	Eucalyptus	parramattensis	Calgaroo
EUPA12	Eugenia	padronii	Padron's stopper
EUPA2	Eugenia	paniculata	Brush cherry
EUPA26	Eucalyptus	parvula	Kybean gum
EUPA3PA	Eucalyptus	pauciflora pauci.	Snow gum
EUPE	Euryops	pectinatus	Euryops pectinatus

EUPE1	Eucalyptus	pellita	Large-fruit red mahogany
EUPE2	Eucalyptus	perriniana	Spinning gum
EUPE8	Euphorbia	petiolaris	Manchineel berry
EUPH5	Euonymus	phellomana	Corktree
EUPI	Eucalyptus	pilularis	Blackbutt
EUPI1	Eucalyptus	pilligaensis	Narrow-leaved grey box
EUPI2	Eucalyptus	piperita	Sydney peppermint
EUPL	Eucalyptus	platypus	Moort
EUPO	Eucalyptus	polyanthemos	Sliver dollar eucalyptus
EUPO1	Eucalyptus	polybractea	Blue-leaved mallee
EUPOPO	Eucalyptus	polyanthemos poly.	Red box
EUPR4	Eugenia	procera	Rockmyrtle
EUPS	Eugenia	pseudopsidium	Christmas cherry
EUPS1	Eucalyptus	pseudoglobulus	Victorian eurabbie
EUPU	Eucalyptus	pulchella	White peppermint
EUPU1	Eucalyptus	punctata	Grey gum
EUPU2	Eucalyptus	pulverulenta	Silverleaf mountain gum
EUPU9	Euphorbia	pulcherrima	Poinsettia
EUQU	Eucalyptus	quadrangulata	White-topped box
EUQU1	Eucalyptus	quadricostata	Square-fruited ironbark
EURA	Eucalyptus	radiata	Narrow-leaved peppermint
EURA4	Eucalyptus	raveretiana	Black ironbox
EURARA	Eucalyptus	radiata radiata	Narrow-leaf peppermint
EURARA1	Eucalyptus	racemosa racemosa	Snappy gum
EURARO	Eucalyptus	racemosa rossii	Inland scribbly gum
EURE	Eucalyptus	redunca	Black marlock
EURE2	Eucalyptus	resinifera	Redmahogany
EURE7	Eugenia	reinwardtiana	Mountain stopper
EURH	Eugenia	rhombea	Red stopper
EURO	Eucalyptus	robusta	Beakpod euclayptus
EURU	Eucalyptus	rudis	Desert gum eucalyptus
EURU1	Eucalyptus	rubida	Candlebark
EURU2	Eucalyptus	rudderi	Rudder's box
EUSA	Eucalyptus	saligna	Sydney blue gum
EUSA1	Eucalyptus	salmonophloia	Salmon gum
EUSA3	Eucalyptus	saxatilis	Suggan Buggan mallee
EUSA6	Eurya	sandwicensis	Anini
EUSABO	Eucalyptus	saligna x botryoides	Eucalyptus saligna
EUSC	Eucalyptus	scoparia	Wallangarra white gum
EUSE	Eucalyptus	seeana	Narrow-leaved red gum
EUSE10	Eugenia	sessiliflora	Sessileleaf stopper
EUSE9	Eugenia	serrasuela	Serrasuela
EUSI	Eucalyptus	sideroxylon	Mugga ironbark
EUSI1	Eucalyptus	sieberi	Silvertop ash

EUSI2	Eucalyptus	simmondsii	Smithton peppermint
EUSM	Syzygium	smithii	Lilly-pilly tree
EUSM1	Eucalyptus	smithii	Gully gum
EUSO	Eucalyptus	socialis	Red mallee
EUSP	Euonymus		spindletree spp
EUSP2	Eucalyptus	spathulata	Narrow-leaved gimlet
EUSQ	Eucalyptus	squamosa	Scaly bark
EUST	Eucalyptus	stellulata	Black sally
EUST1	Eucalyptus	stricta	Blue Mountains mallee ash
EUST3	Eugenia	stahlii	Stahl's stopper
EUST6	Eugenia	stewardsonii	Stewardson's stopper
EUTE	Eucalyptus	tereticornis	Horn cap eucalyptus
EUTE1	Eucalyptus	pleurocarpa	Tallerack
EUTI	Euphorbia	tirucalli	Indiantree spurge
EUTO11	Eucalyptus	torquata	Coral gum
EUTR	Eucalyptus	tricarpa	Red ironbark
EUUL	Eucommia	ulmoides	Hardy rubber tree
EUUN	Eugenia	underwoodii	Underwood's stopper
EUUN2	Eugenia	uniflora	Surinam cherry
EUUR	Eucalyptus	urophylla	Eucalyptus urophylla
EUVE	Eucalyptus	verrucata	Mt Abrupt stringybark
EUVI	Eucalyptus	viminalis	Ribbon gum eucalyptus
EUVI1	Eucalyptus	viridis	Green mallee
EUVIPR	Eucalyptus	viminalis pryoriana	Gippsland manna gum
EUVIVI	Eucalyptus	viminalis viminalis	Manna gum
EUVIWI	Eucalyptus	viridis wimmerensis	Eucalyptus viridis
EUWO2	Eugenia	woodburyana	Woodbury's stopper
EUXE	Eugenia	xerophytica	Aridland stopper
EUYA	Eucalyptus	yarraensis	Yarra gum
EUYO	Eucalyptus	youmanii	Yourman's stringybark
EX1	Exocarpos		exocarpos spp
EX2	Exochorda		pearlbrush spp
EX3	Exostema		exostema spp
EX4	Exothea		exothea spp
EXCA	Exostema	caribaeum	Princewood
EXCU	Exocarpos	cupressiformis	Cherry Ballart
EXEL	Exostema	ellipticum	Plateado
EXGA	Exocarpos	gaudichaudii	Hulumoa
EXLU	Exocarpos	luteolus	Leafy ballart
EXME	Exocarpos	menziesii	Menzies' ballart
EXPA	Exothea	paniculata	Butterbough
EXRA	Exochorda	racemosa	Common pearlbrush
EY1	Eysenhardtia		kidneywood spp
EYOR	Eysenhardtia	orthocarpa	Tahitian kidneywood
EYPO	Eysenhardtia	polystachya	Mexican kidneywood
EYSP	Eysenhardtia	spinosa	Spiny kidneywood

EYTE	Eysenhardtia	texana	Texas kidneywood
FA	Fagus		beech spp
FA1	Fagraea		fagraea spp
FA2	Falcataria		peacocksplume spp
FA3	Fallugia		Apache plume spp
FA4	Faramea		false coffee spp
FA5	Fatsia		fatsia spp
FABE	Fagraea	berteroana	Pua kenikeni
FACR	Fagus	crenata	Japanese beech
FAGR	Fagus	grandifolia	American beech
FAJA	Fatsia	japonica	Japanese aralia
FAOC	Faramea	occidentalis	False coffee
FAPA	Fallugia	paradoxa	Apache plume
FASY	Fagus	sylvatica	European beech
FASYPU	Fagus	sylvatica 'Purpurea'	Copper beech
FE	Feijoa		feijoa spp
FE1	Fendlera		fendlerbush spp
FE2	Fendlerella		Utah fendlerbush spp
FE3	Ferocactus		barrel cactus spp
FERI2	Fendlera	rigida	Stiff fendlerbush
FERU	Fendlera	rupicola	Cliff fendlerbush
FESE	Feijoa	sellowiana	Pineapple guava
FEUT	Fendlerella	utahensis	Utah fendlerbush
FEWI	Ferocactus	wislizeni	Candy barrelcactus
FEWR	Fendlera	wrightii	Wright's fendlerbush
FI	Filicium		filicium spp
FI1	Ficus		fig spp
FI3	Firmiana		parasoltree spp
FI4	Fitchia		fitchia spp
FIAL4	Ficus	altissima	Council tree
FIAM	Ficus	americana	Jamaican cherry fig
FIAU	Ficus	aurea	Florida strangler fig
FIBE	Ficus	benjamina	Benjamin fig
FIBE2	Ficus	benghalensis	Indian banyan
FICA	Ficus	carica	Common fig
FICI	Ficus	citrifolia	Wild banyantree
FICO	Ficus	coronata	Sandpaper Fig
FIDE	Ficus	destruens	Boonjee
FIDE6	Filicium	decipiens	Fern tree
FIDR3	Ficus	drupacea	Brown-woolly fig
FIEL	Ficus	elastica	Rubber plant
FIEN	Ficus	enormis	Figueira
FILY	Ficus	lyrata	Fiddle leaf fig
FIMA	Ficus	macrocarpa	Ficus macrocarpa
FIMA1	Ficus	macrophylla	Moreton bay fig
FIMAAL	Ficus	maclellandii v alii	Dwarf rubber plant

FIMI	Ficus	thonningii	Figueira benjamin
FIMIHI	Ficus	microcarpa hillii	Hill's weeping fig
FIMINI	Ficus	microcarpa nitida	Green indian laurel fig
FIMINI1	Ficus	microcarpa nitida v Grn Gem	Grn gem indian laurel fig
FINE	Ficus	lutea	Lagos rubbertree
FINO3	Ficus	nota	Tibig
FIOB	Ficus	obtusifolia	Amate
FIOB1	Ficus	obliqua	Small-leaved Fig
FIOR	Ficus	organensis	Figueira nativa
FIPA2	Ficus	palmata	Punjab fig
FIPL	Ficus	platypoda	Rock fig
FIPU2	Ficus	pumila	Climbingfig
FIRE3	Ficus	religiosa	Peepul tree
FIRE4	Ficus	retusa ssp nitida	Indian laurel fig
FIRU	Ficus	rubiginosa	Rustyleaf fig
FISI	Firmiana	simplex	Chinese parasoltree
FISP3	Fitchia	speciosa	Burrdaisytree
FIST	Ficus	stahlii	Jaguey
FISU	Ficus	henneana	Sea Fig
FITR	Ficus	trigonata	Jaguey blanco
FIVI	Ficus	virens	White Fig
FIWA	Ficus	watkinsiana	Watkins fig
FL1	Flacourtia		flacourtia spp
FL5	Flindersia		flindersia spp
FL6	Flourensia		tarwort spp
FL7	Flueggea		bushweed spp
FLAC	Flueggea	acidoton	Simpleleaf bushweed
FLAU	Flindersia	australis	Crows Ash
FLBR	Flindersia	brayleyana	Queensland maple
FLCE	Flourensia	cernua	American tarwort
FLIN	Flacourtia	indica	Governor's plum
FLIN3	Flacourtia	inermis	Batoko plum
FLNE	Flueggea	neowawraea	Mehamehame
FO1	Fontanesia		fontanesia spp
FO2	Forchhammeria		forchhammeria spp
FO3	Forestiera		swampprivet spp
FO4	Fortunella		kumquat spp
FO5	Fothergilla		witchalder spp
FO6	Fouquieria		ocotillo spp
FOAC	Forestiera	acuminata	Swamp privet
FOAN	Forestiera	angustifolia	Texas swampprivet
FOBR2	Forchhammeria	brevipes	Shortstalk forchhammeria
FOEG	Forestiera	eggersiana	Inkbush
FOGA	Fothergilla	gardenii	Dwarf witchalder
FOGO	Forestiera	godfreyi	Godfrey's swampprivet
FOIN3	Forsythia	x intermedia	Showy forsythia

FOJA	Fortunella	japonica	Round kumquat
FOLI	Forestiera	ligustrina	Upland swampprivet
FOMA	Fothergilla	major	Mountain witchalder
FOMA2	Fortunella	margarita	Oval kumquat
FOOV80	Forsythia	ovata	Early forsythia
FOPH2	Fontanesia	phillyreoides	Syrian-privet
FOPO3	Forchhammeria	polyandra	Manystamen forchhammeria
FOPU2	Forestiera	pubescens	Stretchberry
FORE	Forestiera	reticulata	Netleaf swampprivet
FORH	Forestiera	rhamnifolia	Caca ravet
FORS	Forsythia		forsythia spp
FOSE	Forestiera	segregata	Florida swampprivet
FOSH	Forestiera	shrevei	Desert olive
FOSP2	Fouquieria	splendens	Ocotillo
FOSU	Forsythia	suspensa	Weeping forsythia
FOVI	Forsythia	viridissima	Greenstem forsythia
FR	Fraxinus		ash spp
FR1	Frangula		buckthorn spp
FR3	Franklinia		Franklin tree spp
FR4	Fremontodendron		flannelbush spp
FRAL	Franklinia	alatamaha	Franklin tree
FRAM	Fraxinus	americana	White ash
FRAMAA	Fraxinus	americana Autumn Applause	Autumn applause ash
FRAMAP	Fraxinus	americana 'Autumn Purple'	Autumn purple ash
FRAMCC	Fraxinus	americana Champaign Cnty	Champaign county ash
FRAMRH	Fraxinus	americana 'Rosehill'	Rosehill ash
FRAN	Fraxinus	anomala	Singleleaf ash
FRAN2	Fraxinus	angustifolia	Narrow-leafed ash
FRAN2AN	Fraxinus	angustifolia angus.	Desert ash
FRANRW	Fraxinus	angustifolia 'Raywood'	Raywood ash
FRBE	Fraxinus	berlandieriana	Arizona ash
FRBE2	Frangula	betulifolia	Beechleaf frangula
FRBL	Frangula	x blumeri	Blumer buckthorn
FRCA	Fraxinus	caroliniana	Carolina ash
FRCA12	Frangula	californica	California buckthorn
FRCA6	Fremontodendron	californicum	California flannelbush
FRCH	Fraxinus	chinensis	Chinese ash
FRCU	Fraxinus	cuspidata	Fragrant ash
FRDE2	Fremontodendron	decumbens	Pine hill flannelbush
FRDI2	Fraxinus	dipetala	California ash
FREX	Fraxinus	excelsior	European ash
FREXAU	Fraxinus	excelsior aurea	Golden ash

FREXHE	Fraxinus	excelsior 'Hessei'	Hesse ash
FREXKI	Fraxinus	excelsior 'Kimberly'	Kimberly ash
FRGO	Fraxinus	gooddingii	Goodding's ash
FRGR	Fraxinus	greggii	Gregg ash
FRGR1	Fraxinus	griffithii	Evergreen Ash
FRHO	Fraxinus	holotricha	Moraine ash
FRLA	Fraxinus	latifolia	Oregon ash
FRMA	Fraxinus	mandshurica	Manchurian ash
FRMA6	Fraxinus	malacophylla	Malacophylla ash
FRME2	Fremontodendron	mexicanum	Mexican flannelbush
FRNI	Fraxinus	nigra	Black ash
FROR	Fraxinus	ornus	Flowering ash
FROX	Fraxinus	oxycarpa	Caucasian ash
FROXAU	Fraxinus	oxycarpa 'Aureafolia'	Golden desert ash
FROXFL	Fraxinus	oxycarpa 'Flame'	Flame ash
FRPA4	Fraxinus	papillosa	Chihuahuan ash
FRPE	Fraxinus	pennsylvanica	Green ash
FRPEMA	Fraxinus	pennsylvanica 'Marshall'	Marshall ash
FRPEPA	Fraxinus	pennsylvanica 'Patmore'	Patmore ash
FRPESG	Fraxinus	pennsylvanica 'Shrwd Glen'	Sherwood glen green ash
FRPESU	Fraxinus	pennsylvanica 'Summit'	Summit ash
FRPR	Fraxinus	profunda	Pumpkin ash
FRQU	Fraxinus	quadrangulata	Blue ash
FRRU	Frangula	rubra	Red buckthorn
FRSP2	Frangula	sphaerosperma	West indian buckthorn
FRTE	Fraxinus	texensis	Texas ash
FRUH	Fraxinus	uhdei	Shamel ash
FRVE	Fraxinus	velutina	Velvet ash
FRVEFW	Fraxinus	velutina 'Fan West'	Velvet ash 'Fan West'
FRVEMO	Fraxinus	velutina 'Modesto'	Modesto ash
FU1	Fuchsia		fuchsia spp
FU2	Funtumia		funtumia spp
FU3	Furcraea		furcraea spp
FUBO	Fuchsia	boliviana	Bolivian fuchsia
FUEL	Funtumia	elastica	Silkrubber
FUHY2	Fuchsia	hybrida	Hybrid fuchsia
FUMA	Fuchsia	magellanica	Hardy fuchsia
FUPA2	Fuchsia	paniculata	Shrubby fuchsia
FUSE	Furcraea	selloa	Wild sisal
GA1	Gaylussacia		huckleberry spp
GA10	Garrya		silktassel spp
GA13	Gaussia		gaussia spp

GA2	Gardenia		gardenia spp
GA5	Galium		bedstraw spp
GA8	Garberia		garberia spp
GA9	Garcinia		saptree spp
GAAN6	Gardenia	angusta	Cape jasmine
GAAT	Gaussia	attenuata	Llume
GABA	Gaylussacia	baccata	Black huckleberry
GABR	Gardenia	brighamii	Forest gardenia
GABU2	Garrya	buxifolia	Dwarf silktassel
GACL2	Galium	cliftonsmithii	Santa barbara bedstraw
GACO9	Garrya	congdonii	Chaparral silktassel
GADU3	Garcinia	dulcis	Gourka
GAEL	Garrya	elliptica	Wavyleaf silktassel
GAFA5	Garrya	fadyenia	Fadyen's silktassel
GAFL	Garrya	flavescens	Silktassel
GAFR	Garrya	fremontii	Silk tassle
GAFR2	Gaylussacia	frondosa	Blue huckleberry
GAHE4	Garberia	heterophylla	Garberia
GAHE5	Garcinia	hessii	Lemon saptree
GAMA10	Garcinia	mangostana	Mangosteen
GAMA6	Gardenia	mannii	Oahu gardenia
GAMO3	Gaylussacia	mosieri	Woolly huckleberry
GANA	Gaylussacia	nana	Confederate huckleberry
GAOV	Garrya	ovata	Eggleaf silktassel
GAPO	Galium	porrigens	Graceful bedstraw
GAPO2	Garcinia	portoricensis	Palo de cruz
GARE	Gardenia	remyi	Remy's gardenia
GATA	Gardenia	taitensis	Tahitian gardenia
GATO5	Gaylussacia	tomentosa	Hairytwig huckleberry
GAUR	Gaylussacia	ursina	Bear huckleberry
GAVE2	Garrya	veatchii	Canyon silktassel
GAWR3	Garrya	wrightii	Wright's silktassel
GE	Geijera		geijera spp
GE1	Geranium		geranium spp
GE2	Gelsemium		trumpetflower spp
GE3	Genipa		genipa spp
GE4	Genista		Genista spp
GE5	Genistidium		brushpea spp
GE6	Gesneria		gesneria spp
GEAM	Genipa	americana	Jagua
GEAR	Geranium	arboreum	Hawai'i red cranesbill
GECA16	Genista	canariensis	Canary broom
GECU	Geranium	cuneatum	Hinahina
GEDU	Genistidium	dumosum	Brushpea
GEHA	Geranium	hanaense	Maui geranium
GELI5	Genista	linifolia	Mediterranean broom
GEMA10	Genista	maderensis	Madeira dyer's greenweed

GEMO2	Genista	monspessulana	French broom
GEMU	Geranium	multiflorum	Manyflower geranium
GEPA	Geijera	parviflora	Wilga; australian willow
GEPE4	Gesneria	pedunculosa	Arbol de navidad
GESE	Gelsemium	sempervirens	Evening trumpetflower
GEST9	Genista	stenopetala	Leafy broom
GETI	Genista	tinctoria	Dyer's greenweed
GEVI7	Gesneria	viridiflora	Grassflower
GI2	Ginkgo		ginkgo spp
GI3	Ginoria		ginoria spp
GIBI	Ginkgo	biloba	Ginkgo
GIBIAG	Ginkgo	biloba 'Autumn Gold'	Ginkgo 'Autumn Gold'
GIBIFA	Ginkgo	biloba 'Fairmont'	Ginkgo 'Fairmont'
GIBIFA2	Ginkgo	biloba 'Fastigiata'	Sentry ginkgo
GIRO	Ginoria	rohrii	Bastard gregre
GL	Glochidion		glochidion spp
GL3	Gleditsia		locust spp
GL4	Gliricidia		quickstick spp
GL5	Glossopetalon		greasebush spp
GL6	Glycosmis		glycosmis spp
GLAQ	Gleditsia	aquatica	Water locust
GLCA	Gleditsia	caspica	Caspina locust
GLCL	Glossopetalon	clokeyi	Clokey's greasebush
GLFE	Glochidion	ferdinandi	Cheese Tree
GLPA4	Glycosmis	parviflora	Flower axistree
GLSE2	Gliricidia	sepium	Quickstick
GLTE	Gleditsia	x texana	Texan locust
GLTE2	Glossopetalon	texense	Texas greasebush
GLTR	Gleditsia	triacanthos	Honeylocust
GLTRIM	Gleditsia	triacanthos 'Imperial'	Imperial honeylocust
GLTRSH	Gleditsia	triacanthos 'Shademaster'	Shademaster honeylocust
GLTRSU	Gleditsia	triacanthos 'Sunburst'	Sunburst honeylocust
GM1	Gmelina		gmelina spp
GMAR	Gmelina	arborea	Gumhar
GMAS	Gmelina	asiatica	Asian bushbeech
GMLE	Gmelina	leichhardtii	White Beech
GO1	Gochnatia		gochnatia spp
GO2	Goetzea		goetzea spp
GO3	Gomidesia		gomidesia spp
GO5	Gonocalyx		brittleleaf spp
GO6	Gonzalagunia		gonzalagunia spp
GO7	Gordonia		gordonia spp
GO8	Gossypium		cotton spp
GO9	Gouania		chewstick spp

GOAX	Gordonia	axillaris	Gordonia
GOBA	Gossypium	barbadense	Creole cotton
GOCO	Gonocalyx	concolor	Island brittleleaf
GOEL	Goetzea	elegans	Mata buey
GOHI	Gossypium	hirsutum	Upland cotton
GOHI2	Gouania	hillebrandii	Hairyfruit chewstick
GOHI4	Gonzalagunia	hirsuta	Mata de mariposa
GOHY	Gochnatia	hypoleuca	Shrubby bullseye
GOLA	Gordonia	lasianthus	Loblolly bay
GOLI	Gomidesia	lindeniana	Grand merisier
GOME	Gouania	meyenii	Smoothfruit chewstick
GOPO	Gouania	polygama	Liane savon
GOPO2	Gonocalyx	portoricensis	Puerto rico brittleleaf
GOTH	Gossypium	thurberi	Thurber's cotton
GOTO	Gossypium	tomentosum	Hawai'i cotton
GOVI	Gouania	vitifolia	Oahu chewstick
GR	Griselinia		griselinia spp
GR1	Graffenrieda		graffenrieda spp
GR2	Graptophyllum		graptophyllum spp
GR4	Grevillea		grevillea spp
GR5	Grewia		grewia spp
GRAS	Grevillea	aspleniifolia	Grevillea aspleniifolia
GRBA	Grevillea	banksii	Kahiliflower
GRBI2	Grewia	biloba	Bilobed grewia
GRLI	Griselinia	littoralis	Kapuka
GRLU	Griselinia	lucida	Akapuka
GRNO	Grevillea	noellii	Grevillea noellii
GROT	Graffenrieda	ottoschulzii	Petites graines camasey
GRPI4	Graptophyllum	pictum	Caricature plant
GRRO	Grevillea	robusta	Silk oak
GU	Guioa		guioa spp
GU1	Guajacum		lignum-vitae spp
GU2	Guapira		guapira spp
GU3	Guarea		guarea spp
GU4	Guatteria		guatteria spp
GU5	Guazuma		guazuma spp
GU6	Guettarda		guettarda spp
GU7	Gundlachia		gundlachia spp
GUAN	Guajacum	angustifolium	Texas lignum-vitae
GUBL	Guatteria	blainii	Haya minga
GUCA2	Guatteria	caribaea	Haya blanca
GUCO	Gundlachia	corymbosa	Yambush
GUDI	Guapira	discolor	Beeftree
GUEL	Guettarda	elliptica	Elliptic leaf velvetseed
GUFR	Guapira	fragrans	Black mampoo
GUGL2	Guapira	globosa	Roundleaf blolly
GUGL3	Guarea	glabra	Alligatorwood

GUGU	Guarea	guidonia	American muskwood
GUKR	Guettarda	krugii	Frogwood
GUOB	Guapira	obtusata	Corcho prieto
GUOD	Guettarda	odorata	Cucubano de vieques
GUOF	Guajacum	officinale	Lignum-vitae
GUOV	Guettarda	ovalifolia	Cucubano
GUPU	Guettarda	pungens	Roseta
GUSA	Guajacum	sanctum	Roughbark lignumvitae
GUSC	Guettarda	scabra	Roughleaf velvet seed
GUSE	Guioa	semiglauca	Guoia
GUUL	Guazuma	ulmifolia	Guacima
GUVA	Guettarda	valenzuelana	Cucubano de monte
GY1	Gyminda		false box spp
GY2	Gymnanthes		gymnanthes spp
GY3	Gymnocladus		coffeetree spp
GYDI	Gymnocladus	dioicus	Kentucky coffeetree
GYLA	Gyminda	latifolia	Falsebox
GYLU	Gymnanthes	lucida	Oysterwood
HA	Halesia		silverbell spp
HA1	Haematoxylum		haematoxylum spp
HA10	Harpullia		harpullia spp
HA12	Harrisia		applecactus spp
HA13	Havardia		havardia spp
HA14	Hazardia		bristleweed spp
HA15	Harpephyllum		harpephyllum spp
HA2	Haenianthus		haenianthus spp
HA3	Halimodendron		halimodendron spp
HA4	Hakea		hakea spp
HA6	Hamamelis		witchhazel spp
HA7	Hamelia		hamelia spp
HAAR4	Harpullia	arborea	Tulip-wood tree
HAAX	Hamelia	axillaris	Balsamillo
HACA	Halesia	carolina	Snowdrop tree
HACA1	Harpephyllum	caffrum	Wild Plum
HACA2	Haematoxylum	campechianum	Bloodwoodtree
HACA3	Harpephyllum	carolina	Kaffir plum
HACA6	Hazardia	cana	Island hazardia
HACO	Halesia	corymbosa	Epaulette tree
HADE4	Hazardia	detonsa	Island bristleweed
HADI	Halesia	diptera	Two-wing silverbell
HAER	Hakea	eriantha	Tree Hakea
HAHA8	Halimodendron	halodendron	Common salttree
HALA	Hakea	laurina	Pincushion tree
HAOR3	Hazardia	orcuttii	Orcutt's bristleweed
HAPA10	Havardia	pallens	Haujillo
HAPA3	Hamelia	patens	Scarletbush
HAPE	Hakea	petiolaris	Sea Urchin Hakea

HAPE1	Harpullia	pendula	Tulipwood
HAPO2	Harrisia	portoricensis	Puerto rico applecactus
HASA	Hakea	salicifolia	Willow-leaved hakea
HASA2	Haenianthus	salicifolius	Palo de hueso
HASU	Hakea	suaveolens	Sweet hakea
HATE3	Halesia	tetraptera	Mountain silverbell
HAVE2	Hamamelis	vernalis	Ozark witchhazel
HAVI	Hamamelis	virginiana	Witch hazel
HE	Heritiera		heritiera spp
HE1	Hebe		hebe spp
HE10	Helicteres		helicteres spp
HE11	Helietta		helietta spp
HE12	Heliocarpus		heliocarpus spp
HE15	Hemizonia		rosinweed spp
HE16	Henriettea		camasey spp
HE18	Hernandia		hernandia spp
HE20	Hesperomannia		island-aster spp
HE22	Heteromeles		toyon spp
HE23	Heteropterys		withe spp
HE25	Heterotrichum		heterotrichum spp
HE4	Hedyosmum		hedyosmum spp
HE5	Hedyotis		starviolet spp
HE6	Heimia		heimia spp
HE9	Helichrysum		strawflower spp
HEAR	Heteromeles	arbutifolia	Toyon
HEAR10	Hesperomannia	arbuscula	Maui island-aster
HEAR2	Hedyosmum	arborescens	Cigarbush
HEAR9	Hesperomannia	arborescens	Lanai island-aster
HECO13	Hedyotis	cookiana	'awiwi
HECO14	Hedyotis	coriacea	Kio'ele
HECY	Heterotrichum	cymosum	Camasey terciopelo
HEDE3	Hedyotis	degeneri	Waianae range starviolet
HEFA5	Henriettea	fasciculatis	Camasey peludo
HEFL6	Hedyotis	fluviatilis	Kamapua'a
HEFO2	Hedyotis	foliosa	Haleakala starviolet
HEFO5	Hedyotis	fosbergii	Fosberg's starviolet
HEFR	Hebe	x franciscana	Francisco hebe
HEHI8	Hedyotis	hillebrandii	Manono
HEJA	Helicteres	jamaicensis	Screwtree
HEKN	Hedyotis	knudsenii	Kokee starviolet
HELA22	Heteropterys	laurifolia	Dragon with
HELI9	Heritiera	littoralis	Looking-glass tree
HELY	Hesperomannia	lydgatei	Kauai island-aster
HEMA11	Henriettea	macfadyenii	Macfadyen's camasey
HEME5	Henriettea	membranifolia	Thinleaf camasey
HEMI6	Hemizonia	minthornii	Santa susana tarweed
HENY	Hernandia	nymphaeifolia	Jack in the box tree

HEPA14	Hedyotis	parvula	Rockface starviolet
HEPA3	Helietta	parvifolia	Barreta
HEPE8	Helichrysum	petiolare	Licorice plant
HEPO4	Heliocarpus	popayanensis	White moho
HESA	Heimia	salicifolia	Shrubby yellowcrest
HESO	Hernandia	sonora	Mago
HESP	Hebe	speciosa	New zealand hebe
HESQ	Henriettea	squamulosum	Jusillo
HETE21	Hedyotis	terminalis	Variable starviolet
HETR6	Hedyotis	tryblium	Kalalau valley starviolet
HI1	Hibiscadelphus		hibiscadelphus spp
HI2	Hillia		hillia spp
HI3	Hippomane		hippomane spp
HI4	Hippophae		seabuckthorn spp
HI5	Hirtella		hirtella spp
HIAR	Hibiscus	arnottianus	White rosemallow
HIBO2	Hibiscadelphus	bombycinus	Hau kuahiwi
HIBR	Hibiscus	brackenridgei	Brackenridge's rosemallow
HICA6	Hibiscus	calyphyllus	Lemonyellow rosemallow
HICL	Hibiscus	clayi	Red kauai rosemallow
HICL2	Hibiscus	clypeatus	Congo mahoe
HICR	Hibiscadelphus	crucibracteatus	Lava hau kuahiwi
HIDI	Hibiscadelphus	distans	Kauai hau kuahiwi
HIEL	Hibiscus	elatus	Mahoe
HIGI	Hibiscadelphus	giffardianus	Kilauea hau kuahiwi
HIGR4	Hibiscus	grandiflorus	Swamp rosemallow
HIHE	Hibiscus	heterophyllus	Native Rosella
HIHU	Hibiscadelphus	hualalaiensis	Hualalai hau kuahiwi
HIKO	Hibiscus	kokio	Red rosemallow
HIMA	Hippomane	mancinella	Manchineel
HIMA5	Hibiscus	macrophyllus	Largeleaf rosemallow
HIMO	Hibiscus	moschuetos	Rose mallow hibiscus
HIMU3	Hibiscus	mutabilis	Dixie rosemallow
HIPA4	Hillia	parasitica	Tibey trepador
HIPE3	Hibiscus	pernambucensis	Seaside mahoe
HIPU2	Hibiscadelphus	x puakuahiwi	Hibiscadelphus
HIRH80	Hippophae	rhamnoides	Seabuckthorn
HIROSI	Hibiscus	rosa-sinensis	Chinese hibiscus
HIRU2	Hirtella	rugosa	Teta de burra cinarron
HISP	Hibiscus		rosemallow spp
HISY	Hibiscus	syriacus	Rose-of-sharon
HITI	Hibiscus	tiliaceus	Sea hibiscus
HITR3	Hirtella	triandra	Pigeonberry
HIVI	Hibiscus	vitifolius	Tropical rose mallow
HIWA	Hibiscus	waimeae	White kauai rosemallow
HIWI	Hibiscadelphus	wilderianus	Maui hau kuahiwi
HIWO	Hibiscadelphus	woodii	Wood's hau kuahiwi

HO	Holocarpha		tarweed spp
HO1	Howea		howea spp
HO2	Homolanthus		homolanthus spp
HO3	Holmskioldia		holmskioldia spp
HO4	Holodiscus		oceanspray spp
HO5	Homalium		homalium spp
HO9	Hovenia		hovenia spp
HOBE	Howea	belmoreana	Curly Palm
HODI	Holodiscus	discolor	Oceanspray
HODU	Hovenia	dulcis	Japanese raisin tree
HODU2	Holodiscus	dumosus	Rockspirea
HOFO	Howea	forsteriana	Kentia palm
HORA	Homalium	racemosum	White cogwood
HOSA2	Holmskioldia	sanguinea	Chinese hatplant
HU4	Hura		sandbox tree spp
HUCR	Hura	crepitans	Sandbox tree
HY	Hyophorbe		hyophorbe spp
HY1	Hyeronima		hyeronima spp
HY2	Hylocereus		nightblooming cactus spp
HY3	Hymenaea		hymenaea spp
HY4	Hymenoclea		burrobrush spp
HY5	Hymenosporum		hymenosporum spp
HY6	Hypelate		hypelate spp
HY7	Hyperbaena		hyperbaena spp
HY8	Hypericum		St. Johnswort spp
HY9	Hyptis		bushmint spp
HYAN8	Hypericum	androsaemum	Sweet amber
HYAR	Hydrangea	arborescens	Wild hydrangea
HYCA11	Hypericum	canariense	Canary isl. st. johnswort
HYCH2	Hypericum	chapmanii	Apalachicola st johnswort
HYCI3	Hydrangea	cinerea	Ashy hydrangea
HYCL	Hyeronima	clusioides	Cedro macho
HYCO	Hymenaea	courbaril	Courbail
HYDE	Hypericum	densiflorum	Bushy st. johnswort
HYDO2	Hyperbaena	domingensis	Forest snakevine
HYED	Hypericum	edisonianum	Arcadian st. johnswort
HYEM	Hyptis	emoryi	Desert lavender
HYEX	Hypericum	exile	Florida sand st johnswort
HYFA	Hypericum	fasciculatum	Peelbark st. johnswort
HYFL	Hymenosporum	flavum	Sweetshade
HYGA	Hypericum	galioides	Bedstraw st. johnswort
HYKA	Hypericum	kalmianum	Kalm's st. johnswort
HYLA	Hyophorbe	lagenicaulis	Bottle palm
HYLA8	Hyperbaena	laurifolia	Limestone snakevine
HYLI4	Hypericum	lissophloeus	Smoothbark st. johnswort
HYLL	Hypericum	lloydii	Sandhill st. johnswort
HYLO2	Hypericum	lobocarpum	Fivelobe st. johnswort

HYMI4	Hypericum	microsepalum	Flatwoods st. johnswort
HYMO2	Hypericum	x moserianum	St. johnswort
HYMY	Hypericum	myrtifolium	Myrtleleaf st. johnswort
HYNI3	Hypericum	nitidum	Carolina st. johnswort
HYNU	Hypericum	nudiflorum	Early st. johnswort
HYPA	Hydrangea	paniculata	Panicled hydrangea
HYPR	Hypericum	prolificum	Shrubby st. johnswort
HYQU3	Hydrangea	quercifolia	Oakleaf hydrangea
HYRA6	Hydrangea	radiata	Silverleaf hydrangea
HYSA	Hymenoclea	salsola	Burrobrush
HYSP	Hydrangea		hydrangea spp
HYSU2	Hypericum	suffruticosum	Pineland st. johnswort
HYTR	Hypelate	trifoliata	Inkwood
HYUN3	Hylocereus	undatus	Nightblooming cactus
HYVE9	Hyophorbe	verschaffeltii	Spindle palm
IL2	Illicium		anisetree spp
ILAL	Ilex	altaclarensis	Wilson holly
ILAM	Ilex	ambigua	Carolina holly
ILAM2	Ilex	amelanchier	Sarvis holly
ILAN	Ilex	anomala	Hawai'i holly
ILAQ	Ilex	aquifolium	English holly
ILAT	Ilex	x attenuata	Topal holly
ILCA	Ilex	cassine	Dahoon
ILCO	Ilex	coriacea	Large gallberry
ILCO2	Ilex	cornuta	Chinese holly
ILCO3	Ilex	cookii	Te
ILCR	Ilex	crenata	Japanese holly
ILCU3	Ilex	cuthbertii	Cuthbert's holly
ILDE	Ilex	decidua	Possum haw
ILFL	Illicium	floridanum	Florida anisetree
ILGL	Ilex	glabra	Inkberry
ILGU	Ilex	guianensis	Maconcona
ILHY	Ilex	hypaneura	Luquillo mountain holly
ILKR	Ilex	krugiana	Tawnyberry holly
ILLA	Ilex	laevigata	Smooth winterberry
ILLO	Ilex	longipes	Georgia holly
ILMA	Ilex	macfadyenii	Caribbean holly
ILMO	Ilex	montana	Mountain winterberry
ILMY	Ilex	myrtifolia	Myrtle dahoon
ILNI	Ilex	nitida	Puerto rico holly
ILOP	Ilex	opaca	American holly
ILPA	Illicium	parviflorum	Yellow anisetree
ILPA2	Ilex	paraguayensis	Paraguay tea
ILSI	Ilex	sideroxyloides	Gongolin
ILSI2	Ilex	sintenisii	Sintenis' holly
ILSP	Ilex		holly spp
ILUR	Ilex	urbaniana	Urban's holly

ILVE	Ilex	verticillata	Common winterberry
ILVO	Ilex	vomitoria	Yaupon
IN1	Indigofera		indigo spp
IN2	Inga		inga spp
INCA	Indigofera	caroliniana	Carolina indigo
INGU	Indigofera	guatemalensis	Guatemalan indigo
ININ	Inga	ingoides	Icecream bean
INKI	Indigofera	kirilowii	Kirilow's indigo
INLA	Inga	laurina	Sweetpea
INMA	Inga	marginata	Inga-feijao
INNO	Inga	nobilis	Guama venezolano
INSP	Indigofera	sphaerocarpa	Sonoran indigo
INTI	Indigofera	tinctoria	True indigo
INUR	Inga	uruguensis	Iganzeiro
INVE	Inga	vera	River koko
IR	Iris		iris spp
IS1	Isocoma		goldenbush spp
IS2	Isodendrion		isodendrion spp
ISAR2	Isocoma	arguta	Carquinez goldenbush
ISHO2	Isodendrion	hosakae	Cindercone isodendrion
ISLA3	Isodendrion	laurifolium	Rockcliff isodendrion
ISLO2	Isodendrion	longifolium	Longleaf isodendrion
ISME5	Isocoma	menziesii	Menzies' goldenbush
ISPY	Isodendrion	pyrifolium	Wahine noho kula
IT1	Itea		sweetspire spp
ITVI	Itea	virginica	Virginia sweetspire
IV1	Iva		marshelder spp
IVFR	Iva	frutescens	Marsh elder
IX1	Ixora		ixora spp
IXAC	Ixora	acuminata	Bola de nieve
IXCO	Ixora	coccinea	Scarlet jungleflame
IXFE	Ixora	ferrea	Palo de hierro
IXPA	Ixora	pavetta	Torch tree
IXTH	Ixora	thwaitesii	White jungleflame
JA1	Jacaranda		jacaranda spp
JA3	Jacquinia		jacquinia spp
JA5	Jamesia		cliffbush spp
JA6	Jasminum		jasmine spp
JA7	Jatropha		nettlespurge spp
JAAM	Jamesia	americana	Fivepetal cliffbush
JAAR2	Jacquinia	armillaris	Braceletwood
JABE	Jacquinia	berteroi	Bois bande
JACA2	Jatropha	cardiophylla	Sangre de cristo
JACI	Jatropha	cinerea	Arizona nettlespurge
JACU	Jatropha	cuneata	Physicnut
JACU2	Jatropha	curcas	Barbados nut
JAHE	Jatropha	hernandiifolia	Wild oilnut

JAIN	Jatropha	integerrima	Peregrina
JAKE	Jacquinia	keyensis	Joewood
JAMI	Jacaranda	mimosifolia	Jacaranda
JAMU	Jatropha	multifida	Coralbush
JAMU2	Jasminum	multiflorum	Star jasmine
JANU	Jasminum	nudiflorum	Winter jasmine
JAOF	Jasminum	officinale	Poet's jasmine
JAPA3	Jacquinia	pauciflora	Thicketwood
JAPO	Jatropha	podagrica	Goutystalk nettlespurge
JASA	Jasminum	sambac	Arabian jasmine
JATE2	Jamesia	tetrapetala	Fourpetal cliffbush
JAUM	Jacquinia	umbellata	Chirriador
JU	Juniperus		juniper spp
JU1	Juglans		walnut spp
JU2	Justicia		water-willow spp
JU3	Jubaea		jubaea spp
JUAI	Juglans	ailanthifolia	Japanese walnut
JUAS	Juniperus	ashei	Ashe juniper
JUBI3	Juglans	x bixbyi	Bixby walnut
JUBR6	Justicia	brandegeeana	Shrimpplant
JUCA1	Juniperus	californica	California juniper
JUCA2	Juglans	californica	Southern cali walnut
JUCA8	Justicia	californica	Beloperone
JUCA9	Justicia	candicans	Arizona water-willow
JUCH	Juniperus	chinensis	Chinese juniper
JUCH1	Jubaea	chilensis	Chilean Wine Palm
JUCHTO	Juniperus	chinensis 'Torulosa'	Hollywood juniper
JUCI	Juglans	cinerea	Butternut
JUCO1	Juniperus	communis	Common juniper
JUCO2	Juniperus	coahuilensis	Redberry juniper
JUCO3	Juniperus	conferta	Shore juniper
JUDE	Juniperus	deppeana	Alligator juniper
JUEX	Juniperus	excelsa	JunÍpero
JUFL	Juniperus	flaccida	Drooping juniper
JUFO	Juniperus	formosana	Formosan juniper
JUHI	Juglans	hindsii	Hind walnut
JUIN3	Juglans	x intermedia	Intermediate walnut
JUJA	Juglans	jamaicensis	West indian walnut
JUMA	Juglans	major	Arizona walnut
JUMI	Juglans	microcarpa	Little walnut
JUMO	Juniperus	monosperma	One seed juniper
JUNI	Juglans	nigra	Black walnut
JUOC	Juniperus	occidentalis	Western juniper
JUOS	Juniperus	osteosperma	Utah juniper
JUPI	Juniperus	pinchotii	Pinchot juniper
JUPR	Juniperus	procumbens	Japanese garden juniper

JUQU	Juglans	x quadrangulata	Juglans x quadrangulata
JURE	Juglans	regia	English walnut
JUSC	Juniperus	scopulorum	Rocky mountain juniper
JUSI	Juniperus	virginiana silicicol	Southern redcedar
JUVI	Juniperus	virginiana	Eastern red cedar
KA1	Kalmiopsis		kalmiopsis spp
KA2	Kalopanax		castor aralia spp
KA3	Kanaloa		kanaloa spp
KA4	Karwinskia		karwinskia spp
KAAN	Kalmia	angustifolia	Sheep laurel
KACA2	Kalmia	carolina	Carolina laurel
KACU	Kalmia	cuneata	Whitewicky
KAHI2	Kalmia	hirsuta	Hairy laurel
KAHU	Karwinskia	humboldtiana	Coyotillo
KAKA	Kanaloa	kahoolawensis	Kanaloa
KALA	Kalmia	latifolia	Mountain laurel
KALE	Kalmiopsis	leachiana	North umpqua kalmiopsis
KAPO	Kalmia	polifolia	Bog laurel
KASE	Kalopanax	septemlobus	Castor aralia
KASP	Kalmia		laurel spp
KE1	Keckiella		keckiella spp
KE3	Kerria		kerria spp
KEAN	Keckiella	antirrhinoides	Snapdragon penstemon
KEBR	Keckiella	breviflora	Bush beardtongue
KECO	Keckiella	cordifolia	Heartleaf keckiella
KEJA	Kerria	japonica	Japanese rose
KELE	Keckiella	lemmonii	Lemmon's keckiella
KERO	Keckiella	rothrockii	Rothrock's keckiella
KETE	Keckiella	ternata	Scarlet keckiella
KH1	Khaya		African mahogany spp
KHNY2	Khaya	nyasica	Nyasaland mahogany
KHSE2	Khaya	senegalensis	Senegal mahogany
KI1	Kigelia		sausage tree spp
KIPI	Kigelia	africana	Sausage tree
KL1	Kleinhovia		kleinhovia spp
KLHO	Kleinhovia	hospita	Guest tree
KO3	Koeberlinia		allthorn spp
KO4	Koelreuteria		koelreuteria spp
KO5	Kokia		treecotton spp
KO6	Kolkwitzia		kolkwitzia spp
KOAM80	Kolkwitzia	amabilis	Beautybush
KOBI	Koelreuteria	bipinnata	Chinese flame tree
KOCO2	Kokia	cookei	Molokai treecotton
KODR	Kokia	drynarioides	Hawai'i treecotton
KOEL	Koelreuteria	elegans	Flamegold
KOKA	Kokia	kauaiensis	Kauai treecotton
KOLA2	Kokia	lanceolata	Wailupe valley treecotton

KOPA	Koelreuteria	paniculata	Goldenrain tree
KOPAFA	Koelreuteria	paniculata Fastigiata	Goldenrain 'Fastigiata'
KOSP	Koeberlinia	spinosa	Crown of thorns
KR1	Krameria		ratany spp
KR3	Krugiodendron		krugiodendron spp
KRFE	Krugiodendron	ferreum	Leadwood
KRIX	Krameria	ixine	Abrojo colorado
KRRA	Krameria	ramosissima	Manystem ratany
LA1	Labordia		labordia spp
LA10	Larix		larch spp
LA11	Larrea		creosote bush spp
LA13	Lasianthus		lasianthus spp
LA14	Laurus		bay tree spp
LA15	Lavandula		lavender spp
LA17	Lawsonia		lawsonia spp
LA2	Laburnum		golden chain tree spp
LA3	Laetia		laetia spp
LA4	Lagascea		lagascea spp
LA5	Lagunaria		lagunaria spp
LA6	Lagerstroemia		lagerstroemia spp
LA7	Laguncularia		laguncularia spp
LA8	Lantana		lantana spp
LA9	Laplacea		laplacea spp
LAAC	Lantana	achyranthifolia	Brushland shrubverbena
LAAN2	Laburnum	anagyroides	Golden chain tree
LAAN81	Lavandula	angustifolia	English lavender
LACA2	Lantana	camara	Lantana
LACA8	Lantana	canescens	Hammock shrubverbena
LACY	Labordia	cyrtandrae	Koolau range labordia
LADE	Larix	decidua	European larch
LADE6	Labordia	degeneri	Degener's labordia
LADE7	Lagascea	decipiens	Doll's head
LADEPE	Larix	decidua 'Pendula'	Weeping european larch
LAEX	Lantana	exarata	Caribbean shrubverbena
LAFA2	Labordia	fagraeoidea	Summit labordia
LAHE2	Labordia	hedyosmifolia	Bog labordia
LAHE3	Labordia	helleri	Napali coast labordia
LAHI5	Labordia	hirtella	Mountain labordia
LAHO3	Labordia	hosakana	Ridgetop labordia
LAIN	Lagerstroemia	indica	Common crapemyrtle
LAIN15	Lantana	insularis	Island lantana
LAIN2	Lantana	involucrata	Buttonsage
LAIN5	Lawsonia	inermis	Henna
LAKA	Labordia	kaalae	Waianae range labordia
LAKA2	Larix	kaempferi	Larix kaempferi
LALA	Larix	laricina	Tamarack

LALA2	Larix	lyallii	Subalpine larch
LALA5	Lasianthus	lanceolatus	Mata de peo
LALE	Larix	leptolepis	Japanese larch
LALY2	Labordia	lydgatei	Wahiawa mountain labordia
LANO	Laurus	nobilis	Laurel de olor
LAOC	Larix	occidentalis	Western larch
LAPA	Lagunaria	patersonii	Primrose tree
LAPO	Laplacea	portoricensis	Nino de cota
LAPR2	Laetia	procera	Cuero de rana
LAPU4	Labordia	pumila	Kauai labordia
LARA	Laguncularia	racemosa	White mangrove
LARE2	Lantana	reticulata	Netted shrubverbena
LASE4	Labordia	sessilis	Thinfruit labordia
LASI	Larix	siberica	Siberian larch
LASP	Lagerstroemia	speciosa	Queens crapemyrtle
LAST2	Lantana	strigosa	Rough shrubverbena
LATI2	Labordia	tinifolia	Paleflower labordia
LATR2	Larrea	tridentata	Creosote bush
LAUR2	Lantana	urticoides	West indian shrubverbena
LAVE3	Labordia	venosa	Maui labordia
LAVE4	Lantana	velutina	Velvet shrubverbena
LAWA	Laburnum	x watereri	Golden-chain tree
LAWA2	Labordia	waialealae	Kamakahala lau li'i
LAWA3	Labordia	waiolani	Nevada peavine
LE1	Leandra		leandra spp
LE10	Lepidospartum		broomsage spp
LE11	Leptocereus		leptocereus spp
LE13	Leptopus		maidenbush spp
LE14	Leptospermum		teatree spp
LE16	Lespedeza		lespedeza spp
LE18	Leucaena		leadtree spp
LE20	Leucophyllum		barometerbush spp
LE21	Leucothoe		doghobble spp
LE22	Leycesteria		leycesteria spp
LE3	Ledum		Labrador tea spp
LE5	Leitneria		corkwood spp
LE6	Leonotis		lion's ear spp
LEAX	Leucothoe	axillaris	Coastal doghobble
LEBU2	Lepidospartum	burgessii	Burgess' broomsage
LECA12	Leucophyllum	candidum	Brewster barometerbush
LECO	Leptospermum	continentale	Tea-tree
LECO8	Ledum	x columbianum	Coast labradortea
LECY80	Lespedeza	cyrtobotrya	Leafy lespedeza
LEDA	Leucothoe	davisiae	Sierra laurel
LEFL	Leitneria	floridana	Corkwood
LEFL3	Leptospermum	flavescens	Common teatree

LEFO	Leucothoe	fontanesiana	Highland doghobble
LEFO2	Leycesteria	formosa	Himalayan honeysuckle
LEFO3	Lespedeza	formosa	Oriental lespedeza
LEFR3	Leucophyllum	frutescens	Texas barometer bush
LEGL	Ledum	glandulosum	Western labrador tea
LEGR	Ledum	groenlandicum	Labrador tea
LEKR	Leandra	krugiana	Krug's roughleaf
LEKR2	Leandra	krugii	Mt. cerrote angleflower
LELA12	Leptospermum	laevigata	Coastal teatree
LELA4	Lepidospartum	latisquamum	Nevada broomsage
LELE	Leucaena	leucocephala	White lead tree
LELE3	Leonotis	leonurus	Lion's ear
LEMI4	Leucophyllum	minus	Big bend barometerbush
LEPA11	Ledum	palustre	Marsh labrador tea
LEPE	Leptospermum	petersonii	Lemon tea-tree
LEPH11	Leptopus	phyllanthoides	Missouri maidenbush
LEPU3	Leucaena	pulverulenta	Great leadtree
LEQU	Leptocereus	quadricostatus	Pitahaya
LERA4	Leucothoe	racemosa	Swamp doghobble
LERE5	Leucaena	retusa	Littleleaf leadtree
LERE6	Leucothoe	recurva	Redtwig doghobble
LESC2	Leptospermum	scoparium	Broom teatree
LESQ	Lepidospartum	squamatum	California broomsage
LI1	Licania		licania spp
LI10	Liriodendron		tuliptree spp
LI12	Litchi		lychee spp
LI13	Lithocarpus		tanoak spp
LI15	Lithraea		Lithraea spp
LI16	Lithrea		lithrea spp
LI17	Litsea		litsea spp
LI18	Livistona		livistona spp
LI2	Licaria		licaria spp
LI3	Limonium		sealavender spp
LI5	Lindera		spicebush spp
LI8	Lippia		lippia spp
LI9	Liquidambar		sweetgum spp
LIAE	Litsea	aestivalis	Pondspice
LIAM	Ligustrum	amurense	Amur privet
LIAR10	Limonium	arborescens	Tree limonium
LIAU	Livistona	australis	Australian fan palm
LIBE	Lindera	benzoin	Spicebush
LIBR5	Licaria	brittoniana	Maria laurel
LICA	Lithraea	caustica	Litre
LICH	Livistona	chinensis	Chinese fan palm
LICH2	Liriodendron	chinense	Chinese tulip tree
LICH4	Litchi	chinensis	Lychee
LIDE	Lithocarpus	densiflorus	Tanoak

LIDE2	Livistona	decipiens	Ribbon palm
LIFO	Liquidambar	formosana	Chinese sweet gum
LIGR6	Lippia	graveolens	Mexican oregano
LIJA	Ligustrum	japonicum	Ligustro
LILU	Ligustrum	lucidum	Glossy privet
LIME7	Lindera	melissifolia	Southern spicebush
LIMI6	Lippia	micromera	Spanish thyme
LIMO4	Lithrea	molleoides	Aroeira blanca
LIOB	Ligustrum	obtusifolium	Border privet
LIOR	Liquidambar	orientalis	Oriental sweetgum
LIOV	Ligustrum	ovalifolium	California privet
LIOVAU	Ligustrum	ovalifolium aurea	Golden privet
LIPA9	Licaria	parvifolia	Puerto rico cinnamon
LIQU2	Ligustrum	quihoui	Waxyleaf privet
LIRI4	Licania	rigida	Oiticica
LISI	Ligustrum	sinense	Chinese privet
LISP	Ligustrum		privet spp
LIST	Liquidambar	styraciflua	Sweetgum
LISU8	Lindera	subcoriacea	Bog spicebush
LITR	Licaria	triandra	Pepperleaf sweetwood
LITU	Liriodendron	tulipifera	Tulip tree
LIVU	Ligustrum	vulgare	Common privet
LO1	Lobelia		lobelia spp
LO4	Lonchocarpus		lancepod spp
LO7	Lophostemon		lophostemon spp
LOAL	Lonicera	albiflora	Western white honeysuckle
LOAR	Lonicera	arizonica	Arizona honeysuckle
LOBE	Lonicera	x bella	Belle honeysuckle
LOBR	Lonicera	x brownii	Brown's honeysuckle
LOCA	Lonicera	canadensis	American fly honeysuckle
LOCA6	Lonicera	caerulea	Sweetberry honeysuckle
LOCI3	Lonicera	ciliosa	Orange honeysuckle
LOCO5	Lonicera	conjugialis	Purpleflower honeysuckle
LOCO9	Lophostemon	confertus	Vinegartree
LODO5	Lonchocarpus	domingensis	Geno geno
LODU2	Lobelia	dunbarii	Waihanau lobelia
LOFL	Lonicera	flava	Yellow honeysuckle
LOFR	Lonicera	fragrantissima	Sweet breath of spring
LOGL2	Lonchocarpus	glaucifolius	Geno
LOGL4	Lobelia	gloria-montis	Bog lobelia
LOGR5	Lobelia	grayana	Haleakala lobelia
LOHE6	Lonicera	x heckrottii	Lonicera x heckrottii
LOHE7	Lonchocarpus	heptaphyllus	Broadleaf lancepod
LOHI4	Lobelia	hillebrandii	Maui lobelia
LOHY	Lobelia	hypoleuca	Kuhi'aikamo'owahie
LOIN	Lonicera	involucrata	Twinberry honeysuckle

LOJA	Lonicera	japonica	Hall's honeysuckle
LOKA2	Lobelia	kauaensis	Lava lobelia
LOKO	Lonicera	korolkowii	Blueleaf honeysuckle
LOMA6	Lonicera	maackii	Amur honeysuckle
LOMI5	Lonicera	x minutiflora	Smallflower honeysuckle
LOMO	Lonicera	morrowii	Morrow honeysuckle
LOMO3	Lobelia	monostachya	Waianae range lobelia
LONI	Lobelia	niihauensis	Niihau lobelia
LONO	Lonicera	x notha	Honeysuckle
LOOA	Lobelia	oahuensis	Oahu lobelia
LOOB	Lonicera	oblongifolia	Swamp fly honeysuckle
LOPU4	Lonchocarpus	punctatus	Dotted lancepod
LORE5	Lonicera	reticulata	Grape honeysuckle
LORU3	Lonicera	ruprechtiana	Manchurian honeysuckle
LOSP	Lonicera		honeysuckle spp
LOST2	Lonicera	standishii	Standish's honeysuckle
LOSU2	Lonicera	subspicata	Southern honeysuckle
LOTA	Lonicera	tatarica	Tartarian honeysuckle
LOUT2	Lonicera	utahensis	Utah honeysuckle
LOVI	Lonicera	villosa	Mountain fly honeysuckle
LOVI3	Lobelia	villosa	Alakai swamp lobelia
LOXY	Lonicera	xylosteum	Dwarf honeysuckle
LOXY2	Lonicera	x xylosteoides	Fly honeysuckle
LU2	Luehea		luehea spp
LU5	Lunania		lunania spp
LU7	Luma		luma spp
LUAP	Eugenia	apiculata	ArrayÁn
LUDI	Luehea	divaricata	Acoita-cavalo
LUEK	Lunania	ekmanii	Mendrina
LUSP11	Luehea	speciosa	Luehea
LY1	Lycianthes		lycianthes spp
LY10	Lysimachia		yellow loosestrife spp
LY2	Lycium		desert-thorn spp
LY3	Lycopersicon		lycopersicon spp
LY6	Lyonia		staggerbush spp
LY7	Lyonothamnus		lyononthmnus spp
LY9	Lysiloma		false tamarind spp
LYAN	Lycium	andersonii	Water jacket
LYAS	Lyonothamnus	f. asplenifol	Fernleaf ironwood
LYBA	Lysiloma	bahamensis	Wild tamarind
LYBA4	Lycium	barbarum	Matrimony vine
LYBE	Lycium	berlandieri	Berlandier's wolfberry
LYCA	Lycium	californicum	California desert-thorn
LYCA2	Lycium	carolinianum	Carolina desert-thorn
LYCH	Lycium	chinense	Chinese desert-thorn
LYCO2	Lycium	cooperi	Peach thorn
LYES	Lycopersicon	esculentum	Tomato

LYEX	Lycium	exsertum	Arizona desert-thorn
LYFE	Lyonia	ferruginea	Lyonia tree
LYFE3	Lycium	ferrocissimum	African boxthorn
LYFL	Lyonothamnus	floribundus	Lyontree
LYFR	Lycium	fremontii	Fremont's desert-thorn
LYFR3	Lyonia	fruticosa	Coastalplain staggerbush
LYHA5	Lycium	hassei	Catalina desert-thorn
LYKA	Lysimachia	kalalauensis	Kauai yellow loosestrife
LYLA	Lysiloma	latisiliquum	Bahama lysiloma
LYLI	Lyonia	ligustrina	Maleberry
LYLU3	Lyonia	lucida	Fetterbush lyonia
LYMA	Lycium	macrodon	Desert wolfberry
LYMA2	Lyonia	mariana	Piedmont staggerbush
LYMA5	Lysimachia	maxima	Pelekunu trl. Loosestrife
LYMI	Lysiloma	microphyllum	Desert fern
LYPA	Lycium	pallidum	Pale desert-thorn
LYPA2	Lycium	parishii	Parish's desert-thorn
LYPU	Lycium	puberulum	Downy desert-thorn
LYRA	Lycianthes	rantonnei	Paraguay nightshade
LYRI	Lycium	richii	Baja desert-thorn
LYRU2	Lyonia	rubiginosa	St. thomas staggerbush
LYSA3	Lycium	sandwicense	Hawai'i desert-thorn
LYSA5	Lysiloma	sabicu	Horseflesh mahogany
LYSH	Lycium	shockleyi	Shockley's desert-thorn
LYTE4	Lycium	texanum	Texas desert-thorn
LYTH	Lysiloma	watsonii	Feather bush
LYTO	Lycium	torreyi	Squawthorn
LYTR3	Lyonia	truncata	Dominican staggerbush
LYTW	Lycium	tweedianum	Tropical desert-thorn
LYVE	Lycium	verrucosum	San nicholas desert-thorn
LYVE6	Lysimachia	venosa	Veined yellow loosestrife
LYVI5	Lycianthes	virgata	Berengena de paloma
MA	Maackia		maackia spp
MA1	Magnolia		magnolia spp
MA10	Maesopsis		umbrella-tree spp
MA11	Mahonia		mahonia spp
MA13	Malacomeles		false serviceberry spp
MA16	Malephora		malephora spp
MA17	Mallotus		mallotus spp
MA18	Malosma		laurel sumac spp
MA19	Malpighia		malpighia spp
MA2	Malus		apple spp
MA21	Malvaviscus		wax mallow spp
MA22	Mammea		mammea spp
MA25	Mangifera		mango spp
MA26	Manglietia		manglietia spp
MA27	Manihot		manihot spp

MA28	Manilkara		manilkara spp
MA3	Macadamia		macadamia spp
MA30	Mappia		mappia spp
MA31	Margaritaria		margaritaria spp
MA33	Marlierea		marlierea spp
MA34	Mastichodendron		mastichodendron spp
MA35	Matayba		matayba spp
MA36	Matelea		milkvine spp
MA38	Maytenus		mayten spp
MA4	Macaranga		macaranga spp
MA5	Markhamia		markhamia spp
MA6	Machaerium		machaerium spp
MA7	Machaonia		machaonia spp
MA8	Maclura		maclura spp
MAAC	Magnolia	acuminata	Cucumber tree
MAAM2	Mammea	americana	Mammee apple
MAAM9	Maackia	amurensis	Amur maackia
MAAN5	Manihot	angustiloba	Desertmountain manihot
MAAR7	Malus	x arnoldiana	Arnold's apple
MAAS	Magnolia	ashei	Ashe magnolia
MABA	Manilkara	bahamensis	Manilkara bahamensis
MABA2	Malus	baccata v purpurea	Manzano de flor
MABE	Mahonia	bealei	Leatherleaf mahonia
MABI	Manilkara	bidentata	Balata
MABO	Maytenus	boaria	Mayten
MACO11	Malpighia	coccigera	Singapore holly
MACR3	Malephora	crocea	Coppery mesemb
MACY2	Maytenus	cymosa	Caribbean mayten
MADA2	Manihot	davisiae	Arizona manihot
MADA5	Malus	x dawsoniana	Malus x dawsoniana
MADE	Magnolia	denudata	Chinese magnolia
MADE5	Malacomeles	denticulata	South false serviceberry
MADI11	Mahonia	dictyota	Shining netvein barberry
MADO	Malus	domestica	Common apple
MADO2	Matayba	domingensis	Negra lora
MAEL3	Maytenus	elongata	Puerto rico mayten
MAEM	Malpighia	emarginata	Barbados cherry
MAEM2	Maesopsis	eminii	Umbrella-tree
MAFL80	Malus	floribunda	Japanese flower crabapple
MAFO	Mastichodendron	foetidissium	False mastic
MAFO2	Manglietia	fortunei	Manglietia fortunei
MAFR	Magnolia	fraseri	Fraser magnolia
MAFR3	Mahonia	fremontii	Fremont's mahonia
MAFU2	Malpighia	fucata	Palo bronco
MAGL11	Malus	glaucescens	Dunbar crabapple
MAGL4	Malus	glabrata	Biltmore crabapple

MAGL5	Manihot	glaziovii	Ceara rubbertree
MAGL6	Malpighia	glabra	Wild crapemyrtle
MAGR	Magnolia	grandiflora	Southern magnolia
MAGR8	Manihot	grahamii	Graham's manihot
MAHA	Malus	'Harvest Gold'	Crabapple 'Harvest Gold'
MAHA4	Mahonia	haematocarpa	Red barberry
MAIN	Mangifera	indica	Mango
MAIN5	Malpighia	infestissima	Cowhage cherry
MAIN8	Macadamia	integrifolia	Macadamia nut
MAIO	Malus	ioensis var. plena	Bechtel crabapple
MAIS	Malus	'Indian Summer'	Crabapple 'Indian Summer'
MAJA	Mahonia	japonica	Japanese mahonia
MAJA2	Manilkara	jaimiqui	Wild dilly
MALA6	Malosma	laurina	Laurel sumac
MALA8	Maytenus	laevigata	White cinnamon
MALI2	Malpighia	linearis	Bastard cherry
MALU2	Machaerium	lunatum	Palo de hoz
MALU4	Markhamia	lutea	Siala
MAMA	Magnolia	macrophylla	Bigleaf magnolia
MAMA28	Macaranga	mappa	Pengua
MAMA29	Malus	x magdeburgensis	Malus x magdeburgensis
MAMA37	Malus	mandshurica	Manchurian crabapple
MANE3	Mahonia	nevinii	Nevin's barberry
MANO	Margaritaria	nobilis	Bastard hogberry
MAOF	Magnolia	officinalis	Magnolia bark
MAPE3	Malvaviscus	penduliflorus	Mazapan
MAPH	Maytenus	phyllanthoides	Florida mayten
MAPH4	Mallotus	philippensis	Kamala tree
MAPI2	Mahonia	pinnata	Wavyleaf barberry
MAPL	Malus	x platycarpa	Bigfruit crab
MAPL2	Manilkara	pleeana	Zapote de costa
MAPO	Maclura	pomifera	Osage orange
MAPO2	Magnolia	portoricensis	Puerto rico magnolia
MAPO5	Maytenus	ponceana	Ponce mayten
MAPO6	Machaonia	portoricensis	Machaonia portoricensis
MAPR	Malus	prunifolia	Plumleaf crabapple
MAPU	Malus	pumila	Paradise apple
MAPUEL	Malus	x purpurea v eleyi	Eleyi crapapple
MAPY	Magnolia	pyramidata	Pyramid magnolia
MARA3	Mappia	racemosa	Palo de cana
MASA4	Matelea	sagittifolia	Arrowleaf milkvine
MASA9	Malus	sargentii	Sargent's apple
MASE	Malpighia	setosa	Bristly stingingbush
MASI3	Marlierea	sintenisii	Beruquillo
MASI80	Malus	sieboldii	Toringa crabapple
MASO	Magnolia	x soulangiana	Saucer magnolia
MASO3	Malus	x soulardii	Soulard crab

MASOGA	Magnolia	x soulangiana 'Galaxy'	Galaxy magnolia
MASP	Magnolia	splendens	Laurel magnolia
MASP1	Malus	spectabilis	Asiatic apple
MAST	Magnolia	stellata	Star magnolia
MASU15	Manihot	subspicata	Spiked manihot
MASW	Mahonia	swaseyi	Texas barberry
MASY2	Malus	sylvestris	European crabapple
MATA3	Macaranga	tanarius	Parasol leaf tree
MATE	Macadamia	tetraphylla	Rough-shell macadamia
MATE1	Macadamia	ternifolia	Sm-fruit Queensland Nut
MATI	Machaerium	tipu	Tipa
MATI3	Maclura	tinctoria	Fustictree
MATO	Malus	toringoides	Cutleaf Crab
MATR	Magnolia	tripetala	Umbrella magnolia
MATR3	Mahonia	trifoliolata	Algerita
MATS	Malus	tschonoskii	crabapple
MAVA3	Manilkara	valenzuela	Nisperillo
MAVI	Magnolia	virginiana	Sweetbay
MAWO	Malpighia	woodburyana	Woodbury's stingingbush
MAWO3	Machaonia	woodburyana	Alfilerillo
MAZA	Manilkara	zapota	Sapodilla
ME10	Melicope		melicope spp
ME11	Meliosma		meliosma spp
ME13	Melochia		melochia spp
ME14	Menodora		menodora spp
ME16	Menziesia		menziesia spp
ME17	Mespilus		mespilus spp
ME18	Metasequoia		dawn redwood spp
ME19	Metopium		Florida poisontree spp
ME2	Mecranium		mecranium spp
ME20	Metrosideros		lehua spp
ME3	Medinilla		medinilla spp
ME4	Melaleuca		melaleuca spp
ME7	Melastoma		melastoma spp
ME8	Melia		melia spp
ME9	Melicoccus		melicoccus spp
MEAD	Melicope	adscendens	Auwahi melicope
MEAN3	Melicope	anisata	Mokihana
MEAR	Melaleuca	armillaris	Drooping melaleuca
MEAZ	Melia	azedarach	Chinaberry
MEBA2	Melicope	balloui	Ballou's melicope
MEBA3	Melicope	barbigera	Uahiapele
MEBI	Melicoccus	bijugatus	Spanish lime
MEBI1	Melaleuca	biconvexa	Biconvex Paperbark
MEBR	Melaleuca	bracteata	River teatree
MECA10	Mespilus	canescens	Stern's medlar

MECA9	Melastoma	candidum	Asian melastome
MECH2	Melicope	christophersenii	Waianae range melicope
MECI6	Melicope	cinerea	Manena
MECL	Melicope	clusiifolia	Kukaemoa
MECR5	Melicope	cruciata	Pilo 'ula
MEDE	Melaleuca	decussata	Melaleuca lilac
MEDE1	Melaleuca	decora	Feather Honey Myrtle
MEDE6	Melicope	degeneri	Kokee stream melicope
MEEL2	Melicope	elliptica	Leiohi'iaka
MEER	Melaleuca	ericifolia	Heath melaleuca
MEEX	Metrosideros	excelsa	New zealand chrstmas tree
MEFE	Menziesia	ferruginea	Rusty menziesia
MEFE2	Melicope	feddei	Hiiaka
MEGE	Mespilus	germanica	European medlar
MEGL	Metasequoia	glyptostroboides	Dawn redwood
MEHA3	Melicope	haupuensis	Haupa mountain melicope
MEHA4	Melicope	hawaiensis	Mokihana kukae moa
MEHA7	Melicope	haleakalae	Haleakala melicope
MEHE	Meliosma	herbertii	Aguacatillo
MEHO2	Melicope	hosakae	Honolulu melicope
MEKA2	Melicope	kaalaensis	Kaala melicope
MEKA3	Melicope	kavaiensis	Kauai melicope
MEKE	Metrosideros	kermadecensis	Kermadec pohutakawa
MEKN	Melicope	knudsenii	Olokele valley melicope
MELA	Melaleuca	lanceolata	Rottnest Teatree
MELA7	Mecranium	latifolium	Camasey almendre
MELE	Melaleuca	leucadendra	White paperbark
MELI7	Melaleuca	linariifolia	Cajeput tree
MELY	Melicope	lydgatei	Koolau range melicope
MEMA	Melastoma	malabathricum	Malabar melastome
MEMA4	Metrosideros	macropus	'ohi'a
MEMA6	Melicope	macropus	Kaholuamanu melicope
MEMA7	Melicope	makahae	Makaha valley melicope
MEMO6	Melicope	molokaiensis	Molokai melicope
MEMU4	Melicope	mucronulata	Alani
MEMU5	Melicope	munroi	Lanahale
MENE	Melaleuca	nesophila	Pink melaleuca
MENE4	Melicope	nealiae	Kokee plateau melicope
MEOA	Melicope	oahuensis	Oahu melicope
MEOB2	Meliosma	obtusifolia	Cacaillo
MEOB4	Melicope	obovata	Makawao melicope
MEOR4	Melicope	orbicularis	Honokahua melicope
MEOV	Melicope	ovalis	Hana melicope
MEOV2	Melicope	ovata	Eggshape melicope
MEPA	Melaleuca	parvistaminea	Broad-leaved paperbark
MEPA6	Melicope	pallida	Pale melicope
MEPA7	Melicope	paniculata	Lihue melicope

MEPE9	Melicope	peduncularis	Boxfruit alani
MEPI2	Menziesia	pilosa	Minniebush
MEPO5	Metrosideros	polymorpha	'ohi'a lehua
MEPS	Melicope	pseudoanisata	Kohala summit melicope
MEPU4	Melicope	puberula	Hairy melicope
MEQU	Melaleuca	quinquenervia	Punk tree
MEQU3	Melicope	quadrangularis	Fourangle melicope
MERA2	Melicope	radiata	Kapu melicope
MERE3	Melicope	reflexa	Lava melicope
MERO3	Melicope	rotundifolia	Roundleaf melicope
MERU2	Metrosideros	rugosa	Lehua papa
MESA3	Melastoma	sanguineum	Red melastome
MESA4	Melicope	saint-johnii	St. john's melicope
MESA5	Melicope	sandwicensis	Mt. kaala melicope
MESP2	Menodora	spinescens	Spiny menodora
MEST	Melaleuca	styphelioides	Melaleuca
METO	Metopium	toxiferum	Florida poisontree
METR5	Metrosideros	tremuloides	Lehua 'ahihi
MEUM3	Melochia	umbellata	Hierba del soldado
MEVE3	Medinilla	venosa	Holdtight
MEVO	Melicope	volcanica	Volcanic melicope
MEWA	Metrosideros	waialealae	Kauai bottlebrush
MEWA2	Melicope	waialealae	Alani wai
MEWA3	Melicope	wailauensis	Wailau valley melicope
MEWA4	Melicope	wawraeana	Monoa melicope
MEZA	Melicope	zahlbruckneri	Kipuka piaula
MI	Mimusops		mimusops spp
MI1	Michelia		michelia spp
MI2	Miconia		johnnyberry spp
MI3	Micropholis		micropholis spp
MI4	Mimosa		sensitive plant spp
MI9	Mitracarpus		girdlepod spp
MIAC3	Mimosa	aculeaticarpa	Catclaw mimosa
MIAF	Miconia	affinis	Saquiyac
MIAR4	Mimosa	arenosa	Elegant mimosa
MIAS3	Mimosa	asperata	Puerto rico briar
MIBI	Mimosa	bimucronata	Marica
MIBO2	Mimosa	borealis	Fragrant mimosa
MICA20	Miconia	calvescens	Velvet tree
MICA21	Mimusops	caffra	Red milkwood
MICE	Mimosa	ceratonia	Black ambret
MICH	Michelia	champaca	Michelia champaca
MIDI8	Mimosa	diplotricha	Giant false sensitive
MIDO	Michelia	doltsopa	Michelia
MIDY	Mimosa	dysocarpa	Velvetpod mimosa
MIEM	Mimosa	emoryana	Emory's mimosa
MIFI	Michelia	figo	Banana shrub

MIFO	Miconia	foveolata	Puerto rico johnnyberry
MIGA	Micropholis	garciniifolia	Caimitillo verde
MIGR2	Mimosa	grahamii	Graham's mimosa
MIGU2	Micropholis	guyanensis	Wild balata
MIIM	Miconia	impetiolaris	Camasey de costilla
MILA10	Miconia	lanata	Hairy johnnyberry
MILA2	Mimosa	laxiflora	Arizona mimosa
MILA8	Miconia	laevigata	Smooth johnnyberry
MIMI3	Miconia	mirabilis	Camasey cuatrocanales
MIPA7	Miconia	pachyphylla	Camasey racimoso
MIPE2	Mimosa	pellita	Lollipop mimosa
MIPI	Mimosa	pigra	Black mimosa
MIPO4	Mitracarpus	portoricensis	Puerto rico girdlepod
MIPR3	Miconia	prasina	Granadillo bobo
MIPU9	Miconia	punctata	Auquey
MIPY2	Miconia	pycnoneura	Ridge johnnyberry
MIRA2	Miconia	racemosa	Camasey felpa
MIRU4	Miconia	rubiginosa	Peralejo
MISE2	Miconia	serrulata	Jau jau
MISI2	Miconia	sintenisii	Mountain johnnyberry
MISP6	Miconia	splendens	White-flower johnnyberry
MISU3	Miconia	subcorymbosa	Forest johnny berry
MITE4	Miconia	tetrandra	Rajador
MITE5	Miconia	tetrastoma	Graceful johnny berry
MITE6	Mimosa	texana	Texas mimosa
MITH	Miconia	thomasiana	Camasey tomaso
MITH4	Miconia	theaezans	Stalk-flower johnnyberry
MITU	Mimosa	turneri	Desert mimosa
MO	Morus		mulberry spp
MO1	Monotoca		monotoca spp
MO10	Mortonia		saddlebush spp
MO11	Mouriri		mouriri spp
MO4	Montanoa		montanoa spp
MO5	Montrichardia		montrichardia spp
MO6	Morella		bayberry spp
MO7	Morinda		morinda spp
MO8	Moringa		moringa spp
MO9	Morisonia		morisonia spp
MOAL	Morus	alba	White mulberry
MOALPE	Morus	alba pendula	White mullberry
MOAM	Morisonia	americana	Ratapple
MOAR	Montanoa	arborescens	Daisy tree
MOAR3	Montrichardia	arborescens	Yautia madera
MOBO	Morus	bombycis	Satin mulberry
MOCI3	Morinda	citrifolia	Indian mulberry
MODO2	Mouriri	domingensis	Murta
MOEL	Monotoca	elliptica	Tree Broom-heath

MOFA	Morella	faya	Firetree
MOGR2	Mortonia	greggii	Gregg's saddlebush
MOHE	Mouriri	helleri	Mameyuelo
MOHI	Montanoa	hibiscifolia	Treedaisy
MOHO3	Morella	holdridgeana	Palo de cera
MOIN	Morella	inodora	Scentless bayberry
MOMA6	Morella	x macfarlanei	Morella x macfarlanei
MOMI	Morus	microphylla	Smallleaf mulbery
MONI	Morus	nigra	Black mulberry
MOOL	Moringa	oleifera	Horseradishtree
MORU	Morus	rubra	Red mulberry
MOSC	Mortonia	scabrella	Rio grande saddlebush
MOSE	Mortonia	sempervirens	Montonia sempervirens
MOSP	Thespesia	grandiflora	Maga
MOTR	Morinda	trimera	Noni kuahiwi
MOUT	Mortonia	utahensis	Utah mortonia
MU1	Muehlenbeckia		maidenhair vine spp
MU2	Munroidendron		munroidendron spp
MU3	Muntingia		muntingia spp
MU4	Murraya		murraya spp
MU5	Musa		banana spp
MUAC	Musa	acuminata	Edible banana
MUAX2	Muehlenbeckia	axillaris	Sprawling wirevine
MUCA4	Muntingia	calabura	Strawberrytree
MUPA	Murraya	exotica	Orange-jessamine
MUPA3	Musa	x paradisiaca	French plantain
MURA3	Munroidendron	racemosum	False 'ohe
MUTR2	Musa	troglodytarum	Fe'i banana
MUVE	Musa	velutina	Hairy banana
MY	Myrocarpus		myrocarpus spp
MY1	Myoporum		myoporum spp
MY2	Myrcia		rodwood spp
MY3	Myrcianthes		myrcianthes spp
MY4	Myrciaria		guavaberry spp
MY5	Myrica		sweetgale spp
MY6	Myristica		nutmeg spp
MY7	Myrospermum		myrospermum spp
MY8	Myrsine		colicwood spp
MY9	Myrtus		myrtus spp
MYAC	Myoporum	acuminatum	Waterbush
MYAL4	Myrsine	alyxifolia	Forest colicwood
MYBO	Myrciaria	borinquena	False tamarisk
MYCA	Morella	californica	Pacific bayberry
MYCA1	Myrciaria	cauliflora	Brazilian Grape Tree
MYCE	Morella	cerifera	Southern bayberry
MYCI	Myrcia	citrifolia	Red rodwood
MYCO	Myrtus	communis	Myrtle

MYCO2	Myrsine	coriacea	Leathery colicwood
MYDE	Myrcia	deflexa	Cieneguillo
MYDE2	Myrsine	degeneri	Summit colicwood
MYDE3	Myrsine	denticulata	Bog colicwood
MYEM	Myrsine	emarginata	Mountain colicwood
MYFA3	Myrcia	fallax	Curame
MYFE	Myrsine	fernseei	Streambank colicwood
MYFL	Myrciaria	floribunda	Guavaberry
MYFO	Myrsine	fosbergii	Koolau range colicwood
MYFR	Myrcianthes	fragrans	Twinberry
MYFR2	Myrospermum	frutescens	Cercipo
MYFR3	Myristica	fragrans	Nutmeg
MYFR4	Myrocarpus	frondosus	Cabriuva
MYGA	Myrica	gale	Sweetgale
MYHA	Myrica	hartwegii	Sierra bayberry
MYHE	Morella	caroliniensis	Evergreen bayberry
MYHE3	Myrsine	helleri	Wahiawa bog colicwood
MYIN	Myoporum	insulare	Boobialla
MYJU	Myrsine	juddii	Cloudswept colicwood
MYKA	Myrsine	kauaiensis	Kauai colicwood
MYKN	Myrsine	knudsenii	Kokee colicwood
MYLA	Myoporum	laetum	Mioporo
MYLA3	Myrsine	lanaiensis	Lanai colicwood
MYLE	Myrcia	leptoclada	Guayabacon
MYLE2	Myrsine	lessertiana	Kolea lau nui
MYLI	Myrsine	linearifolia	Narrowleaf colicwood
MYMA4	Myrcia	margarettiae	Margarett's myrcia
MYMA5	Myrcia	maricaensis	Maricao rodwood
MYME2	Myrsine	mezii	Hanapepe river colicwood
MYMY	Myrciaria	myrtifolia	Ridgetop guavaberry
MYPA	Myrcia	paganii	Ausu
MYPE	Morella	pensylvanica	Bayberry
MYPE3	Myrsine	petiolata	Swamp colicwood
MYPU2	Myrsine	pukooensis	Molokai colicwood
MYPU3	Myrsine	punctata	Dotted colicwood
MYSA	Myoporum	sandwicense	Naio
MYSA2	Myrsine	sandwicensis	Kokea lau li'i
MYSP	Myrcia	splendens	Punchberry
MYVA	Myrsine	vaccinioides	Violet lake colicwood
MYWA	Myrsine	wawraea	Mt. kahili colicwood
NA2	Nandina		nandina spp
NADO	Nandina	domestica	Heavenly bamboo
NE1	Nectandra		nectandra spp
NE11	Nerium		oleander spp
NE13	Nesoluma		nesoluma spp
NE14	Nestegis		nestegis spp
NE15	Nestronia		nestronia spp

NE17	Neviusia		snow-wreath spp
NE2	Neea		saltwood spp
NE3	Nemopanthus		nemopanthus spp
NE4	Neolamarckia		neolamarckia spp
NE5	Neolaugeria		neolaugeria spp
NE9	Neraudia		ma'oloa spp
NEAL	Neviusia	alabamensis	Alabama snow-wreath
NEAN	Neraudia	angulata	Angularfruit ma'oloa
NEBU	Neea	buxifolia	Saltwood
NECA7	Neolamarckia	cadamba	Kadam
NECL	Neviusia	cliftonii	Shasta snow-wreath
NECO	Nectandra	coriacea	Lancewood
NEHI2	Nectandra	hihua	Shinglewood
NEKA2	Neraudia	kauaiensis	Kauai ma'oloa
NEKR	Nectandra	krugii	Krug's sweetwood
NEME3	Nectandra	membranacea	Sweetwood
NEME5	Neraudia	melastomifolia	Ma'aloa
NEMU2	Nemopanthus	mucronatus	Catberry
NEOL	Nerium	oleander	Oleander
NEOV	Neraudia	ovata	Big island ma'oloa
NEPA4	Nectandra	patens	Capberry
NEPO	Nesoluma	polynesicum	Keahi
NERE2	Neolaugeria	resinosa	Aquilon
NESA2	Nestegis	sandwicensis	Hawai'i olive
NESE2	Neraudia	sericea	Woodland ma'oloa
NETU	Nectandra	turbacensis	Laurel amarillo
NEUM	Nestronia	umbellula	Leechbrush
NI1	Nicotiana		tobacco spp
NI2	Nierembergia		cupflower spp
NIFR	Nierembergia	frutescens	Tall cupflower
NIGL	Nicotiana	glauca	Tree tobacco
NO1	Nolina		beargrass spp
NO2	Nothocestrum		aiea spp
NO4	Nothofagus		nothofagus spp
NO5	Nototrichium		rockwort spp
NOAL	Nothofagus	alpina	RaulÍ
NOBI	Nolina	bigelovii	Bigelow's nolina
NOBR2	Nothocestrum	breviflorum	Smallflower aiea
NODO	Nothofagus	dombeyi	CoigÜe
NOHU	Nototrichium	humile	Kaala rockwort
NOLA	Nothocestrum	latifolium	Broadleaf aiea
NOLO	Nothocestrum	longifolium	Longleaf aiea
NOOB	Nothofagus	obliqua	Roble
NOPA	Nolina	parryi	Parry's beargrass
NOPE	Nothocestrum	peltatum	Oahu aiea
NOSA	Nototrichium	sandwicense	Hawai'i rockwort
NY1	Nypa		nypa spp

NY2	Nyssa		tupelo spp
NYAQ	Nyssa	aquatica	Water tupelo
NYBI	Nyssa	biflora	Swamp tupelo
NYFR2	Nypa	fruticans	Nipa palm
NYOG	Nyssa	ogeche	Ogeechee tupelo
NYSY	Nyssa	sylvatica	Black tupelo
NYUR2	Nyssa	ursina	Bear tupelo
OC1	Ochna		ochna spp
OC2	Ochroma		ochroma spp
OC3	Ochrosia		yellowwood spp
OC4	Ocotea		sweetwood spp
OCCO	Ochrosia	compta	Holei
OCEL	Ochrosia	elliptica	Elliptic yellowwood
OCFL	Ocotea	floribunda	Laurel espada
OCFO	Ocotea	foeniculacea	Black sweetwood
OCHA	Ochrosia	haleakalae	Island yellowwood
OCJA	Ochna	jabotapita	Bird's-eye bush
OCKA	Ochrosia	kauaiensis	Kauai yellowwood
OCKI	Ochrosia	kilaueaensis	Hawai'i yellowwood
OCLE	Ocotea	leucoxylon	Loblolly sweetwood
OCMO	Ocotea	moschata	Nemoca
OCNE	Ocotea	nemodaphne	Laurel sassafras
OCPO	Ocotea	portoricensis	Laurel de paloma
OCPY	Ochroma	pyramidale	West indian balsa
OCSE2	Ochna	serrulata	Mickey mouse plant
OCSP	Ocotea	spathulata	Nemoca cimarrona
OCTH	Ochna	thomasiana	Thomas' bird's-eye bush
OCWR	Ocotea	wrightii	Wright's laurel canelon
OD1	Odontonema		toothedthread spp
ODNI	Odontonema	nitidum	Shrubby toothedthread
ODTU	Odontonema	tubiforme	Firespike
OE1	Oemleria		oemleria spp
OECE	Oemleria	cerasiformis	Indian plum
OL2	Olea		olive spp
OL3	Olneya		olneya spp
OLEM	Olea	emarginata	Madagascar olive
OLEU	Olea	europaea	Olive
OLEU2	Olea	europaea 'Swan Hill'	Swan hill olive
OLTE	Olneya	tesota	Tesota
OMPO	Homolanthus	populifolius	Bleeding heart
ON1	Ononis		restharrow spp
ONAR	Ononis	arvensis	Field restharrow
OP1	Oplonia		oplonia spp
OP2	Oplopanax		oplopanax spp
OP3	Opuntia		pricklypear spp
OPAU10	Opuntia	aurantiaca	Tiger-pear

OPAU2	Opuntia	aurea	Golden pricklypear
OPBA2	Opuntia	basilaris	Beavertail pricklypear
OPBR2	Opuntia	brasiliensis	Brazilian pricklypear
OPCO4	Opuntia	cochenillifera	Cochineal nopal cactus
OPFI	Opuntia	ficus-indica	Tuna cactus
OPFU	Opuntia	fulgida	Jumping cholla
OPGO	Opuntia	gosseliniana	Violet pricklypear
OPHO	Oplopanax	horridus	Devilsclub
OPIM	Opuntia	imbricata	Tree cholla
OPMA8	Opuntia	macrocentra	Purple pricklypear
OPMI	Oplonia	microphylla	Thicketwort
OPMO2	Opuntia	moniliformis	Tuna
OPMO5	Opuntia	monacantha	Common pricklypear
OPPI3	Opuntia	pinkavae	Pinkava's pricklypear
OPRU	Opuntia	rubescens	Sour pricklypear
OPSA	Opuntia	santa-rita	Santa rita pricklypear
OPSP4	Oplonia	spinosa	Pricklybush
OPTO2	Opuntia	tomentosa	Woollyjoint pricklypear
OR	Orbignya		orbignya spp
OR1	Ormosia		ormosia spp
OR2	Ornithostaphyls		ornithostaphylos spp
ORCO9	Orbignya	cohune	Cohune palm
ORKR	Ormosia	krugii	Peronia
OROP	Ornithostaphylos	oppositifolia	Baja birdbush
OS1	Osmanthus		devilwood spp
OS2	Osteomeles		osteomeles spp
OS4	Ostrya		hophornbean spp
OSAM	Osmanthus	americanus	Devilwood
OSAN	Osteomeles	anthyllidifolia	Hawai'i hawthorn
OSCA	Ostrya	carpinifolia	Hop hornbeam
OSFR	Osmanthus	fragrans	Sweet olive
OSHE	Osmanthus	heterophyllus	Holly osmanthus
OSKN	Ostrya	knowltonii	Knowlton hophornbeam
OSVI	Ostrya	virginiana	Eastern hophornbeam
OT1	Ottoschulzia		ottoschulzia spp
OTRH	Ottoschulzia	rhodoxylon	Pincho palo de rosa
OU1	Ouratea		ouratea spp
OUIL	Ouratea	ilicifolia	Chicharron amarillo
OULI	Ouratea	littoralis	Abey amarillo
OUST	Ouratea	striata	Guanabanilla
OX2	Oxandra		oxandra spp
OX3	Oxydendrum		swamp cranberry spp
OXAR	Oxydendrum	arboreum	Sourwood
OXLA4	Oxandra	lanceolata	Blacklancewood
OXLA5	Oxandra	laurifolia	Haya
PA	Parrotia		ironwood spp
PA1	Pachira		pachira spp

PA10	Pandanus		screwpine spp
PA11	Paraserianthes		paraserianthes spp
PA12	Parathesis		parathesis spp
PA13	Parkinsonia		paloverde spp
PA14	Parmentiera		parmentiera spp
PA16	Parryella		parryella spp
PA17	Parthenium		feverfew spp
PA18	Parthenocissus		creeper spp
PA19	Paulownia		paulownia spp
PA2	Pachycereus		pachycereus spp
PA21	Paxistima		paxistima spp
PA3	Patagonula		patagonula spp
PA4	Parapiptadenia		parapiptadenia spp
PA5	Paederia		sewer vine spp
PA7	Palicourea		cappel spp
PA8	Paliurus		Jeruselem thorn spp
PAAC	Parkinsonia	aculeata	Jerusalem thorn
PAAC13	Parmentiera	aculeata	Cuachilote
PAAL9	Palicourea	alpina	Tafetan
PAAM	Patagonula	americana	Guajuvira
PAAR5	Parthenium	argentatum	Guayule
PACE8	Parmentiera	cereifera	Candle tree
PACR18	Palicourea	croceoides	Yellow cedar
PACR2	Parathesis	crenulata	Scratchthroat
PACR3	Palicourea	crocea	Red cappel
PAFI4	Parryella	filifolia	Common dunebroom
PAFO3	Paederia	foetida	Stinkvine
PAGU	Palicourea	guianensis	Showy cappel
PAIN2	Parthenium	incanum	Mariola
PAIN7	Pachira	insignis	Wild chestnut
PALO8	Paraserianthes	lophantha	Plume albizia
PALO8LO	Paraserianthes	lophantha lop.	Cape leeuwin wattle
PAMY	Paxistima	myrsinites	Oregon boxleaf
PAPE	Parrotia	persica	Persian ironwood
PAPR	Parkinsonia	praecox	Sonoran palo verde
PAQU	Parthenocissus	quinquefolia	Virginia creeper
PARI	Parapiptadenia	rigida	Angico vermelho
PASC14	Pachycereus	schottii	Senita cactus
PASP16	Paliurus	spina-christi	Jeruselem thorn
PATE10	Parkinsonia	texana	Texas paloverde
PATE2	Pandanus	tectorius	Tahitian screwpine
PATO	Paulownia	tomentosa	Royal paulownia
PATR	Parthenocissus	tricuspidata	Boston ivy
PAUT	Pandanus	utilis	Common screwpine
PAVE6	Pandanus	veitchii	Veitch's screwpine
PE11	Pentzia		pentzia spp
PE12	Pera		pera spp

PE13	Peraphyllum		peraphyllum spp
PE14	Pereskia		pereskia spp
PE17	Perrottetia		perrottetia spp
PE18	Persea		bay spp
PE20	Petitia		petitia spp
PE25	Peucephyllum		pygmycedar spp
PE26	Peumus		peumus spp
PE3	Pedilanthus		pedilanthus spp
PE6	Peltophorum		peltophorum spp
PEAC2	Pereskia	aculeata	Barbados shrub
PEAM	Persea	americana	Avocado
PEBO	Persea	borbonia	Redbay
PEBO2	Peumus	boldus	Boldo
PEBU2	Pera	bumeliifolia	Jiqi
PEDO	Petitia	domingensis	Bastard stopper
PEDU3	Peltophorum	dubia	Horsebush
PEGR14	Pereskia	grandifolia	Rose cactus
PEHU2	Persea	humilis	Silk bay
PEIN17	Persea	indica	Indian bay
PEIN4	Pentzia	incana	African sheepbush
PEKR	Persea	krugii	Canela
PELI	Persea	lingue	Lingue
PEPA37	Persea	palustris	Swamp bay
PEPT	Peltophorum	pterocarpum	Peltophorum
PERA4	Peraphyllum	ramosissimum	Squaw apple
PESA3	Perrottetia	sandwicensis	Olomea
PESC4	Peucephyllum	schottii	Schott's pygmycedar
PETI	Pedilanthus	tithymaloides	Redbird flower
PEUR2	Persea	urbaniana	Aquacatillo
PH	Phillyrea		phillyrea spp
PH11	Phyllanthus		leafflower spp
PH15	Physalis		groundcherry spp
PH16	Physocarpus		ninebark spp
PH17	Phytolacca		pokeweed spp
PH18	Phyllostachys		tropical bamboo spp
PH2	Phaulothamnus		phaulothamnus spp
PH3	Phellodendron		corktree spp
PH4	Phialanthus		phialanthus spp
PH5	Phlomis		jerusalem sage spp
PH7	Phoenix		date palm spp
PHAC3	Phyllanthus	acidus	Tahitian gooseberry tree
PHAC7	Phyllanthus	acuminatus	Jamaican gooseberry tree
PHAL7	Physocarpus	alternans	Dwarf ninebark
PHAM	Phellodendron	amurense	Amur corktree
PHAN9	Phyllanthus	angustifolius	Foliage flower
PHAR10	Philadelphus	argyrocalyx	Silvercup mock orange
PHAR12	Philadelphus	argenteus	Silver mock orange

PHBO9	Phytolacca	bogotensis	Southern pokeweed
PHCA	Phoenix	canariensis	Canary island date palm
PHCA11	Physocarpus	capitatus	Pacific ninebark
PHCA18	Philadelphus	californicus	California mock orange
PHCO	Philadelphus	coronarius	Sweet mock orange
PHCO25	Philadelphus	confusus	Piper's mock orange
PHCO32	Philadelphus	cordifolius	Heartleaf mock orange
PHCR3	Philadelphus	crinitus	Transpecos mock orange
PHCU4	Phyllanthus	cuneifolius	Wedge leaf-flower
PHDA4	Phoenix	dactylifera	Date palm
PHDA5	Photinia	davidiana	Chinese photinia
PHDI	Phytolacca	dioica	OmbÚ
PHDI8	Phyllanthus	distichus	Pamakani mahu
PHEM2	Phyllanthus	emblica	Emblic
PHEP	Phyllanthus	epiphyllanthus	Swordbush
PHER	Philadelphus	ernestii	Canyon mock orange
PHFL4	Philadelphus	floridus	Florida mock orange
PHFL9	Photinia	floribunda	Purple chokeberry
PHFR	Photinia	x fraseri	Fraser photinia
PHFR4	Phlomis	fruticosa	Shrubby jerusalem sage
PHGA	Philadelphus	gattingeri	Gattinger's mock orange
PHGL	Photinia	glabra	Japanese photinia
PHGR11	Phialanthus	grandifolius	Aquilon prieto
PHHE8	Phytolacca	heteropetala	Mexican pokeweed
PHHI2	Philadelphus	hirsutus	Streambank mock orange
PHHI3	Philadelphus	hitchcockianus	Hitchcock's mock orange
PHIN21	Philadelphus	insignis	Summer mock orange
PHIN5	Philadelphus	inodorus	Scentless mock orange
PHJA	Phellodendron	japonicum	Japanese corktree
PHJU2	Phyllanthus	juglandifolius	Gamo de costa
PHKA4	Philadelphus	karwinskianus	Evergreen mock orange
PHLA	Phillyrea	latifolia	Broad-leaved phillyrea
PHLE	Philadelphus	lewisii	Wild mock orange
PHMA5	Physocarpus	malvaceus	Mallow ninebark
PHMA7	Philadelphus	maculatus	Spotted mock orange
PHMA8	Philadelphus	madrensis	Desert mock orange
PHME13	Photinia	melanocarpa	Black chokeberry
PHME4	Philadelphus	mearnsii	Mearns' mock orange
PHMI4	Philadelphus	microphyllus	Littleleaf mock orange
PHMO4	Physocarpus	monogynus	Mountain ninebark
PHMY	Phialanthus	myrtilloides	Candlewood
PHOC2	Philadelphus	occidentalis	Western mock orange
PHOP	Physocarpus	opulifolius	Common ninebark
PHOR4	Philadelphus	oreganus	Oregon mock orange
PHPA11	Philadelphus	palmeri	Palmer's mock orange
PHPE4	Physalis	peruviana	Peruvian groundcherry
PHPU11	Phyllanthus	pulcher	Tropical leaf-flower

PHPU15	Philadelphus	pumilus	Dwarf mock orange
PHPU4	Philadelphus	pubescens	Hoary mock orange
PHPY4	Photinia	pyrifolia	Red chokeberry
PHRE	Phoenix	reclinata	Senegal date palm
PHRECA	Phoenix	reclinata x canariensis	Senegal Date hybrid
PHRESY	Phoenix	reclinata x sylvestris	Senegal date
PHRO	Phoenix	roebelenii	Pygmy date palm
PHSE	Photinia	serratifolia	Taiwanese photinia
PHSE1	Photinia	serrulata	Photinia
PHSE2	Philadelphus	serpyllifolius	Thymeleaf mock orange
PHSH	Philadelphus	sharpianus	Sharp's mock orange
PHSP	Philadelphus		mock orange spp
PHSP2	Photinia		chokeberry spp
PHSP4	Phaulothamnus	spinescens	Devilqueen
PHSY	Phoenix	sylvestris	Wild date palm
PHTE3	Philadelphus	texensis	Texas mock orange
PHTO7	Philadelphus	tomentosus	Fuzzy mock orange
PHTR3	Philadelphus	trichothecus	Columbian mock orange
PHVI	Photinia	villosa	Oriental photinia
PHWO	Philadelphus	wootonii	Wooton's mock orange
PHZE	Philadelphus	zelleri	Zeller's mock orange
PI1	Picea		spruce spp
PI10	Pilocarpus		pilocarpus spp
PI11	Pilosocereus		tree cactus spp
PI12	Pimenta		pimenta spp
PI13	Pinckneya		pinckneya spp
PI14	Piper		pepper spp
PI15	Piptocarpha		ashdaisy spp
PI16	Piptocoma		velvetshrub spp
PI17	Pipturus		pipturus spp
PI19	Piscidia		piscidia spp
PI2	Pinus		pine spp
PI20	Pisonia		catchbirdtree spp
PI21	Pistacia		pistache spp
PI22	Pithecellobium		blackbead spp
PI23	Pittosporum		cheesewood spp
PI3	Pickeringia		chaparral pea spp
PI5	Picramnia		bitterbush spp
PI6	Picrasma		picrasma spp
PI8	Pictetia		pictetia spp
PI9	Piloblephis		piloblephis spp
PIAB	Picea	abies	Norway spruce
PIABAS	Picea	abies x asperata	Norway x chinese spruce
PIAC	Pictetia	aculeata	Fustic
PIAC2	Pisonia	aculeata	Pullback

PIAC6	Piptocoma	acevedoi	Acevedo's velvetshrub
PIAD	Piper	aduncum	Higuillo de hoja menuda
PIAL	Pinus	albicaulis	Whitebark pine
PIAL2	Pipturus	albidus	Waimea pipturus
PIAL3	Pisonia	albida	Corcho bobo
PIAM2	Piper	amalago	Higuillo de limon
PIAN2	Picrasma	antillana	Bitter ash
PIAN4	Piptocoma	antillana	Antilles velvetshrub
PIAR	Pinus	aristata	Bristlecone pine
PIAR2	Pinus	armandii	David's pine
PIAR3	Cojoba	arborea	Cojoba
PIAR4	Pittosporum	argentifolium	Hawai'i poisonberry tree
PIAR5	Pinus	arizonica	Arizona pine
PIAR9	Pittosporum	arborescens	Pittosporum
PIAS	Picea	asperata	Chinese spruce
PIAT	Pinus	attenuata	Knobcone pine
PIAT2	Pinus	x attenuradiata	Pinus x attenuradiata
PIAT4	Pistacia	atlantica	Mt. atlas mastic tree
PIAU	Piper	auritum	Vera cruz pepper
PIAY	Pinus	ayacahuite	Mexican White Pine
PIBA	Pinus	banksiana	Jack pine
PIBA2	Pinus	balfouriana	Foxtail pine
PIBI	Picea	bicolor	Alcock spruce
PIBL	Piper	blattarum	Moth pepper
PIBR	Picea	brewerana	Brewer spruce
PIBR2	Pinus	brutia	Turkish pine
PIBR3	Pisonia	brunoniana	Australasia catchbirdtree
PIBU	Pinus	bungeana	Lacebark pine
PICA	Pinus	canariensis	Canary island pine
PICA14	Pisonia	capitata	Mexican devil's-claws
PICA16	Pinus	californiarum	California pine
PICA5	Piscidia	carthagenensis	Stinkwood
PICE	Pinus	cembroides	Mexican pinyon
PICE2	Pinus	cembra	Swiss stone pine
PICH	Pistacia	chinensis	Chinese pistache
PICHPS	Pistacia	chinensis 'Pearl Street'	Chinese pistache Pearl St
PICL	Pinus	clausa	Sand pine
PICO	Pinus	contorta	Lodgepole pine
PICO2	Pinus	coulteri	Coulter pine
PICO4	Pittosporum	confertiflorum	Ho'awa
PICO5	Pinus	contorta var. bolanderi	Bolander beach pine
PICO6	Pinus	contorta var. latifolia	Tall lodgepole pine
PICO7	Pinus	contorta v murrayana	Murray lodgepole pine
PICR	Pittosporum	crassifolium	Stiffleaf cheesewood

PIDE	Pinus	densiflora	Japanese red pine
PIDI	Pinus	discolor	Border pinyon
PIDI2	Piper	dilatatum	Higuillo
PIDI3	Pimenta	dioica	Allspice
PIDU	Pithecellobium	dulce	Monkeypod
PIEC	Pinus	echinata	Shortleaf pine
PIED	Pinus	edulis	Pinyon pine
PIEL	Pinus	elliottii	Slash pine
PIEL2	Pinus	eldarica	Afghan pine
PIEN	Picea	engelmannii	Engelmann spruce
PIEN3	Pinus	engelmannii	Apache pine
PIEU	Pittosporum	eugenioides	Tarata
PIEU1	Pittosporum	eugenoides	Lemonwood
PIEUVA	Pittosporum	eugenioides vrgtd.	Variegated pittosporum
PIEX	Picrasma	excelsa	Bitterwood
PIFE	Pittosporum	ferrugineum	Rusty pittosporum
PIFL	Pinus	flexilis	Limber pine
PIFL2	Pieris	floribunda	Mountain fetterbush
PIFL4	Pittosporum	flocculosum	Waianae range cheesewood
PIFL6	Pisonia	floridana	Rock key devil's-claws
PIFO2	Pipturus	forbesii	Forbes' pipturus
PIGA2	Pittosporum	gayanum	Waialeale cheesewood
PIGL1	Picea	glauca	White spruce
PIGL2	Pinus	glabra	Spruce pine
PIGL3	Picea	glehnii	Sagholia spruce
PIGL4	Pittosporum	glabrum	Koolau range cheesewood
PIGL5	Piper	glabrescens	Guyanese pepper
PIGR5	Pithecellobium	graciliflorum	Guadeloupe blackbead
PIGR6	Pisonia	grandis	Grand devil's-claws
PIHA	Pinus	halepensis	Aleppo pine
PIHA4	Pittosporum	hawaiiense	Hawai'i cheesewood
PIHI2	Piper	hispidum	Jamaican pepper
PIHO	Pittosporum	hosmeri	Kona cheesewood
PIJA	Pieris	japonica	Japanese pieris
PIJE	Picea	jezoensis	Yeddo spruce
PIJE2	Pinus	jeffreyi	Jeffery pine
PIKA	Pipturus	kauaiensis	Kauai pipturus
PIKA3	Pittosporum	kauaiense	Kauai cheesewood
PIKE	Pithecellobium	keyense	Florida keys blackbead
PIKH	Pinus	kesiya	Khasia pine; thông ba lá
PIKO1	Picea	koraiensis	Korean spruce
PIKO2	Picea	koyamai	Picea koyamai
PILA	Pinus	lambertiana	Sugar pine
PILE	Pinus	leiophylla	Chihuahua pine
PILE2	Pinus	leucodermis	Bosnian pine
PILO	Pinus	longaeva	Intermtn bristlecone pine

PILU	Picea	x lutzii	Lutz's spruce
PIMA	Picea	mariana	Black spruce
PIMA2	Pinus	massoniana	Chinese red pine
PIMA3	Pinus	maritima	Pinus maritima
PIMA4	Piper	marginatum	Marigold pepper
PIME	Piper	methysticum	Kava
PIMO	Picea	montigena	Picea montigena
PIMO2	Pinus	monophylla	Singleleaf pinyon
PIMO3	Pinus	monticola	Western white pine
PIMO4	Pittosporum	x monae	Mona cheesewood
PIMO5	Pickeringia	montana	Montana chaparral pea
PIMO6	Pinus	montezumae	Pinus montezumae
PIMU	Pinus	mugo	Sweet mountain pine
PIMU2	Pinus	muricata	Bishop pine
PINA	Pittosporum	napaliense	Royal cheesewood
PINI	Pinus	nigra	Austrian pine
PINI2	Pinus	nigricans	Pinus nigricans
PINI4	Pinus	nigra ssp. salzmannii	Corsican pine
PIOM	Picea	omorika	Serbian spruce
PIOR	Picea	orientalis	Oriental spruce
PIPA	Pinus	palustris	Longleaf pine
PIPA2	Pinus	parviflora	Japanese white pine
PIPA3	Pinus	pallasiana	Pinus pallasiana
PIPA4	Pinus	patula	Mexican weeping pine
PIPE	Picramnia	pentandra	Bitterbush
PIPE8	Pittosporum	pentandrum	Taiwanese cheesewood
PIPH	Pieris	phillyreifolia	Climbing fetterbush
PIPH2	Pittosporum	phillyraeoides	Pittosporum willow
PIPI	Pinus	pithyusa	Pinus pithyusa
PIPI1	Piscidia	piscipula	Florida fishpoision tree
PIPI2	Pinus	pinea	Itailian stone pine
PIPI6	Pinus	pinaster	Maritime pine
PIPO	Pinus	ponderosa	Ponderosa pine
PIPU	Picea	pungens	Blue spruce
PIPU2	Pinckneya	bracteata	Fever bark
PIPU3	Pinus	pungens	Table mountain pine
PIQU	Pinus	quadrifolia	Parry pinyon
PIRA	Pinus	radiata	Monterey pine
PIRA2	Pimenta	racemosa	Bay rum tree
PIRA3	Pilocarpus	racemosus	Aceitillo
PIRE	Pinus	resinosa	Red pine
PIRE5	Pinus	remota	Papershell pinyon
PIRH	Pittosporum	rhombifolium	Queensland pittosporum
PIRI	Pinus	rigida	Pitch pine
PIRI5	Piloblephis	rigida	Wild pennyroyal
PIRO	Pinus	roxburghii	Chir pine

PIRO3	Pisonia	rotundata	Smooth devil's-claws
PIRO5	Pilosocereus	robinii	Key tree cactus
PIRO6	Pilosocereus	royenii	Royen's tree cactus
PIRU	Picea	rubens	Red spruce
PIRU2	Pipturus	ruber	Red pipturus
PISA	Pinus	sabiniana	Digger pine
PISA2	Samanea	saman	Raintree
PISA5	Pisonia	sandwicensis	Aulu
PISE	Pinus	serotina	Pond pine
PISI	Picea	sitchensis	Sitka spruce
PISO	Pinus	x sondereggeri	Pinus x sondereggeri
PISP	Pieris		fetterbush spp
PIST	Pinus	strobus	Eastern white pine
PIST2	Pinus	strobiformis	Southwestern white pine
PISU	Pisonia	subcordata	Water mampoo
PISW	Piper	swartzianum	Spanish elder
PISY	Pinus	sylvestris	Scotch pine
PITA	Pinus	taeda	Loblolly pine
PITA2	Pinus	tabulaeformis	Southern chinese pine
PITE	Pistacia	mexicana	Texas pistache
PITE11	Pittosporum	tenuifolium	Tawhiwhi
PITE11VA	Pittosporum	tenuifolium vrgtd.	Cheesewood
PITE5	Pittosporum	terminalioides	Cream cheesewood
PITE6	Piptocarpha	tetrantha	Mountain ashdaisy
PITH	Pinus	thunbergiana	Japanese black pine
PITO	Pittosporum	tobira	Japanese pittosporum
PITO2	Pinus	torreyana	Torrey pine
PIUM2	Pisonia	umbellifera	Umbrella catchbirdtree
PIUN	Pittosporum	undulatum	Victorian box
PIUN2	Pithecellobium	unguis-cati	Catclaw blackbead
PIUN3	Pinus	uncinata	Mountain pine
PIVE	Pistacia	vera	Pistachio
PIVI	Pinus	virginiana	Virginia pine
PIVI5	Pittosporum	viridiflorum	Cape cheesewood
PIWA	Pinus	washoensis	Washoe pine
PIWA1	Pinus	wallichiana	Bhutan pine
PIWA2	Pisonia	wagneriana	Kauai catchbirdtree
PIYU	Pinus	yunnanensis	Yunnan pine
PL	Planchonella		planchonella spp
PL1	Planera		planertree spp
PL11	Pluchea		camphorweed spp
PL13	Plumeria		plumeria spp
PL2	Platymiscium		platymiscium spp
PL3	Platanus		sycamore spp
PL4	Platycladus		platycladus spp
PL5	Platydesma		platydesma spp
PL7	Plectranthus		plectranthus spp

PL8	Pleodendron		pleodendron spp
PL9	Pleomele		hala pepe spp
PLAC	Platanus	hybrida	London planetree
PLAC1	Platanus	x acerifolia	London plane
PLAC2	Plumeria	acuminata	Fragipani
PLACBL	Platanus	acerifolia 'Bloodgood'	Lndon planetree Bloodgood
PLACCO	Platanus	acerifolia 'Columbia'	London planetree Columbia
PLAL	Plumeria	alba	Nosegay tree
PLAM2	Plectranthus	amboinicus	Mexican mint
PLAQ	Planera	aquatica	Water elm
PLAU	Planchonella	australis	Black plum
PLAU2	Pleomele	aurea	Golden hala pepe
PLAU5	Pleomele	auwahiensis	Maui hala pepe
PLCA10	Pluchea	carolinensis	Cure for all
PLCO6	Platydesma	cornuta	Oahu pilo kea
PLFE	Pleomele	fernaldii	Lanai hala pepe
PLFO2	Pleomele	forbesii	Waianae range hala pepe
PLHA3	Pleomele	halapepe	Royal hala pepe
PLHA4	Pleomele	hawaiiensis	Hawai'i hala pepe
PLMA6	Pleodendron	macranthum	Chupa gallo
PLOB2	Plumeria	obtusa	Singapore graveyard
PLOC	Platanus	occidentalis	American sycamore
PLOR	Platanus	orientalis	Oriental planetree
PLORDI	Platanus	orientalis digitata	Cut leaf plane
PLORIN	Platanus	insularis	Cyprus plane
PLPI4	Platymiscium	pinnatum	Chachimbo
PLRA	Platanus	racemosa	California sycamore
PLRE4	Platydesma	remyi	Hawai'i pilo kea
PLRO2	Platydesma	rostrata	Pilo kea lau li'i
PLRU	Plumeria	rubra	Frangipani
PLSE	Pluchea	sericea	Arrowweed
PLSP3	Platydesma	spathulata	Maui pilo kea
PLWR	Platanus	wrightii	Arizona sycamore
PO	Populus		cottonwood spp
PO1	Polyalthia		polyalthia spp
PO10	Polyscias		aralia spp
PO11	Poncirus		poncirus spp
PO12	Pontederia		pontederia spp
PO15	Pouteria		pouteria spp
PO16	Pouzolzia		pouzolzia spp
PO17	Pongamia		pongame spp
PO2	Potentilla		cinquefoil spp
PO3	Podocarpus		plum pine spp
PO4	Poitea		wattapama spp
PO7	Polygala		polygala spp

PO9	Polygonum		knotweed spp
POAC5	Populus	x acuminata	Lanceleaf cottonwood
POAL	Populus	alba	White poplar
POAN	Populus	angustifolia	Narrowleaf cottonwood
POAN1	Prumnopitys	andina	Lleuque
POBA	Populus	balsamifera	Balsam poplar
POBABA	Populus	balsamifera ssp balsamifera	Balsam poplar Balsamifera
POBR7	Populus	x brayshawii	Hybrid balsam poplar
POCA	Populus	x canescens	Gray poplar
POCA2	Populus	x canadensis	Carolina poplar
POCA23	Pouteria	campechiana	Canistel
POCO3	Podocarpus	coriaceus	Yucca plum pine
POCO5	Polygala	cowellii	Violet tree
POCU	Polygonum	cuspidatum	Japanese knotweed
POCU14	Polyscias	cumingiana	Malaysian aralia
PODE	Populus	deltoides	Eastern cottonwood
PODI5	Pouteria	dictyoneura	Cocuyo
PODO5	Pouteria	dominigensis	Jacana
POEL	Podocarpus	elatus	Plum pine
POEL1	Polyscias	elegans	Celerywood
POFL20	Poitea	florida	Wattapama
POFR	Populus	fremontii	Fremont cottonwood
POFR2	Dasiphora	floribunda	Shrubby cinquefoil
POFR3	Potentilla	fruiticosa	Shrubby cinquifoil
POFR5	Polyscias	fruticosa	Ming aralia
POGR	Populus	grandidentata	Bigtooth aspen
POGR2	Podocarpus	gracilior	Fern pine
POGU	Polyscias	guilfoylei	Geranium aralia
POHE	Populus	heterophylla	Swamp cottonwood
POHE2	Podocarpus	henkelii	Long-leafed yellowwood
POHE5	Populus	x heimburgeri	Heiburger's poplar
POHE7	Polygala	heterorhyncha	Beaked spiny polygala
POHI8	Populus	x hinckleyana	Hinckley poplar
POHO4	Pouteria	hotteana	Redmammee
POIN23	Populus	x inopina	Populus x inopina
POJA2	Populus	x jackii	Balm-of-gilead
POLO21	Polyalthia	longifolia	Cemetery tree
POMA	Podocarpus	macrophyllus	Yew podocarpus
POMA2	Populus	maximowiczii	Japanese poplar
POMU6	Pouteria	multiflora	Bullytree
PONA	Podocarpus	nagi	Broad leaf podocarpus
PONE21	Podocarpus	neriifoluis	Brown pine
PONI	Populus	nigra	Black poplar
PONIIT	Populus	nigra 'Italica'	Lombardy poplar
POOC4	Pouzolzia	occidentalis	Coamo river pouzolzsbush
POPA11	Populus	x parryi	Parry's cottonwood

POPA34	Poitea	paucifolia	Retama
POPE13	Polygala	penaea	Crevajosa
POPI	Derris	indica	Poonga oil tree
POPU19	Poitea	punicea	Caracol illo
PORO12	Pontederia	rotundifolia	Tropical pickerelweed
PORO4	Populus	x rouleauiana	Populus x rouleauiana
POSA	Populus	deltoides s monilifera	Plains cottonwood
POSA11	Pouteria	sandwicensis	'ala'a
POSA13	Pouteria	sapota	Naseberry
POSA2	Podocarpus	saligna	MaÑio de hojas largas
POSC10	Polyscias	scutellaria	Shield aralia
POSI	Populus	simonii	Chinese popular
POSIFA	Populus	simonii fastigiata	Simon poplar
POSM2	Populus	x smithii	Smith's poplar
POTO	Populus	tomentosa	Chinese white poplar
POTO1	Podocarpus	totara	Totara
POTR	Populus	trichocarpa	Black cottonwood
POTR1	Populus	tremuloides	Quaking aspen
POTR10	Populus	tremula	European aspen
POTR2	Populus	balsamifera trichocarp	Brayshaw black cottonwood
POTR4	Poncirus	trifoliata	Hardy orange
POUS2	Podocarpus	usambarensis	East african yellow wood
POYU	Populus	yunnanensis	Yunnan poplar
PR	Prunus		plum spp
PR1	Premna		premna spp
PR2	Prestoea		prestoea spp
PR3	Prumnopitys		prumnopitys spp
PR4	Pritchardia		pritchardia spp
PR5	Prockia		prockia spp
PR6	Prosopis		mesquite spp
PR7	Proustia		proustia spp
PRAC	Prestoea	acuminata	Sierran palm
PRAF	Pritchardia	affinis	Hawai'i pritchardia
PRAL	Prunus	alleghaniensis	Allegheny plum
PRAL11	Prosopis	alpataco	Prosopis alpataco
PRAL2	Prosopis	alba	Argentine mesquite
PRAL7	Prunus	alabamensis	Alabama cherry
PRAM	Prunus	americana	American plum
PRAM2	Prunus	amygdalus	Almendro
PRAN	Prunus	angustifolia	Chickasaw plum
PRAN2	Prunus	andersonii	Desert peach
PRAR	Prunus	armeniaca	Apricot
PRAR2	Pritchardia	arecina	Maui pritchardia
PRAR6	Prosopis	argentina	Prosopis argentina
PRAV	Prunus	avium	Sweet cherry

PRBE	Pritchardia	beccariana	Kilauea pritchardia
PRBL	Prunus	blieriana	Blierana plum
PRBU2	Prosopis	burkartii	Prosopis burkartii
PRCA	Prunus	caroliniana	Carolina laurelcherry
PRCA10	Prosopis	calingastana	Cusqui
PRCA11	Prosopis	campestris	Prosopis campestris
PRCA12	Prosopis	castellanosii	Prosopis castellanosii
PRCA2	Prunus	campanulata	Taiwan cherry
PRCA9	Prosopis	caldenia	the Caldén
PRCE	Prunus	cerasifera	Cherry plum
PRCE2	Prunus	cerasifera var. nigra	Ciruelo rojo
PRCEKV	Prunus	cerasifera Krauter Vesuvius	Krauter vesuvius plum
PRCETH	Prunus	cerasifera 'Thundercloud'	Thundercloud purple plum
PRCH	Prosopis	chilensis	Algarrobo
PRCI	Prunus	x cistena	Purpleleaf sand cherry
PRCR2	Prockia	crucis	Guasimilla
PRDE4	Prosopis	denudans	Prosopis denudans
PRDO	Prunus	domestica	Common plum
PRDU	Prunus	dulcis	Sweet almond
PREL5	Prosopis	elata	Prosopis elata
PREM	Prunus	emarginata	Bitter cherry
PRFA	Prunus	fasciculata	Desert almond
PRFA2	Prosopis	farcta	Syrian mesquite
PRFE2	Prosopis	ferox	Prosopis ferox
PRFI4	Prosopis	fiebrigii	Prosopis fiebrigii
PRFO	Pritchardia	forbesiana	Mt. eke pritchardia
PRFR	Prunus	fremontii	Desert apricot
PRFR2	Prunus	fruticosa	European dwarf cherry
PRGE	Prunus	geniculata	Scrub plum
PRGL	Prunus	glandulosa	Dwarf flowering almond
PRGL2	Prosopis	glandulosa	Honey mesquite
PRGR	Prunus	gracilis	Oklahoma plum
PRHA	Prunus	havardii	Havard's plum
PRHA2	Pritchardia	hardyi	Makaleha pritchardia
PRHA4	Prosopis	hassleri	Prosopis hassleri
PRHAJO	Prunus	'Hally Jolivette'	Hally jolivette cherry
PRHI	Pritchardia	hillebrandii	Lo'ulu lelo
PRHO	Prunus	hortulana	Hortulan plum
PRHU3	Prosopis	humilis	Prosopis humilis
PRIL	Prunus	ilicifolia	Hollyleaf cherry
PRIN	Prunus	x incam 'okame'	Okame cherry
PRJA	Prunus	japonica	Japanese plum
PRJU3	Prosopis	juliflora	Mesquite
PRKA	Pritchardia	kaalae	Waianae range pritchardia

PRKU2	Prosopis	kuntzei	Prosopis kuntzei
PRLA	Prunus	laurocerasus	Common cherry laurel
PRLA3	Pritchardia	lanaiensis	Lanai pritchardia
PRLA4	Pritchardia	lanigera	Lo'ulu
PRLA6	Prosopis	laevigata	Smooth mesquite
PRLI2	Pritchardia	limahuliensis	Limahuli pritchardia
PRLO2	Pritchardia	lowreyana	Molokai pritchardia
PRLU	Prunus	lusitanica	Portugal laurel
PRLY	Prunus	ilicifolia ssp. lyonii	Catalina cherry
PRMA	Prunus	maackii	Amur chokecherry
PRMA2	Prunus	maritima	Beach plum
PRMA5	Pritchardia	martii	Koolau range pritchardia
PRME	Prunus	mexicana	Mexican plum
PRMI2	Prunus	minutiflora	Texas almond
PRMI3	Pritchardia	minor	Alakai swamp pritchardia
PRMU	Prunus	munsoniana	Wildgoose plum
PRMU2	Prunus	mume	Japanese apricot
PRMU3	Pritchardia	munroi	Kamalo pritchardia
PRMU4	Prunus	murrayana	Murray's plum
PRMY	Prunus	myrtifolia	West indies cherry
PRNI	Prunus	nigra	Canada plum
PROC	Prunus	occidentalis	Western cherry laurel
PROD	Premna	odorata	Fragrant premna
PROR	Prunus	x orthosepala	Prunus
PRPA	Prunus	padus	European bird cherry
PRPA10	Prosopis	palmeri	Prosopis palmeri
PRPA11	Pritchardia	pacifica	Fiji fan palm
PRPA2	Prosopis	pallida	Kiawe
PRPA8	Prunus	x palmeri	Palmer's prunus
PRPE1	Prunus	pensylvanica	Pin cherry
PRPE2	Prunus	persica	Peach
PRPE7	Pritchardia	perlmanii	Wai'oli pritchardia
PRPEN2	Prunus	persica v nucipersica	Nectarine
PRPI	Prunus	pissardii	Purpleleaf plum
PRPL3	Prunus	pleuradenia	antilles cherry
PRPU1	Prunus	pumila	Sand cherry
PRPU2	Prosopis	pubescens	Screwbean mesquite
PRRE	Pritchardia	remota	Nihoa pritchardia
PRRI	Prunus	rivularis	Creek plum
PRRO4	Prosopis	rojasiana	Prosopis rojasiana
PRRU4	Prosopis	ruizlealii	Prosopis ruizlealii
PRRU5	Prosopis	ruscifolia	Prosopis ruscifolia
PRSA	Prunus	sargentii	Sargent cherry
PRSC	Pritchardia	schattaueri	Lands of papa pritchardia
PRSE1	Prunus	serotina	Black cherry
PRSE2	Prunus	serrulata	Kwanzan cherry

PRSE5	Prosopis	sericantha	Prosopis sericantha
PRSEAM	Prunus	serrulata 'Amanogawa'	Amanogawa cherry
PRSESH	Prunus	serrulata 'Shirofugen'	Shirofugen cherry
PRSESO	Prunus	serrulata 'Shirotae'	Shirotae cherry
PRSH	Prunus	x shirotae	Mount fuji cherry
PRSL	Prunus	x slavinii	Slavin's prunus
PRSP2	Prunus	spinosa	Blackthorn
PRSP3	Prunus	spachiana f. ascendens	Usuzumi cherry
PRST3	Prosopis	strombulifera	Argentine screwbean
PRSU	Prunus	subhirtella	Higan cherry
PRSU2	Prunus	subcordata	Klamath plum
PRTA	Prunus	takesimensis	Korean cherry
PRTE	Prunus	texana	Peachbush
PRTO	Prunus	tomentosa	Manchu cherry
PRTO3	Prosopis	torquata	Prosopis torquata
PRTR	Prunus	triloba	Flowering plum
PRUM	Prunus	umbellata	Flatwods plum
PRVA	Proustia	vanillosma	Sweet yellowcrown
PRVE	Prosopis	velutina	Velvet mesquite
PRVI	Prunus	virginiana	Common chokecherry
PRVI2	Pritchardia	viscosa	Stickybud pritchardia
PRVISH	Prunus	virginiana 'Shubert'	Shubert chokecherry
PRVU	Prunus	vulgaris	Prunus vulgaris
PRWA	Pritchardia	waialealeana	Poleline pritchardia
PRX	Prunus	x blireana	Blireana plum
PRYE	Prunus	yedoensis	Yoshino flowering cherry
PS	Psoralea		psoralea spp
PS1	Pseudobombax		pseudobombax spp
PS10	Pseudophoenix		pseudophoenix spp
PS12	Pseudotsuga		douglas-fir spp
PS13	Psidium		guava spp
PS15	Psoralidium		scurfpea spp
PS16	Psorothamnus		dalea spp
PS17	Psychotria		wild coffee spp
PS3	Pseudanamomis		pseudanamomis spp
PS4	Pseuderanthemum		pseuderanthemum spp
PS6	Pseudocydonia		chinese-quince spp
PS8	Pseudolarix		golden larch spp
PS9	Pseudolmedia		pseudolmedia spp
PSAM	Pseudolarix	amabilis	Golden larch
PSAM2	Psidium	amplexicaule	Mountain guava
PSAR4	Psorothamnus	arborescens	Mojave indigobush
PSBE	Psychotria	berteriana	Cachimbo-cumun
PSBR2	Psychotria	brachiata	Palo de cachimbo

PSBR3	Psychotria	brownei	Browne's wild coffee
PSCA	Psidium	cattleianum	Strawberry guava
PSCA16	Pseuderanthemum	carruthersii	Carruthers' falseface
PSCA5	Psidium	calyptranthoides	Luquillo mountain guava
PSDE	Psychotria	deflexa	Nodding wild coffee
PSDO2	Psychotria	domingensis	Cheakyberry
PSEL5	Pseudobombax	ellipticum	Shaving brush tree
PSFA	Psychotria	fauriei	Koolau range wild coffee
PSFR	Psorothamnus	fremontii	Fremont's dalea
PSGR	Psychotria	grandiflora	Largeflower wild coffee
PSGR2	Psychotria	grandis	Cachimbo grande
PSGR3	Psychotria	greenwelliae	Kauai wild coffee
PSGU	Psidium	guajava	Common guava
PSHA2	Psychotria	hathewayi	Waianae range wild coffee
PSHA3	Psychotria	hawaiiensis	Kopiko 'ula
PSHE2	Psychotria	hexandra	Woodland wild coffee
PSHO	Psychotria	hobdyi	Milolii kopiwai
PSHO2	Psychotria	hoffmannseggiana	Hoffmannsegg wild coffee
PSJU2	Psoralidium	junceum	Rush lemonweed
PSKA	Psychotria	kaduana	Kopiko kea
PSLI2	Psychotria	ligustrifolia	Bahama wild coffee
PSLO2	Psidium	longipes	Mangroveberry
PSMA	Pseudotsuga	macrocarpa	Bigcone douglas fir
PSMA4	Psychotria	maleolens	Cachimbo de gato
PSMA5	Psychotria	maricaensis	Cachimbo de maricao
PSMA6	Psychotria	mariniana	Forest wild coffee
PSMA7	Psychotria	mauiensis	'opiko
PSME	Pseudotsuga	menziesii	Douglas fir
PSMI	Psychotria	microdon	Thicket wild coffee
PSNE	Psychotria	nervosa	Seminole balsamo
PSNU2	Psychotria	nutans	Floating balsamo
PSPI	Psoralea	pinnata	African Scurfpea
PSPO	Psorothamnus	polydenius	Nevada dalea
PSPU	Psychotria	pubescens	Hairy wild coffee
PSPU2	Psychotria	punctata	Dotted wild coffee
PSRE2	Psychotria	revoluta	Curl-leaf wild coffee
PSSA	Pseudophoenix	sargentii	Buccaneer palm
PSSC5	Psorothamnus	schottii	Schott's dalea
PSSI2	Psidium	sintenisii	Sintenis' guava
PSSI4	Pseudocydonia	sinensis	Chinese-quince
PSSP2	Pseudolmedia	spuria	False breadnut
PSTE4	Psychotria	tenuifolia	Shortleaf wild coffee
PSTH	Psorothamnus	thompsoniae	Thompson's dalea
PSUM	Pseudanamomis	umbellulifera	Ciruelas
PSWA2	Psychotria	wawrae	Leatherleaf wild coffee
PT1	Ptelea		hoptree spp
PT2	Pteralyxia		pteralyxia spp

PT3	Pterocarpus		pterocarpus spp
PT4	Pterocarya		pterocarya spp
PT7	Ptychosperma		ptychosperma spp
PTCR3	Ptelea	crenulata	California hoptree
PTEL	Ptychosperma	elegans	Alexander palm
PTFR	Pterocarya	fraxinifolia	Caucasian Wingnut
PTIN	Pterocarpus	indicus	India paduak
PTKA	Pteralyxia	kauaiensis	Kauai pteralyxia
PTMA	Pterocarpus	macrocarpus	Burma paduk
PTMA8	Ptychosperma	macarthurii	Macarthur palm
PTOF	Pterocarpus	officinalis	Dragonsblood tree
PTST	Pterocarya	stenoptera	Chinese wingnut
PTTR	Ptelea	trifoliata	Common hoptree
PU	Punica		pomegranate spp
PU2	Purshia		cliff rose spp
PU3	Pueraria		kudzu spp
PUER2	Purshia	ericifolia	Heath cliffrose
PUGL2	Purshia	glandulosa	Desert bitterbrush
PUGR	Punica	granatum	Pomegranate
PULO	Pueraria	lobata	Kudzu
PUPI	Purshia	pinkavae	Pinkava's cliffrose
PUST	Purshia	stansburiana	Stansbury cliffrose
PUSU2	Purshia	x subintegra	Arizona cliffrose
PUTR2	Purshia	tridentata	Antelope bitterbrush
PY	Pyrus		pear spp
PY3	Pyrularia		pyrularia spp
PYAN	Malus	angustifolia	Southern crabapple
PYAN2	Pyracantha	angustifolia	Narrowleaf firethorn
PYBA	Malus	baccata	Siberian crabapple
PYCA	Pyrus	calleryana	Callery pear
PYCAAR	Pyrus	calleryana 'Aristocrat'	Callery pear 'Aristocrat'
PYCABR	Pyrus	calleryana 'Bradford	Callery pear 'Bradford'
PYCACA	Pyrus	calleryana 'Capital'	Callery pear 'Capital'
PYCACH	Pyrus	calleryana 'Chanticleer'	Callery pear Chanticleer
PYCACL	Pyrus	calleryana 'Cleveland'	Cleveland pear
PYCARS	Pyrus	calleryana 'Red Spire'	Callery pear 'Redspire'
PYCATR	Pyrus	calleryana 'Trinity'	Callery pear 'Trinity'
PYCAWH	Pyrus	calleryana 'Whitehouse'	Callery pear Whitehouse
PYCO	Pyrus	communis	Common pear
PYCO2	Pyracantha	coccinea	Fire thorn
PYCO3	Malus	coronaria	Sweet crabapple
PYCR7	Pyracantha	crenulata	Nepalese firethorn

PYFA	Pyrus	fauriei	Korean sun pear
PYFO	Pyracantha	fortuneana	Chinese firethorn
PYFU	Malus	fusca	Oregon crabapple
PYIO	Malus	ioensis	Prairie crabapple
PYKA	Pyrus	kawakamii	Evergreen pear
PYKO	Pyracantha	koidzumii	Formosa firethorn
PYPA	Pyrus	pashia	Wild pear
PYPU	Pyrularia	pubera	Buffalo nut
PYPY2	Pyrus	pyrifolia	Pyrus pyrifolia
PYSA	Pyrus	salicifolia	Willow-leaved Pear
PYSP	Pyracantha		firethorn spp
PYUS	Pyrus	ussuriensis	Chinese pear
QU	Quercus		oak spp
QU1	Quararibea		quararibea spp
QU2	Quassia		quassia spp
QU3	Quillaja		quillaja spp
QUAC	Quercus	acutissima	Sawtooth oak
QUAC2	Quercus	acerifolia	Mapleleaf oak
QUAC3	Quercus	x acutidens	Quercus x acutidens
QUAG	Quercus/live	agrifolia	Coastal live oak
QUAJ	Quercus	ajoensis	Ajo mountain scrub oak
QUAL	Quercus	alba	White oak
QUAL2	Quercus	x alvordiana	Alvord oak
QUAL3	Quercus	aliena	Oriental white oak
QUAM	Quassia	amara	Quassia wood
QUAR	Quercus/live	arizonica	Arizona white oak
QUAR2	Quercus	arkansana	Arkansas oak
QUAS3	Quercus	x ashei	Ash's oak
QUAT	Quercus	x atlantica	Atlantic oak
QUAU	Quercus	austrina	Bluff oak
QUBE	Quercus	berberidifolia	Scrub oak
QUBE2	Quercus	x beaumontiana	Beaumont's oak
QUBE3	Quercus	x bebbiana	Bebb's oak
QUBE4	Quercus	x bernardiensis	Bernard's oak
QUBE5	Quercus	x beadlei	Beadle's oak
QUBE8	Quercus	x beckyae	Becky's oak
QUBE9	Quercus	x benderi	Bender oak
QUBI	Quercus	bicolor	Swamp white oak
QUBI2	Quercus	x bimundorum	Quercus x bimundorum
QUBL	Quercus	x blufftonensis	Bluffton's oak
QUBO2	Quercus	boyntonii	Boynton sand post oak
QUBR	Quercus	x brittonii	Britton's oak
QUBU	Quercus	x bushii	Bush's oak
QUBU2	Quercus	buckleyi	Buckley oak
QUBU3	Quercus	x burnetensis	Burnet's oak
QUBY	Quercus	x byarsii	Byars' oak
QUCA	Quercus	x caduca	Quercus x caduca

QUCA2	Quercus	x capesii	Cape oak
QUCA3	Quercus	x caesariensis	Caesar oak
QUCA7	Quercus	carmenensis	Mexican oak
QUCA8	Quercus	canariensis	Algerian Oak
QUCA9	Quercus	castaneifolia	Chestnut-leaved oak
QUCE	Quercus	cerris	European turkey oak
QUCH	Quercus/live	chrysolepis	Canyon live oak
QUCH2	Quercus	chapmanii	Chapman oak
QUCH4	Quercus	chihuahuensis	Chihuahuan oak
QUCI	Quercus	incana	Bluejack oak
QUCO	Quercus	coccinea	Scarlet oak
QUCO3	Quercus	x comptoniae	Compton's oak
QUCO4	Quercus	x columnaris	Column oak
QUCO5	Quercus	x cocksii	Cock's oak
QUCO7	Quercus	cornelius-mulleri	Muller oak
QUCR	Quercus	x cravenensis	Quercus x cravenensis
QUDE	Quercus	x deamii	Deam's oak
QUDE1	Quercus	dentata	Daimio oak
QUDE2	Quercus	bemareei	Quercus bemareei
QUDE3	Quercus	depressipes	Davis mountain oak
QUDI	Quercus	x discreta	Discreet oak
QUDI2	Quercus	x diversiloba	Manylobed oak
QUDO	Quercus	douglasii	Blue oak
QUDU	Quercus	dumosa	Coastal sage scrub oak
QUDU2	Quercus	dunnii	Dunn oak
QUDU4	Quercus	durata	Leather oak
QUEG	Quercus	x egglestonii	Eggleston's oak
QUEL	Quercus	ellipsoidalis	Northern pin oak
QUEM	Quercus/live	emoryi	Emory oak
QUEN	Quercus	engelmannii	Engelmann oak
QUEP	Quercus	x eplingii	Epling's oak
QUEX	Quercus	x exacta	Quercus x exacta
QUFA	Quercus	falcata	Southern red oak
QUFA2	Quercus	x faxonii	Faxon's oak
QUFE	Quercus	x fernaldii	Fernald's oak
QUFE2	Quercus	x fernowii	Fernow's oak
QUFI	Quercus	x filialis	Quercus x filialis
QUFO	Quercus	x fontana	Fontana oak
QUFU	Quercus/live	fusiformis	Plateau oak
QUGA	Quercus	gambelii	Gambel oak
QUGA2	Quercus	garryana	Oregon white oak
QUGA3	Quercus	x garlandensis	Garland oak
QUGA4	Quercus	x ganderi	Gander oak
QUGE	Quercus	georgiana	Georgia oak
QUGE2	Quercus/live	geminata	Sand live oak
QUGI	Quercus	x giffordii	Gifford's oak
QUGR	Quercus	grisea	Arizona grey oak

QUGR2	Quercus	gravesii	Chisos red oak
QUGR3	Quercus	graciliformis	Chisos oak
QUGR4	Quercus	x grandidentata	Largeleaf oak
QUGU	Quercus	x guadalupensis	Guadalupe oak
QUHA	Quercus	x harbisonii	Harbison's oak
QUHA2	Quercus	x hastingsii	Hasting's oak
QUHA3	Quercus	havardii	Havard oak
QUHA4	Quercus	x hawkinsiae	Hawkins' oak
QUHE	Quercus	hemisphaerica	Darlington oak
QUHE2	Quercus	x heterophylla	Oddleaf oak
QUHI	Quercus	hinckleyi	Hinckley oak
QUHO	Quercus	x howellii	Howell's oak
QUHU	Quercus	x humidicola	Quercus x humidicola
QUHY	Quercus/live	hypoleucoides	Silver leaf oak
QUIL	Quercus	ilicifolia	Bear oak
QUIL2	Quercus/live	ilex	Holly oak
QUIM	Quercus	imbricaria	Shingle oak
QUIN2	Quercus	x inconstans	Quercus x inconstans
QUIN3	Quercus	intricata	Dwarf oak
QUIN4	Quercus	x introgressa	Quercus x introgressa
QUIN5	Quercus	x incomita	Quercus x incomita
QUIN7	Quercus	inopina	Sandhill oak
QUJA	Quercus	x jackiana	Jack's oak
QUJO	Quercus	x jolonensis	Jolon's oak
QUJO3	Quercus	john-tuckeri	Tucker oak
QUJO4	Quercus	x joorii	Jorr's oak
QUKE	Quercus	kelloggii	California black oak
QULA	Quercus	laceyi	Lacey oak
QULA1	Quercus	laevis	Turkey oak
QULA2	Quercus	laurifolia	Laurel oak
QULE	Quercus	x leana	Quercus x leana
QULO	Quercus	lobata	California white oak
QULU	Quercus	x ludoviciana	Quercus x ludoviciana
QULY	Quercus	lyrata	Overcup oak
QUMA	Quercus	x macnabiana	Macnab's oak
QUMA1	Quercus	macrocarpa	Bur oak
QUMA2	Quercus	marilandica	Blackjack oak
QUMA3	Quercus	margaretta	Sand post oak
QUMA4	Quercus	x macdonaldii	Macdonald oak
QUMA6	Quercus	margarettiae	Runner oak
QUME	Quercus	x mellichampii	Mellichamp's oak
QUME2	Quercus	x megaleia	Quercus x megaleia
QUMI	Quercus	michauxii	Swamp chestnut oak
QUMI2	Quercus	minima	Dwarf live oak
QUMO	Quercus	mohriana	Mohr oak
QUMO1	Quercus	mongolica	Mongolian oak
QUMO2	Quercus	x moreha	Oracle oak

QUMO3	Quercus	x moultonensis	Moulton's oak
QUMU	Quercus	muehlenbergii	Chinkapin oak
QUMU2	Quercus	x mutabilis	Quercus x mutabilis
QUMU3	Quercus	x munzii	Munz's oak
QUMY	Quercus	myrtifolia	Myrtle oak
QUNE	Quercus	x neopalmeri	Quercus x neopalmeri
QUNE2	Quercus	x neotharpii	Quercus x neotharpii
QUNE3	Quercus	x nessiana	Ness's oak
QUNI	Quercus	nigra	Water oak
QUNU	Quercus	texana	Texas red oak
QUOB	Quercus/live	oblongifolia	Mexican blue oak
QUOG	Quercus	oglethorpensis	Oglethorpe oak
QUOR	Quercus	x organensis	Organ oak
QUOV	Quercus	x oviedoensis	Quercus x oviedoensis
QUPA	Quercus	palustris	Pin oak
QUPA2	Quercus	pagoda	Cherrybark oak
QUPA3	Quercus	x palmeriana	Palmer's oak
QUPA4	Quercus	x pauciloba	Wavyleaf oak
QUPA5	Quercus	x palaeolithicola	Quercus x palaeolithicola
QUPA6	Quercus	pacifica	Channel island scrub oak
QUPA8	Quercus	parvula	Coast oak
QUPAFA	Quercus	palustris fastigiata	Fastigiate pin oak
QUPE	Quercus	petraea	Durmast oak
QUPH	Quercus	phellos	Willow oak
QUPO	Quercus	x podophylla	Quercus x podophylla
QUPO2	Quercus/live	polymorpha	Netleaf white oak
QUPR	Quercus	prinus	Chestnut oak
QUPR2	Quercus	prinoides	Dwarf chinkapin oak
QUPS	Quercus	x pseudomargarettiae	False sand post oak
QUPU	Quercus/live	pungens	Pungent oak
QUPU1	Quercus	pubescens	Downy Oak
QUPU80	Quercus	pumila	Running oak
QUPY	Quercus	pyrenaica	Pyrenean Oak
QURE	Quercus	x rehderi	Rehder's oak
QURI	Quercus	x riparia	Riparian oak
QURO	Quercus	robur	English oak
QURO2	Quercus	x robbinsii	Robinn's oak
QURO3	Quercus	robusta	Robust oak
QURO4	Quercus	x rolfsii	Rolf's oak
QUROFA	Quercus	robur 'Fastigiata'	Columnar english oak
QURU	Quercus	rubra	Northern red oak
QURU2	Quercus	x rudkinii	Rudkin's oak
QURU3	Quercus	x runcinata	Quercus x runcinata
QURU4	Quercus	rugosa	Netleaf oak
QUSA	Quercus	x saulii	Saul's oak

QUSA2	Quillaja	saponaria	Quillay
QUSA3	Quercus	x sargentii	Sargent's oak
QUSA4	Quercus	sadleriana	Deer oak
QUSC	Quercus	x schochiana	Quercus x schochiana
QUSC2	Quercus	x schuettei	Quercus x schuettei
QUSE	Quercus	glandulifera	Konara oak
QUSH	Quercus	shumardii	Shumard oak
QUSI	Quercus	sinuata	Bastard oak
QUSI2	Quercus	similis	Bottomland post oak
QUSM	Quercus	x smallii	Small's oak
QUST	Quercus	stellata	Post oak
QUST2	Quercus	x stelloides	Quercus x stelloides
QUST3	Quercus	x sterilis	Quercus x sterilis
QUST4	Quercus	x sterretii	Sterret's oak
QUSU	Quercus/live	suber	Cork oak
QUSU2	Quercus	x subintegra	Quercus x subintegra
QUSU3	Quercus	x substellata	Quercus x substellata
QUSU4	Quercus	x subconvexa	Quercus x subconvexa
QUSU6	Quercus	x subfalcata	Quercus x subfalcata
QUTA	Quercus	tardifolia	Lateleaf oak
QUTH	Quercus	x tharpii	Tharp's oak
QUTO	Quercus/live	tomentella	Island live oak
QUTO2	Quercus	toumeyi	Toumey oak
QUTO3	Quercus	x townei	Towne's oak
QUTO4	Quercus	x tottenii	Totten's oak
QUTR	Quercus	x tridentata	Tridentata oak
QUTU	Quararibea	turbinata	Swizzlestick tree
QUTU2	Quercus/live	turbinella	Sonoran scrub oak
QUVA	Quercus/live	vacciniifolia	Huckleberry oak
QUVA2	Quercus	x vaga	Quercus x vaga
QUVA5	Quercus	vaseyana	Sandpaper oak
QUVE	Quercus	velutina	Black oak
QUVE2	Quercus	x venulosa	Quercus x venulosa
QUVI	Quercus/live	virginiana	Live oak
QUVI2	Quercus	viminea	Sonoran oak
QUWA	Quercus	x walteriana	Walter's oak
QUWA2	Quercus	x wagneri	Wagner's oak
QUWI	Quercus/live	wislizeni	Interior live oak
QUWI2	Quercus	x willdenowiana	Willdenow's oak
RA	Ravenea		ravenea spp
RA1	Randia		indigoberry spp
RA2	Raphiolepis		raphiolepis spp
RA3	Rauvolfia		devil's-pepper spp
RA4	Ravenala		traveler's tree spp
RA5	Ravenia		ravenia spp
RA6	Rapanea		rapanea spp
RA7	Radermachera		radermachera spp

RAAC	Randia	aculeata	White indigoberry
RAFO2	Randia	formosa	Jasmin de rosa
RAGU	Myrsine	floridana	Guianese colicwood
RAHO	Rapanea	howittiana	Turnipwood
RAIN	Raphiolepis	indica	India hawthorn
RAMA	Ravenala	madagascariensis	Traveler's tree
RANI	Rauvolfia	nitida	Bitter-ash
RAPA4	Randia	parvifolia	Smallflower indigoberry
RAPO2	Randia	portoricensis	Puerto rico indigoberry
RARH2	Randia	rhagocarpa	Crucillo
RARI	Ravenea	rivularis	Majesty palm
RASA3	Rauvolfia	sandwicensis	Devil's-pepper
RASA5	Rauvolfia	samarensis	Rauvolfia
RASI	Radermachera	sinica	Serpent Tree
RATE8	Rauvolfia	tetraphylla	Be still tree
RAUM	Rapanea	umbrellata	Capororoca
RAUR	Ravenia	urbanii	Tortugo prieto
RAVI	Rauvolfia	viridis	Milkbush
RAVO	Rauvolfia	vomitoria	Poison devil's-pepper
RE1	Remya		remya spp
RE2	Reynoldsia		reynoldsia spp
RE3	Reynosia		darlingplum spp
REGU	Reynosia	guama	Guama
REKA	Remya	kauaiensis	Kauai remya
REKR	Reynosia	krugii	Krug's darlingplum
REMA2	Remya	mauiensis	Maui remya
REMO	Remya	montgomeryi	Kalalau valley remya
RESA	Reynoldsia	sandwicensis	'ohe makai
RESE	Reynosia	septentrionalis	Darling plum
REUN	Reynosia	uncinata	Sloe
RH	Rhaphiolepis		rhaphiolepis spp
RH1	Rhapidophyllum		rhapidophyllum spp
RH2	Rhapis		rhapis spp
RH3	Rhizophora		true mangrove spp
RH4	Rhodomyrtus		rhodomyrtus spp
RH5	Rhodotypos		rhodotypos spp
RH6	Rhopalostylis		rhopalostylis spp
RH7	Rhytidophyllum		tibey-amarillo spp
RHAL	Rhamnus	alnifolia	Alderleaf buckthorn
RHAL2	Rhododendron	albiflorum	Cascade azalea
RHAL5	Rhododendron	alabamense	Alabama azalea
RHAR3	Rhododendron	arborescens	Smooth azalea
RHAR4	Rhus	aromatica	Fragrant sumac
RHAR6	Rhamnus	arguta	Sharp tooth buckthorn
RHAS	Rhus	x ashei	Ash'c sumac
RHAT	Rhododendron	atlanticum	Dwarf azalea
RHAU	Rhododendron	austrinum	Orange azalea

RHAU2	Rhytidophyllum	auriculatum	Tibey-amarillo
RHAZ	Rhododendron	azalea	Azalea
RHBA4	Rhododendron	x bakeri	Bajer's rhododendron
RHBA7	Rhopalostylis	baueri	Norfolk island palm
RHCA	Rhamnus	cathartica	European buckthorn
RHCA14	Rhododendron	carolinianum	Carolina azalea
RHCA2	Frangula	caroliniana	Carolina buckthorn
RHCA4	Rhododendron	calendulaceum	Flame azalea
RHCA5	Rhododendron	camtschaticum	Kamchatka rhododendron
RHCA6	Rhododendron	canadense	Rhodora
RHCA7	Rhododendron	canescens	Mountain azalea
RHCA8	Rhododendron	catawbiense	Catawba rosebay
RHCH	Rhus	chinensis	Chinese sumac
RHCH5	Rhododendron	chapmanii	Chapman's rhododendron
RHCO	Rhus	copallina	Shining sumac
RHCR	Rhamnus	crocea	Redberry
RHCU	Rhododendron	cumberlandense	Cumberland rhododendron
RHDA	Rhamnus	davurica	Dahurian buckthorn
RHEX	Rhapis	excelsa	Bamboo palm
RHFL	Rhododendron	flammeum	Piedmont azalea
RHFR	Frangula	alnus	Glossy buckthorn
RHGL	Rhus	glabra	Smooth sumac
RHHY	Rhapidophyllum	hystrix	Needle palm
RHIL	Rhamnus	ilicifolia	Hollyleaf redberry
RHIN	Rhus	integrifolia	Lemonade berry
RHIN21	Rhaphiolepis	indica	Indian hawthorn
RHJA2	Rhododendron	japonicum	Japanese azalea
RHJA8	Rhamnus	japonica	Japanese buckthorn
RHKE	Rhus	kearneyi	Kearney's sumac
RHLA	Rhus	lancea	African sumac
RHLA2	Rhododendron	lapponicum	Lapland rosebay
RHLA3	Rhus	lanceolata	Prairie sumac
RHLA4	Rhamnus	lanceolata	Lanceleaf buckthorn
RHMA	Rhododendron	maximum	Rosebay rhododendron
RHMA2	Rhizophora	mangle	Red mangrove
RHMA3	Rhododendron	macrophyllum	Pacific rhododendron
RHMI2	Rhododendron	minus	Piedmont rhododendron
RHMI3	Rhus	microphylla	Littleleaf sumac
RHMU	Rhizophora	mucronata	Mangrove
RHOB	Rhododendron	oblongifolium	Texas azalea
RHOC	Rhododendron	occidentale	Western azalea
RHOV	Rhus	ovata	Sugar sumac
RHPE3	Rhododendron	x pennsylvanicum	Pennsylvania rhododendron
RHPE4	Rhododendron	periclymenoides	Pink azalea
RHPI	Rhamnus	pirifolia	Island redberry
RHPR	Rhododendron	prinophyllum	Early azalea
RHPR2	Rhododendron	prunifolium	Plumleaf azalea

RHPU	Frangula	purshiana	Cascara buckthorn
RHPU2	Rhus	x pulvinata	Pulvinate sumac
RHSA2	Rhus	sandwicensis	Neneleau
RHSC3	Rhodotypos	scandens	Jetbead
RHSE3	Rhamnus	serrata	Sawleaf buckthorn
RHSM	Rhamnus	smithii	Smith's buckthorn
RHSP	Rhus		sumac spp
RHSP1	Rhododendron		rhododendron spp
RHSP2	Rhamnus		Rhamnus spp
RHTO	Rhodomyrtus	tomentosus	Rose myrtle
RHTR	Rhus	trilobata	Skunkbush sumac
RHTY	Rhus	hirta	Staghorn sumac
RHUT80	Rhamnus	utilis	Chinese buckthorn
RHVA	Rhododendron	vaseyi	Pinkshell azalea
RHVI2	Rhododendron	viscosum	Swamp azalea
RHVI3	Rhus	virens	Evergreen sumac
RHWE	Rhododendron	x welleslyanum	Wellesly rhododendron
RI	Rinorea		Rinorea spp
RI1	Ricinus		ricinus spp
RIAC	Ribes	acerifolium	Mapleleaf currant
RIAL2	Ribes	alpinum	Alpine currant
RIAM	Ribes	amarum	Bitter gooseberry
RIAM2	Ribes	americanum	American black currant
RIAU	Ribes	aureum	Golden currant
RIBI	Ribes	binominatum	Ground gooseberry
RIBR	Ribes	bracteosum	Stink currant
RICA	Ribes	californicum	Hillside gooseberry
RICA2	Ribes	canthariforme	Moreno currant
RICE	Ribes	cereum	Wax currant
RICO3	Ricinus	communis	Castorbean
RICR	Ribes	cruentum	Shinyleaf currant
RICU	Ribes	curvatum	Granite gooseberry
RICY	Ribes	cynosbati	East prickly gooseberry
RIDI	Ribes	divaricatum	Spreading gooseberry
RIEC	Ribes	echinellum	Miccosukee gooseberry
RIER	Ribes	erythrocarpum	Crater lake currant
RIGL	Ribes	glandulosum	Skunk currant
RIHI	Ribes	hirtellum	Hairystem gooseberry
RIHU	Ribes	hudsonianum	Northern black currant
RIIN	Ribes	indecorum	Whiteflower currant
RIIN2	Ribes	inerme	Whitestem gooseberry
RILA	Ribes	lacustre	Prickly currant
RILA2	Ribes	lasianthum	Alpine gooseberry
RILA3	Ribes	laxiflorum	Trailing black currant
RILE	Ribes	leptanthum	Trumpet gooseberry
RILO	Ribes	lobbii	Gummy gooseberry
RIMA	Ribes	malvaceum	Chaparral currant

RIMA2	Ribes	marshallii	Hupa gooseberry
RIME	Ribes	menziesii	Canyon gooseberry
RIME2	Ribes	mescalerium	Mescalero currant
RIMI	Ribes	missouriense	Missouri gooseberry
RIMO2	Ribes	montigenum	Gooseberry currant
RINE	Ribes	nevadense	Sierra currant
RINI	Ribes	nigrum	European black currant
RINI2	Ribes	niveum	Snow currant
RIOX	Ribes	oxyacanthoides	Canadian gooseberry
RIPI	Ribes	pinetorum	Orange gooseberry
RIQU	Ribes	quercetorum	Rock gooseberry
RIRO	Ribes	roezlii	Sierra gooseberry
RIRO2	Ribes	rotundifolium	Appalachian gooseberry
RIRU80	Ribes	rubrum	Cultivated currant
RISA	Ribes	sanguineum	Redflower currant
RISE	Ribes	sericeum	Lucia gooseberry
RISP	Ribes		currant spp
RISP2	Ribes	speciosum	Fuchsiaflower gooseberry
RITH	Ribes	thacherianum	Santa cruz gooseberry
RITR	Ribes	triste	Red currant
RITU	Ribes	tularense	Tulare gooseberry
RIUV80	Ribes	uva-crispa	European gooseberry
RIVE	Ribes	velutinum	Desert gooseberry
RIVI	Ribes	viburnifolium	Island gooseberry
RIVI2	Ribes	victoris	Victor's gooseberry
RIVI3	Ribes	viscosissimum	Sticky currant
RIWA	Ribes	watsonianum	Spring gooseberry
RIWO	Ribes	wolfii	Wolf's currant
RO	Rosa		rose spp
RO1	Rochefortia		rochefortia spp
RO2	Rolandra		yerba de plata spp
RO3	Rothmannia		rothmannia spp
RO4	Rollinia		rollinia spp
RO6	Rondeletia		cordobancillo spp
RO7	Rosmarinus		rosemary spp
RO8	Rourea		rourea spp
RO9	Roystonea		royal palm spp
ROAC	Rosa	acicularis	Prickly rose
ROAC2	Rochefortia	acanthophora	Greenheart ebony
ROAL3	Rosa	x alba	White rose of york
ROAM2	Robinia	x ambigua	Pink locust
ROAMID	Robinia	x ambigua 'Idahoenis'	Idaho locust
ROBA	Rosa	banksiae	Banksian rose
ROBL	Rosa	blanda	Smooth rose
ROBO	Roystonea	borinquena	Puerto rico royal palm
ROBO3	Rosa	x borboniana	Bourbon rose

ROBR	Rosa	bracteata	Macartney rose
ROCA2	Rosa	californica	California wildrose
ROCA3	Rosa	canina	Dog rose
ROCE	Rosa	centifolia	Cabbage rose
ROCH	Rosa	chinensis	Chinese rose
ROCI	Rosa	cinnamomea	Cinnamon rose
RODA	Rosa	x damascena	Damask rose
RODU	Rosa	x dulcissima	Rosa x dulcissima
RODU80	Rosa	dumetorum	Corymb rose
ROEG	Rosa	eglanteria	Sweetbriar rose
ROEL	Roystonea	elata	Florida royalpalm
ROFR	Rolandra	fruticosa	Yerba de plata
ROGA	Rosa	gallica	French rose
ROGL	Rothmannia	globosa	September Bells
ROHA4	Rosa	x harisonii	Harrison's yellow rose
ROHI	Robinia	hispida	Bristly locust
ROHO	Robinia	x holdtii	Holdt's locust
ROHO3	Rosa	x housei	House's rose
ROIN4	Rondeletia	inermis	Cordobancillo
ROIN5	Rosa	indica	Cyme rose
ROLO2	Robinia	x longiloba	Locust
ROMA	Robinia	x margarettiae	Margarett's locust
ROMA3	Rosa	manca	Mancos rose
ROMA81	Rosa	majalis	Double cinnamon rose
ROMI	Rosa	micrantha	Smallflower sweetbrier
ROMI80	Rosa	minutifolia	Baja rose
ROMO	Rosa	moschata	Musk rose
ROMU	Rosa	multiflora	Multiflora rose
ROMU3	Rollinia	mucosa	Wild sugar apple
ROMY	Rosa	myriadenia	Glandular rose
RONE	Robinia	neomexicana	New mexico locust
RONI	Rosa	nitida	Shining rose
RONU	Rosa	nutkana	Nootka rose
ROOB2	Rosa	obtusiuscula	Appalachian valley rose
ROOD	Rosa	odorata	Tea rose
ROOF	Rosmarinus	officinalis	Rosemary
ROPA	Rosa	palustris	Swamp rose
ROPA4	Rosa	x palustriformis	Rosa x palustriformis
ROPI2	Rosa	pisocarpa	Cluster rose
ROPI3	Rondeletia	pilosa	Cordobancillo peludo
ROPO	Rondeletia	portoricensis	Juan tomas
ROPS	Robinia	pseudoacacia	Black locust
ROPSPR	Robinia	pseudoacacia 'Purple Robe'	Black locust Purple Robe
RORE3	Rosa	x rehderiana	Polyantha rose
RORU	Rosa	rugosa	Rugosa rose
RORU2	Rosa	rubrifolia	Redleaf rose

RORU3	Rosa	x rudiuscula	Rosa x rudiuscula
ROSE2	Rosa	setigera	Climbing prarie rose
ROSE3	Rosa	sempervirens	Evergreen rose
ROSE8	Rosa	serafinii	Mediterranean rose
ROSP2	Robinia		Robinia spp
ROSP3	Rosa	spithamea	Ground rose
ROSP4	Rosa	spinosissima	Scotch rose
ROSP8	Rochefortia	spinosa	Espino
ROST	Rosa	stellata	Desert rose
ROSU4	Rourea	surinamensis	Juan caliente
ROTO	Rosa	tomentosa	Whitewoolly rose
ROVI	Robinia	viscosa	Clammy locust
ROVI2	Rosa	virginiana	Virginia rose
ROVI80	Rosa	villosa	Apple rose
ROWI	Rosa	wichuraiana	Memorial rose
ROWO	Rosa	woodsii	Woods' rose
ROXA2	Rosa	xanthina	Yellow rose
ROYA	Rosa	yainacensis	Cascade rose
RU	Rubus		blackberry spp
RUAB	Rubus	aboriginum	Garden dewberry
RUAC5	Rubus	aculiferus	Thorny dewberry
RUAD2	Rubus	adjacens	Peaty dewberry
RUAL	Rubus	allegheniensis	Allegheny blackberry
RUAL7	Rubus	aliceae	Roadside raspberry
RUAL8	Rubus	alter	Maine dewberry
RUAL9	Rubus	alumnus	Oldfield blackberry
RUAN2	Rubus	andrewsianus	Andrews' blackberry
RUAP	Rubus	apogaeus	Falling dewberry
RUAP2	Rubus	aptatus	Drybank dewberry
RUAR2	Rubus	argutus	Sawtooth blackberry
RUAR3	Rubus	arizonensis	Arizona dewberry
RUAR5	Rubus	arvensis	Field blackberry
RUAR7	Rubus	arenicola	Sanddwelling dewberry
RUAR8	Rubus	arcuans	Wand dewberry
RUAU	Rubus	audax	Tampa blackberry
RUBA	Rubus	bartonianus	Barton's raspberry
RUBA2	Rubus	baileyanus	Bailey's dewberry
RUBE	Rubus	bellobatus	Kittatinny blackberry
RUBI	Rubus	bifrons	Himalayan berry
RUBI2	Rubus	bicknellii	Nantucket blackberry
RUBI3	Rubus	biformispinus	Pasture dewberry
RUBI4	Rubus	bigelovianus	Lowland blackberry
RUBL2	Rubus	blanchardianus	Blanchard's dewberry
RUBO	Rubus	boyntonii	Boynton's dewberry
RUBU	Rubus	burnhamii	Burnham's blackberry
RUBU2	Rubus	bushii	Bush's blackberry
RUCA	Rubus	caesius	European dewberry

RUCA16	Rubus	canadensis	Smooth blackberry
RUCE2	Rubus	centralis	Illinois dewberry
RUCL	Rubus	clarus	Mt. vernon dewberry
RUCO3	Rubus	concameratus	West virginia blackberry
RUCO4	Rubus	coronarius	Cultivated raspberry
RUCO9	Rubus	conanictuensis	Conanicut blackberry
RUCU	Rubus	cuneifolius	Sand blackberry
RUCU3	Rubus	cubitans	Sprawling dewberry
RUCU4	Rubus	curtipes	Shortstalk dewberry
RUDE	Rubus	deliciosus	Delicious raspberry
RUDE4	Rubus	deamii	Deam's dewberry
RUDE6	Rubus	defectionis	Eclipse blackberry
RUDE7	Rubus	densissimus	Morgantown blackberry
RUDE8	Rubus	depavitus	Aberdeen dewberry
RUDI2	Rubus	discolor	Himalayan blackberry
RUDI3	Rubus	dissimilis	Bristly oswego blackberry
RUEL2	Rubus	elegantulus	Showy blackberry
RUEL3	Rubus	ellipticus	Yellow himalaya raspberry
RUEX2	Rubus	exsularis	Fenceline dewberry
RUEX3	Rubus	exeter	Baton rouge blackberry
RUFE	Rubus	fecundus	Dc dewberry
RUFE2	Rubus	felix	Woodland dewberry
RUFL	Rubus	flagellaris	Northern dewberry
RUFL3	Rubus	flavinanus	Windham county blackberry
RUFL4	Rubus	floricomus	Manyflower blackberry
RUFL6	Rubus	florulentus	Big blackberry
RUFR2	Rubus	fraternalis	Northeastern dewberry
RUFR3	Rubus	frondisentis	Leafy blackberry
RUFR4	Rubus	frondosus	Yankee blackberry
RUFR5	Rubus	fryei	Cacapon river blackberry
RUFR80	Rubus	fruticosus	Shrubby blackberry
RUFU4	Rubus	furtivus	Openground dewberry
RUGE	Rubus	geniculatus	False himalayan berry
RUGL	Rubus	glaucifolius	San diego raspberry
RUGL2	Rubus	glandicaulis	Glandstem blackberry
RUGN	Rubus	gnarus	Pollock's mill blackberry
RUGR5	Rubus	grimesii	Grimes' dewberry
RUGR9	Rubus	griseus	Loogootee blackberry
RUGU	Rubus	gulosus	New brunswick blackberry
RUHA	Rubus	hawaiensis	Hawai'i blackberry
RUHA3	Rubus	hancinianus	Windswpt prairie dewberry
RUHA4	Rubus	harmonicus	Kennebunkport dewberry
RUHA6	Rubus	hanesii	Hanes' blackberry
RUHE2	Rubus	heterophyllus	Ecotone blackberry
RUHI	Rubus	hispidus	Bristly dewberry
RUHI3	Rubus	hispidoides	Bog dewberry

RUHU2	Rubus	huttonii	Hutton's dewberry
RUHY2	Rubus	hypolasius	Pineland dewberry
RUIC	Rubus	ictus	Savannah dewberry
RUID	Rubus	idaeus	American red raspberry
RUIM	Rubus	immanis	Watauga river blackberry
RUIM2	Rubus	impar	Posey county blackberry
RUIN3	Rubus	insons	New england blackberry
RUIN4	Rubus	insulanus	Island blackberry
RUIN5	Rubus	invisus	Upland dewberry
RUIN6	Rubus	inclinis	Marshland blackberry
RUIN8	Rubus	inferior	Ocala blackberry
RUIN9	Rubus	iniens	Sandyfield dewberry
RUIT	Rubus	ithacanus	Ithaca blackberry
RUJA	Rubus	jacens	Spreading dewberry
RUJU2	Rubus	junceus	Herbaceous blackberry
RUKE2	Rubus	kelloggii	Kellogg's blackberry
RUKE3	Rubus	kennedyanus	Kennedy's blackberry
RULA5	Rubus	largus	Oakwoods dewberry
RULA6	Rubus	laudatus	Plains blackberry
RULA7	Rubus	lawrencei	Adirondack blackberry
RULA8	Rubus	latens	Massachusetts blackberry
RULE	Rubus	leucodermis	Whitebark raspberry
RULE3	Rubus	leviculus	Bottomland dewberry
RULI2	Rubus	linkianus	Link's blackberry
RULO4	Rubus	longii	Long's blackberry
RULU	Rubus	lucidus	Manatee dewberry
RUMA	Rubus	macrophyllus	Largeleaf blackberry
RUMA2	Rubus	macvaughii	Macvaugh's dewberry
RUMA6	Rubus	macraei	'akala
RUMA8	Rubus	maniseesensis	Mohican trail dewberry
RUME3	Rubus	meracus	Dryslope dewberry
RUMI2	Rubus	michiganensis	Michigan dewberry
RUMI3	Rubus	mirus	Marvel dewberry
RUMI4	Rubus	missouricus	Missouri dewberry
RUMO3	Rubus	mollior	Softleaf blackberry
RUMO4	Rubus	moluccanus	Eelkek
RUMO5	Rubus	montensis	Mountaintop blackberry
RUMU2	Rubus	multifer	Kinnickinnick dewberry
RUMU3	Rubus	multiformis	Variable blackberry
RUMU4	Rubus	multispinus	Devil's blackberry
RUMU5	Rubus	mundus	Oldfield dewberry
RUNA	Rubus	navus	Grand lake blackberry
RUNE	Rubus	neomexicanus	New mexico raspberry
RUNE2	Rubus	nefrens	Prickless dewberry
RUNI	Rubus	nigerrimus	Dark raspberry
RUNI4	Rubus	niveus	Snowpeaks raspberry
RUNO2	Rubus	notatus	Bristle berry

RUNO3	Rubus	novanglicus	New england dewberry
RUNO4	Rubus	noveboracus	New york blackberry
RUNO5	Rubus	novocaesarius	Tuckahoe dewberry
RUOB2	Rubus	obsessus	New york dewberry
RUOB4	Rubus	obvius	Woodborder dewberry
RUOC	Rubus	occidentalis	Black raspberry
RUOD	Rubus	odoratus	Purpleflowering raspberry
RUOK	Rubus	oklahomus	Oklahoma blackberry
RUOR4	Rubus	originalis	Cold spring blackberry
RUOR5	Rubus	ortivus	Desert island blackberry
RUOS	Rubus	ostryifolius	Highbush blackberry
RUPA	Rubus	parviflorus	Thimbleberry
RUPA10	Rubus	particeps	Kingston dewberry
RUPA11	Rubus	pascuus	Chesapeake blackberry
RUPA13	Rubus	parcifrondifer	Silver creek blackberry
RUPA14	Rubus	particularis	West virginia dewberry
RUPA25	Rubus	paludivagus	Cape cod blackberry
RUPA7	Rubus	paganus	St. lawrence dewberry
RUPA8	Rubus	x paracaulis	Blackberry
RUPA9	Rubus	parlinii	Parlin's dewberry
RUPE10	Rubus	pervarius	Westminster dewberry
RUPE20	Rubus	pernagaeus	Smithfield blackberry
RUPE3	Rubus	pensilvanicus	Pennsylvania blackberry
RUPE6	Rubus	pergratus	Upland blackberry
RUPE7	Rubus	permixtus	Thicket dewberry
RUPE8	Rubus	persistens	Persistent blackberry
RUPE9	Rubus	perspicuus	Great lakes dewberry
RUPH	Rubus	phoenicolasius	Wine raspberry
RUPH2	Rubus	philadelphicus	Philadelphia blackberry
RUPL	Rubus	plicatifolius	Plaitleaf dewberry
RUPL2	Rubus	plus	Hairyleaf dewberry
RUPL3	Rubus	plexus	Tangled dewberry
RUPO	Rubus	porteri	Pocono plateau dewberry
RUPO2	Rubus	positivus	New london dewberry
RUPR11	Rubus	prosper	Rhode island dewberry
RUPR3	Rubus	prestonensis	Terra alta blackberry
RUPR4	Rubus	probabilis	Tree blackberry
RUPR5	Rubus	probativus	Birmingham blackberry
RUPR6	Rubus	probus	Queensland raspberry
RUPR9	Rubus	provincialis	Groundberry
RUPU4	Rubus	pubifolius	Eagle rock blackberry
RUPU5	Rubus	pugnax	Pugnacious blackberry
RURA	Rubus	racemiger	Racemed dewberry
RURA2	Rubus	randolphiorum	Plymouth blackberry
RURE	Rubus	recurvans	Recurved blackberry
RURE2	Rubus	recurvicaulis	Arching dewberry
RURE3	Rubus	regionalis	Wisconsin dewberry

RURI	Rubus	riograndis	Rio grande dewberry
RURO2	Rubus	roribaccus	Lucretia dewberry
RURO3	Rubus	rosa	Rose blackberry
RURO4	Rubus	rossbergianus	Connecticut blackberry
RURO5	Rubus	rosarius	James river blackberry
RURU2	Rubus	russeus	Halifax blackberry
RURY	Rubus	rydbergianus	Rydberg's blackberry
RUSA4	Rubus	saltuensis	Tolland county blackberry
RUSC	Rubus	scambens	Springtime dewberry
RUSC2	Rubus	sceleratus	Androscoggin blackberry
RUSC3	Rubus	schoolcraftianus	Schoolcraft's dewberry
RUSE	Rubus	setosus	Setose blackberry
RUSE2	Rubus	segnis	Nova scotia dewberry
RUSE3	Rubus	semisetosus	Swamp blackberry
RUSE4	Rubus	severus	Harsh dewberry
RUSE6	Rubus	sewardianus	Seward's blackberry
RUSI2	Rubus	signatus	Sphagnum dewberry
RUSI4	Rubus	sieboldii	Palmleaf dewberry
RUSO	Rubus	sons	New orleans dewberry
RUSP	Rubus	spectabilis	Salmonberry
RUSP4	Rubus	spectatus	Sphagnum blackberry
RUST5	Rubus	steelei	Steele's dewberry
RUST7	Rubus	stipulatus	Horseshoe lake dewberry
RUSU4	Rubus	suus	Branched blackberry
RUTA2	Rubus	tardatus	Wet thicket dewberry
RUTH	Rubus	tholiformis	Domeshape dewberry
RUTH2	Rubus	thyrsoides	Great britain blackberry
RUTO2	Rubus	tomentosus	Woolly blackberry
RUTR	Rubus	trivialis	Southern dewberry
RUTR4	Rubus	trifrons	Threeleaflet dewberry
RUTR5	Rubus	triphyllus	Threeleaf blackberry
RUTR6	Rubus	trux	Lookout mtn blackberry
RUTY	Rubus	tygartensis	Taylor county blackberry
RUUC	Rubus	ucetanus	Hillsborough blackberry
RUUL	Rubus	ulmifolius	Elmleaf blackberry
RUUN	Rubus	uniformis	Thornless dewberry
RUUR	Rubus	ursinus	California blackberry
RUUV	Rubus	uvidus	Kalamazoo dewberry
RUVA	Rubus	vagus	Rambling dewberry
RUVA3	Rubus	variispinus	Vicksburg blackberry
RUVE	Rubus	vestitus	European blackberry
RUVE5	Rubus	vermontanus	Vermont blackberry
RUVE6	Rubus	velox	Fuzzy dewberry
RUVI11	Rubus	vigilis	Missouri blackberry
RUVI3	Rubus	vigoratus	Essex dewberry
RUWH	Rubus	whartoniae	Wharton's dewberry
RUWH2	Rubus	wheeleri	Wheeler's blackberry

RUWI	Rubus	wisconsinensis	Wisconsin blackberry
SA	Salix		willow spp
SA1	Sarcomelicope		sarcomelicope spp
SA10	Salmea		bejuco de miel spp
SA12	Salvia		sage spp
SA13	Samanea		raintree spp
SA14	Samyda		samyda spp
SA15	Sanchezia		sanchezia spp
SA16	Santalum		sandalwood spp
SA18	Sapindus		soapberry spp
SA19	Sapium		milktree spp
SA2	Sambucus		elderberry spp
SA20	Sarcobatus		greasewood spp
SA23	Sassafras		sassafras spp
SA26	Savia		savia spp
SA3	Sabal		palmetto spp
SA4	Sabicea		woodvine spp
SA5	Sadleria		sadleria spp
SA6	Sageretia		mock buckthorn spp
SA7	Sagraea		hogwood spp
SA9	Salazaria		bladdersage spp
SAAL	Sassafras	albidum	Sassafras
SAAL3	Salix	alaxensis	Feltleaf willow
SAAL4	Salix	alba	White willow
SAALTR	Salix	alba 'Tristis'	Golden weeping willow
SAAM	Salix	amygdaloides	Peachleaf willow
SAAR14	Salix	arizonica	Arizona willow
SAAR3	Salix	arbusculoides	Littletree willow
SAAR7	Salix	argyrocarpa	Labrador willow
SAAT	Salix	athabascensis	Athabasca willow
SAAU9	Salix	aurita	Eared willow
SABA	Salix	x sepulcralis Simonkai	Weeping willow
SABA3	Salix	barclayi	Barclay's willow
SABA4	Salix	barrattiana	Barratt's willow
SABA6	Savia	bahamensis	Bahama maidenbush
SABE	Salix	bebbiana	Bebb willow
SABE4	Salix	x bebbii	Bebb's willow
SABE5	Salix	x beschelii	Beschel's willow
SABO	Salix	bonplandiana	Bonpland willow
SABO2	Salix	boothii	Booth's willow
SABR	Salix	brachycarpa	Shortfruit willow
SABR2	Salix	breweri	Brewer's willow
SACA	Sambucus	nigra s canadensis	Common elderberry
SACA2	Salix	candida	Sageleaf willow
SACA25	Sapium	caribaeum	Gumtree

SACA3	Salix	caroliniana	Costal plain willow
SACA37	Salix	calcicola	Woolly willow
SACA4	Salix	caprea	Goat willow
SACA5	Sabal	causiarum	Puerto rico palmetto
SACA6	Salix	cascadensis	Cascade willow
SACANE	Sambucus	caerulea v mexicana	Neomexican elderberry
SACI	Salix	cinerea	Large gray willow
SACI2	Sabicea	cinerea	Largeflower woodvine
SACO	Salix	cordata	Heart leaved willow
SACO10	Salix	x conifera	Conifer willow
SACO2	Salix	commutata	Undergreen willow
SACR10	Salix	x cryptodonta	Smalltoothed willow
SACY3	Sadleria	cyatheoides	Amaumau fern
SADE2	Salix	delnortensis	Del norte willow
SADI	Salix	discolor	Pussy willow
SADI3	Salix	x dieckiana	Dieck's willow
SADO12	Sagraea	domingensis	Woodland hogwood
SADR	Sapindus	saponaria drummondii	Western soapberry
SADR2	Salix	drummondiana	Drummond's willow
SAEA	Salix	eastwoodiae	Mountain willow
SAEH	Salix	x ehrhartiana	Ehrhart's willow
SAEL	Salix	elaeagnos	Elaeagnus willow
SAEL2	Santalum	ellipticum	Coastal sandalwood
SAER	Salix	eriocephala	Diamond willow
SAET	Sabal	etonia	Scrub palmetto
SAEX	Salix	exigua	Narrowleaf willow
SAFA	Salix	farriae	Farr's willow
SAFL	Salix	floridana	Florida willow
SAFL2	Salix	fluviatilis	River willow
SAFR	Salix	fragilis	Crack willow
SAFR4	Santalum	freycinetianum	Forest sandalwood
SAGE2	Salix	geyeriana	Geyer's willow
SAGL	Salix	glauca	Grayleaf willow
SAGL3	Salix	x glatfelteri	Glatfelter's willow
SAGO	Salix	gooddingii	Goodding's willow
SAGR	Salix	gracilistyla	Black pussy willow
SAGR7	Salix	x grayi	Gray's willow
SAHA	Salix	hastata	Halberd willow
SAHA3	Santalum	haleakalae	Haleakala sandalwood
SAHE2	Salix	herbacea	Snowbed willow
SAHO	Salix	hookeriana	Hooker willow
SAHU	Salix	humboldtiana	Humboldt's willow
SAHU2	Salix	humilis	Prairie willow
SAIN3	Salix	interior	Sandbar willow
SAIR	Salix	irrorata	Dewystem willow

SAJE	Salix	jepsonii	Jepson's willow
SAKO3	Salix	koriyanagi	Kori-yanagi
SALA1	Salix	lasiolepis	Arroya willow
SALA2	Salix	lucida ssp. lasiandra	Pacific willow
SALA25	Sapium	laurifolium	Hinchahuevos
SALA3	Salix	laevigata	Red willow
SALA8	Sapium	laurocerasus	Milktree
SALE	Salvia	leucophylla	Purple sage
SALE2	Salix	lemmonii	Lemmon's willow
SALI	Salix	ligulifolia	Strapleaf willow
SALU	Salix	lucida	Shining willow
SALU2	Salix	lutea	Yellow willow
SAMA	Salix	matsudana	Corkscrew willow
SAMA1	Salix	matsundana tortuosa	Tortured willow
SAMA12	Salix	maccalliana	Mccalla's willow
SAMA2	Salix	prolixa	Macenzie willow
SAME	Salazaria	mexicana	Mexican bladdersage
SAME2	Salix	melanopsis	Dusky willow
SAME8	Sabal	mexicana	Rio grande palmetto
SAMI10	Sageretia	minutiflora	Sm-flower mock buckthorn
SAMI8	Sabal	minor	Dwarf palmetto
SAMO2	Salix	monticola	Park willow
SAMO4	Salix	monochroma	Onecolor willow
SAMU	Sapindus	mukorossi	Sapindus mukorossi
SAMY	Salix	myrtillifolia	Blueberry willow
SAMY2	Salix	myricoides	Bayberry willow
SANI	Salix	nigra	Black willow
SANI10	Salix	niphoclada	Barrenground willow
SANI4	Sambucus	nigra	European black elderberry
SAOA2	Sapindus	oahuensis	Lonomea
SAOR	Salix	orestera	Sierra willow
SAPA	Sabal	palmetto	Cabbage palmetto
SAPA7	Santalum	paniculatum	Mountain sandalwood
SAPE	Salix	pentandra	Laurel leaved willow
SAPE12	Salix	x pendulina Wenderoth	Wisconsin weeping willow
SAPE18	Salix	petrophila	Alpine willow
SAPE2	Salix	pedicellaris	Bog willow
SAPE3	Salix	pellita	Satiny willow
SAPE5	Salix	petiolaris	Meadow willow
SAPE9	Salix	x peasei	Salix x peasei
SAPL2	Salix	planifolia	Diamondleaf willow
SAPR7	Salix	x princeps-ourayi	Ouray willow
SAPS	Salix	pseudomonticola	False mountain willow
SAPS8	Salix	pseudomyrsinites	Firmleaf willow

SAPU15	Salix	pulchra	Tealeaf willow
SAPU2	Salix	purpurea	Purpleosier willow
SAPY	Salix	pyrifolia	Balsam willow
SARA2	Sambucus	racemosa	Red elderberry
SARI4	Salix	richardsonii	Richardson's willow
SARU2	Salix	x rubella	Rubella willow
SARU3	Salix	x rubens	Hybrid crack willow
SASA	Sapindus	saponaria	Wingleaf soapberry
SASA8	Santalum	salicifolium	Willowleaf sandalwood
SASC	Salix	scouleriana	Scouler willow
SASC3	Salmea	scandens	Bejuco de miel
SASC7	Sagraea	scabrosa	Sevennerve roughleaf
SASC8	Sagraea	scalpta	Threenerve roughleaf
SASE	Salix	sericea	Silky willow
SASE2	Salix	serissima	Autumn willow
SASE3	Salix	sessilifolia	Northwest sandbar willow
SASE6	Savia	sessiliflora	Amansa guapo
SASI	Sarcomelicope	simplicifolia	Big yellowwood
SASI2	Salix	sitchensis	Sitka willow
SASM2	Salix	x smithiana	Silky-leaf osier
SASO4	Salix	x solheimii	Solheim's willow
SASP5	Samyda	spinulosa	Soldier crabtree
SASP7	Sanchezia	speciosa	Shrubby whitevein
SATA	Salix	taxifolia	Yewleaf willow
SATH5	Sageretia	thea	Pauper's-tea
SATW	Salix	tweedyi	Tweedy's willow
SAUM3	Sagraea	umbrosa	White hogwood
SAUV	Salix	uva-ursi	Bearberry willow
SAVE	Salix	vestita	Rock willow
SAVE4	Sarcobatus	vermiculatus	Greasewood
SAVI	Salix	viminalis	Basket willow
SAWA	Salix	x waghornei	Waghorn's willow
SAWO	Salix	wolfii	Wolf's willow
SAWR	Sageretia	wrightii	Wright's mock buckthorn
SC	Sciadopitys		sciadopitys spp
SC1	Scaevola		naupaka spp
SC11	Schoepfia		schoepfia spp
SC12	Schradera		schradera spp
SC14	Scolosanthus		scolosanthus spp
SC2	Schaefferia		schaefferia spp
SC3	Schefflera		schefflera spp
SC4	Schiedea		schiedea spp
SC5	Schinus		peppertree spp
SC6	Schisandra		schisandra spp
SC7	Schizolobium		Brazilian firetree spp
SC8	Schizomeria		schizomeria spp
SC9	Schlegelia		Schlegelia spp

SCAD	Schiedea	adamantis	Diamond head schiedea
SCAP	Schiedea	apokremnos	Kauai schiedea
SCAR	Schefflera	arboricola	Dwarf Umbrella Tree
SCAR2	Schoepfia	arenaria	Arana
SCBR5	Schlegelia	brachyantha	Higuerito de sierra
SCCE3	Scaevola	x cerasifolia	Naupaka
SCCH3	Scaevola	chamissoniana	Naupaka kuahiwi
SCCU4	Schaefferia	cuneifolia	Desert yaupon
SCEX2	Schradera	exotica	Yellowshrub
SCFR	Schaefferia	frutescens	Florida boxwood
SCGA2	Scaevola	gaudichaudiana	Mountain naupaka
SCGA3	Scaevola	gaudichaudii	Ridgetop naupaka
SCGL5	Scaevola	glabra	'ohe naupaka
SCGL6	Schefflera	gleasonii	Yuquilla
SCGL7	Schisandra	glabra	Bay starvine
SCGR5	Scolosanthus	grandifolius	Espuela de galan
SCHA4	Schiedea	haleakalensis	Haleakala schiedea
SCKI	Scaevola	kilaueae	Huahekili uka
SCLI4	Schiedea	ligustrina	Privetleaf schiedea
SCLO2	Schinus	longifolius	Longleaf peppertree
SCMA4	Schiedea	mannii	Ridgetop schiedea
SCMO	Schinus	molle	California peppertree
SCMO10	Schefflera	morototonii	Matchwood
SCMO5	Scaevola	mollis	Purple naupaka
SCOB	Schoepfia	obovata	White beefwood
SCOV	Schizomeria	ovata	Cherry Birch
SCPA23	Schizolobium	parahybum	Brazilian firetree
SCPO	Schinus	polygamus	Huingan
SCPO9	Scolosanthus	portoricensis	Maricao
SCPR	Scaevola	procera	Forest naupaka
SCSC3	Schoepfia	schreberi	Gulf graytwig
SCSE6	Scaevola	sericea	Beach naupaka
SCTE	Schinus	terebinthifolius	Brazilian pepper
SCVE	Sciadopitys	verticillata	Umbrella pine
SCVE4	Scolosanthus	versicolor	Puerto rico devilbrush
SE	Sequoia		redwood spp
SE1	Sebastiania		Sebastian-bush spp
SE10	Serianthes		Serianthes spp
SE12	Serissa		snowrose spp
SE13	Sesbania		riverhemp spp
SE14	Severinia		severinia spp
SE2	Securidaca		securidaca spp
SE3	Sedum		stonecrop spp
SE7	Senna		senna spp
SE8	Sequoiadendron		giant sequoia spp
SE9	Serenoa		serenoa spp
SEAL4	Senna	alata	Emperor's candlesticks

SEAR8	Senna	armata	Desertsenna
SEAT3	Senna	atomaria	Flor de san jose
SEBA2	Senna	bacillaris	Whitebark senna
SEBI5	Senna	bicapsularis	Christmasbush
SEBI9	Sebastiania	bilocularis	Arrow poision plant
SECO9	Senna	corymbosa	Argentine senna
SEDE8	Sedum	dendroideum	Tree stonecrop
SEDI8	Senna	didymobotrya	African senna
SEFL4	Senna	x floribunda	Floribunda senna
SEFO2	Serissa	foetida	Snowrose
SEFR	Sebastiania	fruticosa	Gulf sebastian-bush
SEGA2	Senna	gaudichaudii	Gaudichaud's senna
SEGI	Sequoiadendron	giganteum	Giant sequoia
SEGR5	Sesbania	grandiflora	Vegetable hummingbird
SEMA	Senna	macranthera	Manduirana
SEME4	Senna	mexicana	Mexican senna
SEMO11	Senna	monozyx	Andean senna
SEMO6	Severinia	monophylla	Chinese boxorange
SEMU5	Senna	multijuga	False sicklepod
SENE9	Serianthes	nelsonii	Hayun lagu
SENI3	Senna	nitida	Hediondilla
SEPE4	Senna	pendula	Valamuerto
SEPO5	Senna	polyphylla	Retama prieta
SERA5	Senna	racemosa	Limestone senna
SERE2	Serenoa	repens	Saw palmetto
SESC	Sebastiania	schottiana	Sarandi
SESE	Sequoia	sempervirens	Coast redwood
SESE8	Sesbania	sesban	Egyptian riverhemp
SESE9	Senna	septentrionalis	Hedionda macho
SESU10	Senna	sulfurea	Smooth senna
SESU4	Senna	surattensis	Glossy shower
SETO3	Sesbania	tomentosa	Oahu riverhemp
SETR	Sesbania	tripetii	Scarlett wisteria
SEVI5	Securidaca	virgata	Bejuco de sopla
SEWI3	Senna	wislizeni	Wislizenus' senna
SH1	Shepherdia		buffaloberry spp
SHAR	Shepherdia	argentea	Silver buffaloberry
SHCA	Shepherdia	canadensis	Russet buffaloberry
SHRO	Shepherdia	rotundifolia	Roundleaf buffaloberry
SI10	Siphoneugena		siphoneugena spp
SI3	Sida		fanpetals spp
SI6	Sideroxylon		bully spp
SI8	Simarouba		simarouba spp
SI9	Simmondsia		goatnut spp
SIAL13	Sideroxylon	alachuense	Alachua bully
SICE2	Sideroxylon	celastrinum	Saffron plum
SICH	Simmondsia	chinensis	Jojoba

SICU7	Sideroxylon	cubense	Espejuelo
SIDE6	Siphoneugena	densiflora	Hoja menuda
SIFA	Sida	fallax	Yellow llima
SIFO	Sideroxylon	foetidissimum	Sideroxylon foetidissimum
SIGL	Simarouba	glauca	Paradise tree
SILA20	Sideroxylon	lanuginosum	Gum bully
SILY	Sideroxylon	lycioides	Buckthorn bully
SIOB	Sideroxylon	obovatum	Breakbill
SIPO3	Sideroxylon	portoricense	Puerto rico bully
SIRE8	Sideroxylon	reclinatum	Florida bully
SITE2	Sideroxylon	tenax	Tough bully
SITH2	Sideroxylon	thornei	Georgia bully
SITU	Simarouba	tulae	Aceitillo falso
SL1	Sloanea		bullwood spp
SLAM	Sloanea	amygdalina	Motillo
SLBE	Sloanea	berteriana	Bullwood
SO	Sorbus		mountain ash spp
SO1	Solanum		nightshade spp
SO3	Sophora		necklacepod spp
SO4	Sorbaria		false spiraea spp
SO5	Sorghum		sorghum spp
SOAF	Sophora	affinis	Texas sophora
SOAL	Sorbus	alnifolia	Korean mountain ash
SOAM	Sorbus	americana	American mountain ash
SOAR3	Sophora	arizonica	Arizona necklacepod
SOAR5	Sorbaria	arborea	Giant false spiraea
SOAU	Sorbus	aucuparia	European mountain ash
SOCA8	Sorbus	californica	California mountain ash
SOCH	Sophora	chrysophylla	Mamani
SODE	Sorbus	decora	Showy mountain ash
SODO	Sorbus	domestica	Service Tree
SODO3	Solanum	donianum	Mullein nightshade
SODR2	Solanum	drymophilum	Erubia
SODU2	Sorbus	dumosa	Arizona mountain ash
SOER2	Solanum	erianthum	Potatotree
SOGR2	Sorbus	groenlandica	Greenland mountain ash
SOGY80	Sophora	gypsophila	Guadalupe mtn necklacepod
SOHUCF	Sorbus	hupehensis v coral fire	Mountain ash 'Coral Fire'
SOHUCQ	Sorbus	hupehensis v columbia	Mtn ash 'Columbia Queen'
SOHY3	Sorbus	hybrida	Oakleaf mountain ash
SOJA	Sophora	japonica	Japanese pagoda tree
SOLE3	Sophora	leachiana	Western necklacepod
SOMA3	Solanum	mauritianum	Earleaf nightshade
SONU4	Solanum	nudum	Forest nightshade

SOPO	Solanum	polygamum	Cakalaka berry
SORU	Solanum	rugosum	Tabacon aspero
SOSA3	Sorbus	sambucifolia	Siberian mountain ash
SOSC2	Sorbus	scopulina	Greene's mountain ash
SOSE	Sophora	secundiflora	Mescalbean
SOSI2	Sorbus	sitchensis	Western mountain ash
SOSO	Sorbaria	sorbifolia	False spiraea
SOTH	Sorbus	x thuringiaca	Mountainash
SOTO3	Sophora	tomentosa	Yellow necklacepod
SOTO4	Solanum	torvum	Turkey berry
SOWO	Solanum	woodburyi	Woodbury's nightshade
SP1	Spartium		spanish broom spp
SP2	Spathodea		spathodea spp
SP7	Spondias		mombin spp
SPAL2	Spiraea	alba	White meadowsweet
SPBE2	Spiraea	betulifolia	White spirea
SPBI2	Spiraea	x billiardii	Billard's spirea
SPBU	Spiraea	x bumalda	Bumald spiraea
SPCA	Spathodea	campanulata	African tulip tree
SPCA10	Spiraea	cantoniensis	Reeves' meadowsweet
SPCH3	Spiraea	chamaedryfolia	Germander meadowsweet
SPDO	Spiraea	douglasii	Rose spirea
SPDU	Spondias	dulcis	Ambarella
SPHY2	Spiraea	hypericifolia	Iberian spirea
SPJA	Spiraea	japonica	Japanese meadowsweet
SPJU	Spartium	junceum	Spanish broom
SPMO	Spondias	mombin	Yellow mombim
SPPR	Spiraea	prunifolia	Bridalwreath spirea
SPPU	Spondias	purpurea	Purple mombin
SPPY	Spiraea	x pyramidata	Pyramid spirea
SPSA2	Spiraea	salicifolia	Willowleaf meadowsweet
SPSE	Spiraea	septentrionalis	Northern meadowsweet
SPSP	Spiraea		spirea spp
SPSP2	Spiraea	splendens	Rose meadowsweet
SPST3	Spiraea	stevenii	Beauverd spirea
SPSU2	Spiraea	x subcanescens	Spirea
SPTH2	Spiraea	thunbergii	Thunberg's meadowsweet
SPTO2	Spiraea	tomentosa	Steeplebush
SPTR2	Spiraea	trilobata	Asian meadowsweet
SPVA2	Spiraea	x vanhouttei	Van houtt's spirea
SPVI2	Spiraea	virginiana	Virginia meadowsweet
ST	Strelitzia		strelitzia spp
ST11	Stephanandra		stephanandra spp
ST13	Sterculia		sterculia spp
ST15	Stewartia		stewartia spp
ST16	Stillingia		toothleaf spp
ST17	Streblus		streblus spp

ST19	Streptosolen		streptosolen spp
ST2	Stachytarpheta		porterweed spp
ST20	Strumpfia		strumpfia spp
ST21	Strychnos		strychnos spp
ST22	Stylogyne		stylogyne spp
ST24	Styphelia		styphelia spp
ST25	Styrax		snowbell spp
ST26	Stenocarpus		stenocarpus spp
ST3	Stahlia		stahlia spp
ST5	Staphylea		bladdernut spp
ST6	Stegnosperma		stegnosperma spp
ST7	Stenocereus		stenocereus spp
ST8	Stenogyne		stenogyne spp
STAM4	Styrax	americanus	American snowbell
STAP	Sterculia	apetala	Panama tree
STBO	Staphylea	bolanderi	Sierra bladdernut
STCA8	Stachytarpheta	cayennensis	Cayenne porterweed
STCU6	Stegnosperma	cubense	Cuban tangle
STDI	Sterculia	discolor	Sterculia rosada
STFI5	Stenocereus	fimbriatus	Spanish stenocereus
STGR4	Styrax	grandifolius	Bigleaf snowbell
STIN12	Stephanandra	incisa	Stephanandra
STJA	Styrax	japonicus	Japanese snowbell
STJA8	Streptosolen	jamesonii	Marmalade bush
STKO	Stewartia	koreana	Stewartia
STLA4	Stylogyne	lateriflora	Quiebrahacha
STMA	Stewartia	malacodendron	Silky camellia
STMA4	Strumpfia	maritima	Pride of big pine
STMO	Stahlia	monosperma	Cobana negra
STNI	Strelitzia	nicolai	Bird of paradise tree
STOV	Stewartia	ovata	Mountain stewartia
STPA5	Stillingia	paucidentata	Mojave toothleaf
STPE3	Streblus	pendulinus	Hawai'i roughbush
STPL3	Styrax	platanifolius	Sycamoreleaf snowbell
STPO3	Styrax	portoricensis	Palo de jazmin
STRE4	Styrax	rediviva	Drug snowbell
STSI	Stenocarpus	sinuatus	Firewheel tree
STSP8	Strychnos	spinosa	Natal orange
STTA	Styphelia	tameiameiae	Pukiawe
STTH3	Stenocereus	thurberi	Organpipe cactus
STTR	Staphylea	trifolia	American bladdernut
STVI7	Stenogyne	viridis	Kaanapali stenogyne
SU2	Suriana		suriana spp
SUMA2	Suriana	maritima	Bay cedar
SW1	Swietenia		mahogany spp
SWMA	Swietenia	mahogani	West indian mahogany
SWMA2	Swietenia	macrophylla	Honduras mahogany

SY1	Syagrus		syagrus spp
SY2	Symphoricarpos		snowberry spp
SY4	Symphysia		symphysia spp
SY5	Symplocos		sweetleaf spp
SY6	Syncarpia		turpentine tree spp
SY8	Syzygium		syzygium spp
SYAC	Symphoricarpos	acutus	Sharpleaf snowberry
SYAL	Symphoricarpos	albus	Common snowberry
SYAU	Syzygium	australe	Scrub Cherry
SYCH	Syringa	x chinensis	Chinese lilac
SYCO	Syagrus	coronata	Licuri palm
SYCU	Syzygium	cumini	Jambolan plum
SYFR	Syzygium	francisii	Giant Water Gum
SYGL	Syncarpia	glomulifera	Turpentine tree
SYGR2	Syzygium	grande	Sea apple
SYGU	Symphoricarpos	guadalupensis	Mckittrick's snowberry
SYHE	Symphoricarpos	hesperius	Trailing snowberry
SYJA	Syzygium	jambos	Malabar plum
SYJO4	Syringa	josikaea	Hungarian lilac
SYLA2	Symplocos	lanata	Nispero cimarron
SYLA8	Symplocos	latifolia	Broad-leaf sweetleaf
SYLO	Symphoricarpos	longiflorus	Desert snowberry
SYLU	Syzygium	luehmannii	Small Leaved Lilly Pilly
SYMA	Symplocos	martinicensis	Martinique sweetleaf
SYMA2	Syzygium	malaccense	Malaysian apple
SYMI2	Symphoricarpos	microphyllus	Pink snowberry
SYMI3	Symplocos	micrantha	Aceitunilla
SYMO	Syzygium	moorei	Coolamon
SYOC	Symphoricarpos	occidentalis	Wolfberry
SYOL	Syzygium	oleosum	Satinash
SYOR	Symphoricarpos	orbiculatus	Coralberry
SYOR2	Symphoricarpos	oreophilus	Mountain snowberry
SYPA	Symphoricarpos	palmeri	Palmer's snowberry
SYPA3	Syringa	patula	Manchurian lilac
SYPE	Syringa	x persica	Persian lilac
SYRA	Symphysia	racemosa	Leatherleaf eelvine
SYRE	Syringa	reticulata	Japanese tree lilac
SYRO2	Symphoricarpos	rotundifolius	Roundleaf snowberry
SYSA	Syzygium	sandwicense	'ohi'a ha
SYSP	Syringa		lilac spp
SYTI	Symplocos	tinctoria	Common sweetleaf
SYVI3	Syringa	villosa	Villous lilac
SYVU	Syringa	vulgaris	Common lilac
SYWI	Syzygium	wilsonii	Powder-puff lilliy pilly
TA	Taxus		yew spp
TA10	Taxodium		bald cypress spp
TA2	Tamarix		tamarisk spp

TA3	Tabernaemontana		milkwood spp
TA7	Tamarindus		tamarind spp
TA9	Tamonea		tamonea spp
TAAF	Tamarix	africana	African tamarisk
TAAL4	Tabernaemontana	alba	White milkwood
TAAP	Tamarix	aphylla	Athel tamarisk
TAAR	Tabebuia	aurea	Caribbean trumpet-tree
TAAR6	Tamarix	aralensis	Russian tamarisk
TAAS	Taxodium	ascendens	Pond cypress
TAAV	Tabebuia	avellanedae	Ipe-roxo
TABA	Taxus	baccata	English yew
TABA2	Tabebuia	bahamensis	White dwarf tabebuia
TABO	Tamonea	boxiana	Crow broom
TABR	Taxus	brevifolia	Pacific yew
TACA	Taxus	canadensis	Canada yew
TACA9	Tamarix	canariensis	Canary island tamarisk
TACH	Tabebuia	chrysantha	Roble amarillo
TACH2	Tamarix	chinensis	Fivestamen tamarisk
TACH3	Tabebuia	chrysotricha	Ipe-amarelo
TACI	Tabernaemontana	citrifolia	Milkwood
TACU	Taxus	cuspidata	Japanese yew
TADI	Taxodium	distichum	Baldcypress
TADI5	Tabernaemontana	divaricata	Pinwheelflower
TADO2	Tabebuia	donnell-smithii	Primavera
TAFL	Taxus	floridana	Florida yew
TAGA	Tamarix	gallica	Tamarisco
TAGL	Tabebuia	glomerata	Tabebuia glomerata
TAHA	Tabebuia	haemantha	Roble cimarron
TAIM	Tabebuia	impetiginosa	Pink trumpet tree
TAIN	Tamarindus	indica	India tamarind
TAMU	Taxodium	mucronatum	Montezuma cypress
TAOCNE	Tabebuia	ochracea ssp neochrysantha	Golden trumpet tree
TAPA	Tabebuia	heterophylla	White cedar
TAPA2	Tamarix	parviflora	Small flower tamerisk
TARA	Tamarix	ramosissima	Saltcedar
TARI	Tabebuia	rigida	Roble de sierra
TARO	Tabebuia	rosea	Apamate
TASC2	Tabebuia	schumanniana	Roble colorado
TASE4	Tabebuia	serratifolia	Yellow poui
TASP	Tabebuia		trumpet-tree spp
TATE7	Tamarix	tetragyna	Tamarix tetragyna
TE1	Tecoma		trumpetbush spp
TE10	Tetragastris		tetragastris spp
TE12	Tetramolopium		tetramolopium spp
TE14	Tetrapanax		tetrapanax spp
TE15	Tetraplasandra		tetraplasandra spp

TE16	Tetrapterys		tetrapterys spp
TE17	Tetrazygia		clover ash spp
TE18	Teucrium		germander spp
TE2	Tectona		tectona spp
TE3	Tephrosia		hoarypea spp
TE4	Terminalia		troipical almond spp
TE6	Ternstroemia		ternstroemia spp
TE8	Tetracoccus		shrubby-spurge spp
TEAN2	Tetrazygia	angustifolia	Stinkingfish
TEAR3	Tetramolopium	arenarium	Maui tetramolopium
TEBA	Tetragastris	balsamifera	Masa
TEBI	Tetrazygia	bicolor	Florida clover ash
TEBI2	Tetrazygia	biflora	Puerto rico clover ash
TECA	Terminalia	catappa	Tropical almond
TECA5	Tephrosia	candida	White hoarypea
TECA7	Tetramolopium	capillare	Pamakani
TECA8	Tecoma	capensis	Cape honeysuckle
TECA9	Tecoma	castanifolia	Chestnutleaf trumpetbush
TECO5	Tetramolopium	consanguineum	Forest tetramolopium
TECO6	Tetramolopium	conyzoides	Smallhead tetramolopium
TECR	Tetrazygia	crotonifolia	Hillside clover ash
TEDI	Tetracoccus	dioicus	Red shrubby-spurge
TEEL	Tetrazygia	elaeagnoides	Krekre
TEFI2	Tetramolopium	filiforme	Ridgetop tetramolopium
TEFR3	Teucrium	fruticans	Shrubby germander
TEGR	Tectona	grandis	Teak
TEGY	Tetraplasandra	gymnocarpa	Koolau range 'ohe
TEHA2	Tetraplasandra	hawaiensis	Hawai'i 'ohe
TEHE3	Ternstroemia	heptasepala	Saintedwood
TEHU	Tetramolopium	humile	Alpine tetramolopium
TEIL	Tetracoccus	ilicifolius	Hollybush
TEIN5	Tetrapterys	inaequalis	Tetrapterys inaequalis
TEIV2	Terminalia	ivorensis	Ivory coast almond
TEKA3	Tetraplasandra	kavaiensis	'ohe'ohe
TELE	Tephrosia	leiocarpa	Smoothpod hoarypea
TELE2	Tetramolopium	lepidotum	Waianae tetramolopium
TELU2	Ternstroemia	luquillensis	Palo colorado
TEMU2	Terminalia	muelleri	Australian almond
TEMY	Terminalia	myriocarpa	East indian almond
TEOA	Tetraplasandra	oahuensis	'ohe mauka
TEOB	Terminalia	oblonga	Peruvian almond
TEOR	Teucrium	orientale	Oriental germander
TEPA	Tetrapanax	papyriferus	Ricepaper plant
TEPE	Ternstroemia	peduncularis	Copey vera
TERE3	Tetramolopium	remyi	Awalua tetramolopium
TERO	Tetramolopium	rockii	Dune tetramolopium
TEST	Tecoma	stans	Ginger-thomas

TEST3	Ternstroemia	stahlii	Mamey de cura
TESU	Ternstroemia	subsessilis	El yunque colorado
TESY	Tetramolopium	sylvae	Seacliff tetramolopium
TETE5	Tetramolopium	tenerrimum	Oahu tetramolopium
TEUR	Tetrazygia	urbanii	Cenizo
TEWA	Tetraplasandra	waialealae	Mt. waialeale 'ohe
TEWA3	Tetraplasandra	waimeae	'ohe kiko 'ola
TH10	Thunbergia		thunbergia spp
TH4	Theobroma		theobroma spp
TH5	Thespesia		thespesia spp
TH6	Thevetia		thevetia spp
TH7	Thouinia		thouinia spp
TH8	Thrinax		thatch palm spp
TH9	Thuja		red cedar spp
THCA	Theobroma	cacao	Cacao
THER	Thunbergia	erecta	Bush clockvine
THMI	Thrinax	morrisii	Key thatch palm
THOC	Thuja	occidentalis	Northern white cedar
THOR	Platycladus	orientalis	Oriental arborvitae
THPA	Thrinax	radiata	Florida thatchpalm
THPE3	Thevetia	peruviana	Luckynut
THPL	Thuja	plicata	Western redcedar
THPU	Thespesia	populnea	Portia tree
THST2	Thouinia	striata	Ceboruquillo
TI	Tilia		basswood spp
TI1	Tibouchina		glorytree spp
TI2	Tipuana		tipuana spp
TIAM	Tilia	americana	American basswood
TICA	Tilia	americana v caroliniana	Carolina basswood
TICO	Tilia	cordata	Littleleaf linden
TICOGR	Tilia	cordata 'Greenspire'	Greenspire linden
TIEU	Tilia	x vulgaris	Common linden
TIEU1	Tilia	x europaea	Common lime
TIEU2	Tilia	euchlora	Crimean linden
TIGR3	Tibouchina	granulosa	Brazilian glorytree
TIHE	Tilia	americana v heterophylla	White basswood
TIMU	Tibouchina	mutabilis	Quaresmeira ou tibuchina
TIPE	Tilia	petiolaris	Pendent silver linden
TIPL	Tilia	platyphyllos	Bigleaf linden
TISP	Tipuana	tipu	Pride of bolivia
TITO	Tilia	tomentosa	Silver linden
TITOSS	Tilia	tomentosa 'Sterling Silver'	Sterling silver linden
TIUR	Tibouchina	urvilleana	Princess-flower
TO	Toxicocendron		toxicocendron spp

TO2	Toona		redcedar spp
TO3	Torralbasia		torralbasia spp
TO4	Torreya		torreya spp
TO5	Touchardia		touchardia spp
TO6	Tournefortia		soldierbush spp
TO7	Toxicodendron		poison oak spp
TOAR2	Tournefortia	argentea	Velvetleaf soldierbush
TOBI	Tournefortia	bicolor	Niguita
TOCA	Torreya	californica	California torreya
TOCI	Toona	ciliata	Australian redcedar
TOCU	Torralbasia	cuneifolia	Boje
TOFI	Tournefortia	filiflora	Cold withe
TOGR	Torreya	grandis	Torreya grandis
TOHI	Tournefortia	hirsutissima	Chiggery grapes
TOLA	Touchardia	latifolia	Olona
TOLA2	Tournefortia	laurifolia	Laurel-leaf soldierbush
TOMA	Tournefortia	maculata	Bejuco de masa
TORA	Toxicodendron	radicans	Poison ivy
TORY	Toxicodendron	rydbergii	Western poison ivy
TOSC3	Tournefortia	scabra	West indian soldierbush
TOSU	Toxicocendron	succedaneum	Rhus Tree
TOTA	Torreya	taxifolia	Florida torreya
TOVE	Toxicodendron	vernix	Poison sumac
TR	Tristaniopsis		tristaniopsis spp
TR1	Trachycarpus		windmill palm spp
TR11	Triphasia		triphasia spp
TR12	Triumfetta		triumfetta spp
TR13	Trixis		threefold spp
TR14	Trophis		trophis spp
TR15	Trithrinax		spiny palm spp
TR4	Trema		trema spp
TR5	Trematolobelia		false lobelia spp
TR7	Triadica		tallowtree spp
TR8	Trichilia		trichilia spp
TRAC	Trithrinax	acanthocoma	Brizilian needle palm
TRBO5	Triumfetta	bogotensis	Parquet burr
TRCO	Tristaniopsis	conferta	Brisbane box
TRFO	Trachycarpus	fortunei	Windmill palm
TRGR8	Trematolobelia	grandifolia	Largeflower false lobelia
TRHI3	Trichilia	hirta	Broomstick
TRIN6	Trixis	inula	Tropical threefold
TRKA2	Trematolobelia	kauaiensis	Kauai false lobelia
TRLA	Tristaniopsis	laurina	Water gum; kanooka
TRLA2	Trema	lamarckianum	Lamarck's trema
TRLAEL	Tristaniopsis	laurina 'Elegans'	Water gum 'Elegans'
TRMA8	Trematolobelia	macrostachys	Koli'i
TRMI	Trema	micrantha	Florida trema

TROR	Trema	orientale	Oriental trema
TRPA2	Trichilia	pallida	Gaita
TRRA4	Trophis	racemosa	White ramoon
TRSE6	Triadica	sebifera	Tallowtree
TRSI5	Trematolobelia	singularis	Lavaslope false lobelia
TRTR7	Triphasia	trifolia	Limeberry
TRTR8	Trichilia	triacantha	Bariaco
TS	Tsuga		hemlock spp
TSCA	Tsuga	canadensis	Eastern hemlock
TSCA2	Tsuga	caroliniana	Carolina hemlock
TSHE	Tsuga	heterophylla	Western hemlock
TSJE	Tsuga	x jeffreyi	Jeffrey hemlock
TSME	Tsuga	mertensiana	Mountain hemlock
TU	Tupidanthus		tupidanthus spp
TU3	Turpinia		turpinia spp
TUCA	Tupidanthus	calyptratus	Tupidanthus
TUOC	Turpinia	occidentalis	Muttonwood
UL1	Ulex		gorse spp
ULAL	Ulmus	alata	Winged elm
ULAM	Ulmus	americana	American elm
ULAMLI	Ulmus	americana 'Liberty'	Liberty elm
ULCAHO	Ulmus	carpinifolia 'Hollandica'	Smoothleaf elm
ULCOFA	Ulmus	cornubiensis fastigiata	Cornish elm
ULCR	Ulmus	crassifolia	Cedar elm
ULEU	Ulex	europaeus	Common gorse
ULGL	Ulmus	glabra	Wych elm
ULGLLU	Ulmus	glabra lutescens	Golden wych elm
ULHO	Ulmus	x hollandica	Dutch elm
ULMI	Ulmus	minor	Smooth-leaf elm
ULNO	Ulmus	x notha	Ulmus x notha
ULPA	Ulmus	parvifolia	Chinese elm
ULPA2	Ulex	parviflorus	African gorse
ULPAEV	Ulmus	parvifolia 'Evergreen'	Chinese evergreen elm
ULPR	Ulmus	procera	English elm
ULPU	Ulmus	pumila	Siberian elm
ULRU	Ulmus	rubra	Slippery elm
ULS	Ulmus		elm spp
ULSE	Ulmus	serotina	September elm
ULTH	Ulmus	thomasii	Rock elm
ULWI	Ulmus	wilsoniana	Wilson elm
UM1	Umbellularia		California laurel spp
UMCA	Umbellularia	californica	California laurel
UN1	Ungnadia		ungnadia spp
UNSP	Ungnadia	speciosa	Mexican buckeye

UR2	Urera		urera spp
UR3	Urvillea		urvillea spp
URBA	Urera	baccifera	Scratchbush
URCA2	Urera	caracasana	Flameberry
URCH2	Urera	chlorocarpa	Ortiga
URGL	Urera	glabra	Hopue
URKA	Urera	kaalae	Opuhe
URUL	Urvillea	ulmacea	Apaac
VA1	Vaccinium		blueberry spp
VA2	Valeriana		valerian spp
VA3	Vallesia		vallesia spp
VA4	Vanclevea		vanclevea spp
VA5	Vangueria		vangueria spp
VA7	Vauquelinia		rosewood spp
VAAN3	Vallesia	antillana	Tearshrub
VAAR	Vaccinium	arboreum	Sparkleberry
VAAT3	Vaccinium	x atlanticum	Atlantic huckleberry
VACA	Vauquelinia	californica	Torrey vauquelinia
VACA11	Vaccinium	x carolinianum	Carolina huckleberry
VACA6	Vaccinium	caesariense	New jersey blueberry
VACA8	Vaccinium	calycinum	Ohelo kau la'au
VACO	Vaccinium	corymbosum	Highbush blueberry
VACO4	Vauquelinia	corymbosa	Slimleaf rosewood
VADE2	Vaccinium	dentatum	Ohelo
VADO	Vaccinium	x dobbinii	Dobbin's huckleberry
VAEL	Vaccinium	elliottii	Elliott's blueberry
VAER	Vaccinium	erythrocarpum	Southern mtn cranberry
VAFO	Vaccinium	formosum	Southern blueberry
VAFU	Vaccinium	fuscatum	Black highbush blueberry
VAGL2	Vallesia	glabra	Pearlberry
VAHI	Vaccinium	hirsutum	Hairy blueberry
VAMA2	Vaccinium	x marianum	Vaccinium
VAMA3	Vaccinium	x margarettiae	Margarett's huckleberry
VAMA5	Vangueria	madagascariensis	Voa vanga
VAME	Vaccinium	membranaceum	Thinleaf huckleberry
VAMY3	Vaccinium	myrsinites	Shiny blueberry
VAOV	Vaccinium	ovalifolium	Oval-leaf blueberry
VAPA	Vaccinium	parvifolium	Red huckleberry
VARE	Vaccinium	reticulatum	Ohelo 'ai
VASI2	Vaccinium	simulatum	Upland highbush blueberry
VAST	Vaccinium	stamineum	Deerberry
VAST3	Vanclevea	stylosa	Pillar false gumweed
VAUL2	Valeriana	uliginosa	Mountain valerian
VAVI2	Vaccinium	virgatum	Smallflower blueberry
VE1	Veitchia		veitchia spp
VE4	Vernicia		vernicia spp
VEFO	Vernicia	fordii	Tungoil tree

VEME	Veitchia	merrillii	Christmas palm
VI	Virola		virola spp
VI1	Viminaria		viminaria spp
VI2	Virgilia		virgilia spp
VI5	Vitex		chastetree spp
VIAC	Viburnum	acerifolium	Maple leaved arrowood
VIAG	Vitex	agnus-castus	Chaste tree
VIBR2	Viburnum	bracteatum	Bracted arrowwood
VIBU3	Viburnum	buddleifolium	Buddlejaleaf viburnum
VIDE	Viburnum	dentatum	Arrowwood
VIDI2	Vitex	divaricata	Higuerillo
VIDI80	Viburnum	dilatatum	Linden arrowwood
VIED	Viburnum	edule	Squashberry
VIEL	Viburnum	ellipticum	Oval leafed vibrunum
VIGL2	Vitex	glabrata	Smooth chastetree
VIJA	Viburnum	japonicum	Japanese viburnum
VIJU	Viminaria	juncea	Golden spray
VILA	Viburnum	lantana	Wayferry tree
VILA11	Viburnum	lantanoides	Hobblebush
VILE	Viburnum	lentago	Nannyberry
VILU6	Vitex	lucens	Puriri
VIMO	Viburnum	molle	Softleaf arrowwood
VINE2	Vitex	negundo	Negundo chastetree
VINU	Viburnum	nudum	Possumhaw
VIOB	Viburnum	obovatum	Small-leaf arrowwood
VIOD	Viburnum	odoratissimum	Sweet viburnum
VIOP	Viburnum	opulus	European cranberry bush
VIOR	Virgilia	oroboides	Keurboom
VIPA6	Vitex	parviflora	Smallflower chastetree
VIPR	Viburnum	prunifolium	Black haw
VIRA	Viburnum	rafinesquianum	Downy arrowwood
VIRH	Viburnum	rhytidophyllum	Leather leaf viburnum
VIRH3	Viburnum	x rhytidophylloides	Lantanaphyllum viburnum
VIRI	Vitis	riparia	Riverbank grape
VIRO80	Vitex	rotundifolia	Roundleaf chastetree
VIRU	Viburnum	rufidulum	Rusty blackhaw
VIRU2	Vitis	rupestris	Sand grape
VISE14	Viburnum	setigerum	Tea viburnum
VISI	Viburnum	sieboldii	Siebold's arrowwood
VISP1	Vitis		grape spp
VISP2	Viburnum		viburnum spp
VITI2	Viburnum	tinus	Laurustinus
VITO	Viburnum	plicatum	Japanese snowball
VITR	Viburnum	opulus v americanum	American cranberrybush
VITR7	Vitex	trifolia	Simpleleaf chastetree
VIVI	Vitis	vinifera	Wine grape

WA1	Wallenia		jacanillo spp
WA3	Waltheria		waltheria spp
WA4	Washingtonia		washingtonia spp
WACA2	Waltheria	calcicola	Raichie
WAFI	Washingtonia	filifera	California palm
WAFL	Syzygium	floribundum	Weeping lilly pilly
WALA	Wallenia	lamarckiana	Jacanillo
WARO	Washingtonia	robusta	Mexican fan palm
WAYU	Wallenia	yunquensis	El yunque jacanillo
WE	Weigela		weigela spp
WE1	Wedelia		creepingoxeye spp
WE3	Weinmannia		weinmannia spp
WEFL	Weigela	floribunda	Crimson weigela
WEFL2	Weigela	florida	Oldfashioned weigela
WEFR	Wedelia	fruticosa	Cstl-plain creepingoxeye
WELA	Wedelia	lanceolata	Riverbank creepingoxeye
WEPA	Wedelia	parviflora	Smallflower creepingoxeye
WEPI	Weinmannia	pinnata	Bastard briziletto
WERE	Wedelia	reticulata	Manazanilla del monte
WI	Wisteria		wisteria spp
WI1	Wigandia		wigandia spp
WI2	Wikstroemia		false ohelo spp
WI3	Wilkesia		iliau spp
WIBI	Wikstroemia	bicornuta	Alpine false ohelo
WIFL	Wisteria	floribunda	Japanese wisteria
WIFLRO	Wisteria	floribunda v rosea	Rose wisteria
WIFU	Wikstroemia	furcata	Forest false ohelo
WIGY	Wilkesia	gymnoxiphium	Iliau
WIHO3	Wilkesia	hobdyi	Dwarf iliau
WIMO	Wikstroemia	monticola	Montane false ohelo
WIOA	Wikstroemia	oahuensis	Oahu false ohelo
WIPH2	Wikstroemia	phillyreifolia	Hawai'i false ohelo
WIPU	Wikstroemia	pulcherrima	Kohala false ohelo
WISA	Wikstroemia	sandwicensis	Variableleaf false ohelo
WISI	Wisteria	sinensis	Purple wisteria
WISK	Wikstroemia	skottsbergiana	Skottsberg's false ohelo
WIUR	Wigandia	urens	Caracus wigandia
WIVI	Wikstroemia	villosa	Hairy false ohelo
WO	Wollemia		wollemia spp
WO1	Wodyetia		wodyetia spp
WOBI2	Wodyetia	bifurcata	Foxtail palm
WONO	Wollemia	nobilis	Wollemi Pine
XA	Xanthostemon		xanthostemon spp
XACH	Xanthostemon	chrysanthus	Golden Penda
XI1	Ximenia		ximenia spp
XIAM	Ximenia	americana	Tallowwood
XY1	Xylococcus		mission manzanita spp

XY3	Xylosma		xylosma spp
XYBI	Xylococcus	bicolor	Mission manzanita
XYBU	Xylosma	buxifolia	Mucha-gente
XYCO	Xylosma	congestum	Shiny xylosma
XYCR	Xylosma	crenata	Sawtooth logwood
XYFL3	Xylosma	flexuosa	Brushholly
XYHA	Xylosma	hawaiiensis	Hawai'i brushholly
XYPA2	Xylosma	pachyphylla	Spiny logwood
XYSC2	Xylosma	schaefferioides	White logwood
XYSC3	Xylosma	schwaneckeana	Schwaneck's logwood
YU1	Yucca		yucca spp
YUAL	Yucca	aloifolia	Aloe yucca
YUBR	Yucca	brevifolia	Joshua tree
YUEL	Yucca	elata	Soaptree yucca
YUFA	Yucca	faxoniana	Eve's needle
YUGL	Yucca	glauca	Soapweed
YUGL2	Yucca	gloriosa	Moundlily yucca
YUGU	Yucca	guatemalensis	Bluestem yucca
YURE	Yucca	recurvifolia	Curveleaf yucca
YUTO	Yucca	torreyi	Torrey yucca
ZA2	Zanthoxylum		pricklyash spp
ZAAM	Zanthoxylum	americanum	Common prickly ash
ZABI	Zanthoxylum	bifoliolatum	Maricao pricklyash
ZACA3	Zanthoxylum	caribaeum	Prickly yellow
ZACL	Zanthoxylum	clava-herculis	Hercules club
ZACO	Zanthoxylum	coriaceum	Biscayne pricklyash
ZADI	Zanthoxylum	dipetalum	Kawa'u
ZAFA	Zanthoxylum	fagara	Lime prickly ash
ZAFL	Zanthoxylum	flavum	West indies satinwood
ZAHA	Zanthoxylum	hawaiiense	Hawai'i pricklyash
ZAHI2	Zanthoxylum	hirsutum	Texas hercules' club
ZAKA	Zanthoxylum	kauaense	Kauai pricklyash
ZAMA	Zanthoxylum	martinicense	White pricklyash
ZAMO	Zanthoxylum	monophyllum	Yellow prickle
ZAOA	Zanthoxylum	oahuense	Oahu pricklyash
ZAPA2	Zanthoxylum	parvum	Tickletongue
ZAPU2	Zanthoxylum	punctatum	Dotted pricklyash
ZASP	Zanthoxylum	spinifex	Niaragato
ZATH	Zanthoxylum	thomasianum	St. thomas pricklyash
ZE	Zelkova		zelkova spp
ZE2	Zenobia		honeycup spp
ZE3	Zea		corn spp
ZECA	Zelkova	carpinifolia	Caucacian zelkova
ZEPU3	Zenobia	pulverulenta	Honeycup
ZESC	Zelkova	schneideriana	Schneider zelkova
ZESE	Zelkova	serrata	Japanese zelkova

ZESEVG	Zelkova	serrata 'Village Green'	Zelkova 'Village Green'
ZESI	Zelkova	sinica	Chinese zelkova
ZI1	Ziziphus		jujube spp
ZICE	Ziziphus	celata	Florida jujube
ZIMA	Ziziphus	mauritiana	Indian jujube
ZIOB	Ziziphus	obtusifolia	Lotebush
ZIPA	Ziziphus	parryi	Parry's jujube
ZIRE	Ziziphus	reticulata	Cacao rojo
ZIRI	Ziziphus	rignonii	Soana
ZITA	Ziziphus	taylorii	Taylor's jujube
ZIZI	Ziziphus	zizyphus	Common jujube
MACLASS			Tree Hardwood
PICLASS			